SURFACE WATER – GROUNDWATER INTERACTIONS: A CASE OF A SHALLOW SEMI-CLOSED LAKE CATCHMENT IN NORTHERN TANZANIA

Gustavio Okwir

A Dissertation Submitted in Partial Fulfilment of the Requirements for the Degree of Doctor of Philosophy in Water Resources Engineering of the Nelson Mandela African Institution of Science and Technology

Arusha, Tanzania

June, 2023

ABSTRACT

Conjunctive use of surface water and groundwater is rapidly growing in many developing countries as an adaptation strategy to climate variability and change. However, the interactions between the groundwater and the surface water systems are not adequately understood, especially among the East African rift valley lakes, where data paucity has limited studies and reporting on the spatial influence of catchment heterogeneity. In its humble contribution to sustainable water development, this study aimed to present a platform for understanding the influence of climatic variation and anthropogenic activities on surface water–groundwater interactions. To be relevant locally, Lake Babati, a freshwater lake in Northern Tanzania that provides the community with fish, freshwater, and a habit for hippopotamus, was studied. The study applied hydrological simulation, grey relational analysis, and stepwise regression analysis to model the hydrological behaviour of the lake. Further, it used hydrogeochemistry and environmental isotopes to identify groundwater fluxes and draw the conceptual understanding of surface water – groundwater interaction and applied topography-based indices to spatially map groundwater potentials within the catchment. The results showed that Lake Babati level is significantly declining (p-value < 0.01) at a rate of 25 mm per annum. The lake level decline could not be explained by climatic variability since the decline occurred when both evaporation and rainfall showed no significant changes either seasonally or annually. Instead, the consistent decline of the lake level in all seasons could be due to the expansion of the spillway, which effectively lowered the lake reservoir level and increased the lake outflow in rainy seasons. The hydro-geochemistry and isotopes data showed that the lake water and groundwater interact and are in hydraulic connections. Further, using Height Above Nearest Drainage based and Topography Wetness Index based methods, the study developed two groundwater potential maps to predict groundwater spatial variability and guide groundwater prospecting efforts and subsequent development. Given that Lake Babati is in a hydraulic connection with the groundwater, its consistent decline will likely impact the groundwater system. Similarly, abstracting groundwater at unsustainable rates could lower the lake levels further. Therefore, integrated water resources management is required for sustainable water resources development and management in the catchment. Mandatory and continuous monitoring of the water resources (groundwater levels, river flows, and lake levels) is recommended to generate quality *in situ* data for future studies.

DECLARATION

I, Gustavio Okwir, do hereby declare to the Senate of the Nelson Mandela African Institution of Science and Technology that this dissertation is my own original work and that it has neither been submitted nor being concurrently submitted for degree award in any other institution.

Gustavio Okwir — Date: 25/8/2023

The above declaration is confirmed by:

Prof. Karoli Nicholas Njau — Date: 25/8/2023

Dr Juma Selemani Rajabu — Date: 27/8/2023

Prof. Sharma Pramod Kumar — Date: 27/8/2023

COPYRIGHT

CERTIFICATION

The undersigned certify that they have read and hereby recommend for acceptance by the Senate of the Nelson Mandela African Institution of Science and Technology a dissertation titled *"Surface water – Groundwater Interactions: A case of a Shallow Semi-closed Lake Catchment in Northern Tanzania"* in partial fulfilment of the requirements for the Degree of Doctor of Philosophy in Water Resources Engineering of the Nelson Mandela African Institution of Science and Technology.

25/8/2023

Prof. Karoli Nicholas Njau — Date

27/8/2023

Dr Juma Selemani Rajabu — Date

27/8/2023

Prof. Sharma Pramod Kumar — Date

ACKNOWLEDGEMENTS

I thank my late father, Eugene Okwang, who motivated and challenged me to seek more profound knowledge. I wish he had lived to see my adventure of self-discovery. Thank you, Dad.

After the Almighty God, who blessed me with life and a desire for advanced studies, came the WISE–FUTURES, who made it possible for me to pursue my PhD studies. I am most grateful for your generosity and favour towards me. WISE – FUTURES did not only sponsor me to study at the prestigious NM – AIST but also sent me on a fully-funded fellowship at the prestigious Indian Institute of Technology Roorkee. I greatly thank WISE–FUTURES and wish that the omnipotent God provides them with more opportunities to sponsor many more studies. My special appreciation goes to Dr. Hans Komakech, Dr. Yusuf Jande, Ms. Grace Cusack and the entire WISE–FUTURES team.

To my supervisors, the late Prof. Alfred N. N. Muzuka, Prof. Njau N. Karoli, Prof. Pramod Kumar Sharma and Dr. Rajabu Selemani, I am exceedingly delighted to have reached the milestone of acknowledging your efforts. I cannot find the best words to express my appreciation for your tremendous and tireless efforts in guiding me to produce this dissertation. The journey has been long, but you made it enjoyable. Thank you so much, and may the omnipresent God bless you abundantly.

Great appreciation goes to my employer, Gulu University and all its administrators for graciously granting me study leave and their general support towards staff development. Particularly, I thank my dean Dr. Collins Okello and the Head of Department, Dr. Nono Denis, for their tireless support. Similarly, NM-AIST is much appreciated for assembling very supportive academic and non-academic teams and providing a conducive learning environment. Notably, I appreciate MEWES deans Prof. Revocatus Machunda and Prof. Kelvin Mtei, and staff Dr. Thomas Kivevele, Prof. Tatiana Pogrebnaya and the entire MEWES team.

Last but most importantly, my classmates and friends: Mohammed Mwambumba, Benard Kivumbi, Latifa Nyembo, Adam Mfargavo, Rosette Nyiranziza, Benjamin Banda, Risala Mureth, Michael Semba, Innocent Lugodisha, Onesmo Sigala Zackaria, and the entire WESE Cohort 7. Thank you very much for the jokes, encouragement, stories, discussions, evening tea and beers. Pombe siyo Chai!! Asanteni sana ndugu zangu!!

DEDICATION

This work is dedicated to my wife, Ireen Akankwasa, and the children, Francis Okwang, Daniella Amollo, Abigail Awor, and the others who are yet to come.

May this work inspire you to seek and love deeper knowledge. May it motivate you to understand the gymnastics of the world. May you do everything for your benefit and the love of others.

TABLE OF CONTENTS

LIST OF TABLES

LIST OF FIGURES

LIST OF APPENDICES

LIST OF ABBREVIATIONS AND SYMBOLS

°C	Degree Centigrade
AHP	Analytical Hierarchy Process
AIC	Akaike Information Criterion
BAWASA	Babati Water Supply Authority
Ca^{2+}	Calcium ions
CI	Consistency Index
Cl^{-}	Chloride ions
CO_3^{2-}	Carbonate ions
DEM	Digital Elevation Model
EARS	East African Rift System
EBBI	Enhanced Built - up and Bareness Index
EC	Electrical Conductivity
EW	Effective Weight
F^{-}	Flouride ions
FAHP	Fuzzy Analytical Hierarchy Process
FMAM	February, March, April and May
GIS	Geographic Information System
GMAO	Global Modelling and Assimilation Office
GMWL	Global Meteoric Water Line
GPS	Global Positioning System
GRA	Grey Relational Analysis
GRACE	Gravity Recovery and Climatic Experiment
GSFLOW	Groundwater and Surface-water FLOW model
GWP	Groundwater Potential
GWPI	Groundwater Potential Index
HAND	Height Above Nearest Drainage
HEC - HMS	Hydrologic Engineering Centre - Hydrologic Modelling System
IOD	Indian Ocean Dipole
IPCC	Internation Panel on Climate Change
ITCZ	Intertropical Convergence Zone
JJAS	June, July, August and September
K^{+}	Potassium ions

km^2	Square Kilometer
LMWL	Local Meteoric Water Line
LULC	Land use and land cover
MASL	Meters Above Sea Level
mbgs	meters below ground surface
MCM	Million Cubic Meters
MERRA 2	Modern-Era Retrospective analysis for Research and Applications, Version 2
Mg^{2+}	Magnesium ions
Na^{+}	Sodium ions
NASA	National Aeronautics and Space Administration
NDBaI	Normalised Difference Barenness Index
NDBI	Normalised Difference Built-up Index
NDVI	Normalised Difference Vegetation Index
NO_3^{-}	Nitrate ions
NPK	Nitrogen, Phosphorus and Potassium
NSE	Nash Sutcliffe Efficiency
ONDJ	October, November, December and January
ONDJFMAM	October, November, December, January, February, March, April and May
PC1	Principal Component One
PC2	Principal Component Two
PCA	Principal Component Analysis
PDSI	Palmer Drought Severity Index
PET	Potential Evapotranspiration
pH	Potential of Hydrogen
PO_4^{3-}	Phosphate ions
RCI	Random Consistency Index
RMSE	Root Means Sqaured Error
RTK GPS	Real Time Kinematic Geographic Information System
SO_4^{2-}	Sulphate ions
SPEI	Standardized Precipitation - Evapotranspiration Index
SPI	Standardised Precipitation Index

SRTM	Shuttle Radar Topographic Mission
SWAT	Soil and Water Assesment Tool
TDS	Total Dissolved Solids
TH	Total Hardness
TMA	Tanzania Meteorological Authority
TWI	Topographic Wetness Index
UH	Unit Hydrograph
UI	Urban Index
USA	United States of America
V-SMOW	Vienna Standard Mean Ocean Water
$\delta^{18}O$	Delta Oxygen - 18 isotope
δD	Delta Hydrogen 2 isotope (Deuterium)

CHAPTER ONE

INTRODUCTION

1.1 Background of the Problem

Safe and clean water access is still low in sub-Saharan Africa (WWAP, 2019). By 2015, as many as 319 million people in the region had no access to safe and clean drinking water (UNICEF, 2015). However, as the population grows, regional governments are exploring opportunities to boost the low per capita food production (Funk & Brown, 2009) through irrigated agriculture which still has a high potential for expansion in sub-Saharan Africa (Mashnik *et al.,* 2017). Similarly, increasing access to improved water supplies is an international priority that will inevitably increase water consumption. Consequently, achieving these objectives implies that the water demand for domestic and economic activities such as agriculture, power generation and industrial purposes will increase (Clifton *et al.,* 2010; WWAP, 2012).

Since fresh surface water fluctuates with seasons and under the influence of climate variability, most people have turned their attention to the exploitation of groundwater (Clifton *et al.,* 2010), which is considered reliable due to its slow response to seasonal variations (Kløve *et al.,* 2014). The decisive role played by groundwater in adapting water resource management to climate variability (Clifton *et al.,* 2010) has accelerated its use for agricultural and industrial purposes. This trend has been described as the ‘‘silent revolution’’ because numerous individual farmers, motivated by short-term benefits provided by groundwater, have drilled an uncountable number of groundwater abstraction wells without government knowledge and approval (Llamas & Martínez-Santos, 2005). Such uncontrolled developments are not incorporated into comprehensive land and water management plans at the basin scale; and, thus, often result in overexploitation and degradation of the groundwater aquifer. Groundwater overexploitation can go on for years because it is difficult to detect. This, coupled with climate variability and uncertainty, significantly challenges sustainable groundwater development worldwide. The East African region is no exception. Tanzania experiences a similar scenario (Mul *et al.,* 2007; Chacha *et al.,* 2018). The unregulated water use in many developing countries threatens the water resources regime (Seeteram *et al.,* 2019; Tolche, 2020). It can also alter the temporal and spatial dynamics of surface water–groundwater interactions (Sakakibara *et al.,* 2016).

As natural resource managers and policymakers embrace evidence-based planning and management, they must be abreast with available water resources, exchange between reservoirs (surface water and groundwater reservoirs), limitations, and vulnerabilities (Biggs *et al.,* 2015) to facilitate sustainable planning and management of the food-water-energy nexus (WWAP, 2012).

The variability of water resources under different stressors has already been widely studied (Christensen *et al.,* 2004; Baguis *et al.,* 2009; Ogiramoi, 2011; Taye *et al.,* 2011; Serdeczny *et al.,* 2016); however, the focus on the lake - groundwater interaction has been limited (Clifton *et al.,* 2010).

Studies on lake responses to climatic and anthropogenic stresses are essential for planning and managing water resources. In semi-arid areas like the East African rift valley regions, surface water and groundwater interactions play vital roles in the eco-hydrological system (Gilfedder *et al.,* 2012). However, these are threatened by unsustainable abstractions of water from shallow lakes and aquifers because they can alter surface water–groundwater interactions and, in the worst case, result in a decline in lake levels or drying of lakes. This can further lead to secondary impacts such as the disturbance of natural habitats of specialist species, the proliferation of nuisance and invasive species, biodiversity loss, and eutrophication in extreme cases (Zohary & Ostrovsky, 2011; Lalika *et al.,* 2015; Kalacska *et al.,* 2017; Seeteram *et al.,* 2019).

A study of several lakes has shown that landscape setting, hydrogeology, and climatic interactions give lakes unique hydrological behaviour (Olaka *et al.,* 2010). The uniqueness of each lake limits the transferability of one study's results to another. Each lake would exhibit different behaviour, thus, justifying the need for site-specific analysis.

1.2 Statement of the Problem

Numerous studies on water balance have used lumped catchment models and ignored the spatial variation of catchment parameters and their impact on water balance components. For example, Swenson and Wahr (2009) and Tate *et al.* (2004) used aggregated and lumped seasonal climatic values to relate the evolution of water storage in Lake Victoria to the impacts of climatic changes and human management. Since such studies often report water balance components in a lumped way, they do not inform policy makers and users on the spatial variation of vital water balance components such as groundwater. Yet groundwater provides half of the world's population with freshwater (WWAP, 2015), and it is a major source of drinking water for rural populations in sub – Saharan Africa (Pavelic *et al.,* 2012)

The increasing dependence of rural communities in developing countries on point boreholes equipped with or without motorized pumps for domestic and agricultural water requirements (Llamas & Martínez-Santos, 2005; Pavelic *et al.,* 2012) have made groundwater a critical resource. However, a survey in Uganda, Malawi, and Ethiopia estimated that 30% of boreholes equipped with hand pumps fail within five years of commissioning, primarily due to low yield, poor quality, and mechanical failure (Macdonald & Helen, 2016). MacDonald *et al.* (2012) attributed this

hidden crisis to the poor understanding of the groundwater system occasioned by the limited instrumental groundwater observation stations across the African continent.

Coupled surface water–groundwater models, which could improve the estimation of fluxes between the surface water and groundwater (Bailey *et al.,* 2016), have been applied with limitations within sub-Saharan Africa. Such models require high quality hydrological and hydrogeological data, which unfortunately, are generally lacking in the region (Deus *et al.,* 2013; WREM International, 2015; Mbanguka *et al.,* 2016; Ligate *et al.,* 2021). The lack of instrumental hydrological (observed) data in sub-Saharan Africa has forced most studies to ignore groundwater or assume it as a negligible water balance component (MacDonald *et al.,* 2012). As a result, the documentation of the groundwater resources is limited and has thus constrained the understanding of the available groundwater resources despite a growing dependence on them (MacDonald *et al.,* 2012; Pavelic *et al.,* 2012). These challenges are more pronounced among the East African Rift Valley lakes as they lack *in situ* hydrological data (Hassan & Jin, 2014; Chacha *et al.,* 2018). Therefore, the interactions between the groundwater and the surface water systems are not adequately understood in most East African Rift Valley lakes.

Mbanguka *et al.* (2016) studied the variability of Lake Babati level and reported cloudiness as a sensitive parameter to the lake's level variability due to its significant influence on evaporation. However, their study used the energy balance equation (Anapalli *et al.,* 2018), which has a higher sensitivity to air temperature and gives inconsistently higher evaporation than the combination methods of estimating evaporation, such as the Penman-Monteith method (Ershadi *et al.,* 2011). Mbanguka *et al.* (2016) further assumed the groundwater influx to be equal to the changes in the lake storage. Their study was based on a rough estimate of the lake's surface area and volume (drawn from five transects of a bathymetric survey of the lake). However, lake size and morphology can significantly influence the sensitivity of lakes to climatic forcing (Olaka *et al.,* 2010). Limited studies have investigated the groundwater dynamics of the Lake Babati catchment. The few studies that have analysed Lake Babati's water balance (Sandstrom, 1995; Lopez, 2011; Mbanguka *et al.,* 2016) lacked observed groundwater data and estimated the groundwater parameters based on the hydraulic properties without verification of the aquifer material.

This study's novelty was centred on analysing the influence of climatic variability on the lake levels, applying hydrogeochemistry and environmental isotopes to identify fluxes of surface–groundwater interactions and topography-based indices to map groundwater potential (GWP). In addition, it incorporated the spatial variabilities of the influencing parameters to map GWP within the catchment. This study further adopted a multi-criteria approach for weighting the influence of hydrological parameters to cover the inadequacies that might result from a single method due to the lack of quality observed data.

1.3 Rationale of the Study

Understanding lake water level dynamics and the variability of hydrological parameters is key for informed and timely management interventions, a prerequisite for sustainable water management. Moreover, as most water resource managers adopt conjunctive use and management of groundwater and surface water (Llamas & Martínez-Santos, 2005), understanding any exchange (interaction) and hydraulic connection between surface water and the groundwater becomes very crucial (Khan & Khan, 2019). This is in consideration that groundwater and surface water reservoirs are coupled and interdependent to the extent that what happens to one part of the system affects the other (Idowu, 2007). In addition to planning conjunctive use, understanding surface water-groundwater interactions is beneficial for many purposes, including the incorporation of groundwater in water resources planning, monitoring the evolution of pollution and control of contamination, water rights issues, and resolution of water-related conflicts (Khan & Khan, 2019)

Lake Babati, whose catchment is the subject of this study, provides the local community with fish and supports several aquatic species like the hippopotamus that inhabit it (Stromquist, 1992; Sandstrom, 1995; Mbanguka *et al.,* 2016). The main economic activities in Babati District (the administrative unit where the Lake Babati catchment lies) are agriculture and livestock production (Hongoa, 2014). Recently, Babati Town has expanded with more settlements, land cover modifications, and an increased population (Hongoa, 2014; Pantaleo *et al.,* 2018). These anthropogenic activities have resulted in the development and construction of more abstraction wells on the lakeshore to supply water to the sprouting Babati town. However, the consistent decline of Lake Babati water levels has made the natural resource managers apprehensive that the abstraction wells around the lake could irrecoverably damage the groundwater–lake dynamics. Despite the importance of the lake, studies relating the wells' abstractions (groundwater dynamics) and anthropogenic activities to the lake's variability are scanty.

Poor understanding of surface water – groundwater interactions challenges the ideals of integrated water resources management as natural resources managers resort to theoretical interactions without verification. For example, the increased number of abstraction wells was thought to drive the observed declines in Lake Babati levels. Unless this knowledge gap is bridged, Lake Babati levels will continue to decline with no remediation efforts or misplaced efforts because the drivers of the lake level decline would be unknown. In the worst case, a consistent lake level decline could lead to lake drying, drying of shallow wells, and disappearance of dependent organisms, which eventually will threaten the livelihood of the fishing community.

This study took innovative approaches applicable in data-scarce catchments to enrich the understanding of interactions between surface water and groundwater sources. It developed a lake

balance model which can be employed to investigate the impacts of future scenarios such as increased pumping, land-use change, or climate change. The sensitivity of different drivers of lake level variability was assessed to inform management and prioritise intervention. Further, it demonstrated how groundwater resources could be mapped in regions lacking *in situ* / observed hydro-meteorological data. The findings of this study have been published in scientific peer-reviewed journals with wide circulations to inform a wider audience of policy makers and the fraternity of the scientific community.

1.4 Research Objectives

1.4.1 General Objective

To investigate the influence of climatic variation and anthropogenic activities on the surface water – groundwater interactions within a semi-closed lake catchment.

1.4.2 Specific Objectives

(i) To assess the influence of climatic variations and anthropogenic activities on the lake level variability

(ii) To identify the sources of groundwater influxes using stable isotopes and hydrogeochemistry and conceptualise the groundwater-lake interactions

(iii) To evaluate the influence of catchment spatial heterogeneity on groundwater distribution

1.5 Research Questions

(i) How do climatic variations and anthropogenic activities impact the water level variability of a semi-closed lake?

(ii) Are the groundwater systems hydraulically connected to Lake Babati, and if so, how?

(iii) How does spatial heterogeneity of catchments influence groundwater distribution on spatial scales?

1.6 Signficance of the Study

The study takes innovative approaches applicable in data-scarce catchments to enrich the understanding of interactions between surface water and groundwater sources. It demonstrates how groundwater resources can be understood in regions lacking insitu / observed hydro-meteorological data. Considering Lake Babati, a shallow lake that responds rapidly to climatic

variations, as a study area, the study aimed at understanding the sensitivity of different drivers of lake level variability to inform management and prioritise intervention.

Lake Babati provides the local community with fish and supports several aquatic species like the hippopotamus that inhabit it (Stromquist, 1992; Sandstrom, 1995; Mbanguka *et al.,* 2016). The main economic activities in Babati District are agriculture and livestock production (Hongoa, 2014). Recently, Babati town has expanded with more settlements, land cover modifications, and increased population (Hongoa, 2014; Pantaleo *et al.,* 2018). These anthropogenic activities have resulted in the development and construction of more abstraction wells on the lakeshore to supply water to the sprouting Babati town. However, despite the importance of the lake, no study has yet analysed the possible influence of anthropogenic activities around Lake Babati and increasing water demand on the lake water level variability. The study further demonstrates a suitable approach for mapping GWP in a data-scarce catchment. The research outputs from this study have been published in scientific peer-reviewed journals.

1.7 Delineation of the Study

The study looked at the Lake Babati level variability trend in response to climatic variability and anthropogenic activities. Due to the lack of measured water abstraction rates and supply, the study was limited to qualitative assessments of whether water abstractions have increased. In addition, land use and land cover changes were used as indicators of anthropogenic interference. The impact of land use and land cover changes on water resources could not be quantified due to the lack of river and lake outflow data.

Whereas surface water – groundwater interactions are as diverse as the surface water and landscape types (Winter, 1995), this study was concerned with identifying fluxes and evidence of interaction between Lake Babati and the groundwater systems. The fluxes of interests were those which could interact with Lake Babati because of the importance of the lake to the community. Surface water – groundwater interactions of rivers were not the subject of this study. The study area was the catchment of Lake Babati. However, it made a worthwhile comparison of hydrogeochemical and isotopic properties of river and lake waters within and outside Lake Babati catchment. Further, the study applied topography-based indices to identify and map the presence of groundwater within the catchment.

CHAPTER TWO

LITERATURE REVIEW

2.1 Overview

The literature review chapter looks at water balance studies within the study region and the studies within the Babati catchment to understand the output of previous studies and the possible knowledge gaps. It further looked at the methods for understanding drought severity, surface water–groundwater interaction analysis methods, and the influence of topography on hydrological processes. Literature specific to methods used in this study has been reviewed under Chapter Three.

2.2 Lake Water Balance

Understanding lake water balance and the drivers of the hydrological systems is very important for the sustenance of ecosystems because an unplanned change may have detrimental effects on all dependent systems and subsequently influence the redistribution and productivity of the ecosystem (Woldeamlak *et al.,* 2007; Stagl *et al.,* 2014). This requires a comprehensive analysis and understanding of the hydrological response, which would be incomplete without considering the water balance of the system. The general equation of the water balance of a system or catchment is based on the continuity equation expressed in Equation (1).

$$Change\ in\ storage = Inputs - Output \tag{1}$$

The continuity equation can be rewritten mathematically for an open lake system as Equation (2) (Chow *et al.,* 1988).

$$\frac{dH}{dt} = P(t) - E(t) + \frac{R_{in}(t) - R_{out}(t) + GW_{in}(t) - GW_{out}(t) - W_{ab}}{A(h)} + \varepsilon_t \tag{2}$$

Whereby, H is the lake level, A(h) is the lake surface area corresponding to a particular lake level h, and P(t) is the precipitation received over the lake area. The E(t) is the lake evaporation rate, and $R_{in}(t)$ and $R_{out}(t)$ are the surface water inflow and outflow to the lake, respectively. Additionally, W_{ab} represents the water abstractions from the lake, GW_{in} and GW_{out} are groundwater inflow and outflow of the lake, and the error term, which is representative of the errors in data and unaccounted-for water losses, is given by ε_t.

Considering a basin at equilibrium where the change in storage is zero or tends towards zero over a long period of time t, the equation can be rewritten as a net basin supply given in Equation (3).

$$N = P(t) + R_{in}(t) - E(t) = P(t) + \alpha P(t)\frac{A_c}{A_L} - E(t) \quad (3)$$

Whereby, N is the net basin supply to the catchment from the climatic sources.

2.3 Studies on Lake Water Balance

Numerous lakes in sub-Saharan Africa have been investigated, with a focus mainly on the lake water balance (Deus *et al.,* 2013; Swenson & Wahr, 2009; Tate *et al.,* 2004). Lake Victoria and the closed basin lakes of the East African Rift System (EARS) (i.e., Lake Ziway-Shalla, Awassa, Turkana, Suguta, Baringo-Bogoria, Nakuru-Elmenteita, Naivasha, Magadi-Natron, Manyara) exhibit high sensitivity to climate, lake size, and morphology (Olaka *et al.,* 2010). However, through water balance analysis, Kebede *et al.* (2006) found that the level variability of Lake Tana neither responds to human impact nor rainfall variability. Lake Malawi, one of the most studied lakes within the region, was investigated for its sensitivity to climate change (Kumambala & Ervine, 2013) and the long-term variations of net inflow to the lake (Sene *et al.,* 2017). Calder *et al.* (1995) also modelled the impact of land cover changes on Lake Malawi water levels, but no studies focused on groundwater–lake interactions. Generally, a few studies within the region have reported exhaustively on the lake–groundwater interactions, probably due to the scarcity of observed data.

The water balance analysis of the lakes mentioned above varied in methods depending on the case, data availability, and study objectives. Due to limitations of observational data, most of the studies explored remote sensing data, while others used environmental isotopes. For example, Weitz and Demlie (2013) used isotopes to conceptually model the groundwater interaction within Lake Sibayi in the eastern part of South Africa. Olaka *et al.* (2010) and Deus *et al.* (2013) modelled the behaviour of Lake Manyara's water balance using remotely sensed data from the Gravity Recovery and Climatic Experiment (GRACE) (Tapley *et al.,* 2004). They reported that the lake undergoes high temporal variations. Kalacska *et al.* (2017) used remotely sensed data to study the land cover and subsurface water changes over Lake Chala. However, none of the studies focused on the groundwater interactions with the lake systems.

Although the balance between input and output controls the changes in lake water levels, complex hydrological processes also drive responses in lakes. The processes themselves are influenced by soil, climate, groundwater, vegetation, and land cover changes, which vary spatially and temporally (Hayashi & Van der Kamp, 2007). However, many regional studies have ignored the influence of spatial variability of water balance components and lumped them.

2.4 Previous studies on Lake Babati

Studies within the Lake Babati catchment have focused on several issues. The earliest study was by Sandstrom (1995), who attempted to relate the lake's flooding to reduced forest cover by developing a lumped catchment model. However, the author reported significant uncertainties in the simulated lake levels, probably because the study did not consider the groundwater influx and interactions. Sjoin (2010) studied the management capacity to deal with the persistent flooding of Lake Babati. A study by Lopez (2011) built a lumped water balance model of Lake Babati, calibrated it using evapotranspiration, and applied the calibrated model to predict the lake's responses to the future climate based on International Panel on Climate Change emission scenarios. Lopez (2011) concluded that the lake's water balance is most sensitive to cloud cover, and precipitation primarily drives outflow. Mbanguka *et al.* (2016), while analysing the sensitivity of Lake Babati to climatic factors such as temperature, precipitation, humidity, and cloudiness, concluded that the lake's water level was most sensitive to cloudiness due to its significant influence on evaporation. Their study solely used the energy balance equation to compute evaporation which gives higher evaporation rates than the combination methods of computing evaporation (Ershadi *et al.,* 2011). Recently, Pantaleo *et al.* (2018), while investigating groundwater pollution by sanitary facilities, established that faecal pollution occurs especially in shallow wells of depths < 30 m.

2.5 Analysis of Drought Variability and Index

Drought is essential in water balance analysis as it defines the moisture availability or deficit in a basin based on meteorological variables. Its determination permits the evaluation of the influence of drought on the hydrological cycle components (Byakatonda *et al.,* 2018). Misidentification of recurring temporal droughts and continued droughts due to long below average rainfall leads to the progression of meteorological drought into a hydrological, agricultural, and economic drought (Byakatonda *et al.,* 2018; Maliva & Missimer, 2012). According to Palmer (1965), drought is a meteorological phenomenon characterized by ''prolonged and abnormal moisture deficiency''. Specifically, drought is an interval of time, generally about months or years, during which the actual moisture supply at a given place consistently falls short of climatically expected or appropriate moisture supply (Palmer, 1965).

Numerous methods based on indices (proxies) are available to quantify drought or estimate the severity of its impacts. Palmer Drought Severity Index (PDSI), developed by Palmer (1965), is a commonly used drought index. The PDSI is a soil moisture balance method that uses precipitation, evapotranspiration computed using the Thornwaite method, and the soil's available water capacity as primary inputs. Limited data, especially the lack of soil available water capacity, limits its

application in many places. Further, the fixed time scale and autoregressive characteristics built in PDSI sometimes influence conditions for unnecessarily a long time (Vicente - Serrano *et al.,* 2010; Yu *et al.,* 2013), and as well its calibration period influences the results (Vicente - Serrano *et al.,* 2010).

Palmer Drought Severity Index and Standardized Precipitation Index (SPI) (Mckee *et al.,* 1993) are the most used among other drought indices because of their low data requirements, ease of calculations, and multi-scaler characteristics, allowing time and space comparison. They, however, use only precipitation data (Yu *et al.,* 2013), leaving out the influence of temperature, soil moisture-holding capacity, and wind speed unaccounted on the estimated drought. The standardized Precipitation Index defines the difference from the mean for a specified period divided by the standard deviation, where the mean and standard deviation are determined from records (Mckee *et al.,* 1993). It is widely accepted because of its versatility in comparing drought at different time and space scales and determining and comparing the temporal changes in drought with respect to other usable water resources. The magnitude of the negative or positive SPI determines the probability of occurrence (or frequency) of the drought severity or extreme wet conditions. When the magnitude of SPI values is 1, it implies the values are within 1 standard deviation or occur 68% of the time, an SPI of 2 means 95% of the time, and an SPI of 3 implies a sigma of 3 or occurs 99% (Hayes *et al.,* 2000). Negative SPI values indicate drought or less than median precipitation values, while the positive values mean vice versa. Mckee *et al.* (1993) classified SPI values with corresponding magnitude and frequencies as in Table 1. A drought with an SPI <-2 is defined as extreme and would occur 2 or 3 times in 100 years.

The importance of the drought indices, which incorporate temperatures such as PDSI and SPEI, cannot be underscored for change studies applications (Yu *et al.,* 2013). Palmer Drought Severity Index requires soil moisture data whose paucity has limited its applications in many places. Although the SPEI was, developed recently, it is gaining popularity because it considers both precipitation and the influence of the ambient conditions in driving drought. Standard precipitation and evapotranspiration index integrates the sensitivity of PDSI to evaporation with the ease of computation and the multi-scaler characters of SPI. Several studies have already implemented SPEI, including Byakatonda *et al.* (2018); Yu *et al.* (2013). Drought severity is classified based on SPEI and SPI values presented in Table 1.

Table 1: Drought Severity classes

SPEI /SPI values	Drought severity class
Less than - 2	Extreme Drought
-1.99 to – 1.50	Severe Drought
-1.49 to 1.00	Moderate Drought
1.00 to 1.49	Near Normal
1.50 to 1.99	Severely Wet
More than >2.00	Extremely Wet

2.6 Groundwater Study Methods

Numerous techniques including field techniques that explore the subsurface to determine groundwater distribution, such as ground invasive techniques like excavation, direct push probes, and drilling, are employed for groundwater investigations. In addition, numerous non-invasive field methods are also in use, including seismic refraction surveys, resistivity, and electromagnetic & radar surveys (Fitts, 2002). However, the field methods are disadvantaged by their inability to predict groundwater levels under varying conditions.

The advent of computers has boosted the popularity of mathematical modelling of groundwater (Anderson, 2005) to disadvantage physical and analogue model methods. The MODFLOW by McDonald and Harbaugh (1988) is the most popular of the numerous existing groundwater modeling codes. Several graphical user interfaces have been developed to ease input and output processing in MODFLOW groundwater models. The graphical user interfaces are either commercially available such as Visual MODFLOW, GMS, or freely available, like Processing MODFLOW (Simcore Software, 2011). Model Muse or FREEWAT are also freely available graphical user interfaces and are equally powerful.

However, the paucity of reliably observational hydrological data in the study area limits the exploitation of the methods mentioned. Proxy methods based on the available topography data and environmental /hydrogeochemical methods present an opportunity to conceptualise the groundwater–lake water interaction in the area. The applications/development of the topography-based method is anchored on the understanding that topography controls groundwater level and saturated overland flow and influences soil and vegetation cover in certain climatic and geological conditions (Savenije, 2010). This study explored the use of readily available topography data to predict the groundwater potential zones.

2.7 Surface Water - Groundwater Interaction Study Methods

Interest in surface water–groundwater interactions has increased steadily within the last two decades (Fleckenstein *et al.,* 2010). The main focus of surface water–groundwater interactions has

been streams–groundwater aquifer interactions (Winter, 1995; Idowu, 2007). The assessment of surface water–groundwater interactions is mainly based on quantifying groundwater recharge and discharge (Idowu, 2007). Groundwater discharge can be baseflow, spring flow, and capillary rise. The increasing interests in surface-groundwater interactions are probably due to the conjunctive use of surface water and groundwater in agriculture, industries, and domestic water supply systems.

The techniques for assessing groundwater-surface water interactions can be hydrological, biogeochemical, ecological, or geological (Idowu, 2007). Although there is no agreement on categorising assessment methods, Winter (1995) identified analytical, field, biogeochemical, and numerical modelling methods. The commonly used methods are hydrograph separation (analytical method), water budgeting of different hydrological components and numerical modelling, and field methods (both ground-invasive methods like drilling and exploration and non-invasive techniques like geophysical surveys) to establish groundwater heads and flow directions (Winter, 1995). The chemical methods use anions, cations, and stable isotopes to trace water, pollutant sources, and dating water (Idowu, 2007).

Due to their ability for prediction, numerical modelling is increasingly applied, with several integrated surface water-groundwater models being developed or improved. The integrated surface water-groundwater models include GSFLOW, which couples the US Geological Survey Precipitation-Runoff Modeling System with MODFLOW (Markstrom *et al.* 2005), SWATMOD, which combines Soil and Water Assessment Tool (SWAT) and MODFLOW (Bailey *et al.,* 2017). SHETRAN is another coupled model that combines and models the flow and transport of sediment and solutes in surface and subsurface systems (Ewen *et al.,* 2000). Similarly, Batelaan and Smedt (2001) developed a WETSPASS model, which can be coupled with MODFLOW to simulate surface water - groundwater interaction (McDonald & Harbaugh, 1988). However, the application of these robust modelling tools is limited by data availability. As such, this study focused on methods applicable to the available datasets.

Environmental isotopes also provide insights into the hydrological processes within a catchment and help assess surface water-groundwater interactions. Differences in the isotopic composition of water from the different sources and the conservative nature of isotopes (Kendall & Doctor, 2003) allow the determination of the relative mixing ratios of different water using isotopic mass balance equations described by Gibson *et al.* (2016). It allows for the separation of groundwater contribution (baseflow) from streamflows (Idowu, 2007), the distinction of young water (recent recharge) from old water, the determination of recharge and discharge points (González-Trinidad *et al.,* 2017), or the development of a conceptual understanding of lake-groundwater interactions

(Weitz & Demlie, 2013). This methodology also helped develop the conceptual model of the study area in the present study.

In the analysis, a linear relation between the deuterium (δD) and Oxygen -18 ($\delta^{18}\mathrm{O}$) isotope values of precipitation that have not been evaporated, first reported by Dansgard (1964) and now termed as the Global Meteoric Water Line (GMWL), expressed mathematically in Equation (4), were usefully applied.

$$\delta^2 H = 8\delta^{18} O + 10 \tag{4}$$

Any variation of the $\delta^{18}\mathrm{O}$ and $\delta^{2}\mathrm{H}$ isotopes that result in a deviation from the GMWL form the basis for studying sources of water because atmospheric processes and groundwater recharge sources influence their compositions (Jabal *et al.,* 2018). However, the interaction of additional factors such as rainfall amount, temperature, and seasonal effect may influence the variations of the isotopic compositions in precipitations in a nonlinear way (Gibson *et al.,* 2016; Gonfiantini *et al.,* 2001; González-Trinidad *et al.,* 2017; Kendall & Doctor, 2003). Deuterium excess (d – excess) is a useful second-order isotope parameter for understanding moisture sources. It is often applied to provide information on the roles of diffusive transport in the atmospheric boundary layer and the effect of temperatures on fractionation (Pfahl & Sodemann, 2014). The applications of the stable isotopes in water are extensive, including establishing aquifer hydrogeological characteristics, groundwater flow dynamics, and interconnections with different sources (Jabal *et al.,* 2018; Krishan *et al.,* 2019; Maurya *et al.,* 2019).

2.8 Influence of Topography on Hydrological Processes

There is a growing interest in how topography (a readily available data) influences water table response (Detty & McGuire, 2010; Condon & Maxwell, 2015). It probably started with Toth (1963), who observed that groundwater level imitates topography. However, Savenije (2010) later demonstrated that topography controls groundwater levels. The study observed that hill slopes generate large floods through Hortonian overland flow. However, little runoff comes from undulating plateaus because vertical flow to recharge groundwater and evaporation losses dominate. Savenije (2010) then related the landscape with dominant hydrological processes irrespective of the geological formation and climate. Savenije (2010) concluded that topography is more important in distinguishing hydrological processes than geology without discounting the influence of soils and climate on hydrological processes. The study further showed that soil characteristics and climate are correlated with topography. For example, he observed that riparian zones tend to be endowed with heavy clayey soils while hill slopes have heterogeneous soils with dual porosity. Therefore, the study concluded that important landscape signatures could be

extracted from topography to build a conceptual architecture for predicting behaviour in an ungauged catchment or an unknown future using a calibrated model (Savenije, 2010; Gao *et al.,* 2014). Further, Condon and Maxwell (2015) observed that topographic gradients drive groundwater fluxes more than pressure head gradients. These linkages between topography or its derivatives with the hydrological processes have been applied to map wetness and wetlands (Grabs *et al.,* 2009) and in modelling studies using TOPMODEL (Nystrom & Burns, 2011) and FLEX - Topo (Gao *et al.,* 2014).

The advances in remote sensing and Geographical Information Systems (GIS) have offered several techniques to extract more hydrological information from topography instead of merely applying altitude, a piece of first-order information. One of these techniques is the Topographic Wetness Index (TWI), developed on the assumption that the local topographic slope equals the hydraulic gradient of a shallow water table (Nystrom & Burns, 2011; Infascelli *et al.,* 2013). The TWI indirectly measures the topographic control of hydrological processes that influence groundwater infiltration rates (Arulbalaji *et al.,* 2019). Several studies (Bretzke *et al.,* 2012; Mallick *et al.,* 2019) have applied TWI as a proxy for surface water availability and subsurface water movement driven by the terrain gradient. Kopecký and Čížková (2010) used it in ecological studies. Height Above the Nearest Drainage (HAND) is the other equally important topography derivative, as it is directly linked to the hydraulic gradient (Nobre *et al.,* 2011). Beyond the topography, usually measured "above mean sea level", HAND can differentiate environmental classes into either wetlands or uplands (plateau and slope) without overlapping (Nobre *et al.,* 2011). The HAND, when combined with slopes, provides sufficient information for landscape classification (Gharari *et al.,* 2011) with broad applications, including soil water condition estimation (Renno *et al.,* 2008), rainfall-runoff modelling (Gao *et al.,* 2019), and identification of groundwater potential (Hamdani & Baali, 2019).

Nobre *et al.* (2011) compared the two topography-based indices but reported a weak correlation between TWI and HAND in the lower Rio Negro catchment in Central Amazonia. Other studies, however, demonstrated that the two topographic indices describe similar parameters. For example, Gharari *et al.* (2011) showed that areas defined by HAND as wetlands and hillslopes in the Wark catchment were the wettest and driest in the TWI map of the same catchment. Thus, high TWI implies areas with a high saturation likelihood and large contributing areas, but with low slopes primarily located in wetlands, along streams, or groundwater discharge areas (Wolock & Price, 1994).

On the other hand, low TWI areas are mainly located on hills and groundwater recharge areas characterised by high slopes and small flow contributing areas (Nystrom & Burns, 2011). While low HAND values generally occur in areas prone to saturation, high HAND areas are either

plateaus or highlands, depending on whether they have low or high slopes. The TWI and HAND have been applied to determine potential groundwater zones (Rahmati *et al.,* 2018; Hamdani & Baali, 2019; Mallick *et al.,* 2019). Although TWI and HAND have been applied to determine the potential groundwater zones (Rahmati *et al.,* 2018; Hamdani & Baali, 2019; Mallick *et al.,* 2019), little information is available on their comparison as predictors of GWP. Groundwater discharge and recharge areas are surface water–groundwater interaction points that should be identified and protected as they can also be points of water contamination. Therefore, groundwater potential maps are proxy indicators of groundwater availability as they assess spatial groundwater discharge and recharge potentials.

CHAPTER THREE

MATERIALS AND METHODS

3.1 Study Area Description

3.1.1 Location and Geology

This study was conducted within the catchment of Lake Babati, which lies between Longitude 35.55° and 35.81° East and Latitude 4.20° and 4.30° South. Figure 1 shows the extent and the location of the catchment within the Manyara Region in Tanzania (The Location of the study area within Africa (a) and Tanzania (b), (c) shows the extent of the catchment, the elevation of the study area, and the meteorological stations within the region). Normal meteorological stations are generally regular stations that observe precipitation and some selected weather parameters, while climatic stations observe all weather parameters.. Based on a 30 m resolution Shuttle Radar Topographic Mission (SRTM) Digital Elevation Model (DEM), the 390 km² catchment was delineated. It lies between an altitude of 1201 meters above sea level (MASL) in the valleys near Lake Babati to 2388 MASL in the boundary hills (Fig. 1). Gentle slopes characterise the land terrain in the lake valley, while steep slopes define highlands at southern and northeast catchment boundaries.

The southwest and western catchment borders lie on the high elevation bounded by an outcrop of the Bubu cataclasites of Precambrian rocks (Mineral Resources Division, 1966). The boundary rocks are mostly granite and gneiss types. Similarly, the southern catchment boundary lies on a range of metasediment mountains of mixed granitoid and permeated gneiss and quartzo – feldspathic gneiss (Fig. 2). The metasediment rocks of micaceous quartzite of the Usagaran formation from the Precambrian era bound the southeast and eastern catchment borders.

The boundary rocks enclose an endowment of superficial and volcanic deposits from the recent Neogene era. There are dark soils from weathered tuffs with quartzo – feldspathic gneiss at some sections interspersed with agglomerate and crystal tuffs from the volcanic formation. Lightly coloured sandy soils (superficial deposits) dominate the valleys, whereas dark brown soils from weathered tuffs cover the eastern side of the lake. The west of the lake is a complex formation with no dominant formation. A combination of red and red-brown soils, dark-brown soils from weathered tuff endows it, sometimes with tuff and lava floats as the superficial deposits. Volcanic formations such as the crystal tuffs and agglomerate intersperse the alluvial deposits of the sand, silt, and clay that form the aquifer surrounding the lake. The Neogene era volcanic materials dominate the northern border of the catchment, forming hills and mountains.

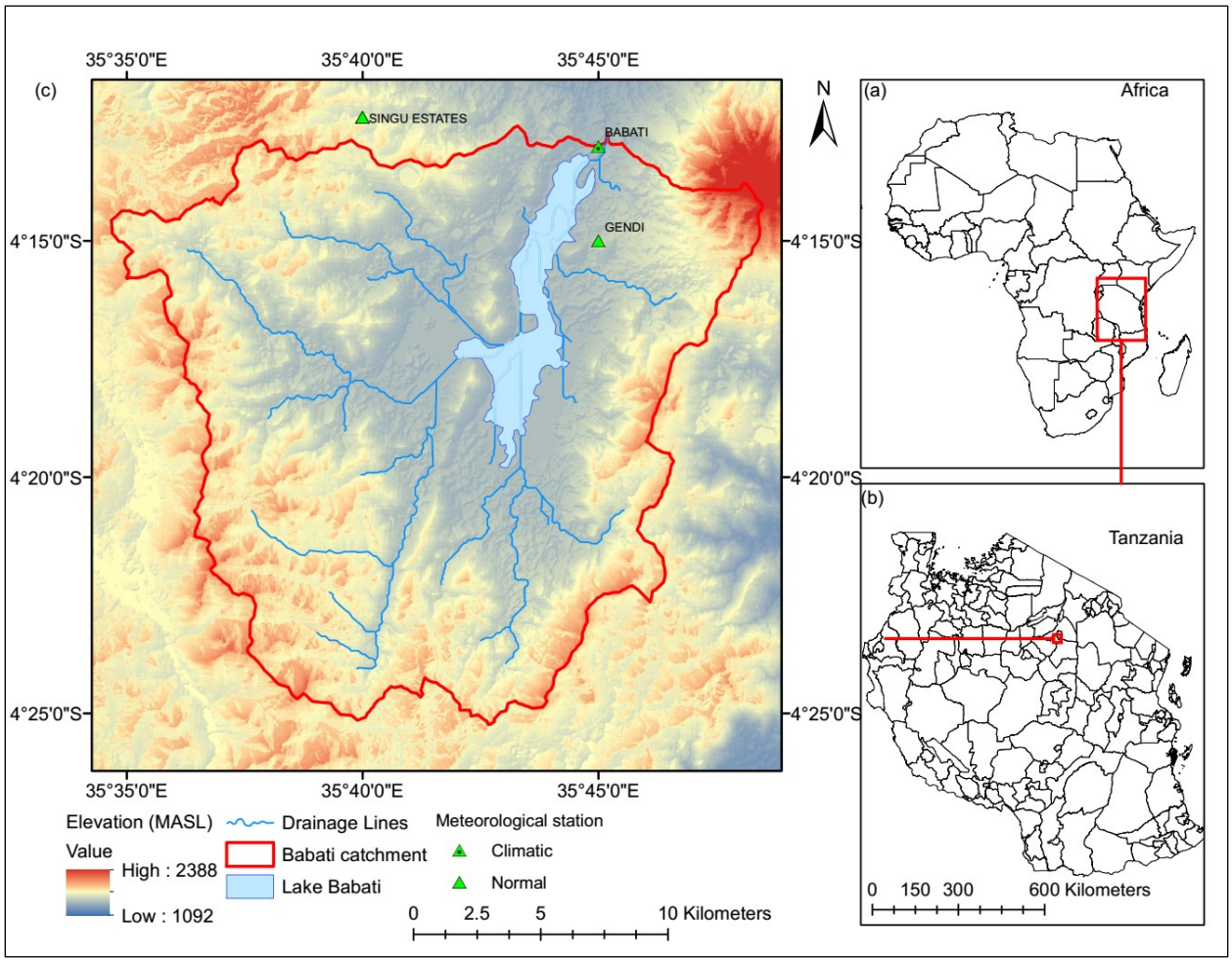

Figure 1: A Map of the Location of the study area

3.1.2 Soils

The soil map of the area was sourced from different agencies. The 1977 soil map from the Geological Survey of Tanzania classified the site with eutric nitosols (with FAO soil code Ne42-2c-837) as the dominant soil in the study catchment, but it was a coarse map. The Soter Map (MARI, 2006) was more detailed and indicated three prevalent soil types within the catchment, distributed as shown in Fig. 2. The luvisols of humi – rhodic luvisols occupy about 57% of the catchment, mainly the flat or gently sloping areas of the southern part of the catchment. Luvisols profiles have less clay at the top but accumulate clay in the subsurface (Driessen *et al.,* 2001). They are moderately weathered soils that overlay unconsolidated materials of alluvial deposits, thus forming the principal aquifer of the catchment.

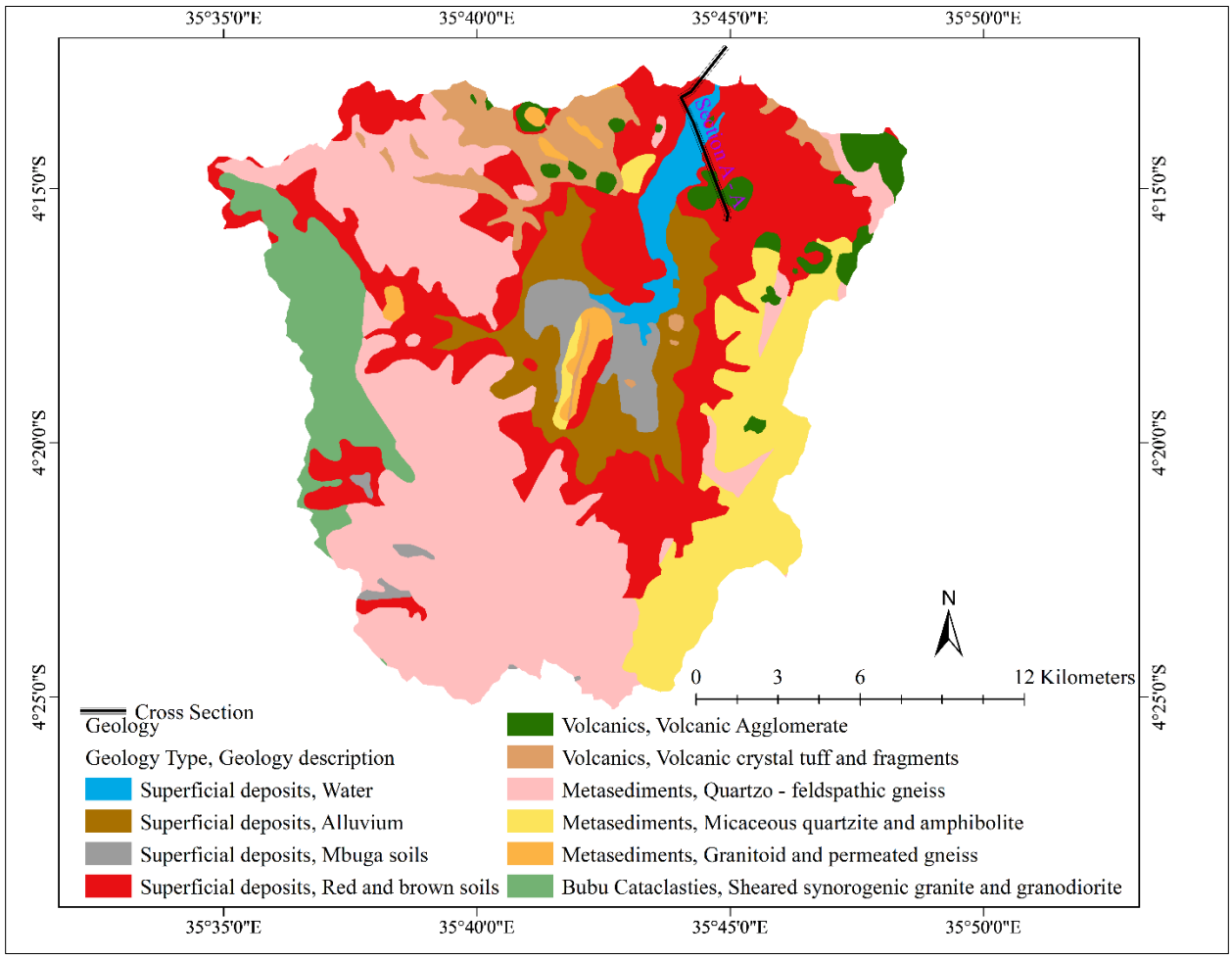

Figure 2: The geology of the study catchment with a detailed specification of the soil types comprised in superficial formation

The eutric leptosols occasionally have shallow groundwater depths and low water holding capacity because of their high gravel content resulting in freely drained soil. Shallow depth to bedrock generally characterises leptosols due to the high erosions on steep slopes (Driessen *et al.,* 2001). Leptosols originate from different rocks with less than 10% finer earth materials. The eutric leptosols comprise 28% of the coverage and occupy the northeast and northwestern parts of the catchment. Meanwhile, chromic – luvi Phaeozams are porous, dark, well-aerated, organic matter-rich soils in flat or gently undulating landforms. Chromic – luvi Phaeozams often cover unconsolidated parent material of either aeolian or alluvial origin (Driessen *et al.,* 2001), thus providing a higher chance of infiltration. Soils with a higher infiltration rate received the highest weight for groundwater potential as they would infiltrate and percolate more water into the groundwater aquifers. The chromic luvi Phaeozams is near the lake and covers 14.6% of the catchment.

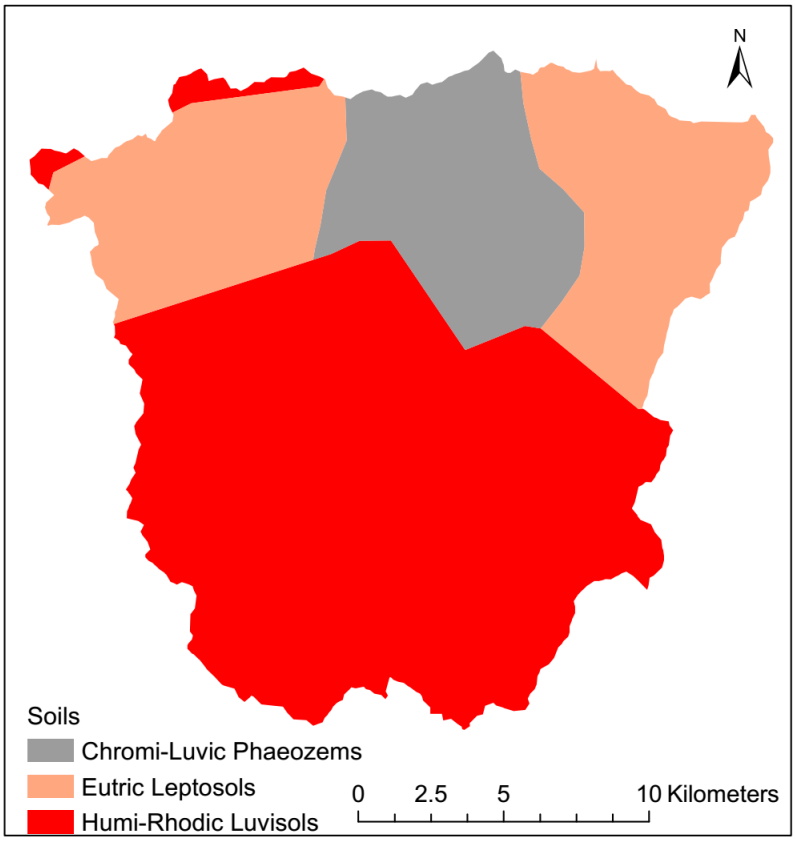

Figure 2: The soil map of the catchment

3.1.3 Climate

The catchment experiences a semi-arid climate (Sandstrom, 1995). The annual rainfall varied between 563 mm (observed in 1995) and 1505 mm (observed in 2006), with an average annual precipitation of 861 mm and a standard deviation of 270 mm. This was according to the 1980 – 2020 rainfall records from Babati meteorological station (Station ID 9435030) maintained by the Tanzania Meteorological Authority. The shifting Intertropical Convergence Zone and the Indian Ocean Dipole (IOD) influence the rainfall distribution (Deus *et al.,* 2013; Awange *et al.,* 2016). For example, the positive IOD of 2006 was responsible for the peak rainfall of 93 mm/day on April 6, 2006, and 85 mm/day on April 7, 2006. Generally, the influence of IOD that year resulted in 1505mm of rainfall compared to the 1377 mm observed in Babati in 1989 without a record of IOD.

The main rainy season of the bimodal distribution occurs from March to May, while a minor rainy season occurs from October to January of the following year (Fig. 4). The June to September period is a long dry but cold season, referred to as a dry season in most parts of this report. A short dry spell in February separates the two rainy seasons.

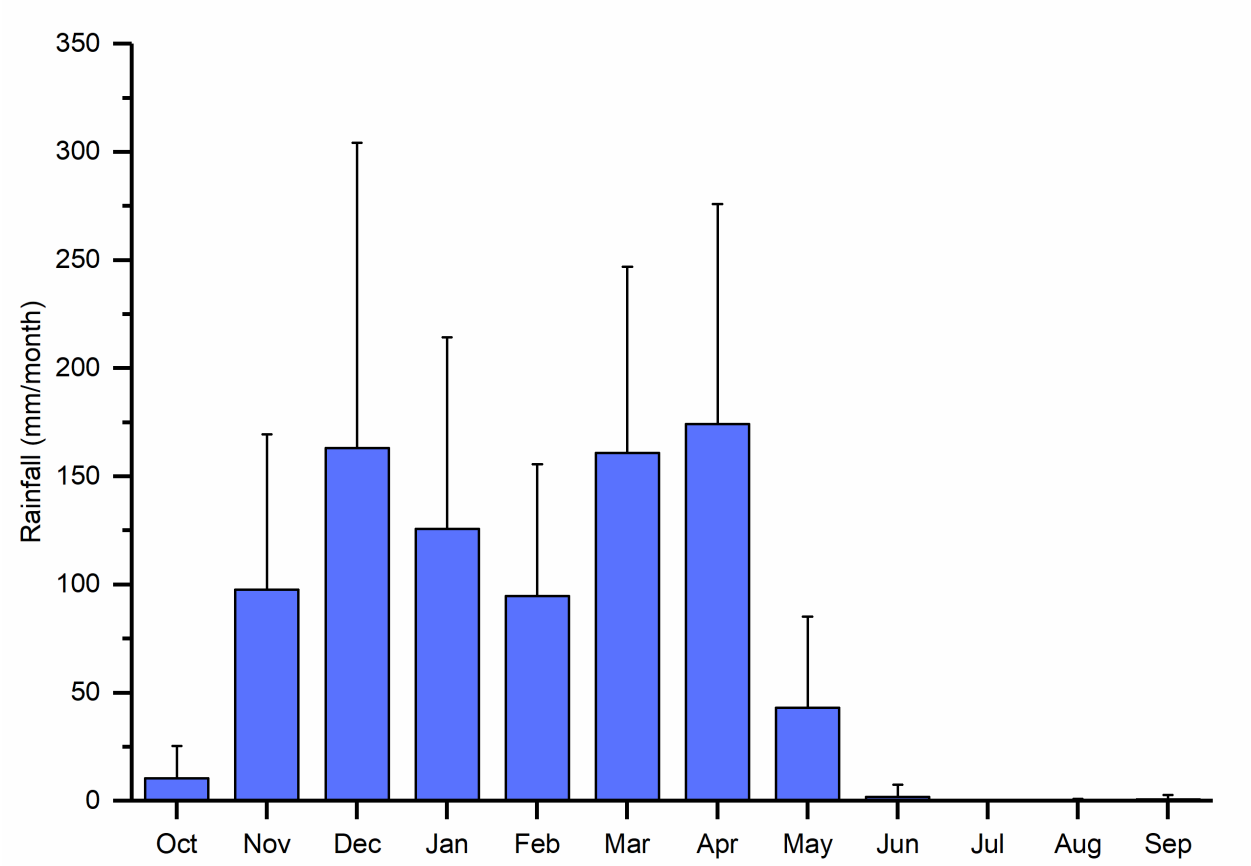

Figure 3: Mean monthly rainfall observed at Babati meteorological station from 1980 to May 2021 (Station ID 9435030). The whisker is plus one standard deviation: Source: Tanzania Meteorological Authority

Except for precipitation data, the other climatic parameters for the study area are scanty. Only monthly minimum and maximum temperatures for 1923 and 1947 for Mbulu, a nearby station to Babati, were obtained. Although the records were old, they were compared to reanalysis temperature data obtained from MERRA 2 for the Babati area. The maximum temperature at Babati was about 2°C higher than Mbulu's maximum temperature from 1923 to 1947, as shown in Fig. 5. Similarly, the minimum temperature of Babati was about 2°C higher than Mbulu's minimum temperature. Due to the time and location difference, it was neither practical to delve further into the possible causes for the observed differences nor prudent to use Mbulu temperature for detailed studies at Babati. Both places, however, exhibited similar temperature patterns. The maximum and minimum temperatures were highest from August to March of the following year, which coincided with the rainfall period. On the other hand, the April to July period had the lowest temperatures and coincided with the dry seasons. This implied that rain falls in the summer while the cooler season is characteristically dry.

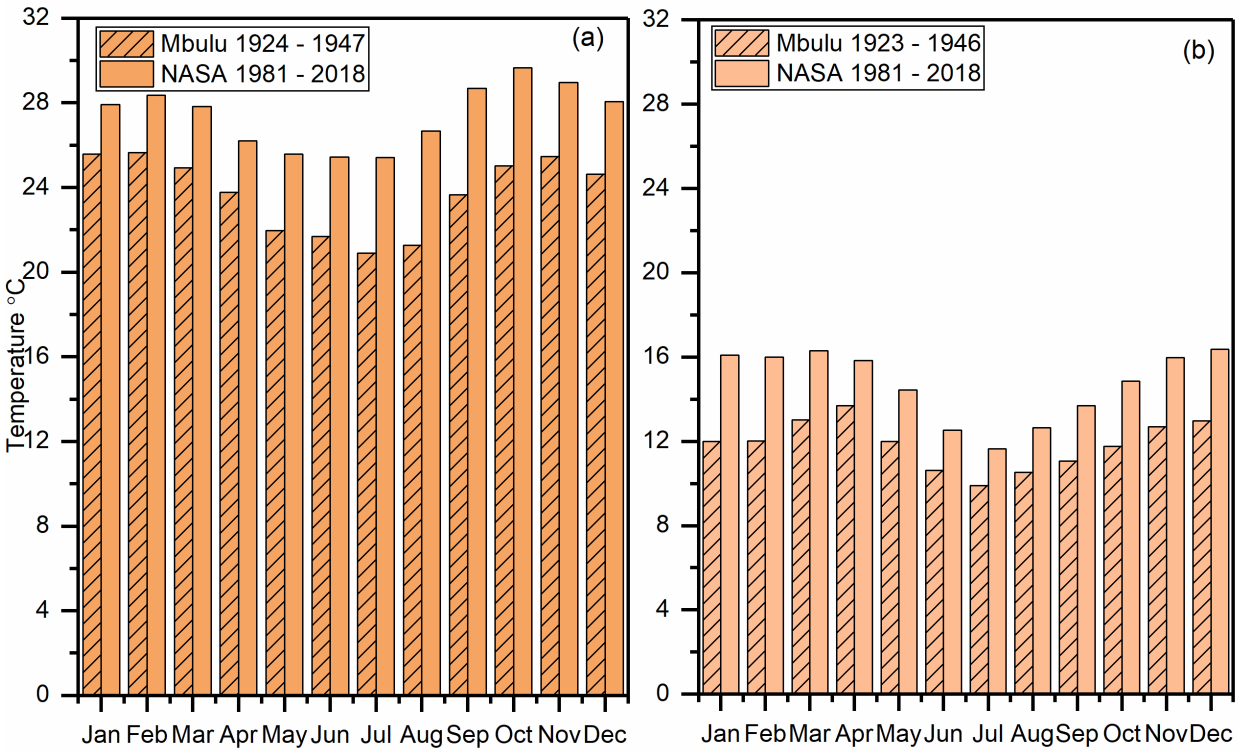

Figure 4: Comparison of the temperature of Babati (from NASA) and Mbulu (from TMA) for different periods for which data was available. (a) is the mean maximum temperature, while (b) is the mean minimum temperature

3.1.4 Lake Babati Hydrology

Lake Babati is among the few freshwater lakes in the East African Rift Valley. It is a graben semi-closed lake formed due to land subsidence within the Internal Drainage Basins of Tanzania. Land subsidence within the region and the lake catchment resulted in several smaller craters observable today in the catchment.

The lake is shallow and reaches its maximum depth of 7 m in mostly the rainy season. Due to its shallowness, the lake rapidly responded to climatic variations and overflooded its banks following episodes of high rainfall in 1964, 1979, and 1990 (Stromquist, 1992). The lake size has since varied many times. The current lake surface area is smaller than shown in Fig. 2. Mbanguka *et al.* (2016) underestimated the current lake size as just 7 km² compared to the 17 km² surface area digitised from the 1966 geological map (Mineral Resources Division, 1966) and 15.9 km² estimated by Yekom (URT, 2014)

As a semi-closed, Lake Babati receives runoffs from surrounding torrential rivers and possibly groundwater flows. However, it generally has no outflow during the low-level seasons except for groundwater fluxes which are not visible. When the lake water level exceeds the levels of the artificial outlet created (usually occurs in rainy seasons), it outflows through River Kiongozi (also called River Farahani). Initially, it had no natural outlet, but an artificial outlet was first constructed after the 1964 floods and modified in 1990 as a relief to protect Babati town from flooding

(Sandstrom, 1995; Mbanguka *et al.,* 2016). By 2013, four box culverts (as spillways), each of 3 m wide box culverts, were constructed on the northeastern part of the lake to relieve its excess water. The outlet level is high enough to allow outflow only when the water elevation exceeds 4.740 m (Lake Stage). The discharge joins the Kiongozi River, which acts as the physical link between Lake Babati and Lake Manyara, located further downstream. Babati catchment lies within the larger basin of Lake Manyara but at a higher elevation, giving it the characteristics of an independent lake.

3.1.5 Groundwater Level and Flow Directions

Data from 323 shallow wells from the catchment showed a contour map of groundwater levels (Fig. 6), and groundwater flow directions were determined from it. The groundwater levels varied with topography but remained shallow in the lake's valleys and flood plains (Fig. 6). Generally, the groundwater contours converged, indicating a flow direction towards the lake. After the lake, the flow directions were in the northeastern part of the catchment, implying that the lake and groundwater precisely drain in the direction of the artificial outlet (channel) constructed to relieve the lake of excess water during floods.

The groundwater contours were steeper in the eastern lake boundary than in the western one, indicating that the former had a more substantial groundwater inflow than the latter. Although the south of the lake had flattened flow contours that signify a low gradient groundwater flow potential, the contours generally indicated a gradient that mobilises the lake flow from the southernmost border to the northeastern part, where it is deepest (Mbanguka *et al.,* 2016).

Since the groundwater level in an unconfined catchment imitates topography and flows to low elevation (Toth, 1963), a general groundwater flow direction towards the lake was assumed in areas without borehole water levels as dictated by the topography.

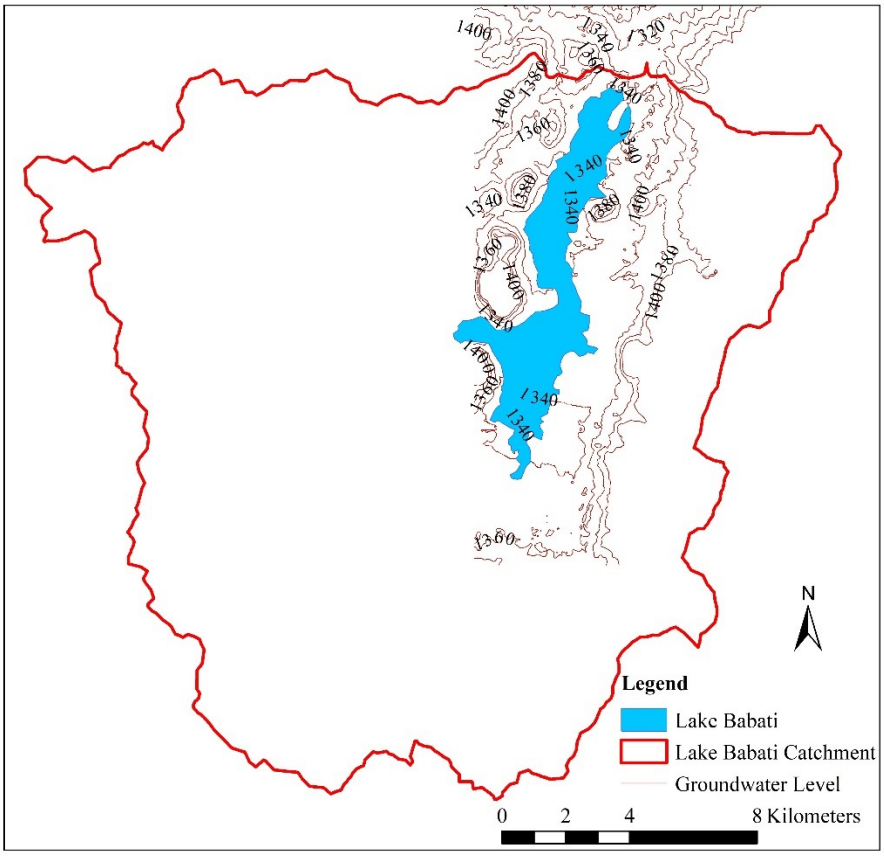

Figure 5: Groundwater level contours in meters above sea level based on the water levels of the shallow wells

The granitic rocks at the southern boundary of the catchment area were believed to establish a no-flow boundary due to the consolidated formation of granite. The mountains are perceived to obstruct any possibility of large-scale regional groundwater flow. Pyroclastic rocks within the watershed provide the opportunity for a localised network of groundwater to interact with the lake. A cross-section A – A (shown in Fig. 2) drawn through deep boreholes drilled to an average depth of 80 m around Lake Babati showed the presence of unconsolidated materials and an aquifer with a high yield of groundwater flow (Fig. 7). From the available data on ten deep boreholes, the first water strike was at an average depth of 12 m, but the piezometric water heads in all the wells averaged 1.5 m. This implies that the deep wells are probably abstracting from confined aquifers with a contribution from the unconfined aquifer since well screens are installed in the unconfined aquifer. A hydrogeological section drawn from the well logs (Fig. 7) shows that clay layers confine the aquifer in the lake area. The presence of clayey sand layers in the lake's neighbourhood as shown in 7 drawn based on the logs of boreholes along Cross Section A – A, shown in Fig. 2, indicates a possibility of interactions between the lake and aquifers through leaky sections.

No-flow boundaries are intimated by steep slopes at the eastern and the western catchment boundaries and the convergences of groundwater head contours towards the lake. In addition, the

contours of the groundwater suggest a northeast groundwater flow after the lake and indicate the possibility of a leaky or flow boundary at the northern catchment boundary.

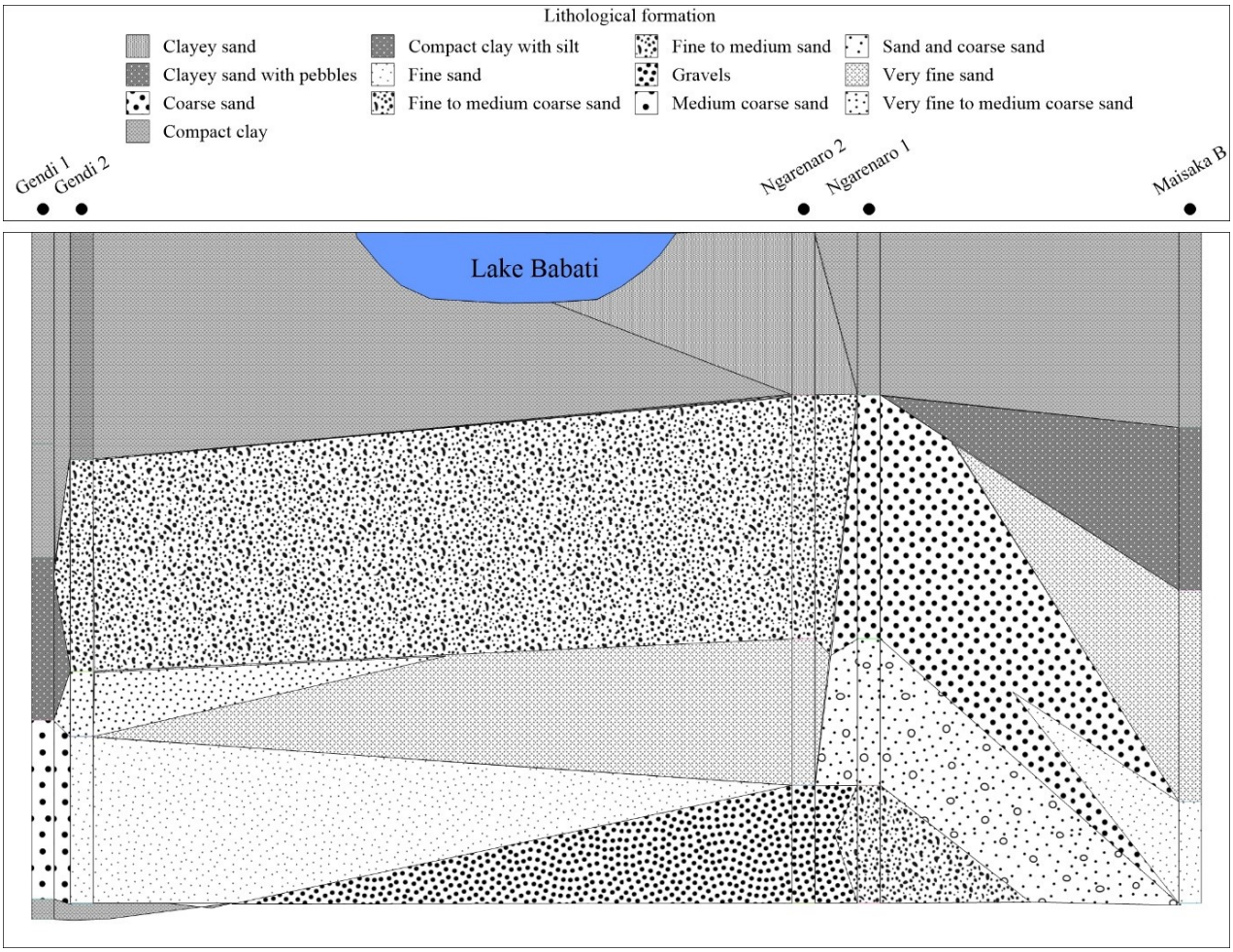

Figure 6: Hydrogeological cross-section A-A beneath Lake Babati

3.2 Data Collection and Analysis

3.2.1 Climatic Data

In the tropics, rainfall is the primary type of precipitation that inputs in the hydrological systems either as a quick runoff or baseflow attenuated through groundwater media and aquifers. On the other hand, evaporation is a derivative parameter of the climate that facilitates water movement within the hydrological cycle by removing water from the reservoirs such as lakes, rivers, and the ground and transferring it to the atmosphere. Therefore, evaporation drives water availability in one reservoir and influences precipitation through a feedback system. As a derivative of climatic parameters, evaporation is influenced by temperature, humidity, water availability in the reservoir, wind speed, and solar radiation, which provides the energy required to convert water from the liquid phase to vapour.

Evaporation pans are crucial for measuring evaporation over an open surface. However, they cannot measure the combined evaporation from soil and plant surfaces, and plant transpiration.

Furthermore, the sparse spatial distributions of measurement instruments do not allow for an excellent spatial assessment of evaporation and evapotranspiration. Therefore, evapotranspiration and evaporation in the present study were estimated from climatic parameters using the methods described in Section 3.2.6.

Some observed climatic data were scarce because of limited *in-situ* observations. The study obtained monthly averages of minimum air temperatures at Mbulu from 1923 to 1946 and maximum temperatures from 1924 to 1947. These old records were used to evaluate and crosscheck the applicability of MERRA 2 data (Global Modeling and Assimilation Office, 2022) in the study area. After satisfactory evaluation, the study downloaded the area's minimum and maximum air temperatures, dew point temperature, relative humidity, wind speed, sunshine hours, and precipitation from the Global Modeling and Assimilation Office (2022). The datasets were essential to study the influence of climatic parameters on the hydrological systems.

(i) Rainfall Data Sources, Quality Check and Covariation Analysis

The study collected rainfall records from the Tanzania Meteorological Authority for stations within Lake Babati catchment and its neighbourhoods (Table 2). The availability of quality data and the relevance of the stations to the study area motivated its choice. The study carefully inspected and evaluated the records to resolve the problems of apparent errors such as outliers and erroneous entries. Graphical plots played critical roles in the identification of errors. After evaluating the records, the analysis omitted years missing more than three months of rainfall in the dry season except when they were used for monthly data computation. A year with at least one month of missing data in the rainy season was also omitted from the computation of annual rainfall. Further data quality analysis was done by testing consistency and homogeneity. Finally, months with more than four days of missing data were omitted from the study.

Table 2: Meteorological and gauging stations within and near the catchment that provided rainfall records

No	Longitude	Latitude	Station ID	From	Name	Elevation (MASL)	Timestep
1	35.5500	-3.8667	9335001	01/06/1990 - 31/01/2017	Mbulu District Office	1737	Monthly rainfall
2	35.3833	-4.0500	9435003	Jan 1960 - Dec 2017	Dongobesh Sec. School	2042	Daily record
3	35.3833	-4.0500	9435003	Jan 1932 - Dec 2008	Dongobesh Sec. School	2042	Monthly rainfall
4	35.3833	-4.5333	9435008	Jan 1980 - Dec 2015	Katesh	1829	Monthly rainfall
5	35.8667	-4.300	9435010	Jan 1980 - Dec 1988	Galappo Mission	1524	Monthly rainfall
6	35.7500	-4.2167	9435030	01/01/1980 - 31/12/2020	Babati	999	Daily record
7	36.5667	-5.2833	9536000	Jan 1980 - Dec 2014	Kibaya	1457	Monthly rainfall
8	35.7395	-4.2369		Jan 1981 – Mar 2019	MERRA 2	1493	Daily rainfall

(ii) Filling gaps in the climatic data

The nearby stations that correlated with records from Babati (Station ID: 9435030) were used for filling in the missing rainfall data of Babati. However, to use portions of dataset X_i to replace Y_i, both datasets X_i, and Y_i had to be homogeneous (Allen *et al.,* 1998). Therefore, the following procedure for substituting data from the nearby station into an incomplete dataset, according to Allen *et al.* (1998), was followed:

(a) Select a nearby weather station for which the dataset length covers all periods of missing data.

(b) Characterise the datasets from the nearby station, X_i, and of the station with missing data, Y_i, by computing the mean $\bar{x}, \bar{y}$ and the standard deviation S_x, S_y for the datasets x_i and y_i using Equation (5) and Equation (6).

$$\bar{x} = \sum_{i=1}^{n} \frac{x_i}{n} \tag{5}$$

$$S_x = \sqrt{\left(\frac{\sum_{i=1}^{n}(x_i - \bar{x})^2}{(n-1)}\right)} \tag{6}$$

The above comparison was applicable for periods when both stations had datasets available. x_i and y_i above are individual observations from datasets X_i and Y_i, and n is the number of observations in each set.

(c) A regression of y on x was performed for the periods when the data in both datasets were available using Equation (7):

$$\hat{y}_i = a + bx_i \tag{7}$$

b is given by Equation (8) and a by Equation (9).

$$b = \frac{cov_{xy}}{{S_x}^2} = \frac{\sum_{i=1}^{n}(x_i - \bar{x})(y_i - \bar{y})}{\sum_{i=1}^{n}(x_i - \bar{x})^2} \tag{8}$$

$$a = \bar{y} - b\bar{x} \tag{9}$$

Whereby, a and b are empirical regression constants, and cov_{xy} is the covariance between X_i and Y_i.

All x_i and y_i and the regression line for the range of observed values were then plotted. Substitution is not recommended if deviations from the regression line increase as y increases. This indicates that the two sites behave differently relative to the weather variable and may not be homogeneous. In that case, another nearby station would be selected and tested. Finally, the procedure for completing datasets was applied after the homogeneity test, and any needed correction for non-homogeneity was performed.

(d) The correlation coefficient r

To measure the relationship among the neighbouring stations, a Spearman rank correlation coefficient r_s (Equation (10)) was preferred to Pearson Moment correlation to eliminate the influence of outliers, the non–linearity, and non–normality of the datasets.

$$r_s = 1 - \left(\frac{6\sum d^2}{n^3 - n}\right) \tag{10}$$

Whereby, n is the sample size, d is the difference between the ranks of the two variables, and r_s the Spearman rank correlation.

The covariation analysis considered the daily, monthly, and annual time scales and was based on hydrological years. The decision to accept or reject Spearman's rank test was based on a comparison of r_s against a critical r value from Spearman's rank table for n < 30 and Pearson's rank table for n > 30. A null hypothesis (H_o) was set that "the variables do not have an order

relationship in the population represented by the sample". The null hypothesis was rejected when the absolute value of the obtained r_s was greater than the critical r values for a 5% significance level. Otherwise, H_o was accepted.

The station for which the H_o was rejected and the value for b was within the range $(0.7 \leq b \leq 1.3)$ was used to replace the missing data in the incomplete data series. The data for the missing periods k = n+1, n+2..., m were computed using the regression equation characterised by the parameters *a* and *b* in Equation (8) and Equation (9) using Equation (11).

$$\hat{y}_k = a + bX_k \tag{11}$$

3.2.2 Hydrological Data – Lake Levels and Well Data

Lake Babati's water level records spanning from November 1964 to December 2020 were obtained from the Internal Drainage Water Basin Authority of Tanzania, which oversees all the water resources within the basin. The water level records, however, had patches of missing data. The main periods with missing observation ran from June 1970 to September 1976, April 1986 to August 1989, and July 2002 to January 2008. The years with data missing for > 4 months were 1979, 1991, 1993, 1994, 1995, 1996, and 1997. Some variations were also observed in the lake level records. Unfortunately, the metadata of the lake level records offers no further information on whether these variations could have resulted from a change of gauging stations, units of measurement, or any changes whatsoever. However, the missing records between 1970 and 1975 may suggest that after 1975, a change occurred either in measurement, the station locations, measurement accuracy, or all together. Due to the inconsistencies in lake level observations before 1975, we selected the portion of the records from August 1976 to December 2020 for further analysis. Graphical plots of time series data were used to detect errors related to entries that were sometimes unrealistically larger or smaller by many fractions than the preceding or succeeding values. This error type occurred in three incidences and was corrected by interpolating the preceding and succeeding values to obtain the erroneously entered value.

The study obtained water levels of 13 deep wells (boreholes with depths > 30 m) and 323 shallow wells (hand-dug wells and boreholes with depths < 30 m) surrounding the lake from the Internal Drainage Basin Authority of Tanzania, research data of Pantaleo *et al.* (2018) and the Babati Water Supply Authority (BAWASA). Out of these, the depths of 12 deep wells and 288 shallow wells were available.

3.2.3 Trends Analysis of Lake Levels and Climatic Variability

Numerous methods, broadly characterized as parametric or non-parametric, are available to analyze the trends of climatic variables. Parametric methods like Pearson Rank Correlation require data with a normally distributed population or those which can be approximated using the central limit theorem (Kwak & Kim, 2017). However, weather-driven events rarely meet this condition (Duan *et al.,* 2018).

The Mann-Kendall method (Kendall, 1975; Mann, 1945) and Spearman rho test are the most used non-parametric methods as they do not require normally distributed data. Most importantly, the two non-parametric methods can handle missing data because they measure or consider ranks of measurements instead of the actual values of measurements and are less sensitive to outliers.

However, Mann-Kendall and Spearman's rho suffer from internal correlation in the time series, leading to a false conclusion of trend or no-trend (Amaya *et al.,* 2018). Therefore, checking the time series data against autocorrelations was vital when using the Mann-Kendall method. The Mann-Kendall method tests for Ho (no trend) and the alternative hypothesis (trend exists). Trends can be either negative or positive. A negative Mann-Kendall coefficient means a decreasing monotonic trend, while a positive one means an increasing monotonic trend.

(i) Homogeneity and Mann-Kendall Tests

Homogeneity tests were performed on all the lake levels and climatic data time series records to check for changes or breakpoints within the time series (Hussain *et al.,* 2023) before the Mann-Kendall analysis. This was a quality check to ensure that trend analyses were performed on datasets without breakpoints and that the data came from the same population distribution.

The lake levels and climatic data were evaluated as an ordered time series, and their Mann-Kendall test statistic S was calculated using the formula adopted from Gilbert (1987) expressed in Equation (12). For example, if the time series is x_j and x_k, the test statistics S increases by one when $x_j - x_k$ is positive and reduces by one if the difference between the successive time-series data is negative but remains constant when successive numbers are equal $(x_j - x_k = 0)$ as summarized in Equations (12) and (13).

$$S = \sum_{k=1}^{n-1} \sum_{j=k+1}^{n} sgn(x_j - x_k) \tag{12}$$

$$sgn(x_j - x_k) = \begin{cases} +1 & if \quad x_j - x_k > 0 \\ 0 & if \quad x_j - x_k = 0 \\ -1 & if \quad x_j - x_k < 0 \end{cases} \tag{13}$$

where x_j and x_k are values in days, months, or years j and k, j >k.

Equations (12) and (13) are valid if the observations (n) are not > 40. The period can be a day, week, month, season, or year. For distribution with > 40 values or with many tied data values, the S statistics are computed by Equation (12), but test statistics Z is computed using Equations (14) and (15).

$$Z = \begin{cases} \dfrac{S-1}{\sqrt{VAR(S)}} & if \quad S > 0 \\ 0 & if \quad S = 0 \\ \dfrac{S+1}{\sqrt{VAR(S)}} & if \quad S < 0 \end{cases} \tag{14}$$

where the variance of S, $VAR(S)$ is computed as in Equation (15).

$$VAR(S) = \frac{1}{18}\left[n(n-1)(2n+5) - \sum_{p=1}^{g} t_p(t_p - 1)(2t_p + 5)\right] \tag{15}$$

g is the number of tied groups and t_p is the number of data in the p^{th} group.

A positive (negative) value of *S* or *Z* indicates an upward (downward) trend. If the null hypothesis (Ho) of no trend is true, the *Z* statistic has a standard normal distribution; thus, the Standard Cumulative normal distribution table is used to decide whether to accept or reject the Ho. To test for either an upward or downward trend (a two-tailed test) at the α level of significance is used; Ho is rejected if the computed probability value (p-value) is less than the specified alpha or if the absolute value of *Z* is greater than $Z_{1-\frac{\alpha}{2}}$, where $Z_{1-\frac{\alpha}{2}}$ is obtained from the standard cumulative normal distribution table.

(ii) Sen's Slope Estimator

The magnitude of trends in the lake levels and climatic datasets were determined using the method of Sen (1968). Although linear regression methods can determine the slope of distributions with a linear trend, outliers or gross errors in the data may influence the slope (Gilbert, 1987). Sen's method provides an opportunity to determine the true slope because it uses a non-parametric procedure that is neither greatly affected by gross data errors nor outliers. It can also be computed

even when some data is missing. Sen's estimate of slope is derived by first computing the N' slope estimates, Q, which for each station is given by Equation (16):

$$Q = \frac{x_{i'} - x_i}{i' - i} \tag{16}$$

where $x_{i'}$ and x_i are data values at times (or during periods) *i'* and *i*, respectively, and *i'* > *i*; N' is the number of data pairs for which $i' > i$. The median of the N' values of Q is Sen's slope estimator.

When one datum exists in each period, then $N' = n(n-1)/2,$ where *n* is the number of periods. However, if multiple observations exist in one or more periods, then $N' < n(n-1)/2$, where n is now the total number of observations, not periods. Since Q cannot be computed with two data from the same period, i.e., when $i' = i$. If x_i is below the detection limit, half of the detection limit may be used for x_i. The median of the N' slope estimates is obtained by ranking Q from the smallest to the largest, and the slope estimator is the median slope obtained as in Equation (17).

$$Sen's\ estimator = \begin{cases} Q_{\frac{[N'+1]}{2}} & if \quad N'\ is\ odd \\ \frac{1}{2}\left(Q_{\frac{[N']}{2}} + Q_{\frac{[N'+2]}{2}}\right) & if \quad N'\ is\ even \end{cases} \tag{17}$$

In addition to statistical methods, graphical plots were used to complement and help identify and present the trends. The variables were plotted against observation time, and a simple linear regression was added to relate the variable to time. A simple t-test was added to ensure the true slope was closer to zero. The t-test, however, can be misleading if seasonal cycles are present, as the data are not normally distributed or are serially correlated (Gilbert, 1987).

(iii) Changepoint Analysis

The non-parametric Pettit Test method was used to analyze abrupt changes in the time series of the datasets. The Ho tested for the absence of a change point within the data series. In contrast, the alternative hypothesis (Ha) tested change point occurrence ($1 \leq t \leq T$) using the non-parametric statistic expressed in Equations (18), (19), and (71).

$$K_T = Max|U_{t,T}|, 1 \leq t \leq T \tag{18}$$

$$U_{t,T} = \sum_{i=1}^{t} \sum_{j=t+1}^{T} sgn(x_i - x_j) \tag{19}$$

$$sgn(x_i - x_j) = \begin{pmatrix} +1 \; if \; x_i - x_j > 0 \\ 0 \; if \; x_i - x_j = 0 \\ -1 \; if \; x_i - x_j < 0 \end{pmatrix} \quad (20)$$

$U_{t,T}$ would continue rising with no turning points when a change point does not exist but the $U_{t,T}$ would decrease, and a turning point would form when a change point exists. The probability of detecting a change point was calculated by Equation (21).

$$P \cong 2 \times exp\left[\frac{6{K_T}^2}{T^3 + T^2}\right] \quad (21)$$

The change was analyzed at a 5% level of significance. The Ho was rejected when the computed p-value was smaller than the 5% significance level, and the appropriate decisions were taken once a change was detected. Pettit tests were run using the XLSTAT software and the Monte Carlo simulations for a quicker determination of the change point. The change point analysis was performed on the lake levels and the climatic datasets to determine if any significant changes occurred in the time series and when the changes occurred. The analysis was aimed to understand the possible triggers for changes in the datasets.

3.2.4 Lake Babati Bathymetry

A bathymetric survey of Lake Babati was done from the 17th to the 19th of July 2020. This study used an echosounder mounted on a motorboat to conduct the survey. The echosounder measured the topography of the lake bottom every second (spaced less than 5 m depending on the boat speed) along the transects. All the crew members used a life jacket, among other safety kits required when in water. Two sets of 12 volts batteries and a power inverter were loaded on the boat to charge and power the surveying equipment and the computers. A Real-Time Kinematic Global Positioning System (RTK GPS) was used to measure the X-Y coordinates of the location of sounding data. The base station of the RTK GPS was located on the lakeshore at the exact location for all three days of the bathymetric survey.

After mounting and setting up the echosounder, transducer, and computer, the sounding depths were verified by comparing them with the manually measured lake depths near the lakeshore each day before and after surveying. The sounding depth was measured by the echosounder, mounted on a motorboat, and the transducer hung 0.5 m below the water level.

Transects spaced at about 100 m drawn on a computer with Eye4Software Hydromagic with the Lake shapefile as a background map were used to guide the field navigation. Figure 7 shows the final hydrographic survey routes followed. Due to thickets of water weeds and grasses, the water banks could not be sounded as the vegetation obstructed the echosounder, and in some cases, the

water depth was shallower than the 0.5 m required for proper sounding. The Hydromagic software monitoring panel was projected on an additional computer monitor configured to display the survey route, the coordinates, and the depths being logged during the survey. An additional computer monitor was included to ease navigation and troubleshoot the survey process whenever any component stopped collecting or logging the sounding data. Routinely, the boat would be stopped to clear the echosounder of any debris or materials obstructing it.

The sounding depth and the X-Y coordinates were logged every second to measure the depth at a specified lake location. A total of 62 048 depths with corresponding coordinates were measured. Subsequent cleaning and processing of the sounding depths were done within the Hydromagic software, including interpolation to visualise the sounding data. On July 19, 2020, the Lake elevation was 1350 MASL, with a lake stage of 4.75 m (given by a limnographic gauge), and a maximum depth of 6.39 m was measured within the lake. It was established that the lake starts to overflow when the lake stage is 4.74 m. The lake was overflowing when the bathymetric survey was undertaken. Figure 8 presents the final bathymetric chart of Lake Babati, which was used to compute the lake stage–surface area and volume relationship.

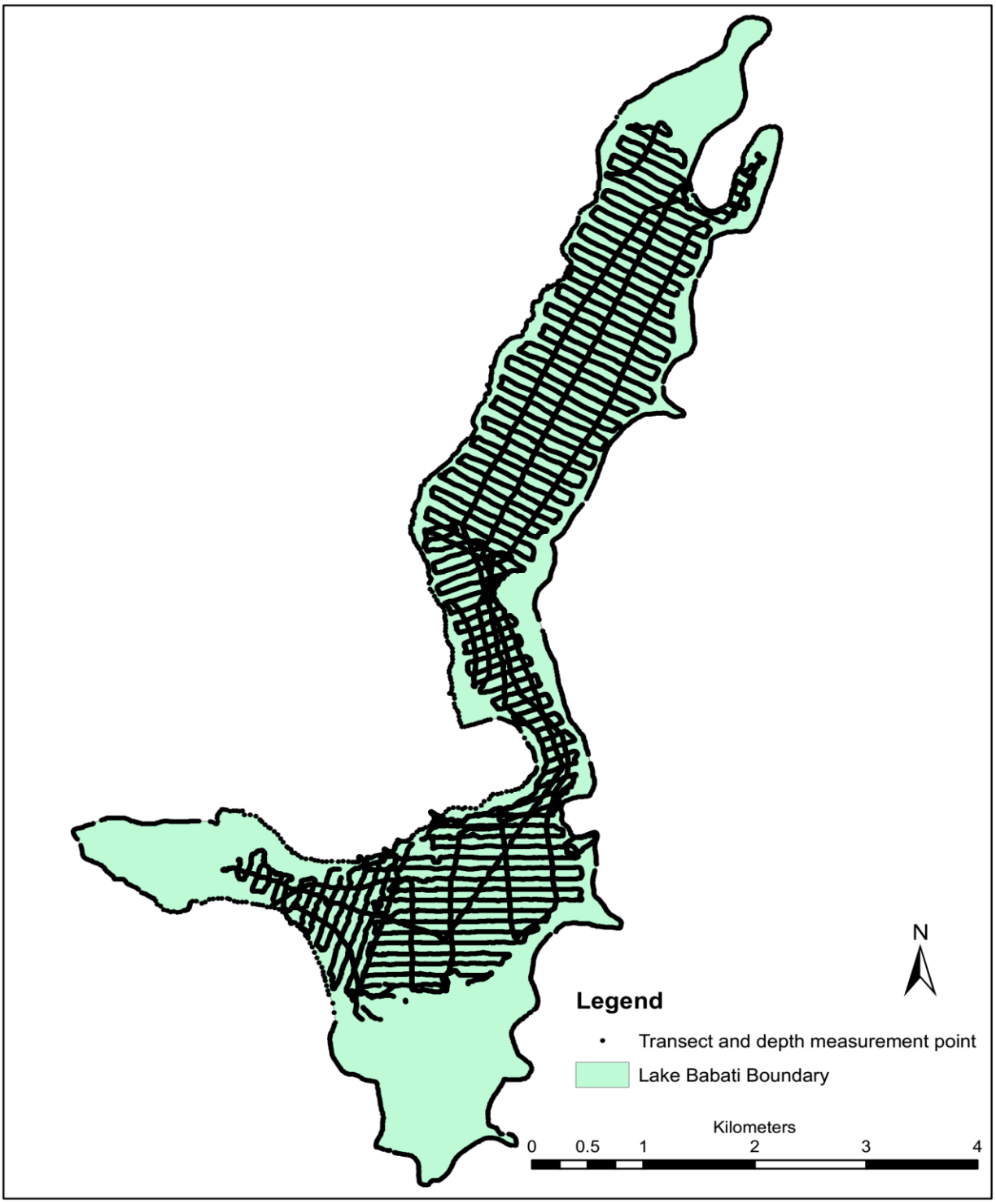

Figure 7: Transect route followed during the bathymetric survey

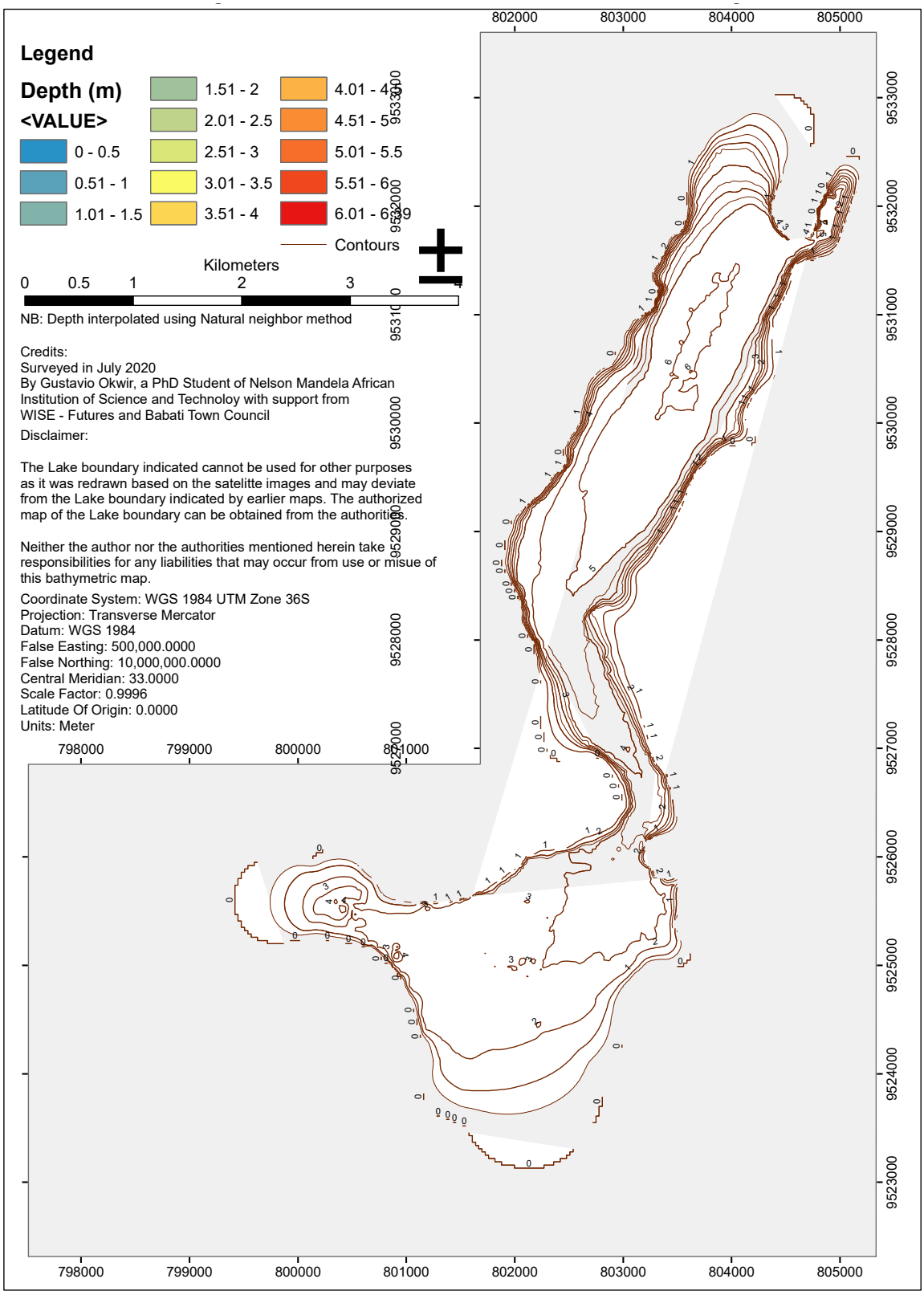

Figure 8: Bathymetric chart of Lake Babati surveyed in July 2020

The lake banks were mapped from Google Earth, and the water level at the banks was set at 0. Next, we extracted the topography of the lake banks and surrounding areas from Google Earth. Finally, the lake depth and bank's topography were combined and interpolated using the natural neighbour method to generate the bathymetric chart in Fig. 8 and compute the lake stage–area–volume relationship in Fig. 9 (The lines poly (Stage – Area) and poly (Stage – Volume) are

polynomial regression lines). Mathematically, the relationships were expressed in Equation (22) and Equation (23).

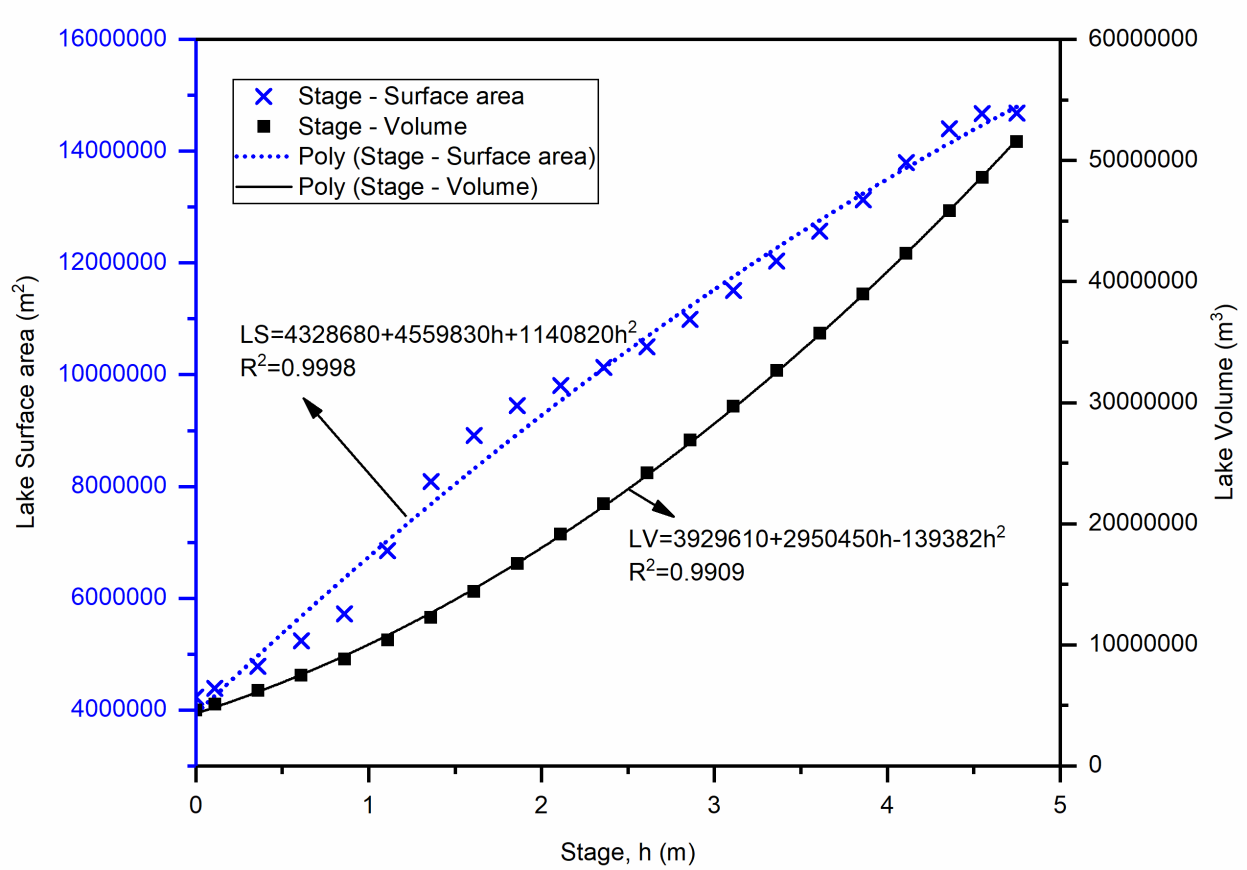

Figure 9: The lake stage - area - volume relationship based on bathymetric (data from this study)

$$LV = 3929610 + 2950450h - 139382h^2 \quad (22)$$

$$LSA = 4328680 + 4559830h + 1140820h^2 \quad (23)$$

where LV is the lake volume in m^3, LSA is the lake surface area in $m^{2,}$ and h is the lake stage in m.

3.2.5 Catchment Geophysical Data and Preparation

The study obtained the geophysical data that influence or describe the aquifer characteristics, groundwater infiltration, recharge, and discharge from various sources. These data included geology, lineament density, altitude, drainage densities, land use, and land cover (Ghorbani *et al.,* 2017; Mallick *et al.,* 2019; Pande *et al.,* 2017; Shekhar & Pandey, 2014; Tolche, 2020).

The geological map was digitised from Quarter degree sheet 85, a geological map for Babati with a scale of 1: 125 000, by Mineral Resources Division (1966). The soil map of the area with a scale of 1: 1 000 000 was obtained from Dijkshoorn (2003). The slope map in degrees was computed as

the maximum rate of change of the neighbouring cells' value using the slope algorithm in the spatial analyst package of ArcGIS 10.5 (Berhanu & Hatiye, 2020). It was based on the 30 m resolution Digital Elevation Model (DEM) obtained from the Shuttle Radar Topographic Mission (USGS, 2018). The same DEM was used to compute the Height Above the Nearest Drainage (HAND), Topographic Wetness Index (TWI), and distance to the streams. The Euclidean distance tool in the ArcGIS tool was used to compute the distance to streams after delineating the streams from the DEM. The distance to a stream is a perpendicular distance measured from the stream centreline. Considering the sensitivity of the stream distance to the initiation point of a stream, the stream threshold was set at 5000 cells implying that a stream begins when the area above it has a catchment area equivalent to 5000 cells.

3.2.6 Determination of drought variability and severity

The study assessed the influence of meteorological drought on the observed lake level variability by analyzing drought in the catchment. The determination of the drought indices was aimed to assess the aggregate influence of precipitation and evapotranspiration on the lake levels. No particular method is, however, recommended for drought analysis, but the choice of methods is motivated mainly by the data availability and the ease of application (Byakatonda *et al.,* 2018). The Standardized Precipitation Index (SPI) and Standardized Precipitation Evapotranspiration Index (SPEI) have been used in this study due to their wide applications in drought severity analysis and because they apply precipitation and evapotranspiration data which are readily available. The SPI and SPEI were compared to assess the influence of evaporation reported by Mbanguka *et al.* (2016) in driving the lake water levels. This study considered drought characteristics at short temporal scales of monthly, seasonal, annual, and bi-annual to account for the long-term influences of drought on surface water resources. The evolution of magnitude and frequency of the drought severity over time was analyzed using SPI and SPEI.

(i) Determination of the SPI

SPI, developed by Mckee *et al.* (1993), is a versatile drought monitoring and analysis tool. It is based on standardized precipitation, the difference between precipitation from the mean for a specified period divided by the standard deviation. The mean and the standard deviation are determined from the records. Mckee *et al.* (1993) proposed the following steps for computing the SPI:

(a) It requires a monthly precipitation data set prepared for 12 months for a continuous period of at least 30 years.

(b) The monthly precipitation is then averaged using the moving average method. Although arbitrary, the averaging periods of 3, 6, 12, 24, or 48 months are commonly used to represent time scales for which precipitation deficits affect the different types of usable water sources: soil moisture, groundwater, snowpack, streamflow, and reservoir storage. The data set is moving in the sense that a new value is determined each month from the previous i months.

(c) The time average values of the precipitation are then fitted to the Gamma function to define the relationship of probability to precipitation.

(d) From the established relationship of probability to precipitation, the probability of any observed precipitation data point is thus calculated and used along with an estimate of the inverse normal to calculate the precipitation deviation for a normally distributed probability density with a mean of zero and a standard deviation of unity. The calculated precipitation value is the SPI for that precipitation data point.

(ii) Determination of SPEI

The following steps developed by Vicente - Serrano *et al.* (2010) and as applied by Yu *et al.* (2013) and Byakatonda *et al.* (2016) were adopted for the computation of SPEI.

Determination of Potential Evapotranspiration

Numerous methods exist for computing evapotranspiration. However, data availability determines the choice of method. The FAO Penman-Monteith method is considered standard and widely accepted for computing evapotranspiration (Allen *et al.,* 1998; Vicente - Serrano *et al.,* 2010) because it is a physically-based method. However, the unavailability of data often limits its application (Trajkovic, 2007) as it requires minimum and maximum temperature, solar radiation, relative humidity, and wind speeds, most of which are often unavailable or have poor quality in sub-Saharan Africa. Although Hargreave's method overestimates evapotranspiration in humid conditions(Trajkovic, 2007), it is widely applicable in data-scarce areas because it requires only minimum and maximum temperatures, which are always available. The lake evaporation was computed using the Penman-Monteith equation to capture the wind and humidity influence which have a substantial effect on lakes.

In contrast, the potential evapotranspiration of the catchment was computed using both the Penman-Monteith and Hargreaves equations. The methods are well elaborated in Allen *et al.* (1998) and Trajkovic (2007) and were applied without repeating for brevity. We used both

methods because Mavromatis (2007) showed that the method of computing PET has significant differences in the Palmer Drought Severity Index (PDSI) results.

Computation of the Climatic Water Balance

The climatic water balance was calculated by taking the difference between precipitation and potential evapotranspiration, as illustrated in Equation (24).

$$D_i = P_i - ETO_i \tag{24}$$

where D_i is the climatic water balance, which measures the water surplus or deficit in the month i measured in mm or inches, P_i is the precipitation in the month i (measured in mm or inches) and ETO_i is the potential evapotranspiration measured in mm or inches.

The Aggregation of Climatic Water Balance

The climatic water balance computed in step 2 is then aggregated for the n^{th} number of months, where n is the drought time scale considered. The drought time scale considered is 1, 3, 6, 12, 18, and 24 months to account for the monthly, quarterly, seasonal, annual, and biannual drought variability.

Aggregating the calculated D_i values at different time scales followed the same procedure as that for the SPI. The aggregated/accumulated climatic water balance denoted as $D_{i,j}^k$ in a given month j and year i depends on the chosen time scale k. For example, the accumulated climatic water balance $D_{i,j}^k$ for one month in a particular year i with a 12–month time scale is calculated using Equation (25).

$$D_{i,j}^k = \sum_{l=13-k+j}^{12} D_{i-1,j} + \sum_{l=1}^{j} D_{i-1,j} \tag{25}$$

Equation (25) is applicable when $j < k$, but for $j \geq k$, $X_{i,j}^k$ is computed as as in Equation (26).

$$D_{i,j}^k = \sum_{l=j-k+1}^{j} D_{i,j} \tag{26}$$

Normalization and Standardization of the Aggregated Climatic Water Balance

The aggregated climatic water balance $D_{i,j}^{k}$ is standardized in a log-logistic distribution whose probability density function is calculated using Equation (27) expressed below

$$f(x) = \frac{\beta}{\alpha}\left(\frac{x-\gamma}{\alpha}\right)\left[1+\left(\frac{x-\gamma}{\alpha}\right)\right]^{-2} \tag{27}$$

where x is the aggregated climatic water balance $D_{i,j}^{k}$ series for all the time scales, α, β, and γ respectively, represent the shape and scale parameters for the climatic water balance values in the range ($\gamma > D < \propto$). This implies the probability distribution function of the climatic water balance $D_{i,j}^{k}$ is calculated as follows:

$$F(x) = \left[1+\left(\frac{x-\gamma}{\alpha}\right)^{\beta}\right]^{-1} \tag{28}$$

The SPEI can be obtained as standardized values of F(x) by following the classical approximation of Abramowitz & Stegun (1970) as used in Yu *et al.* (2013)

$$SPEI = W - \frac{C_0 + C_1 W + C_2 W^2}{1 + d_1 W + d_2 W^2 + d_3 W^3} \tag{29}$$

where $W = \sqrt{-2ln(P)}$ for $P \leq 0.5$, and P is the probability of exceeding a determined $D_{i,j}^{k}$ value, $P = 1 - F(x)$. For $P > 0.5$, P is replaced by 1 – P, and the sign of SPEI computed is reversed. The constants are: $C_0 = 2.515517$, $C_1 = 0.802853$, $C_2 = 0.010328$, $d_1 = 1.432788$, $d_2 = 0.189269$ and $d_3 = 0.001308$. These SPEI and SPI were computed using the SPEI package within the R Programming language.

The study analyzed the area's drought using both the SPI and SPEI. The SPEI was based on the potential evapotranspiration computed using the Hargreaves and Penman-Monteith methods. In addition to the minimum and maximum temperature required by the Hargreaves method, the Penman-Monteith uses more parameters to determine potential evapotranspiration. Therefore, in most cases, the PET computed using the Penman-Monteith method was more conservative than that computed using the Hargreaves method. Whereas Penman-Monteith caters for the influence of additional parameters, such as the effect of wind and sunshine hours on evapotranspiration, Hargreaves is known to overestimate PET in humid conditions (Trajkovic, 2007). Therefore, the PET computed by the Penman-Monteith and Hargreaves methods has been used in the present study with caution that the latter predicts the worst-case scenario and the former moderate conditions.

3.2.7 Assessment of Anthropogenic Activities

Numerous anthropogenic activities influence hydrological regimes, but the key activities are groundwater and surface water exploitation. They increase groundwater discharge, alter the natural hydrological regime, runoff harvesting, and natural land cover alterations. Section 3.2.8 exhaustively covers the effect of the land cover modification. The key anthropogenic activities considered in this section are related to the abstraction and use of water resources.

The catchment of Lake Babati extends within Babati Town Council and Babati Rural, where domestic and non-domestic water is abstracted from groundwater sources. The information on water use was not readily available. However, this study used population data to project future water consumption. The demand of the study areas was scaled from the estimated water demand of the Internal Drainage Basin Authority by URT (2014). At the time of this study, the BAWASA was already supplying about 50 000 m^3 per week to households within their coverage area. Communities outside the BAWASA service area used water from shallow wells for domestic and agricultural activities. There were no inter-catchment water transfers by any known means except the lake, which outpours to the Kiongozi River and drains into Lake Manyara when it floods. Therefore, regional groundwater flows, as defined by (Toth, 1963), were considered minimal and balanced by the regional groundwater outflows, if any.

3.2.8 Land Use and Land Cover Classification

(i) Satellite Image Acquisition and Classification

Land cover links humans to the physical environment (Foody, 2002). Therefore, the study determined land cover changes to assess the degree of interference of the natural environment by anthropogenic activities and estimate the possible influence of the changes on the water resources. The detection of land use and land cover changes was conducted by analysing the multispectral Landsat images from 1991 to 2019 obtained from the Earth Explorer website by the U.S. Geological Services (https://earthexplorer.usgs.gov/). A large part of the Lake Babati catchment falls within the images from Landsat zone/path 169 and row 063, while a small portion lies on images from path 168 and row 063.

Images from 1991 to 1999 were from Landsat 4 – 5, which had a 30 m resolution, except band 6, whose resolution was 120 m but was resampled to 30m to match others. The Landsat 8 images were collected from 2013 to 2019. The cloud cover of the images was high for some years, while bar errors shaded other images. The images of the study area had, in most cases, the thickest cloud cover during the rainfall season. Most cloud-free images were only available for the dry seasons month of September, October, December, and February. No cloud-free images were available for

the rainy season. This hampered the possibility of studying the seasonal variation of land use. In addition, the scan liner error, which occurred after the failure of the Scan Line Corrector aboard the satellite systems, affected the Landsat 7 images from March 2003. Despite attempts to correct the errors, the images were erroneous for such a small study area and were discarded from the analysis.

Given that the available images were only for the dry season, it was challenging to distinguish between the urban land cover (or buildings) and bare land. As practiced in this area, agricultural land is prepared during the dry season; therefore, agricultural land is highly likely to be converted to bare land in the dry season. Consequently, the main index used for classification was the Normalized Difference Vegetation Index (NDVI). In addition, indices such as the Normalized Difference Built-up Index (NDBI), Normalized Difference Bareness Index (NDBaI), and Urban index (UI) (Meijerink *et al.,* 2007; As-syakur *et al.,* 2012) were used for a better distinction between bare land and built-up surfaces and vegetated surfaces during classification. Based on the digital values of the image bands, the indices were calculated as illustrated in Equation (30) to Equation (34) (Rahman *et al.,* 2004; As-syakur *et al.,* 2012).

$$NDVI = \frac{Band\ 4 - Band\ 3}{Band\ 4 + Band\ 3} \tag{30}$$

$$NDBI = \frac{Band\ 5 - Band\ 4}{Band\ 5 + Band\ 4} \tag{31}$$

$$UI = \frac{Band\ 7 - Band\ 4}{Band\ 7 + Band\ 4} \tag{32}$$

$$NDBaI = \frac{Band\ 5 - Band\ 6}{Band\ 5 + Band\ 6} \tag{33}$$

$$EBBI = \frac{Band\ 5 - Band\ 4}{10\sqrt{Band\ 5 - Band\ 4}} \tag{34}$$

Because no single method is better at distinguishing bare land and urban, a combination of the methods with ranges defined in Table 3 was used to distinguish the land cover classes. A location identified by more than one method as bare land was accepted. The urban index could not distinguish between the bare land and buildings as it categorized both as one unit. Therefore, the NDVI values were used with reference values of EBBI, NDBI, and NDBaI to distinguish the bare land from built-up portions of the land use and categorize the different land cover types.

The Google Earth images, old topographic maps from the Tanzania Survey Division (1967), the open street map, and the ground truth data about the spatial extent of specific land cover types and

categories collected during fieldwork provided instrumental data for determining the spectral signatures in supervised classification and validating the land use and land cover classification. Further, interviews with the local community about spots of unchanged land use and the historical land uses and cover changes were useful for verifying classification results. Finally, using the supervised classification method in ArcGIS version 10.5, the land cover and the land use were classified into the five main and easily identifiable classes presented in Table 4.

Table 3: Land cover classification criteria and classes

	Index	Values range	Values interpretation / Land cover class
No	NDVI values range		Interpretation
1		-1<NDVI<-0.1	Water bodies, cloud cover
		-0.1<NDVI<0.1	Bare soil surface, including open agricultural land, and man-made structures
		0.1<NDVI<0.2	Roads, bare surfaces with sparse vegetation
		0.2 < NDVI < 0.4	Shrubs, grassland, and farmland
		NDVI > 0.4	Dense forests
2	Enhanced Built-up and Bareness Index (EBBI)	0.10<EBBI< 0.35	Built up area
		EBBI > 0.35	Bare land
3	Normalized Difference Built-up Index (NDBI)	0.10<NDBI<0.30	Built-up area
		NDBI > 0.30	Bare land
4	Normalized Difference Bareness Index (NDBaI)	NDBaI < -0.15	Other land cover types
		NDBaI > -0.15	Bare land or clouds

Rahman *et al.* (2004)

Table 4: The main land cover and land use classes identified in the classification

Class No	Main Classes	Description
1	Water	Open water such as Lake, lagoons, and crater water
2	Built-up and bare land	Buildings, paved roads and surfaces, Bare soils, bare rocks, and unpaved roads
3	Agricultural land and grassland	Agricultural land and grassland
4	Shrubs and scattered trees	Shrubs and scattered trees
5	Forests	Dense forests

(ii) Accuracy assessment of land-use classification

Accuracy assessment is an essential process of quantifying and checking the quality/validity of classified images (Debnath *et al.,* 2017). At least 150 sample points were randomly picked (to incorporate probability sampling) from the classified maps for accuracy assessment following the recommendations of Olofsson *et al.* (2014). The sampling was controlled and stratified to ensure that at least 20 points were taken from each land-use class. The study avoided using non-probability sampling techniques such as sampling points of convenience and sampling from homogenous areas.

Numerous stratification methods exist, but each has a benefit and a shortcoming. For example, proportional allocation produces a smaller standard deviation for estimating producer accuracy and overall accuracy than equal allocation, while equal allocation favours the user's accuracy over the overall accuracy (Olofsson *et al.,* 2014). This study compromised and balanced the benefits of the two methods by taking the average of two sample allocation criteria, i.e., weighted/proportional allocation and equal distribution allocation. This increases the sampling points for the rarer class above the proportional limit but to a number less than that of the equal allocation, as recommended by Olofsson *et al.* (2014), thus improving classification accuracy.

Several accuracy assessment methods exist, but no single method has been standardized. The choice of analysis method was motivated by the ability of the method to measure the accuracy assessments with the available resources. In the present study, a confusion matrix (error matrix), due to its limited computational requirement, was applied to evaluate the accuracy of the classified maps. The accuracy assessments determined how well the land use and land cover were classified. Higher producer accuracy, user accuracy, overall accuracy, and kappa coefficient imply the suitability of classified land use and land cover maps for land use change and impact analysis.

A confusion matrix compares the generated land use maps against the reference information (in this case, from Google Earth images and old topographical maps) regarded as the truth. It summarizes the relationship between the classified map and the reference data in an error matrix (Olofsson *et al.,* 2014). The confusion matrix table eases the computation of the overall accuracy of the classification, the percent correct, the user's accuracy, the producer's accuracy, and the kappa coefficient. The main diagonal in the error matrix shows the correct classification, while the omission and commission areas are presented in the off-diagonal, as Foody (2002) illustrated in Fig. 10.

Figure 10 shows an array of cells with column letters indicating the actual classes (reference class) and row letters indicating classes in the predicted (classified map). The letters in the cells, for example, n_{AC} mean the number of cells that have been predicted (classified) to be in class A but belong to class C in the actual map. Correctly classified cells have the same letter codes in their subscript. For example, n_{DD} is the number of cells predicted (or classified) as class D and actually belong to class D in the actual class (original map). n_{A+} is the summation of the number of cells in row A (predicted class A), and n_{+D} is the summation of the number of cells in column D (in actual class D).

Actual Class

Predicted classes

	A	B	C	D	Σ
A	n_{AA}	n_{AB}	n_{AC}	n_{AD}	n_{A+}
B	n_{BA}	n_{BB}	n_{BC}	n_{BD}	n_{B+}
C	n_{CA}	n_{CB}	n_{CC}	n_{CD}	n_{C+}
D	n_{DA}	n_{DB}	n_{DC}	n_{DD}	n_{D+}
Σ	n_{+A}	n_{+B}	n_{+C}	n_{+D}	n

Figure 10: Demonstration of the error matrix of classification adapted from Foody (2002)

From the illustration in Fig. 10, Foody (2002) presented the formula for computing the user's accuracy, producer's accuracy, error of commission, error of omission, overall efficiency, and the Kappa coefficient as in Equation (35) to Equation (41).

$$P_c = \frac{\sum_{k=1}^{q} n_{kk}}{n} \times 100 \tag{35}$$

where q is the number of land use classes, P_c is the percent correct and n_{kk} is the number of correctly classified cells (the sum of the numbers in the diagonal of Fig. 10).

The user's accuracy of class i is the proportion of area mapped as class i and has reference (actual) class i. User accuracy, U_i is computed by taking the ratio of the cells mapped as of class i in the classified map against the number of cells in the reference (actual) map with class i.

$$U_i = \frac{n_{ii}}{n_{i+}} \tag{36}$$

The commission error for class i, C_{ei} is complementary to the user's accuracy, and it is measured as in Equation (37):

$$C_{ei} = 1 - U_i = 1 - \frac{n_{ii}}{n_{i+}} \tag{37}$$

Producers accuracy, P_i measures the ratio of the cells referenced (actual map) as class i and mapped as class i as expressed in Equation (38):

$$P_i = \frac{n_{ii}}{n_{+i}} \tag{38}$$

The error of omission, O_{ei} is computed from the producer's accuracy as in Equation (39):

$$O_{ei} = 1 - P_i = 1 - \frac{n_{ii}}{n_{+i}} \tag{39}$$

Other complementary methods of assessing accuracy exist; however, the Kappa coefficient is the most popular method. Olofsson *et al.* (2014) propound that correction of chance agreement in the Kappa coefficient is unreasonable. Its strong correlation to the user's accuracy makes using both the Kappa coefficient and the user's accuracy redundant. Kappa coefficient, K_C (computed by Equation (40)) was adopted in the present study to reinforce the user's accuracy.

$$K_C = n\frac{\sum_{k=1}^{q} n_{kk} - \sum_{k=1}^{q} n_{k+n_{+k}}}{n^2 - \sum_{k=1}^{q} n_{k+n_{+k}}} \tag{40}$$

Similarly, the overall accuracy of the classification was computed as follows in Equation (41):

$$Overall\ accuracy\ (\%) = \frac{\sum_{k=1}^{q} n_{kk}}{n} \times 100 \tag{41}$$

3.3 Hydrological modelling of Lake Babati catchment

3.3.1 The Hydrologic Engineering Centre – Hydrologic Modelling System

Hydrological modelling of Lake Babati catchment was undertaken using the Hydrologic Engineering Centre – Hydrologic Modelling System (HEC-HMS) computer program version 4.8 (HEC, 2000, 2021). The HEC-HMS has several models, sometimes called packages, which are sets of equations representing the behaviour of hydrological components (HEC, 2000).

The HEC-HMS was chosen from numerous tools, such as SWAT and GSFLOW, to simulate the Babati catchment's continuous response because it can model and be calibrated by the reservoir levels. Models such as SWAT and MIKE SHE use outflow data which was unavailable for calibration in this case. The HEC-HMS models conceptualize rainfall-runoff response in both events and continuous storms. The continuous models can simulate the streamflow over a long time because they maintain soil moisture balance (Razmkhah, 2016). In addition, the model packages can be fully lumped or distributed to account for the spatial variations of parameters that influence hydrological responses.

3.3.2 The Modelling Equations

The Deficit and constant rate method (HEC, 2000, 2021) was chosen to model runoff volume, i.e., to model the loss of water to interception, evaporation, and infiltration before the runoff, while the Snyder's Unit Hydrograph method (Chow *et al.,* 1988) was preferred to simulate the direct runoff on the ground surface. The study chose the deficit and constant rate loss method because it could perform continuous rainfall-runoff modelling with fewer input data and calibrate with the available data. Although the Soil Moisture Accounting method (HEC, 2000) is also suitable for continuous modelling, it requires numerous input data, including soil parameters that were unavailable. The baseflow (groundwater) was routed using the Linear Reservoir model. The channel flow was not routed since all the rivers were seasonal, and the channel characteristics were unknown. Instead, the sub-basins were assumed to drain directly into the lake since each sub-basin ends in the lake, as depicted in Fig. 11.

The HEC (2000) conceptualizes the deficit and constant loss method clearly with the computation proceeding as follows: The precipitation first fills the canopy-interception storage, and only the excess precipitation is available for infiltration. If the excess precipitation exceeds the available soil storage or the computed potential infiltration cannot deplete the volume, the excess volume fills the surface-depression storage. The runoff will only occur when the surface depression storage is full. The evaporation is modelled when no precipitation occurs within the interval (HEC, 2000). Otherwise, its computation proceeds in the following order: The model first satisfies the potential evapotranspiration needs from canopy storage, then surface storage. Water is extracted from the upper soil storage profile if the surface storage does not satisfy evapotranspiration (HEC, 2000).

The Deficit and Constant Loss method is a modification of the Initial and Constant Loss method (HEC, 2000), which assumes that the maximum rate of precipitation loss f_c is constant throughout the rainfall event. Therefore, if P_t is the mean areal precipitation in a time interval Δt from t to $t + \Delta t$, then HEC (2000) computes the excess precipitation Pe_t in the initial and constant loss model as shown in Equation (42).

$$Pe_t = \begin{cases} P_t - f_c & if \quad P_t > f_c \\ 0, & otherwise \end{cases} \tag{42}$$

When the initial loss to interception and detention storage, I_a is added to Equation (42), the runoff would not occur until the initial losses are exceeded, and Equation (42) becomes Equation (43).

$$Pe_t = \begin{cases} 0 & if \quad \sum P_i < I_a \\ P_t - f_c & if \quad \sum P_i > I_a \; and \; P_t > f_c \\ 0 & if \quad \sum P_i > I_a \; and \; P_t < f_c \end{cases} \tag{43}$$

The deficit and constant loss methods differ from Equation (43) because the initial loss can recover after a long drought. The application of the model requires the specification of the initial loss, constant loss rate, and recovery rate. The model continuously tracks the moisture deficit, computed as the sum of the initial abstraction value and the recovery volume in the precipitation-free period and less by the precipitation volume. Therefore, the sum of the evaporation and the percolation rates is a reasonable estimate of the recovery rates (HEC, 2000).

The Snyder Unit Hydrograph (UH), developed by Snyder in 1938 to analyze runoff in the ungauged catchments of Appalachians Highlands in the USA (Chow *et al.,* 1988), was used in the present study. This method was chosen because the study catchment is ungauged, and parsimony was believed to be achievable since the Snyder UH has only two parameters. The parameters are the t_p which is the basin lag between the rainfall peak and the hydrograph peak, and C_p, a peaking coefficient that varies from 0.4 to 0.8 (HEC, 2000). More importantly, t_p can be determined from the basin parameters using Equation (44) (Chow *et al.,* 1988).

$$t_p = CC_t(LL_c)^{0.3} \tag{44}$$

where C_t is the basin coefficient, L is the length of the mainstream from the outlet to the catchment divide, L_c is the length along the mainstream from the outlet to a point nearest to the centroid, and C is the conversion factor which is 0.75 for the SI units and 1 for the foot-pound system. The basin coefficient C_t is not a physically based parameter and is best determined through calibration. Bedient *et al.* (2013) reported that C_t varies from 1.8 to 2.2 but also noted that it varied from 0.4 in mountainous areas to 8.0 along the Gulf of Mexico.

The USACE (1994) provides an alternative method for estimating the basin lag t_p as shown in Equation (45).

$$t_p = CC_t\left(\frac{LL_c}{\sqrt{S}}\right)^N \tag{45}$$

Where S is the slope of the longest watercourse from the point of concentration to the boundary of the drainage basin, and N is an exponent commonly considered as 0.33. Both methods (Equations (44) and (71)) were applied to determine the probable ranges for the basin lag. Other studies have also estimated the basin lag as 50 – 75% of the time of concentration. The linear reservoir volume

accounting model modelled the baseflow, which applies a cascade of reservoirs whose outflows are linearly proportional to the storage volume.

3.3.3 The Model Setup

Based on a 30 m resolution DEM from SRTM (USGS, 2018), six small sub-basins were delineated using the GIS package of HEC-HMS (Fig. 11) to represent the different hydrological responses better. The catchment characteristics derived from the delineated sub-basins (Table 5) were used to estimate realistic ranges of hydrological basin parameters.

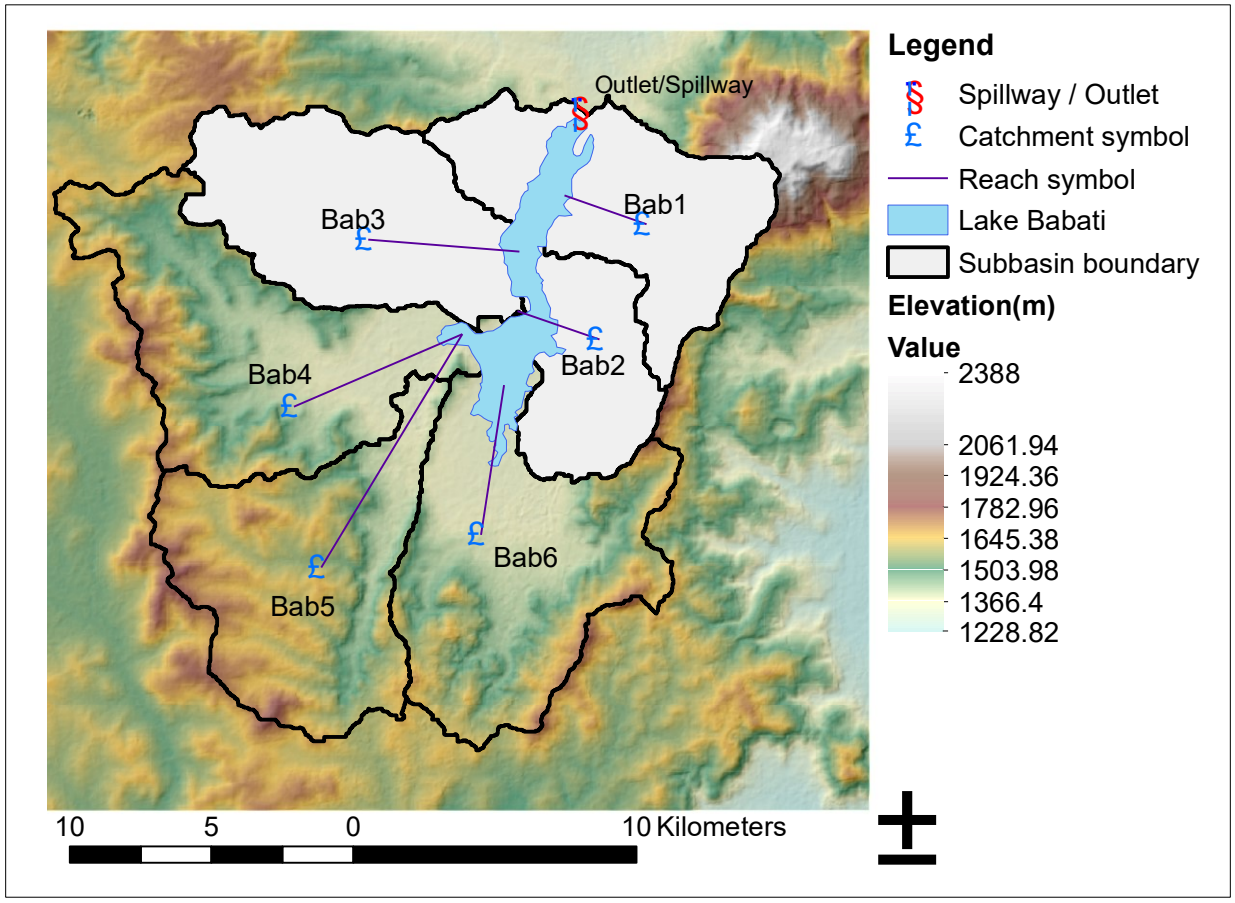

Figure 11: Delineated sub-basins within the Lake Babati catchment and their schematic representation in the HEC-HMS model

Table 5: Sub-basin properties applied for estimation of the sub-basin hydrological parameters

Parameters	Area (km^2)	Longest flow path Length (km)	Longest Flow path slope	Centroidal Flow path Length (km)	Centroidal Flow path Slope	10 - 85 Flow path Length (km)	10 - 85 Flow path Slope	Basin Slope	Basin Relief (m)	Relief Ratio	Elongation Ratio	Drainage Density (km/Km^2)
Bab1	58.48	18.26	0.0572	10.60	0.0055	13.70	0.0251	0.1326	1047.0	0.0573	0.4725	0.1563
Bab2	33.2	12.03	0.0211	5.76	0.0010	9.02	0.0023	0.1164	467.0	0.0388	0.5404	0.0750
Bab3	62.86	16.70	0.0238	7.34	0.0077	12.52	0.0199	0.1302	409.0	0.0245	0.5357	0.1614
Bab4	80.55	23.25	0.0139	12.35	0.0034	17.43	0.0092	0.1422	448.0	0.0193	0.4356	0.1835
Bab5	72.97	20.42	0.0235	15.26	0.0165	15.31	0.0188	0.1430	483.0	0.0237	0.4721	0.1695
Bab6	81.89	19.68	0.0174	10.51	0.0035	14.76	0.0133	0.1367	458.0	0.0233	0.5188	0.1565

Bains relief is measured in meters as the high above the lowest elevation

3.3.4 Model Calibration

Calibration is tuning the model parameters to match (improve) the prediction of the outputs with the observations or the field-measured data (HEC, 2000). Model calibrations take a trial-and-error approach to find the best sets of parameters. First, a trial set of parameter values is chosen, the model is run, and the errors are computed. Another set of trial parameter values is chosen when the computed errors are unacceptable and the program is simulated iteratively. The iterations continue until the model errors are within the acceptable ranges or the stopping number of iterations is reached.

The automatic calibration implements a computerized numerical mathematical solution and can quickly produce good model outputs due to the faster iteration rates. However, automatic calibration can produce a good model output but with unrealistic sets of parameter values, especially from the wide search space of parameter values. Therefore, the modeller must use intuition to restrict the parameter space to realistic ranges that describe the observed catchment characteristics. Thus, the expertise of the modeller is essential for calibration. On the other hand, the hydrological experts, although time-consuming, can achieve good agreement with manual calibration.

The calibration process ends when the model outputs are closest to the observations as measured by goodness of fit statistics and graphical representations. In the present study, the automatic calibration did not improve the pool level shape since the automatic calibration was restricted to measuring only the goodness of fit with the maximum peak pool elevation. Therefore, manual calibration was adopted after automatic calibration to preserve the pool-level hydrograph shape and optimize the Root Mean Square Error (RMSE) and the Nash Sutcliffe Efficiency (NSE) objective functions. Other goodness of fit measures applied includes a scatterplot of the predicted lake pool level against the observations, the sum of absolute errors (Equation (46)), the sum of squared residuals (Equation (47)), the percent error in peak (Equation (48)), and the peak weighted root means squared errors (Equation (49)). The goodness of fit measures in Equations (46) - (49) was computed from outside the model using Microsoft Excel because the model was not built to compute them.

The sum of absolute errors:

$$Z = \sum_{i=1}^{n} |q_{o(i)} - q_{s(i)}| \tag{46}$$

The sum of Squared residuals as cited in HEC (2000):

$$Z = \sum_{i=1}^{n} \left[q_{o(i)} - q_{s(i)} \right]^2 \tag{47}$$

The percent error in peak (HEC, 2000):

$$Z = 100 \left| \frac{q_{s(peak)} - q_{o(peak)}}{q_{o(peak)}} \right| \tag{48}$$

The peak weighted root means square objective function by USACE (1998) was applied for optimization as in Equation (49).

$$Z = \left\{ \frac{1}{n} \left[\sum_{i=1}^{n} \left[q_{o(i)} - q_{s(i)} \right]^2 \left(\frac{q_{o(i)} - \overline{q_o}}{2\overline{q_o}} \right) \right] \right\}^{\frac{1}{2}} \tag{49}$$

The NSE was applied to measure the goodness of fit for the calibration and validation phase. It varies from negative infinity to 1. When NSE < 0, it implies that the mean of the variation is a better predictor than the model, while an NSE = 0 indicates that the mean of the distribution is as good a predictor as the model. A model is considered worthy for prediction purposes when its NSE > 0.6. Moriasi *et al.* (2015) considered a daily flow model with 0.5 < NSE < 0.7 as satisfactory and a model with 0.7 < NSE < 0.8.5 as a good one. A daily flow model was considered very good when NSE > 0.85 (Moriasi *et al.,* 2015). NSE is calculated using Equation (50) and (71).

$$NSE = 1 - \frac{\sum_{i=1}^{n} \left(q_{s(i)} - q_{o(i)} \right)^2}{\sum_{i=1}^{n} \left(q_{o(i)} - \overline{q_o} \right)^2} \tag{50}$$

where $q_{o(i)}$ is the observed output at time step i, $q_{s(i)}$ is the simulated output (discharge or pool level) at time step i, n is the number of computed hydrograph ordinates, $q_{s(peak)}$ is the peak simulated discharge and $q_{o(peak)}$ is the peak observed discharge. The calibrated parameters of the model are presented in Table 6, Table 7, and Table 8.

Table 6: The initial and calibrated parameters for initial abstraction, runoff volume, and catchment runoff routing

	Simple Canopy							Simple Surface						Snyder Transform					
	Initial Storage (%)			Maximum Storage (mm)				Initial Storage (%)			Maximum Storage (mm)			Lag Time (HR)			Peaking Coefficient		
	Minimum	Maximum	Calibrated	Minimum	Maximum	Calibrated	Crop Coefficient (-)	Minimum	Maximum	Calibrated	Minimum	Maximum	Calibrated	Minimum	Maximum	Calibrated	Minimum	Maximum	Calibrated
Bab4	0	100	0.0267	0	10	1	1	0	100	100	0	100	1	0.1	500	7.3743	0.4	0.8	0.4
Bab5	0	100	0.0294	0	10	1	1	0	100	100	0	100	1	0.1	500	7.558	0.4	0.8	0.4
Bab6	0	100	0.0315	0	10	1	1	0	100	100	0	100	1	0.1	500	6.6849	0.4	0.8	0.4
Bab3	0	100	0.0329	0	10	1	1	0	100	100	0	100	1	0.1	500	5.7119	0.4	0.8	0.4
Bab2	0	100	0.0336	0	10	1	1	0	100	100	0	100	1	0.1	500	4.8154	0.4	0.8	0.4
Bab1	0	100	0.0338	0	10	1	1	0	100	100	0	100	1	0.1	500	6.5522	0.4	0.8	0.4

Table 7: The initial and calibrated linear Reservoir model parameters for modelling groundwater in the catchment

	Number of Layers	GW 1 Initial – Discharge per unit area ($m^3/s/km^2$)			GW 1 Fraction (-)	GW 1 Coefficient (HR)			GW 1 Steps	GW 2 Initial Discharge per unit area ($m^3/s/km^2$)			GW 2 Fraction (-)	GW 2 Coefficient (HR)			GW 2 Steps
		Minimum	Maximum	Calibrated		Minimum	Maximum	Calibrated		Minimum	Maximum	Calibrated		Minimum	Maximum	Calibrated	
Bab4	2	0	0.4	0.0001	0.2	0.1	1000	59.407	1	0	0.15	0.0015	0.15	1	5000	1232	2
Bab5	2	0	0.4	0.0001	0.2	0.1	1000	57.855	1	0	0.15	0.0015	0.12	1	5000	1204	2
Bab6	2	0	0.4	0.0001	0.2	0.1	1000	52.671	1	0	0.15	0.0015	0.10	1	5000	1197	2
Bab3	2	0	0.4	0.0001	0.2	0.1	1000	43.658	1	0	0.15	0.0015	0.10	1	5000	1167	2
Bab2	2	0	0.4	0.0001	0.2	0.1	1000	37.235	1	0	0.15	0.0015	0.15	1	5000	1120	2
Bab1	2	0	0.4	0.0001	0.2	0.1	1000	46.156	1	0	0.15	0.0015	0.15	1	5000	1183	2

Table 8: Parameter ranges and calibrated values for the deficit and constant rate methods of accounting infiltration rates

	Deficit and Constant									
	Initial Deficit (mm)	Initial Deficit (mm)	Initial Deficit (mm)	Maximum Storage (mm)	Maximum Storage (mm)	Maximum Storage (mm)	Constant Rate (mm/HR)	Constant Rate (mm/HR)	Constant Rate (mm/HR)	Impervious (%)
	Minimum	Maximum	Calibrated	Minimum	Maximum	Calibrated	Minimum	Maximum	Calibrated	
Bab4	0	5	0.14196	0.001	1000	5	0.001	30	3	0
Bab5	0	5	0.11462	0.001	1000	5	0.001	30	3	0
Bab6	0	5	0.087282	0.001	1000	5	0.001	30	3	0
Bab3	0	5	0.059943	0.001	1000	5	0.001	30	3	0
Bab2	0	5	0.032604	0.001	1000	5	0.001	30	3	0
Bab1	0	5	0.005265	0.001	1000	5	0.001	30	3	0

3.3.5 Model Validation

Models are simple representations of the complex system, which may still be inaccurate. Calibrations attempt to improve model accuracy. However, the calibrated parameters may only correctly represent the scenario/dataset used for calibrations because models are simplified representations of a complex system. Therefore, hydrological model validation attempts to test the accuracy of the model calibration efforts by measuring how best the calibrated model predicts the known observed hydrological output with a set of stress conditions different from the calibration datasets. This study used rainfall and evapotranspiration data from August 2020 to March 2021 as validation datasets, and the lake's level measured at a 30-minute interval using an automatic pressure transducer (diver) installed in the Lake.

A model is deemed unreliable when the validation test fails; thus, it is not recommended for use. Therefore, the model was iteratively recalibrated until it satisfactorily met the objective functions in both calibration and validation. The satisfaction of the objective functions was measured using the goodness of fit statistics presented in Table 19 and the graphical comparison of the simulation in the calibration and validation phase with the observed lake level.

3.4 Sensitivity Analysis and Attribution of Water Level Drivers

3.4.1 Grey Relational Analysis

Grey Relational Analysis (GRA) and multi-stepwise regression were applied to analyse the sensitivity of the net basin supply parameters. The GRA determines the most sensitive parameters without showing the direction of effect (Wong *et al.,* 2006), while multi-stepwise regression analysis attempts to quantify the direction of changes and trends.

Wong *et al.* (2006) developed the GRA to measure the degree of influence of one sequence over a reference sequence. The GRA determines geometrical proximity between different discrete sequences and at least one comparison sequence in a system (Li *et al.,* 2014). The proximity, a measure of similarities between discrete data arranged in sequential order, is expressed in grey relational grade. A higher grey relational grade implies a higher similarity between the sequential parameters (Li *et al.,* 2014; Wong *et al.,* 2006).

The GRA and grey system theory has been widely used to analyze uncertainties in systems with imprecise information, including finance and hydrology (Wong *et al.,* 2006; Kung & Wen, 2007; Li *et al.,* 2014), optimization of the manufacturing process and quality (Tzeng *et al.,* 2009). This technique was adopted to analyze the sensitivity of natural and anthropogenic factors that drive the water level variability of Lake Babati. Li *et al.* (2014) similarly applied GRA techniques to

identify significant factors that influenced groundwater change in North China Plains. Li *et al.* (2014) simplified the steps of using GRA proposed by Wong *et al.* (2006) as follows:

(i) Determination of the Reference and Comparison Series

The reference time series denoted as X_0' represents the system's characteristics, while the comparison time series denoted by Xi' is a series of factors that influence the system characteristics. The series is represented by Equation (51) and Equation (71).

$$X_0' = \{x_0'(k) | k = 1,2, \dots n\} \tag{51}$$

$$X_i' = \{x_i'(k) | k = 1,2, \dots n; i = 1,2, \dots, m\} \tag{52}$$

The k represents the period; thus, n is the number of periods while *i* represents the evaluating factors, with m as the total number of influencing factors evaluated.

(ii) Data Processing

Data preprocessing is necessary to ensure that all evaluated factors are of the same units or that the original series are transformed into comparable sequences. Kung & Wen (2007) and Li *et al.* (2014) proposed these three linear normalization methods (Equations (53), (54), and (71)) to avoid distortion of data in preprocessing.

$$X_i'(k) = \frac{X_i(k)}{\overline{X_i}} \ (i = 0,1, \dots m; k = 12 \dots n) \tag{53}$$

$$X_i'(k) = \frac{X_i(k)}{X_i(1)} \ (i = 0,1, \dots m; k = 12 \dots n) \tag{54}$$

If a larger value is expected, like in benefits, Equation (55) can be used to determine $X_i'(k)$.

$$X_i'(k) = \frac{x_i^{(0)}(k) - min\, x_i^{(0)}(k)}{max\, x_i^{(0)}(k) - min\, x_i^{(0)}(k)} \tag{55}$$

Equation (56) is applicable for determining $X_i'(k)$ when a lower value like in costs is anticipated.

$$X_i'(k) = \frac{max\, x_i^{(0)}(k) - x_i^{(0)}(k)}{max\, x_i^{(0)}(k) - min\, x_i^{(0)}(k)} \tag{56}$$

When the expected distribution is normally distributed, like for age, Equation (57) is used.

$$X_i'(k) = 1 - \frac{\left| x_i^{(0)}(k) - OB \right|}{max.\{Max.[x_i^{(0)}(k)] - OB, OB - Min.[x_i^{(0)}(k)]\}} \tag{57}$$

where $X_i'(k)$ is the value of the grey relation, $\max x_i^{(0)}(k)$ is the maximum value of the $x_i^{(0)}(k)$ and $\min x_i^{(0)}(k)$ is the minimum value of $x_i^{(0)}(k)$. OB is the objective value.

(iii) Determination of the Deviation Sequences

The deviation sequences $\Delta_{0i}(k)$ between the corresponding values in the reference and comparison series are determined by Equation (58):

$$\Delta_{0i}(k) = |x_0(k) - x_i(k)| \tag{58}$$

From these deviation sequences, the maximum $max\Delta_{0i}(k)$ and minimum $min\Delta_{0i}(k)$ values are determined.

(iv) Calculation of the Grey Relational Coefficient ξi(k)

For each series, the grey relational coefficient is calculated using Equation (59):

$$\xi_i(k) = \frac{min\Delta_{0i}(k) + \rho max\Delta_{0i}(k)}{\Delta_{0i}(k) + \rho max\Delta_{0i}(k)} \tag{59}$$

Where ρ is the distinguishing coefficient whose value is $0 \leq \rho \leq 1$, and differentiates the degree of proximity of X_0 and Xi, such that $\xi_i(k)$ is between 0 and 1. $\in[0,1]$. ρ can be adjusted based on the actual system requirements but is generally taken to be 0.5.

(v) The Grey Relational Grade γi

The grey relational grade γ_i is calculated as in Equation (60).

$$\gamma_i = \frac{1}{n}\sum_{k=1}^{n} \xi_i(k) \tag{60}$$

3.4.2 Stepwise Regression Analysis

The methods of stepwise regression analysis of multiple variables described in Draper and Smith (1998) and Rawlings and Dickey (1998) were followed to determine the partial regression coefficients for each independent variable responsible for lake water level variations. The multiple regression analysis was performed on daily precipitation, lake evaporation, inflow to the lake, and lake outflow to determine the most influencing factors. The inflow was obtained from the HEC-HMS model from August 2019 to March 2021 to ensure all the data had the same length.

The forward selection, backward elimination, and stepwise selection of model variables developed the stepwise regression models relating lake levels to the different variables. First, a simple model

with no predictors was selected. Then, the model variables or predictors were iteratively added using forward selection until an optimized fit of the model variables was reached. At the optimized stage, adding more variables produced no statistically significant improvement. In the backward elimination method, the regression was started with a complex model which included all model parameters. The model variables were eliminated at each backward step until an optimized model fit where all the variables were statistically significant. Forward and backward methods ensured the results were triangulated, consistent, and reliable. Irrespective of the chosen stepwise method, the model converged to the same optimal solution.

The Akaike Information Criterion (AIC) (Akaike, 1973) was applied to measure the quality of the resulting model relative to other models after adding or eliminating parameters. The parameter sets that gave a model with the lowest AIC was deemed the optimal sets of sensitive parameters. Therefore a smaller AIC was used as a stopping criterion in the stepwise model regression. Based on the AIC, the best model was chosen, and the goodness of fit tests was done. F- tests on each partial regression coefficient were conducted to determine the most significant variable that could be retained or eliminated to simplify the model.

3.5 Sampling and Analysis of Hydrogeochemical and Isotopic Data

3.5.1 Water Sample Collection

(i) Preparation for Water Sampling Campaign

While preparing for the water sampling campaign, the study followed Brassington (2007) and the American Public Health Association (2017) protocols for sampling, handling, storing, and transporting water samples. For example, the study prepared beforehand a sampling equipment checklist, a list of sample sites, the type of sample to be taken at each location, a list of parameters to be determined at each site, and a route map to the sample locations before the sampling campaigns. The additional items mobilized were pretreatment equipment, including cold boxes to suppress evaporation, the first-aid box, personal protective equipment, appropriate sample bottles with spares packed in cold boxes with ice packs, and suitable packing material. Other equipment included beakers for on-site measurement and a HANNA multiparameter set (model HI 9829) of complete probes to measure temperature, the potential of Hydrogen ion (pH), the electrical conductivity (EC), and dissolved oxygen. We also carried blank and standard solutions for multiparameter calibration, de-ionized water, and tissue for cleaning instruments. After each sampling or at the end of each working day, the samplers (a bailer, buckets, and beakers) were washed in a cleaning solution, and the samplers rinsed well in de-ionized water to avoid sample adulteration.

(ii) Water Sampling

Water samples were collected on the 22nd and the 23rd of May 2019 (towards the end of the major rainy season). The samples were taken from different points and depths in Lake Babati, shallow and deep wells, and the rivers within and outside of Lake Babati's catchments, as shown in Fig. 12. Coordinates of sampling points were determined using a handheld Global Positioning System (GPS) handset (Garmin etrex 30 model), and the sampling depth was measured using a dipping tape.

The lake water was sampled using a bailer from 1m below the surface and 2/3rd of the lake depth using a lake water sampler. Further, the study sampled water from two points on Lake Manyara (one from about the lake middle and another from its northernmost boundary near a river input) for comparison purposes with Lake Babati.

Water was collected from shallow open wells using a bucket which was cleaned and rinsed several times with the well water. Deep and shallow wells installed with pumps were sampled from the pump outlet after pumping out for 5 – 10 minutes to avoid sampling standing water. The main interests were to collect representative groundwater samples from the exact productive aquifer. In addition, we sampled river water from where the river was flowing to avoid sampling standing water. After sampling, the study followed the standard methods for preserving and examining water and wastewater chemistry prescribed by the America Public Health Association (2017).

The temperature, pH, Total Dissolved Solids (TDS), and EC were measured onsite immediately after sampling using a HANNA multi-parameter test kit (model HI 9829). The multi-parameter kit was calibrated for EC and pH by taking readings from standard solutions of both. The kit was reset and recalibrated whenever necessary according to the manufacturer’s specifications.

The water samples were filled into cleaned dry bottles, decontaminated in Nitric Acid, and rinsed with deionized water a day before the field excursion. Immediately after sampling, the samples were placed into cooler boxes packed with ice cubes to keep the samples cold. The water samples were placed in different but appropriate bottles and treated differently depending on the parameters to be tested. The samples for isotopes were filled and capped airtight underwater into 100 ml high-density polyethylene bottles to avoid the introduction of air bubbles. No further treatments were performed on the samples, but they were stored in a low-temperature room to avoid evaporation. Water samples for cation and anion analysis were kept in polyethylene bottles and maintained at 4˚C without further treatment.

3.5.2 Water Chemistry Analysis

Immediately after fieldwork, the carbonate, bicarbonate, and total alkalinity of the samples were determined by titrating with sulphuric acid with methyl orange and phenolphthalein as endpoint indicators following titration method 2320B (America Public Health Association, 2017).

The major cations and anions were analyzed using Ion Chromatography (ICS – 5000) at the National Institute of Hydrology Laboratory Roorkee, Uttarakhand State, India. The samples were filtered using a 0.45μm pore diameter membrane filter and diluted with distilled water to ensure EC < 10 μS/cm before analysis. The ionic balance of the major cations and anions in the samples was a criterion for assessing the accuracy of the hydro-geochemical analysis. Sample analysis was repeated where the ionic balance errors of major cations and anions were >10%. Finally, 86% of the 29 samples had ionic balance errors of < 5%, while one sample still had an ionic balance error of >10% after repeated analysis. These results were accepted as most had a minor ionic balance error of less than the acceptable 5%.

3.5.3 Laboratory Analysis of Isotopes in Water

Water samples for isotope analysis were analyzed for deuterium (^{2}H) and oxygen – 18 (^{18}O) isotopes at the Nuclear Laboratory of the National Institute of Hydrology, Roorkee, Uttarakhand, India, using a Dual Inlet Isotope Mass Ratio Spectrometer. The unit of measurement was per mil deviations from Vienna Standard Mean Ocean Water (denoted as δ of V-SMOW). About 3 mL of the sample was first equilibrated with hydrogen gas in the presence of a platinum catalyst for 3 hours before determining deuterium. Before determining the oxygen - 18 isotope fractionation, the samples were equilibrated for about 7 hours in carbon dioxide. The isotope composition δ (delta values) of deuterium and oxygen – 18, defined as isotopic ratios reflecting deviation in per mil (‰) from Vienna - Standard Mean Ocean Water (Vienna - SMOW), were calculated from Equation (61) (Kendall & Doctor, 2003)

$$\delta_{Sample} = \left(\frac{R_{sample}}{R_{standard}} - 1\right) \times 1000 \tag{61}$$

where R_{sample} is the concentration ratio of the heavy isotope to the more abundant light isotope of the same atom, for example, the ratios of $^{18}O/^{16}O$ or $^{2}H/^{1}H$. The $R_{standard}$ and R_{sample} were derived from beam currents integrated over time for a sample gas against a reference gas. A positive δ_{Sample} means the isotopic ratio is higher than the standards and vice versa.

Isotopes in precipitation data are important for drawing the local meteoric water lines upon which the interpretation of isotopic compositions in different water sources can be based. The study area did not have isotopes in precipitation observed over time. However, the Global Network of Isotope

in Precipitation (IAEA, 2019) had 117 monthly isotopic datasets (of deuterium and oxygen – 18) in precipitation in Tanzania collected from Dar es Salaam between March 1961 to October 1973 and another 18 monthly measurements from Dodoma collected between January 2014 and April 2016. The Dodoma station is at an altitude of 1150 m, 213 km south of the study area, while Dar es Salaam is at 55 m altitude and 480 km southeast. These isotopes in precipitation data were collected in all the months with rainfall and were thus representative of the seasonal variations of isotopes in precipitation for Tanzania. In assessing the possible interaction among different water sources, the composition of isotopes in water was compared with the Local Meteoric Water Lines (LMWL) based isotopic composition in precipitation.

3.5.4 Statistical and Graphical Analysis

We applied descriptive statistics using the Excel analysis tools and the R – Packages (Version 3.6.1) to analyze hydrogeochemical parameters and isotopic compositions. Each parameter's box and whisker plots were applied to compare the relative variations of the parameter among different water sources. Pearson's correlation was used to determine the relationships between different chemical parameters in the water samples. At the same time, the Principal Component Analysis (PCA), performed using R-packages (prcomp package), was employed to identify multicollinearity issues. In the PCA, the missing values were omitted, and variables were scaled since they had different units of measurement. The spatial autocorrelation of the hydro-geochemical parameter was checked using the Moran autocorrelation coefficient. We followed the procedures of computing Moran I statistics described by Ijumulana *et al.* (2020) and Quino-lima *et al.* (2020) without repeating them here for brevity. Based on the relative abundance of major cations and anions, we used the Piper Diagram (Piper, 1944) to identify the dominant hydro-geochemical facies and their evolution in the water.

To understand the relationship in isotopic variations, a scatter plot of the δD and $\delta^{18}\mathrm{O}$ values were made while the $\delta^{18}\mathrm{O}$ values were spatially interpolated using the Kriging method to appreciate its evolution in the lake surface and bottom. Further, the deuterium excess (d^*) expressed in Equation (62), a second-order isotope parameter sensitive to the conditions during the evaporation of water from the source (Liliane & Jouzel, 1979; Pfahl & Sodemann, 2014) has been applied to understand moisture sources (Jabal *et al.,* 2018). Deuterium excess, d^* was plotted against $\delta^{18}0$ to explore the water sources.

$$d^* = \delta D - 8\delta^{18}O \tag{62}$$

With δD and $\delta^{18}0$ as the measured deuterium and oxygen – 18 relative abundance to V-SMOW

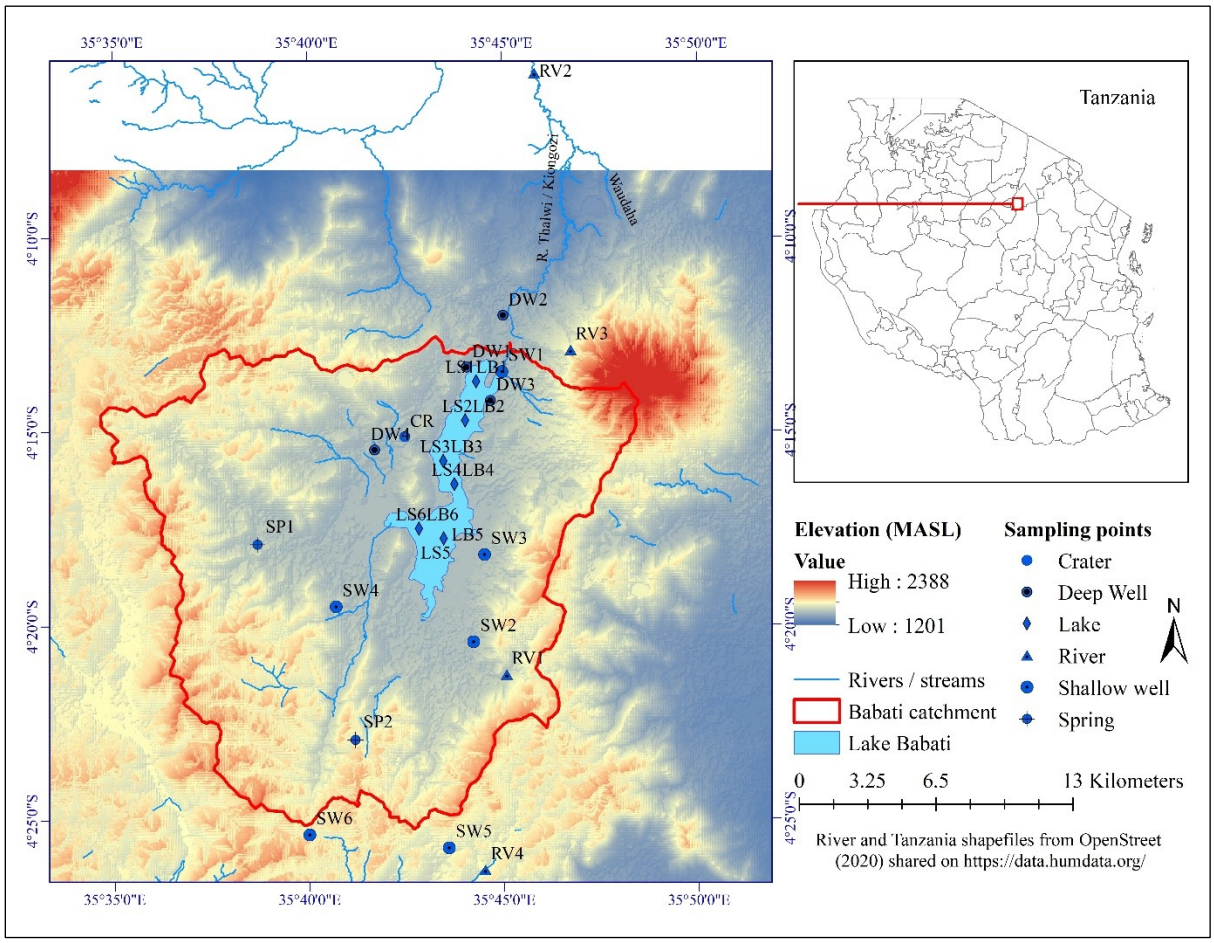

Figure 12: The elevation in Meters Above Sea Level (MASL) with sampling locations of the Lake Babati catchment

3.6 Mapping Groundwater Potential

3.6.1 The General Method and Workflow

While cognizant of the data limitation, this section explored alternative methods to map and classify the GWP while incorporating the spatial variability of the input parameters to support the sustainable development and management of groundwater resources. It applied remote sensing and GIS techniques to explore the nonlinear interactions of topography, geology, land cover, and other catchment properties (connected to recharge), which primarily control the groundwater configurations (Condon & Maxwell, 2015) to map GWP. The study adopted and adapted methods from Andualem and Demeke (2019) and Das *et al.* (2019) to map and zone GWP according to the workflow summarized in Fig. 13.

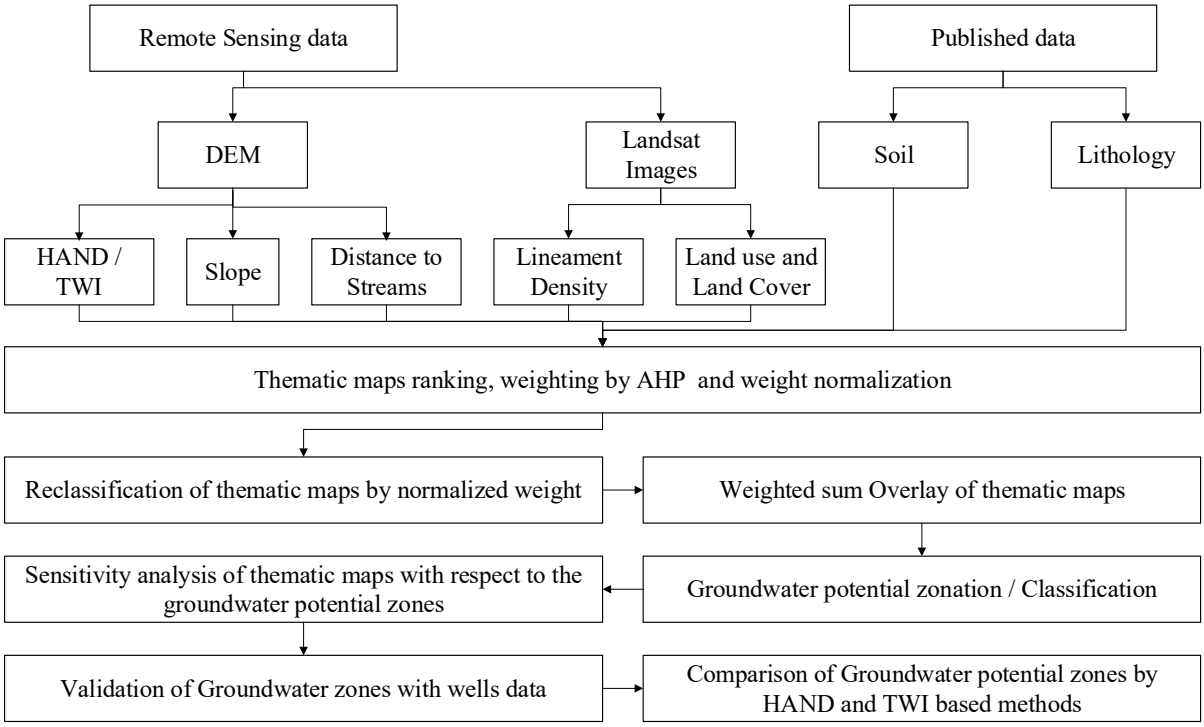

Figure 13: Schematic workflow adopted and adapted from Andualem and Demeke (2019) and Das *et al.* (2019) to map the groundwater potential zones

3.6.2 Lineament Extraction

Lineaments are expressions of geomorphological structures such as cliffs, faults, fractures, joints, terraces, structural ridges, and valley segments that result in vegetation variations, soil moisture content, rocks, or soils (Salui, 2018). The detection of geomorphological features is often based on aerial photographs, satellite images, and shaded relief images created from digital elevation models (Abdullah *et al.,* 2010; Prasad *et al.,* 2013; Salui, 2018). Various scholars (Abdullah *et al.,* 2010; Salui, 2018; Fajri *et al.,* 2019) have used digital elevation models for tectonic geomorphological studies and lineaments.

In all cases, lineament extraction is based on edge detection techniques, which enhance image pixels to detect abnormalities on the Earth's surface. Manual detection using expert opinions has been used, but of late, automatic algorithms are available (Salui, 2018; Berhanu & Hatiye, 2020) to speed up and eliminate the subjectivity involved in manual lineaments extraction. Based on the shaded relief map built on the Shuttle Radar Topographic Mission's 30 m resolution DEM (USGS, 2018), lineaments were extracted using the Line algorithm in PCI Geomatica (PCI, 2019).

Lineament identification from the DEM was initiated by generating eight shaded terrain maps using the Hillshade tool in ArcGIS version 10.5. The first shaded relief map had a solar azimuth set at 0° and an altitude angle of 45° for the sun (light source). From the second to the eighth shaded relief maps, the solar azimuth was set at 45°, 90°, 135°, 180°, 225°, 270°, and 315°, respectively, but the same altitude set for the angle of 45° for the light source was maintained for all as Abdullah *et al.* (2010) applied. Then, as Abdullah *et al.* (2010) executed, two overlay relief

maps were created by combining the relief maps. The first combined shaded relief map (referred to hereafter as the combined shaded relief map 1) had the shaded relief maps with the solar azimuth of 0°, 45°, 90°, and 135° combined using a weighted sum overlay operation. Each map was given equal weight while overlaying (equivalent to merely adding the relief maps). Similarly, the shaded relief maps with solar azimuths of 180°, 225°, 270°, and 315° were combined (summed with each map allocated equal weight) to form the combined relief map 2.

The parameters of the line algorithm elaborated by Salui (2018) were iteratively varied until the derived lineaments from the combined relief maps matched and agreed in direction with some of the faults indicated in the geological map by the Mineral Resources Division (1966). The following optimal parameters were used: Filter Radius (RADI), a specification of the edge detection filter, was set at 10 pixels, while the edge gradient (GTHR), a threshold for the minimum gradient level for an edge pixel, was set at 100 pixels. LTHR (set to 30 pixels) is the minimum wavelength considered a lineament or for further analysis. Three pixels were considered FTHR, the maximum error allowed in pixels when fitting the polyline. The ATHR, the parameter which specifies the maximum angle in degrees, was set to 30 degrees. When the angle exceeds the ATHR, the algorithm divides the polyline into two or three vectors. The DTHR is the minimum distance measured in pixels between the endpoints of two vectors for them to be connected. The DTHR was set at 20 pixels.

Two lineament maps were generated based on the parameter sets described above. The lineaments from combined shaded relief maps 1 and 2 were compared, and the most representative of the observed lineament directions on the geological map by the Mineral Resources Division (1966) was chosen. Rose diagrams of the lineaments were drawn using the Rockworks software showed with ease the general lineaments directions.

A comparison of rose diagrams of lineaments from the combination of shaded relief maps illuminated from different angles is presented in Fig. 14. Most lineaments were oriented in the northwest and southeast directions, with some in the north-south orientation, which agrees with the lineaments identified in the geological map of Babati by the Mineral Resources Division (1966). However, since the rose diagrams are not significantly different, the lineaments derived from shaded relief maps combination illuminated in the 0°, 45°, 90°, and 135° directions were selected for further analysis because they represented the observable lineaments well and had far more lineaments. The lineament density was calculated with the line density algorithm in ArcGIS 10.5 based on the selected shaded relief maps combination.

(a) (b)

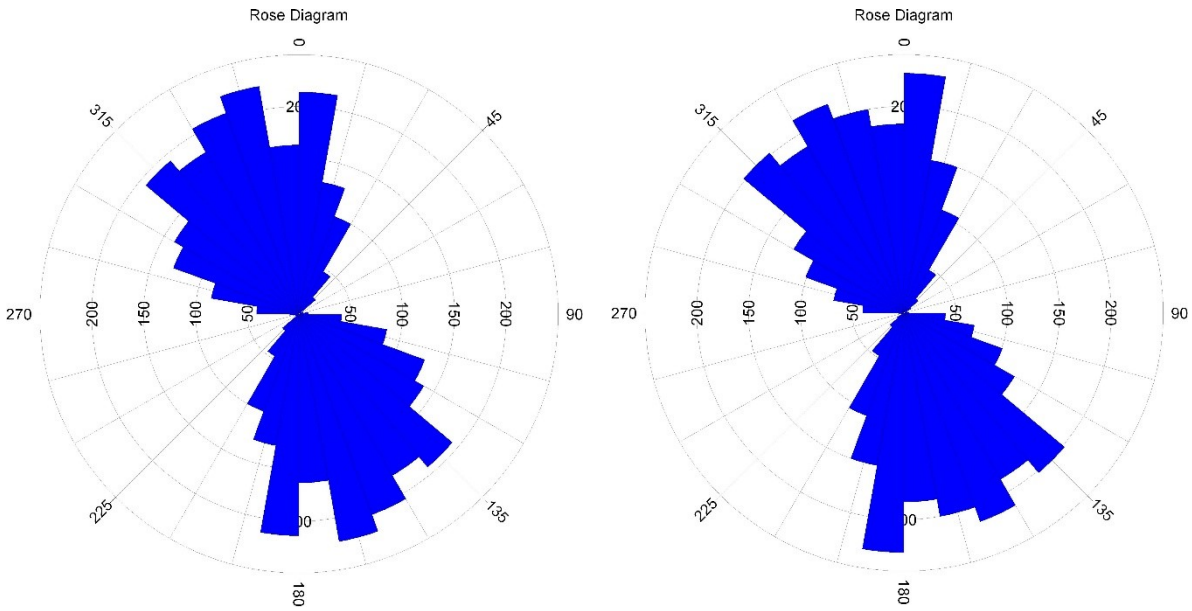

Figure 14: Rose diagram of lineaments derived from the combination of shaded relief maps (a) derived from the combination of shaded relief maps illuminated from 0°, 45°, 90°, and 135°, while (b) is for lineaments derived from shaded relief maps illuminated from 180°, 225°, 270°, and 315°

3.6.3 TWI and HAND Computation

(i) TWI

The TWI was computed based on a 30 m by 30 m resolution DEM obtained from Shuttle Radar Topographic Mission (USGS, 2018). The DEM was first filled to create a depression-less and hydrologically correct DEM using Pit – Removed tools of TauDEM by Tarboron (1997) in the ArcGIS Spatial Analyst tools environment. Based on the filled DEM, the D-infinity flow directions algorithm by Tarboron (1997) for multiple flow directions was applied to determine the grid's possible flow directions and the slope, S. The slope S is a tangent of the slope angle equal to $tan\beta$ in Equation (63). Using the same D – Infinity algorithm, flow accumulation raster (sca) was generated from the flow direction map created earlier. The sca is the specific catchment area in length units (the area of upstream cells that drain into a cell per unit cell width) and equals to the α of Equation (63). The slope S ($tan\beta$) cells with 0 (zero) values were replaced with a small value (0.002) to avoid infinity complications that occur when a number is divided by zero. Finally, using the Raster Calculator, Equation (63)was applied to compute TWI based on the contributing area and the surface slope:

$$TWI = ln\left(\frac{\alpha}{tan\beta}\right) \tag{63}$$

where ln is the natural logarithm, α is the upslope contributing area per unit length of a contour in meters, and $tan\beta$ is the computed local slope, S.

(ii) HAND

The HAND computation was based on the same DEM as the TWI with depressions filled and hydrologically correct DEM. The D – Infinity algorithm by Tarboron (1997) was used to create the flow direction grid, the slope, and the flow accumulation grid. The HAND was determined as the vertical distance in the D – Infinity Distance Down operations using the Taudem ArcGIS toolbox (Tarboron, 1997). Conscious of the sensitivity of HAND to the stream initiation threshold (Gharari *et al.,* 2011), the threshold upslope contributing area for calculating the stream network using the D8 algorithm was fixed at 5000 cells (equivalent to 4.5 km^2). Finally, the distance to streams (drainage) was computed from the same stream network using the Euclidean distance tool in ArcGIS.

3.6.4 Parameter Weighting and Multicriteria Analysis

(i) Parameter Identification

The input parameters considered were the HAND /TWI, geology, land cover and land use, lineaments density, distance to streams, slope, and soil. Although precipitation is a primary source of groundwater recharge, it was assumed to be uniformly distributed in intensity and amount over the catchment due to its small size of only 390 km^2. Therefore, its spatial variation within the catchment was assumed to have no significant differences in GWP.

The numerically based input maps were classified into five groups based on the natural breaks algorithm developed by Jenk (1967), which identifies logical breaks in data and creates groups (classes) by minimizing differences within the same class while maximizing the differences between classes.

The study considered HAND and TWI to represent the same groundwater properties because either parameter was believed to produce the same GWP map. Therefore, the TWI and HAND were weighted equally for a meaningful comparison. Since HAND and TWI are secondary parameters derived from functions related to river networks, the river density was deemed a repetition, but the distance to drainage was used instead.

The present study adopted the multi-influencing criteria which Magesh *et al.* (2012) used to minimize the weighting bias imposed by the researcher's subjectivity. This method assigns verifiable weightings based on the number and perceived strength of influences of the parameters. The interrelationship among the identified multi-parameters influencing the GWP was identified

and classified as a major or minor effect, as presented in Fig. 15. The major effect was weighed as one, whereas a minor effect was weighted as 0.5. Finally, the weights of each parameter were summed and provided as representative weights in Table 9. From this comparison, geology emerged as the most important with a representative weight of 3.5, followed by HAND / TWI with a representative weight of 3. According to the weighting, the least important parameter was the lineament density, and land use and land cover, each with a representative weight of 1.5.

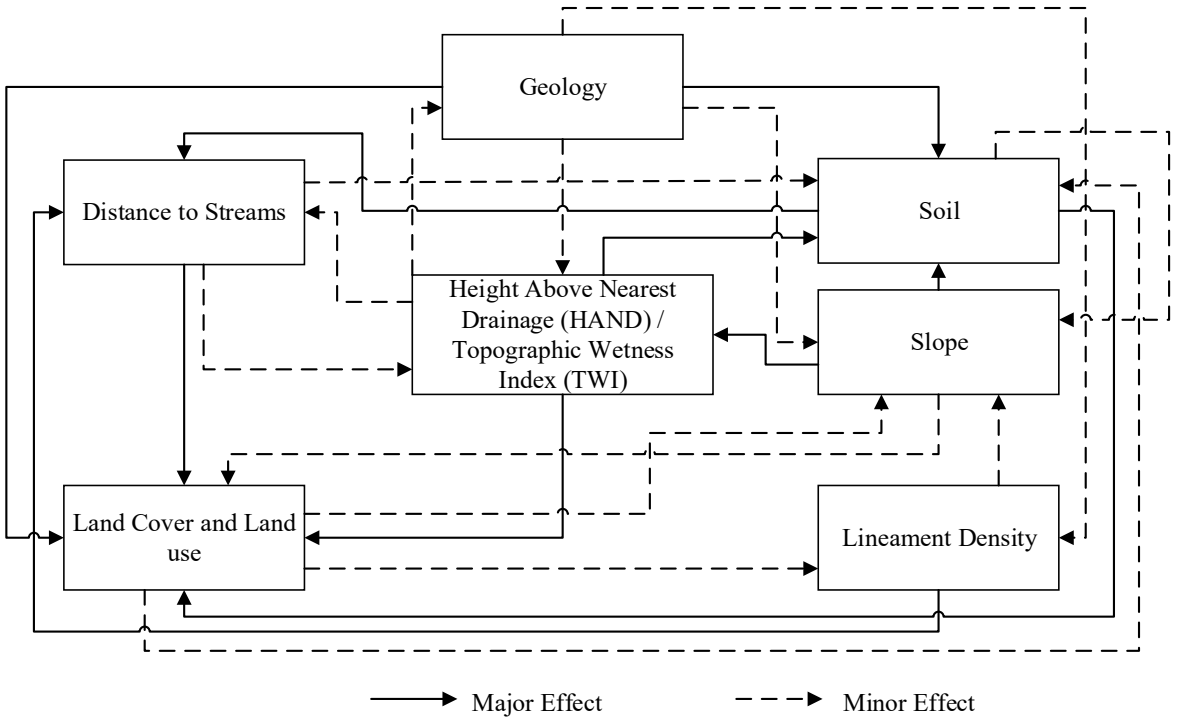

Figure 15: Interrelationship among different parameters identified to influence groundwater potential

(ii) Parameter Weighting

Several multi-criteria decision-making methods, including Fuzzy Logic, Artificial Neural Network, and the Analytical Hierarchy Process (AHP) developed by Saaty (1987), are available to analyze complex issues. Each method has its strengths and weaknesses, which Ishizaka (2014) elaborates very well. The AHP is commended for its prowess in consistently capturing both the subjective and objective parts of the complex decision-making process to allow process evaluation and feedback. However, the AHP is criticized for harbouring imprecise and subjective assessment of parameters resulting from vague linguistic assessments (Ishizaka, 2014; Reig-Mullor *et al.,* 2020). The Fuzzy – Analytical Hierarchy Process (FAHP), which combines the benefits of the Fuzzy logic method and AHP (Ishizaka, 2014), is viewed as an improvement of the AHP. However, Mallick *et al.* (2019) noted that integrating the flexibility of the fuzzy membership achieved using FAHP does not improve the accuracy of the resultant GWP maps. Therefore, despite the limitation, the AHP method, motivated by its popularity in natural resources management, suitability analysis, and site selection, where multiple parameters influence a

decision (Malczewski, 2006; Das *et al.,* 2019; Mallick *et al.,* 2019; Saranya & Saravanan, 2020) was applied for parameter weighting to reduce biases.

The parameters were arranged in rows and columns (as in Table 9). Then, the pairwise matrix was developed by dividing the weight of each row parameter against the weight of the column parameter to determine the relative weight of each parameter influencing GWP. The diagonal gives the relative importance of 1 (Table 9), meaning equal importance because the parameter is compared against itself. Similarly, each of the five parameter classes (for numerical parameters such as HAND and TWI) and parameter types such as geology were ranked based on the relative importance of the Saaty (1987) scale. For example, the most important parameter for groundwater availability received a scale of 9, while the least important parameter was given a scale of 1. The final decision on the input parameters' weighting was informed by the researchers' opinions and literature, including Arulbalaji *et al.* (2019) and Mallick *et al.* (2019).

The normalized parameter weight was obtained by dividing its geometric mean by the sum of the parameters' geometric means. The pairwise matrix of relative importance was accepted if it had a consistency ratio of less than 0.1. Otherwise, another matrix was developed, and normalized weights were recomputed after eliminating errors or using different weights altogether. Finally, the consistency index was used to check the matrix for errors or subjectivity in assigning relative weights and was calculated using Equations (64) and (71) (Shekhar & Pandey, 2014).

$$CI = \frac{\lambda_{max} - n}{n} \tag{64}$$

$$CR = \frac{CI}{RCI} \tag{65}$$

where RCI is the random consistency index by Saaty (1987) and depends on the number of parameters, λ_{max} is the maximum eigen value of the pairwise matrix and n is the number of parameters considered.

Table 9: Pairwise comparison matrix of parameter weights and computation of normalized parameter weight

	Representative weight	HAND /TWI	Geology	LULC	Lineament Density	Drainage Density	Slope	Soil	Geometric mean	Normalized weight
HAND/TWI	3	1.00	0.86	2.00	2.00	1.50	1.20	1.50	1.37	0.19
Geology	3.5	1.17	1.00	2.33	2.33	1.75	1.40	1.75	1.60	0.22
LULC	1.5	0.50	0.43	1.00	1.00	0.75	0.60	0.75	0.69	0.09
Lineament Density	1.5	0.50	0.43	1.00	1.00	0.75	0.60	0.75	0.69	0.09
Distance to stream	2	0.67	0.57	1.33	1.33	1.00	0.80	1.00	0.92	0.13
Slope	2.5	0.83	0.71	1.67	1.67	1.25	1.00	1.25	1.14	0.15
Soil	2	0.67	0.57	1.33	1.33	1.00	0.80	1.00	0.92	0.13

LULC = Land use and land cover. The table presents the representative weights (sum of major and minor effects) based on the multi influencing criteria applied by Magesh et al. (2012), the AHP pairwise weighting of the relative weights, geometric mean, and the normalized weights of each parameter class and types.

(iii) Multicriteria Analysis and Map Overlay

We opted for the normalized and weighted sum overlay analysis of the input layers (thematic maps) among the different multi-criteria analysis techniques because it is popular (Andualem & Demeke, 2019; Hamdani & Baali, 2019; Tolche, 2020). First, the thematic maps were reclassified by assigning each class with a score of influencing parameters, as presented in Appendix A to Appendix H. Then, using the Raster Calculator in ArcGIS 10.5, the groundwater potential index (GWPI) map was computed using the weighted sum overlay concept expressed in Equation (66) adopted from Tolche (2020). The resultant GWP map was categorized into five classes: Very Good, Good, Moderate, Poor, and Very Poor classes of GWP zones based on Jenk's natural break algorithm (Jenk, 1967).

$$GwPI = \sum_{j=1}^{m} \sum_{i=1}^{n} W_j X_i \tag{66}$$

where W_j is the normalized weight of the parameter given in Table 9 and X_i the thematic map i reclassified according to the weights of the parameter classes. $GwPI$ is the Groundwater Potential Index [-], the subscript j is the count of parameters, m is the total number of parameters, subscript i is the count of classes within each parameter, and n is the total number of parameter classes.

3.6.5 Sensitivity Analysis of Parameters

The sensitivity of the input parameters was tested using a method adopted from Mallick *et al.* (2019), which compares the theoretical weight assigned and the parameter's effective weight (EW) as expressed in Equation (67).

$$EW = \frac{W_j \times X_j}{GwPI} \times 100 \quad (67)$$

where W_j is the normalized weight of the parameter j, and X_j the thematic map of the parameter j is classified by class weight, and $GwPI$ is the GWP indices computed by Equation (66).

3.6.6 Validation of the Groundwater Potential Zones

The study used a correlation analysis of the depths to the water levels and the wells' depths with GWP to validate the GWP classification. Test pumping results would be a good alternative for validating GWP classification; however, no test pumping was carried out on the available shallow wells. Test pumping is so expensive and was outside the budget of this study.

3.6.7 Comparison of Groundwater Potential Maps

In the absence of an agreed-upon method for comparing raster maps (Grabs *et al.,* 2009), the present study used Cohen's kappa coefficient, producers' accuracy, and users' accuracy to determine the degree of agreement between the GWP zones developed based on the two methods. The maps' agreement was compared on a cell-by-cell basis. The Kappa coefficient provides an overall assessment of the agreement. A negative Kappa coefficient implies a lower comparison than a random predictor, while a Kappa coefficient of 1 means a perfect agreement (Grabs *et al.,* 2009). In addition, the producer's and user's errors have been determined to gain insights into agreements between different classes. The methods of determining these measures of agreement and comparisons have been elaborated on earlier in Section 3.2.8.

CHAPTER FOUR

RESULTS AND DISCUSSION

4.1 Drivers of Lake Babati level

4.1.1 The Lake Babati Water Level History and Variability

Since gauging Lake Babati in 1964, the water levels have fluctuated. Before 1970, the records showed that the lake level varied between 1 - 14 m deep, while after 1975, the lake depth varied within a narrower range of 3 – 9 m. A Pettit test for homogeneity for the water level after 1975 was significant (p-value < 0.01) as the mean water level shifted from 5.461 m between 1976 and 1991 to 4.829 m between 1991 and 2020, as shown in Fig. 17. The Pettit test revealed July 14, 1991, as the date of shift (Fig. 17). The shift followed a 1990 flooding of Lake Babati that caused severe damage. After the 1990 flood, 13 large culverts with an estimated flow rate of 4 m^3/s were installed lower than the previous outflow levels to help relieve the lake of excess water (Sandstrom, 1995). Mbanguka *et al.* (2016) studied the variability in the lake levels from 1978 to 2012 and noted the records as disjointed into two periods. The first period from 1978 – 1984 was reported with an average level of 5.27 m, while 2008 – 2012 had an increase in average levels to 5.75 m. Their analysis deviated from this study because they did not utilize or access the lake level records between 1984 and 2008.

Based on the homogenous lake level records from September 26, 1976, to December 31, 2020, the Mann-Kendall analysis revealed that Lake Babati level is undergoing a significant ($p < 0.05$) decline (Fig. 18). Furthermore, Sen's slope (Table 11), a non-parametric method that accounts for the effects of the outliers and gross errors on the trend, indicated an overall lake level decline of 0.025 m yearly. Apparently, this is the first quantification of the lake level decline, as previous studies were concerned with lake flooding (Sandstrom, 1995; Sjoin, 2010) and the general lake level variability (Mbanguka *et al.,* 2016). Subsequent analysis of the lake levels aggregated at monthly and seasonal time steps showed significant lake level declines (p-value < 0.05) in all the months and seasons, as summarized in Table 11. The lake's level decline in other months was insignificant (p-value > 0.05). Contrary to expectations, both rainy and dry seasons experienced a decline. The minor rainy season (from October to January), characterized by higher temperatures, experienced a lake level decline of 0.021 m, comparable to the major rainy season lake level decline of 0.022 m given by the Sen's slope (Table 11). The subsequent sections analyzed the exact driver of the lake level decline in both rainy and dry seasons. Whereas lakes in the region, such as Lake Manyara, further downstream of Lake Babati, have shown variability in levels, reflecting the high and low rainfall seasons (Deus *et al.,* 2013), none has consistently declined in lake levels, even in rainy seasons. The decline observed was unique to Lake Babati.

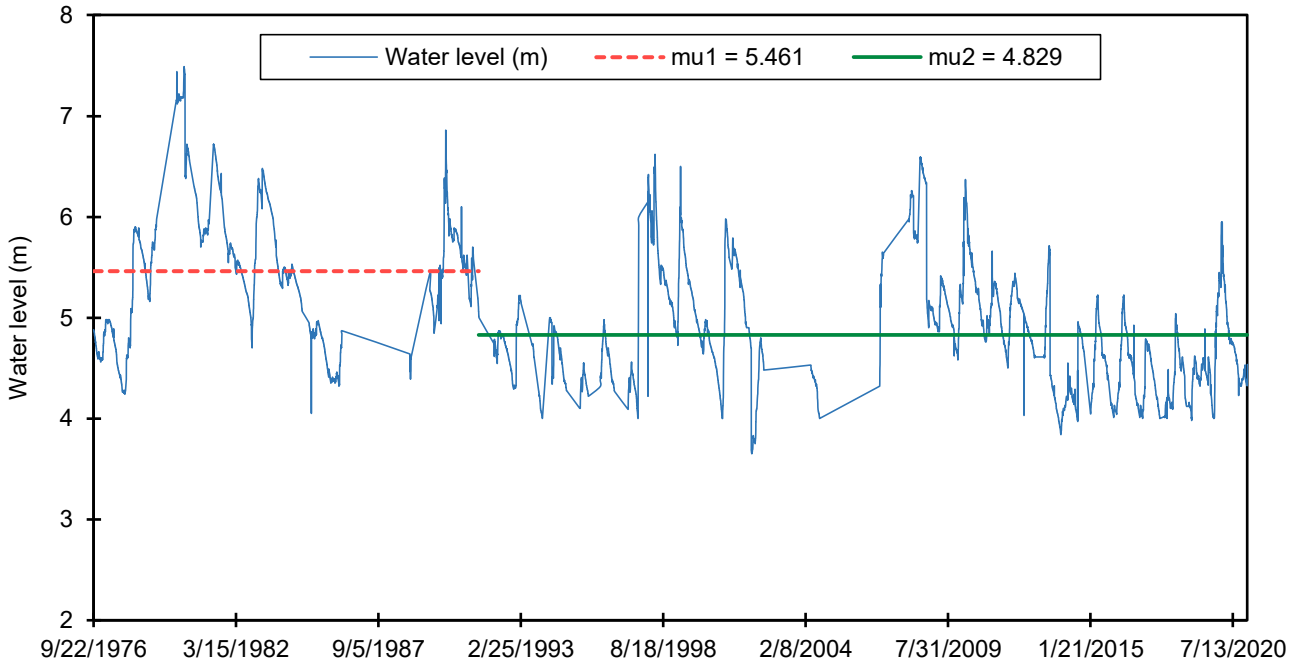

Figure 16: Homogeneity test of the water level records of Lake Babati. The mu1 is the mean lake level before July 8, 1991, while mu2 is the mean lake level from April 1992 to 2020

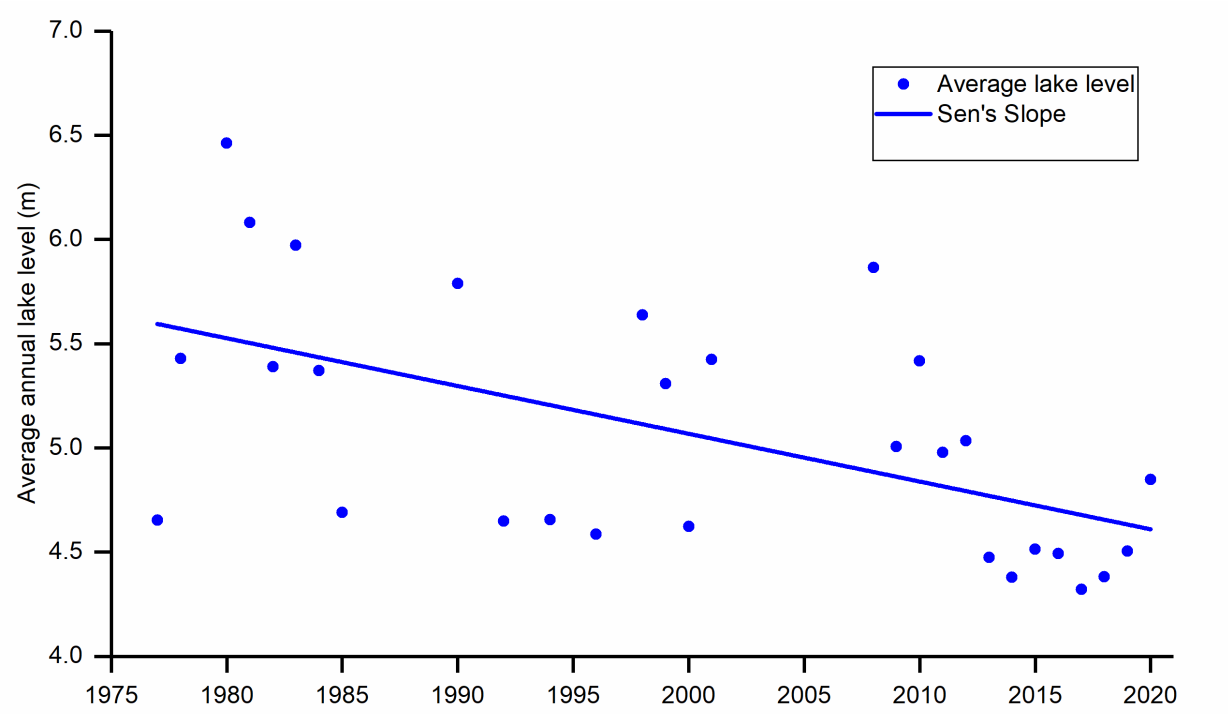

Figure 17: Trend of average annual lake levels

4.1.2 Spatial Rainfall Variability

The Spearman rank correlation analysis of rainfall records from nearby Mbulu and Dongobesh Secondary School climatic stations (shown in Table 10) revealed that Babati rainfall was positively correlated with the neighbouring stations at *p*-value < 0.01 significance levels. The computed Spearman rank correlation is higher than the critical r - values of 0.195 and 0.254 for 95% and 99% confidence intervals. The positive correlation indicated that higher precipitation in either of

the stations implied higher precipitation at Babati and vice versa. Figure 18 compares the average monthly rainfall of Babati and the neighbouring climatic stations.

Whereas rainfall at Babati station showed a positive correlation with the neighbouring stations, the correlation was weak at daily time steps. For example, rainfall records at Mbulu station, the most strongly correlated to Babati at daily time step (r = 0.4716), could explain only 22.24% (r^2 =0.2224) of the rainfall observed in Babati. In comparison, only 16.77% (r^2 = 0.1677) of rainfall measured at Dongobesh station matched the observations at Babati. Similarly, MERRA – 2 (NASA) precipitation records explained only 19.76% (r^2=0.1976) of the rainfall variations observed in Babati. Babati rainfall did not strongly correlate with the neighbouring Mbulu rainfall stations at a daily time step. Instead, the records showed very distinctive statistics at daily time steps (Table 10), implying they were unsuitable for filling in the missing daily rainfall data at Babati. These findings agreed with Mbanguka *et al.* (2016), who also observed a poor correlation of rainfall at Babati meteorological station with its neighbouring stations like Haubi Mission, Galappo Mission, and Mbulu. Mbanguka *et al.* (2016) suggested that different processes and terrain could be responsible for the rainfall variations observed in the area.

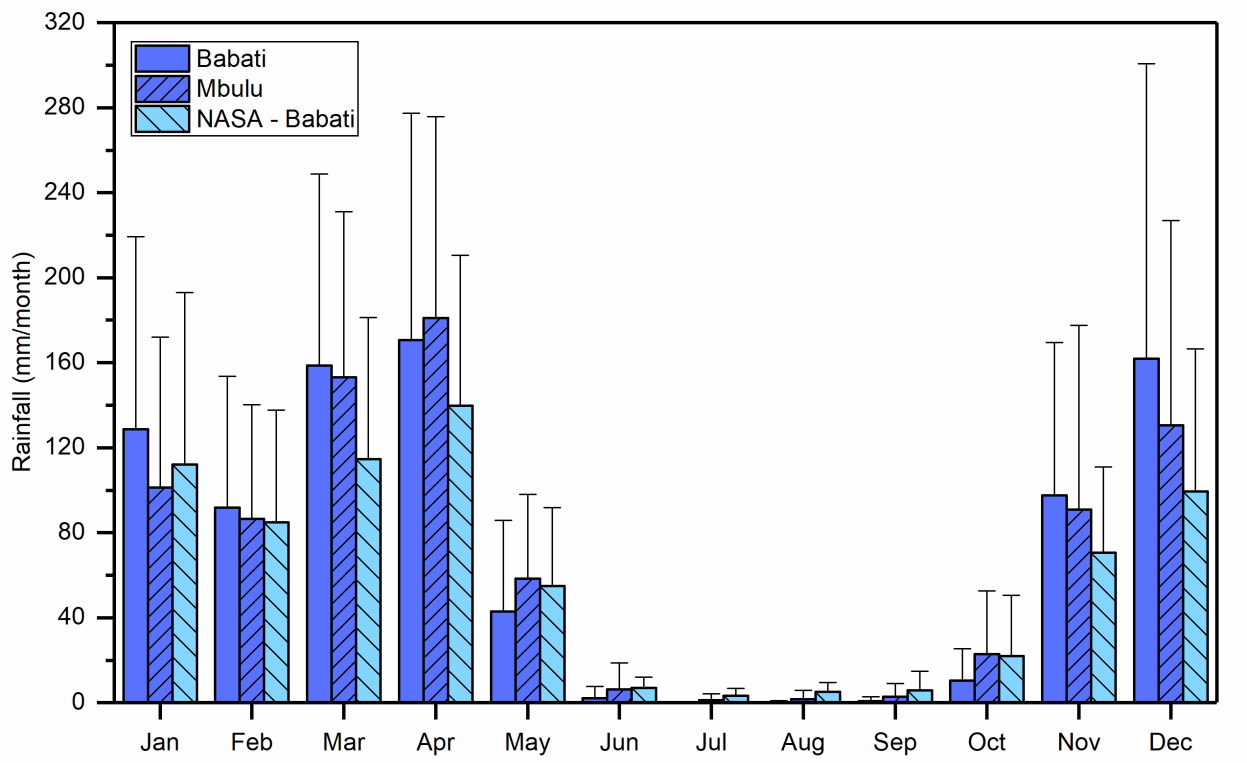

Figure 18: Comparison of monthly rainfall received in the area based on rainfall records of Babati and NASA from 1980 - 2020 (The limit of the whisker is plus one standard deviation) (MERRA 2 and TMA)

Table 10: Spearman's rank relationship between Babati station with other neighbouring stations

Stations compared	Daily time step		Monthly time step		Annual time step	
	Spearman rank correlation coefficient, r_s	Coefficient of correlation r_s^2	Spearman rank correlation coefficient, r_s	Coefficient of correlation r_s^2	Spearman rank correlation coefficient, r_s	Coefficient of correlation r_s^2
NASA and Babati	0.4445	0.1976	0.8591	0.7381	0.4649	0.2161
Babati and Mbulu	0.4716	0.2224	0.8807	0.7757	0.5071	0.2572
Babati and Dongobesh	0.4095	0.1677	0.8616	0.7423	0.6500	0.4225

However, correlations of rainfall between neighboring stations improved at the monthly time steps and became significant (p-value < 0.01). The Spearman's rank correlation coefficient of Mbulu and Babati improved to 0.8807, implying that Mbulu rainfall records explained 77.57% (r^2 = 0.7757) (Table 10) of the observed rainfall variations at Babati. Correlation with other rainfall stations equally improved. The monthly rainfall at Dongobesh and NASA explained 74.23% and 73.81%, respectively, of the monthly rainfall variations in Babati.

The correlation between Babati and Mbulu, Dongobesh, and NASA dropped to 25.72%, 42.25%, and 21.61%, respectively, when the precipitation data were aggregated into annual time steps. Furthermore, the best Spearman Correlation coefficient r_s was only 0.65 for Babati and Dongobesh stations. At the same time, the correlation between Babati and Mbulu dropped to 0.5071 at the annual time step compared to 0.8807 at the monthly time step. This means data from different stations were relevant for gap-filling the Babati rainfall records at a monthly time scale.

The stronger correlation in monthly rainfall between different stations may suggest that the influence of regional factors wanes with higher time steps. The variations in correlation at daily and monthly time steps suggested that regional factors such as the Inter-Tropical Convergence Zones could be driving the monthly and seasonal rainfall. The daily rainfall distribution may also be modified by location-specific factors such as topography due to mountains and rift valley escarpments. For example, all the stations experienced the positive IOD of 1997 and 2006, which brought extreme rainfall recorded by all the stations. The influence of IOD was also reported by Awange *et al.* (2016), who observed a strong correlation between the hydrological droughts in the Great Horn of Africa and IOD. Therefore, daily precipitation records from NASA, Mbulu, and Dongobesh stations were unsuitable for gap-filling Babati precipitation records. Instead, the monthly rainfall recorded at Dongobesh and Mbulu stations was used for gap-filling where necessary. Where monthly records for Dongobesh and Mbulu stations were insufficient, NASA precipitations were used.

4.1.3 Rainfall Trend and Influence on Lake Level Variability

The lake level increases in the rainy season and recedes in the dry season (Fig. 20), suggesting that rainfall is responsible for some variations. However, the relationship between lake level and rainfall was neither direct nor linear, probably because of the time delay between rainfall and runoff peaks. Whereas the peak lake level corresponded to periods of high rainfall, the peak did not occur precisely on the day of rainfall but was offset (or delayed). This suggests that peak lake levels may be due to runoff, which is often delayed from the rainfall due to catchment processes.

A deeper assessment of the rainfall variability using the Mann-Kendall statistics and Sen's slope (shown in Table 11) indicated no significant decline or increase in rainfall. However, some

insignificant decline was observed in April, May, and November. Similarly, Sen's statistics indicated an insignificant decline (p-value >0.05) in the rainy season (October through May). Generally, no significant trends were observed in rainfall either seasonally or annually. As Sandstrom (1995) reported earlier, no significant trends could be discerned in the catchment rainfall. This implied that the trends of lake level declines could not be due to rainfall as rainfall showed no significant trends before and after 1995.

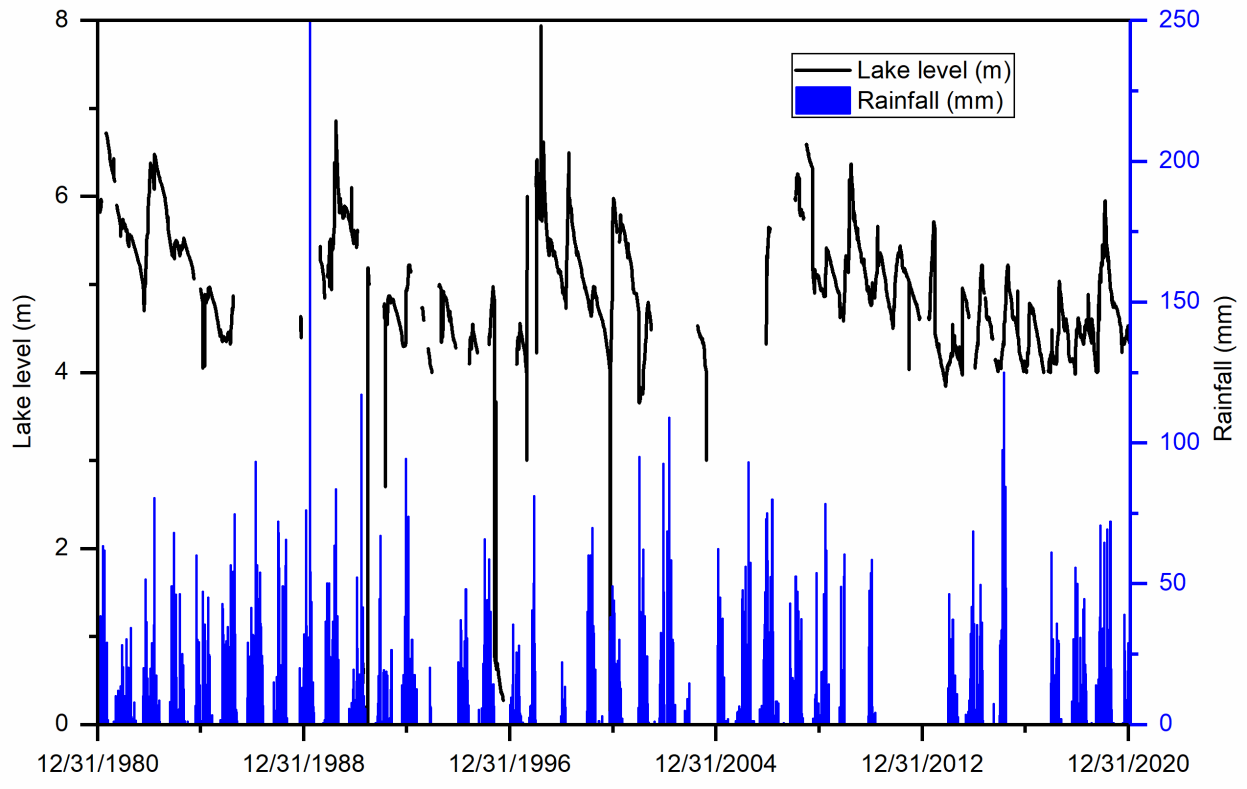

Figure 19: Comparison of water level against daily rainfall from 1980 - 2020

The precipitation was averaged over varying periods using the moving average method and correlation with the lake level measured. The precipitation showed a weak and insignificant positive correlation (p-value > 0.05) with the lake level at the monthly time step. The best correlation occurred when the rainfall was averaged over nine months (Fig. 21). At 18 months moving average period again, the correlation was as good as at nine months; thus, the sequence was doubled. This suggested that the residual influence of the rainfall has a nine months delay or period in driving the lake levels.

Table 11: Summary of the Mann-Kendall trend test statistics of the monthly and seasonal Lake Babati levels and rainfall observed at Babati

Series\Test	Lake Babati Level (m)			Babati Rainfall (mm)		
	Kendall's tau	p-value	Sen's slope	Kendall's tau	p-value	Sen's slope
Jan	-0.310	0.015	-0.026	0.103	0.442	1.574
Feb	-0.290	0.023	-0.023	0.109	0.390	0.980
Mar	-0.300	0.026	-0.020	0.067	0.610	0.577
Apr	-0.310	0.006	-0.021	-0.117	0.404	-1.460
May	-0.359	0.000	-0.030	-0.145	0.269	-0.548
Jun	-0.308	0.016	-0.020	-0.040	0.804	0.000
Jul	-0.359	0.004	-0.023	-0.193	0.225	0.000
Aug	-0.333	0.001	-0.022	-0.109	0.491	0.000
Sep	-0.335	0.001	-0.021	0.080	0.644	0.000
Oct	-0.382	0.007	-0.021	0.003	1.000	0.000
Nov	-0.384	0.004	-0.021	-0.013	0.944	-0.081
Dec	-0.360	0.007	-0.026	0.080	0.591	1.663
Annual	-0.468	0.000	-0.025	-0.046	0.758	-2.233
Minor Rainy (ONDJ)	-0.394	0.001	-0.021	0.072	0.637	2.068
Major Rainy (FMAM)	-0.324	0.005	-0.022	-0.094	0.505	-1.858
Rainy (ONDJFMAM)	-0.387	0.000	-0.020	-0.093	0.528	-4.337
Dry (JJAS)	-0.363	0.02	-0.020	-0.100	0.509	0.000

ONDJ is the Minor wet season from October to January, FMAM means February, March, April and May, ONDJFMAM is wet season from October to May and JJAS are dry months of June, July, August and September

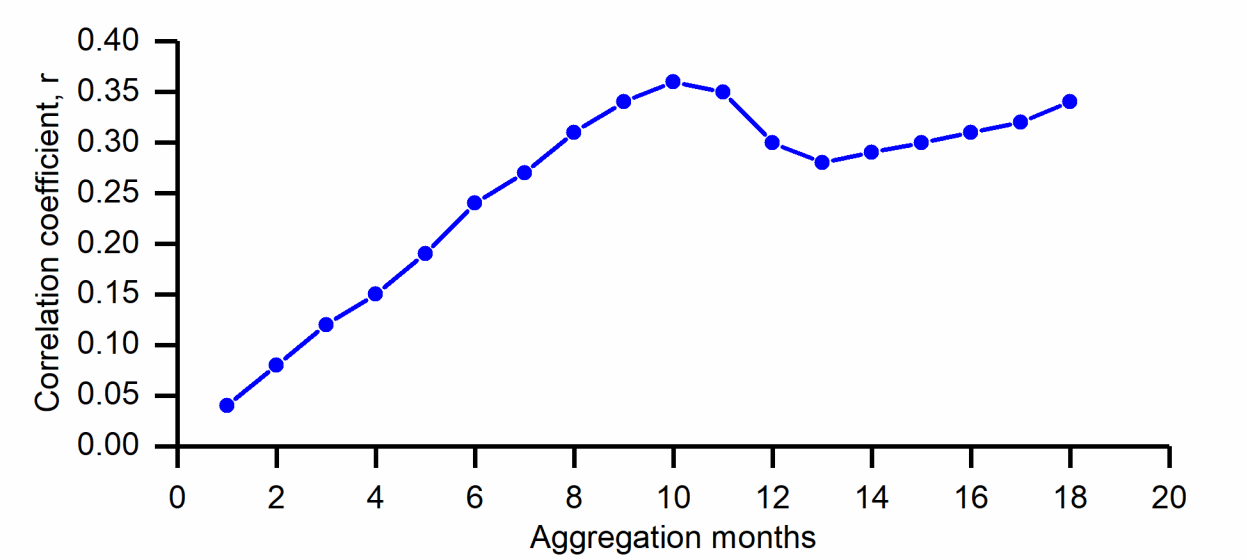

Figure 20: Variation of correlation coefficient r with rainfall at different aggregation levels with the mean monthly lake level

4.1.4 Trend Analysis of the Temperature and other Climatic Parameters

(i) The Maximum Temperature

During the 1980 – 2020 period, the daily maximum temperature showed no significant change except in August, September, and October, when the temperatures rose significantly (Fig. 22). Annually, no significant rise was observed; however, in the dry season between June to September, a significant rise (p-value <0.05) in maximum temperature was observed.

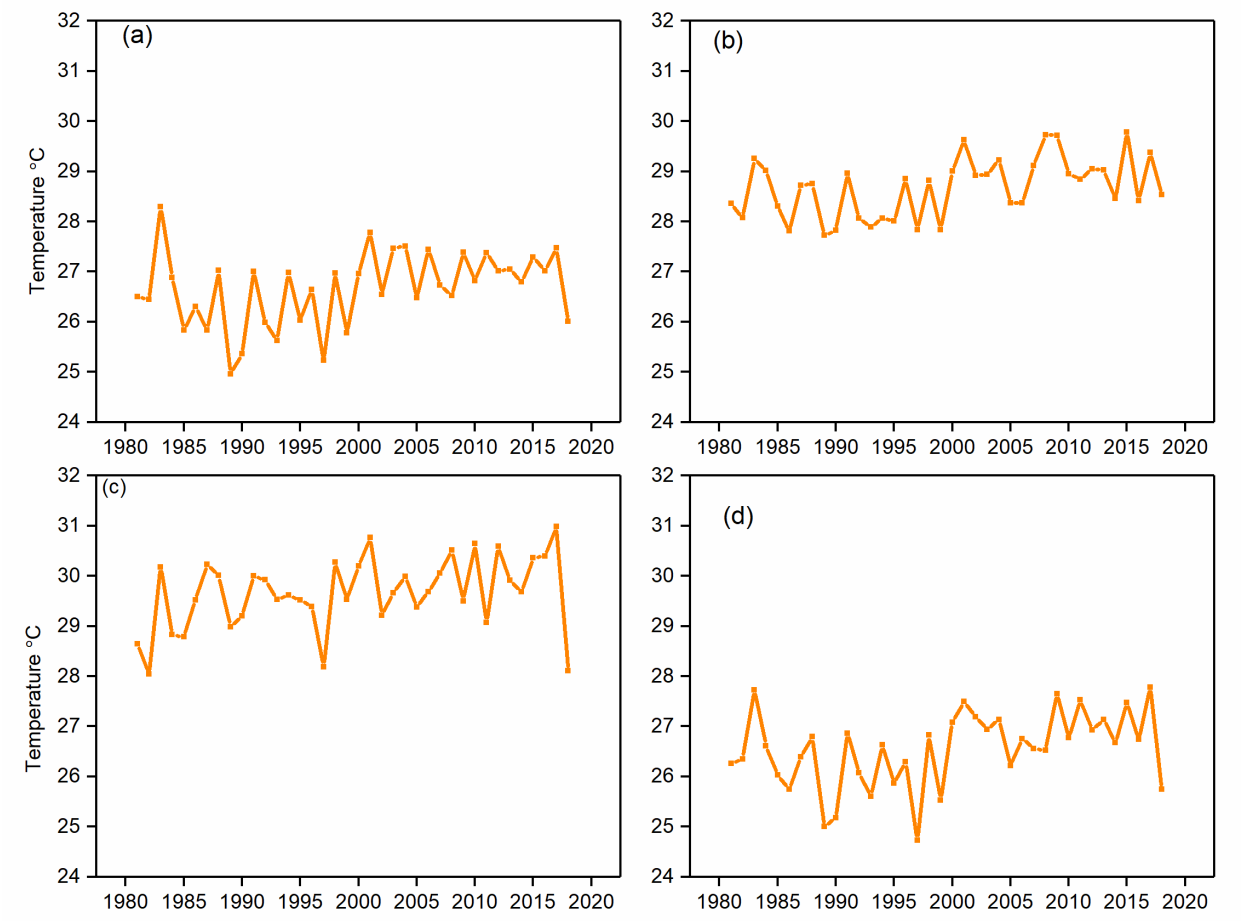

Figure 21: Variation of maximum temperature for months that show the significant change (°C): (a) is for August, (b) for September, (c) for October, and (d) for the dry season, which runs from June to September

(ii) The Minimum Temperature

The daily minimum temperature from 1980 – 2020 showed significant changes for most of the year, with February, June, July, August, September, October, November, and December showing a significant increase (p-value < 0.05). Most of the increments occurred after 2000, as captured in Fig. 23. Consequently, in all the rainy and dry seasons, the increase in the minimum temperature has a high potential to increase the evaporative power of the atmosphere and the drought severity in the study area.

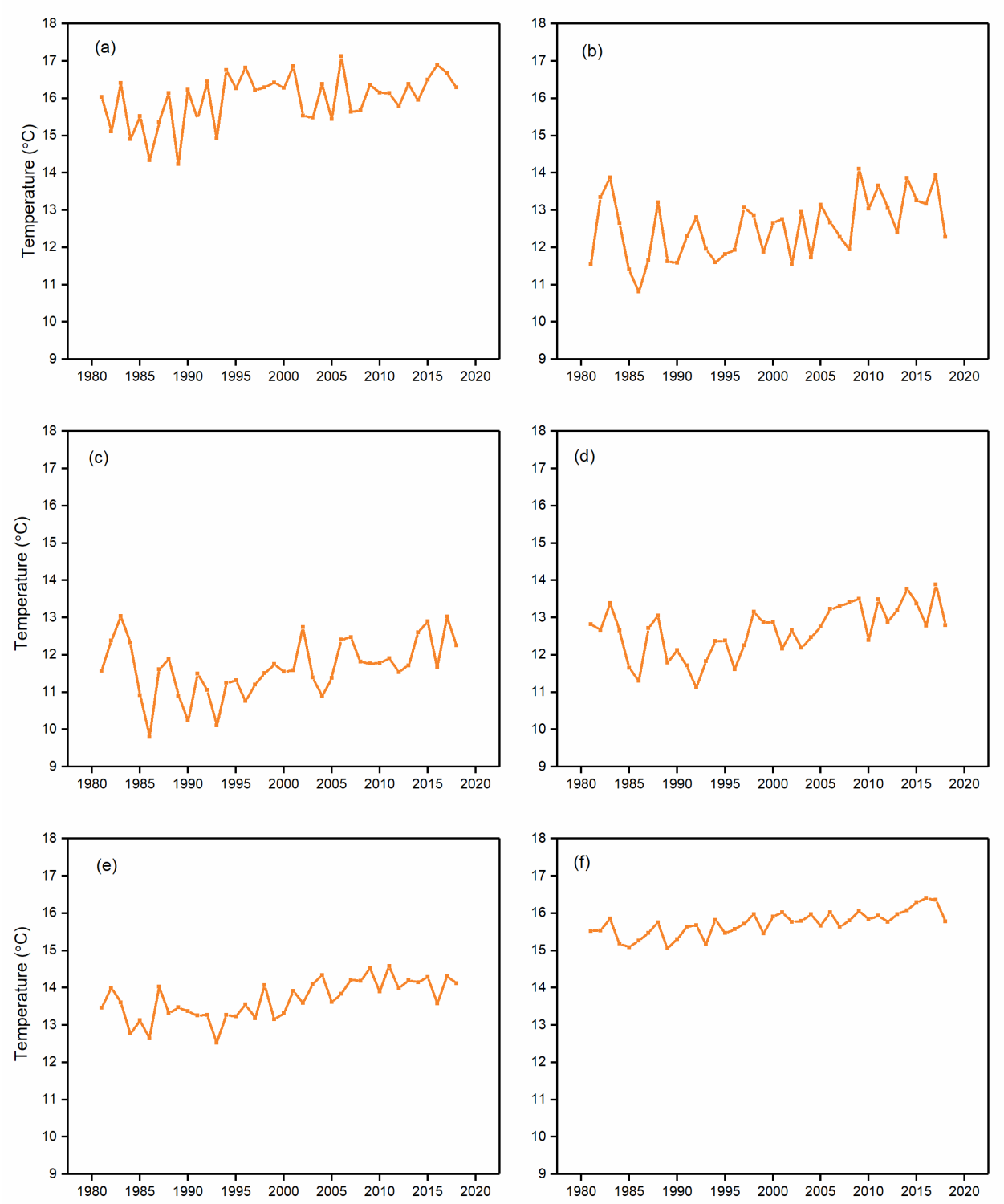

Figure 22: Plots of months through years with significant increases in the minimum temperature. Figure (a) is a plot of temperature in February, (b)in June, (c)in July, (d) in August, (e) in September, and (f) for the rainy season from October to May of the following year

(iii) The Wind Speeds

For most of the year, the wind speed significantly reduced (p-value < 0.05) in January, March, April, May, July, October, November, and December. Thus, the wind speed showed an annual reduction, as depicted in Fig. 24.

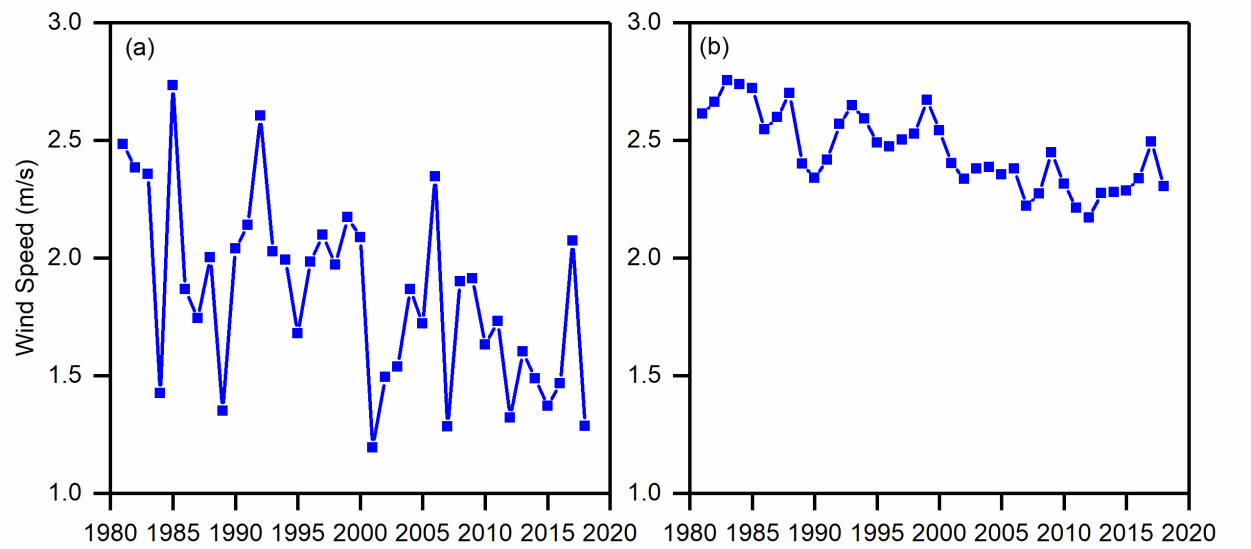

Figure 23: Plot showing the variation of the wind during January in (a) and the annual average in (b) over the years

(iv) Trends of Potential Evapotranspiration

The trends of evapotranspiration computed by Penman and Hargreaves were analyzed. Both methods agreed that March experienced a significant decline in potential evapotranspiration. Evapotranspiration declined in January, February, April, June, August, November, and December but was insignificant (p-value > 0.05). Only May, July, and October showed an insignificant increase in potential evapotranspiration computed using Penman-Monteith. From the Hargreaves method, January, February, November, and December indicated an insignificant reduction. Evapotranspiration significantly declined (p-value < 0.05) in July, while May, June, August, September, and October experienced an insignificant increase (p-value > 0.05). The time series generally showed no significant change in trend.

Generally, in the Mann-Kendall trend analysis of the wind, the minimum and maximum temperatures showed no significant trend in the maximum temperature. In addition, the relative humidity over the years remained constant except in March, when it significantly increased. The significant decline in evapotranspiration in March might be related to the high relative humidity reported in March. The insignificant trends in evapotranspiration in other months appear realistic since temperature, relative humidity, and wind speed, as drivers of evapotranspiration, showed no significant trends.

(v) Lake Evaporation

Since the lake evaporation was not monitored, it was computed using the Penman-Monteith formula. The lake evaporation varies from a minimum of 158.4 mm per month in June 1990 (dry and cold season) to a maximum of 286.3 mm per month in October 1987 (dry and hot season),

while the monthly mean and median were 216.6 mm and 218.0 mm, respectively. The slight difference between the mean and median implies stable lake evaporation with few outliers.

Seasonal and interannual trend analysis using Mann-Kendall showed an insignificant decline in lake evaporation. An insignificant increase was observed in the dry season months of February, May, June, July, August, September, and October, while January, March, April, November, and December (rainy season) showed an insignificant decline in lake evaporation. In addition, the minor and major rainy seasons experienced an insignificant decline in evaporation, while dry seasons experienced an insignificant increase in lake evaporation. Generally, no significant change has been observed in lake evaporation since 1981.

4.1.5 Drought and Lake Level Variations

(i) Comparison of Drought Indices

The evapotranspiration computed by both methods was strongly correlated (r = 0.8879) (Fig. 25), translating to r^2 of 0.7884. This meant that the potential evapotranspiration from the Hargreaves method explained 78.84% of the variations in the potential evapotranspiration by the Penman-Monteith method. Indirectly, this implied that the climatic parameters of wind speed and sunshine hours account for about 21.16% of evapotranspiration. This considerable influence suggested that these parameters are important in estimating the evaporative power of the atmosphere in the study area.

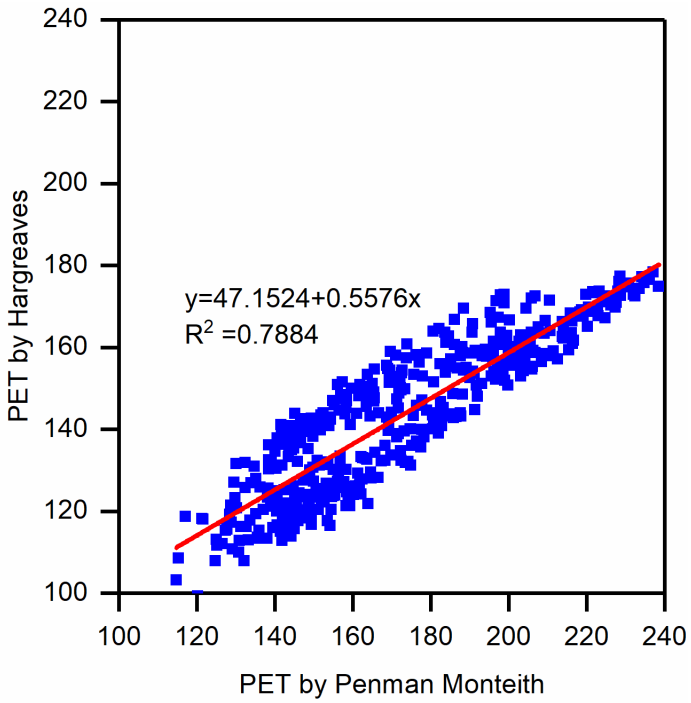

Figure 24: Correlation between evapotranspiration computed using the Penman-Monteith method and the Hargreaves method

(ii) Drought Temporal Variations

The temporal drought variation was assessed at different aggregation levels. As a result, the drought severity by SPEI and SPI varied considerably, as presented in Table 12. The differences in extremities were probably because of how the two methods computed the drought and wet extremities. However, SPEI and SPI agreed that January 2017 was the wettest month, probably because of the extremely wet conditions driven by excess rainfall but minimal evapotranspiration influence.

This study compared the regression of water level and the SPEI based on evapotranspiration computed using Penman-Monteith and Hargreaves. The slope of the regression was insignificantly different (*p*-value of 0.8795). Therefore, using evapotranspiration computed by either Penman-Monteith or Hargreaves method to calculate the SPEI did not result in statistically different drought severity and wetness extremities. The wind speed was generally low in the area, with the sunshine hours averaging five hours per day. This probably made the Penman-Monteith method yield no better results than the Hargreaves method, which computes evapotranspiration using only the minimum and maximum temperature. In addition, the reported reduction in the wind speed was perhaps countering the influence of increased minimum and maximum temperature (discussed in Section 4.1.4) to increase potential evapotranspiration. Nonetheless, the Penman–Monteith method offered a more comprehensive approach to compute drought. It considers the additional influence of winds, humidity, and aerodynamic resistance of vegetation on evapotranspiration, which the Hargreaves method omits.

Table 12: Extreme drought and wet periods determined by the different methods: SPEI_Hargreaves is the SPEI based on Hargreaves, and SPEI_Penman is based on the Penman-Monteith method

Methods	Driest condition		Wettest condition		Driest condition		Wettest condition	
	1 Month	When	1 Month	When	3 Month	When	3 Month	When
SPI					-5.56	May-2011	2.66	Jan-2017
SPEI_Hargreaves	-3.50	Jun-2002	2.42	Jan-2017	-2.24	May-2011	2.27	Jan-2017
SPEI_Penman	-2.47	Aug-1983	2.37	Jan-2017	-2.33	Sep-1983	2.25	Jan-2017

The Mann-Kendall trend tests (Table 13) on the SPEI and SPI indicated no significant change in the drought severity at a 5% significance level. This agrees with Keijzer (2020), who observed no clear trend in the drought severity time series of Lake Manyara but noted an increase in drought frequency in the last century. However, this study noted an exception with the SPEI based on the Penman-Monteith computed evapotranspiration, which indicated a significant increase in drought when SPEI was aggregated at a time scale longer than 6 months.

Table 13: Mann - Kendall trends of the drought indices aggregated at different time scales

Sample	Z	n	S	Var(S)	Kendall's tau	p-value
SPEI_Penman_1mon	0.3161	433	952.00	9 051 428	0.0102	0.7519
SPEI_Harg_1mon	-1.8989	433	-5714.00	9 051 428	-0.0611	**0.0576**
SPEI_Penman_3mon	0.5767	431	1724.00	8 926 727	0.0186	0.5642
SPEI_Harg_3mon	-1.7086	431	-5106.00	8 926 727	-0.0551	0.0875
SPEI_Penman_6mon	1.1063	428	3272.00	8 741 827	0.0358	0.2686
SPEI_Harg_6mon	-0.4488	428	-1328.00	8 741 827	-0.0145	0.6536
SPI_6mon	-0.2976	428	-881.00	8 741 824	-0.0096	0.766
SPEI_Penman_9mon	1.9770	425	5785.00	8 559 499	0.0642	**0.0480**
SPEI_Harg_9mon	0.1870	425	548.00	8 559 498	0.0061	0.8517
SPI_9mon	0.0519	425	153.00	8 559 491	0.0017	0.9586
SPEI_Penman_12mon	2.8869	422	8358.00	8 379 721	0.0941	**0.0039**
SPEI_Harg_12mon	0.6702	422	1941.00	8 379 722	0.0218	0.5027
SPI_12mon	0.2028	422	588.00	8 379 715	0.0218	0.8393
SPEI_Penman_24mon	3.0043	410	8330.00	7 685 791	0.0994	**0.0026**
SPEI_Harg_24mon	0.3629	410	1007.00	7 685 790	0.0120	0.7167
SPI_24mon	-0.2947	410	-818.00	7 685 769	-0.0097	0.7682

1mon means one – month, Three – months denoted as 3 mon, Six – months as 6 mon, Nine – months as 9 mon,12 – months as 12 mon and 24 – months as 24 mon and SPEI_Harg means SPEI based on Hargreaves and SPEI_Penman is SPEI based on Penman – Monteith computed potential evapotranspiration

(iii) Influence of Drought on the Lake Level Variability

Generally, the lake levels were more tied to extreme rainfall conditions, as shown in Fig. 20. When SPI indicated severely wet conditions, such as in November 1982 and August 1998, or during the prolonged highly wet conditions of December 2006 through February 2007 (Fig. 27 to Fig. 31), the lake levels increased significantly. Similarly, the lake levels declined during a negative SPEI, indicating drought conditions (Fig. 26 to Fig. 31). The lake levels increased when SPEI showed humid conditions, such as prolonged normal conditions from December 2009 to April 2010. Lower lake levels occurred during prolonged moderate or severe drought conditions, such as from May 2010 to March 2011. Such trends are realistic, and Keijzer (2020) reported a similar response by Lake Manyara, whose volume and lake surface area increased with wetness and reduced in seasons of prolonged drought severity.

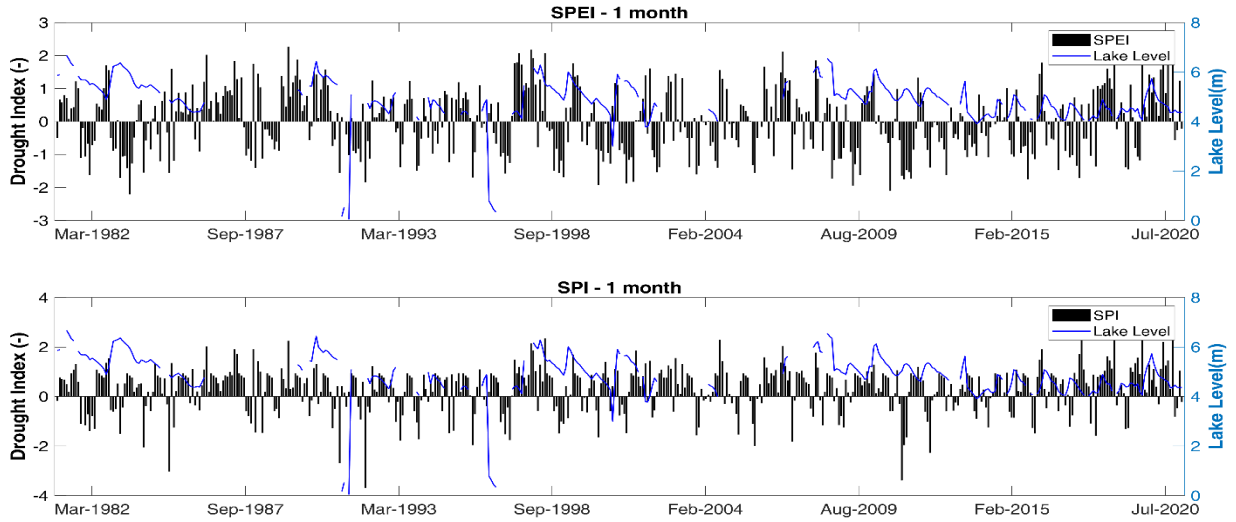

Figure 25: Variation of lake level with drought severity computed at 1-month aggregation level

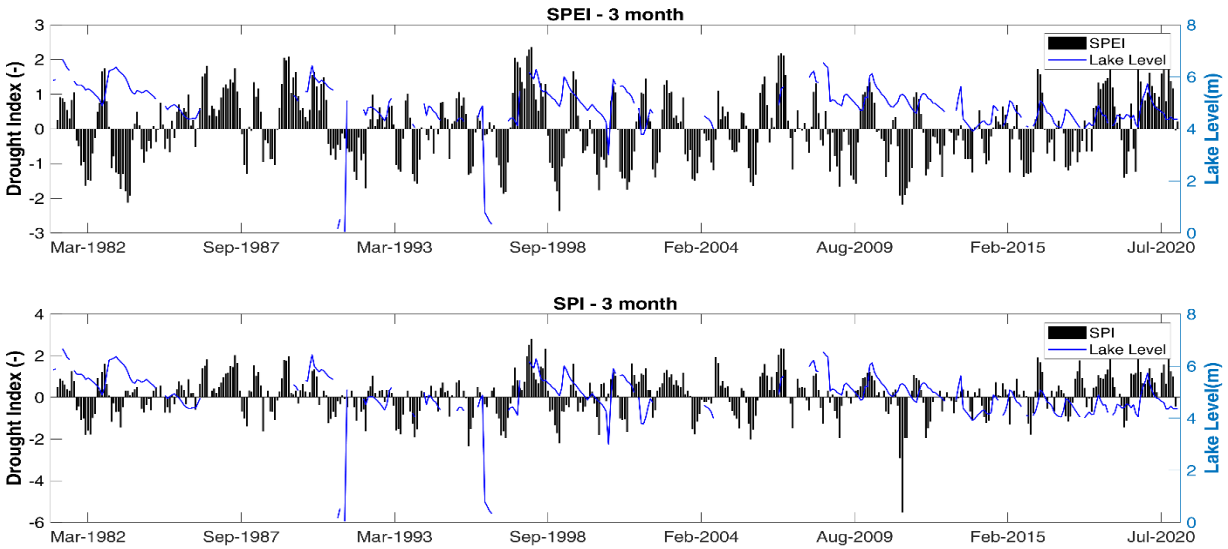

Figure 26: Comparison of lake-level variations in comparison to the drought severity at three months aggregation

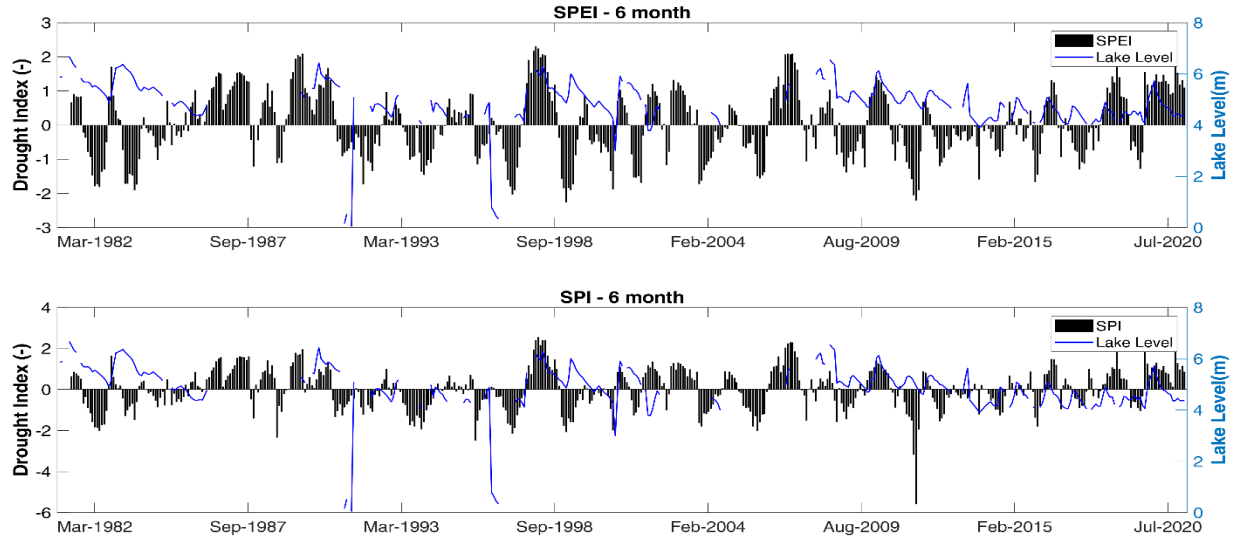

Figure 27: Variation of Lake level against Severity index aggregated at six months period

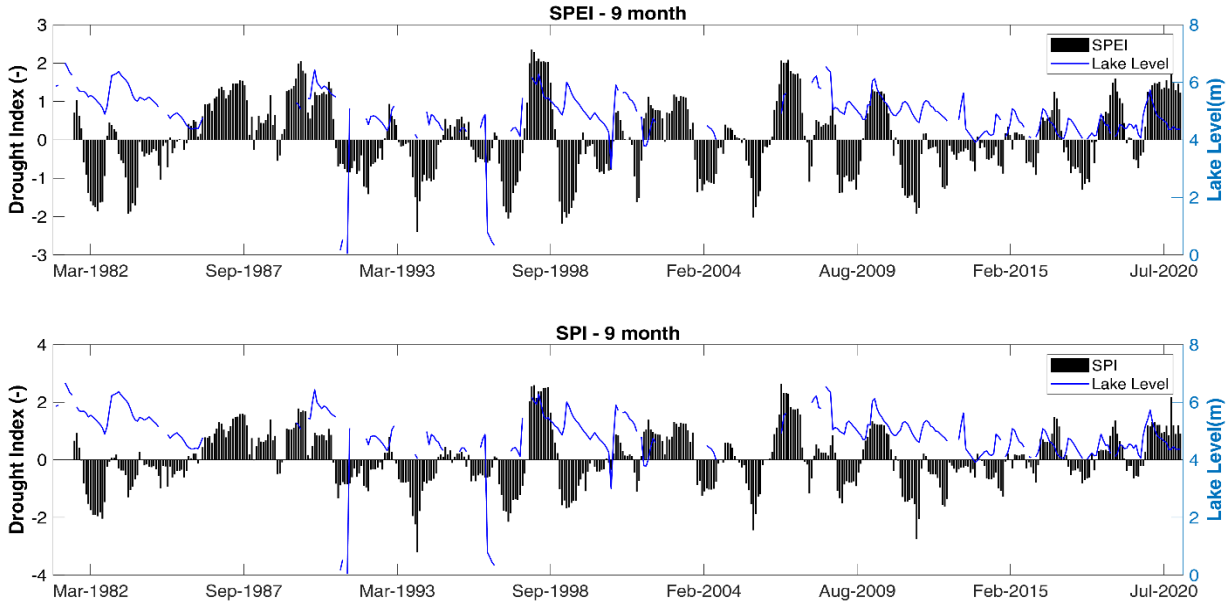

Figure 28: Variation of Lake level against drought severity at nine months aggregation

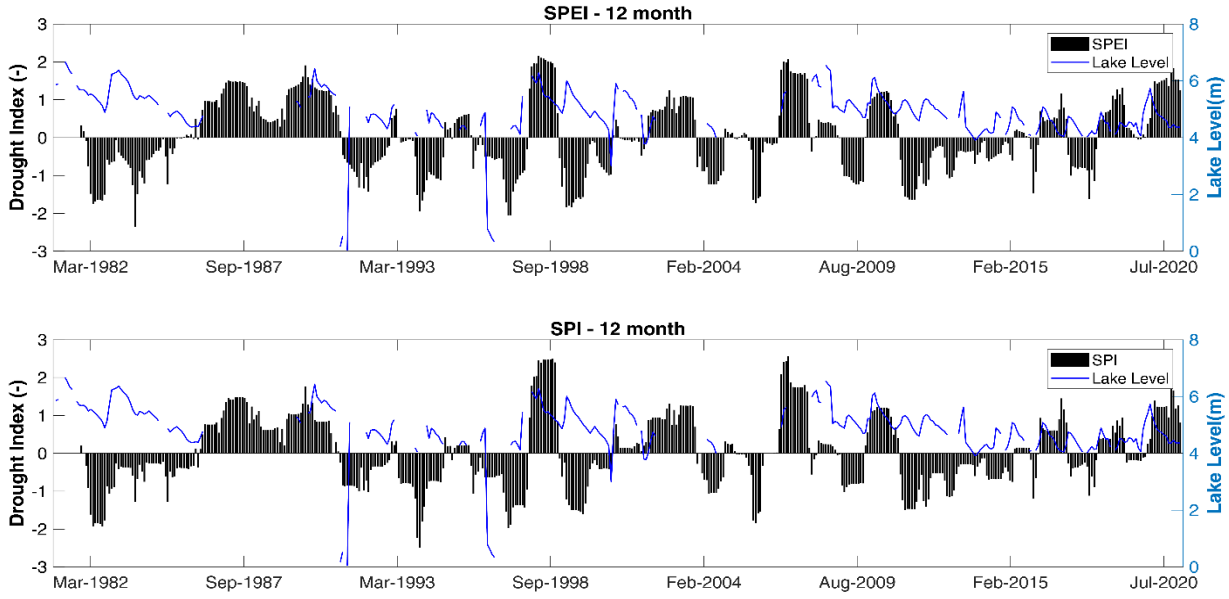

Figure 29: Variation of Lake level against drought severity at 12 months aggregation

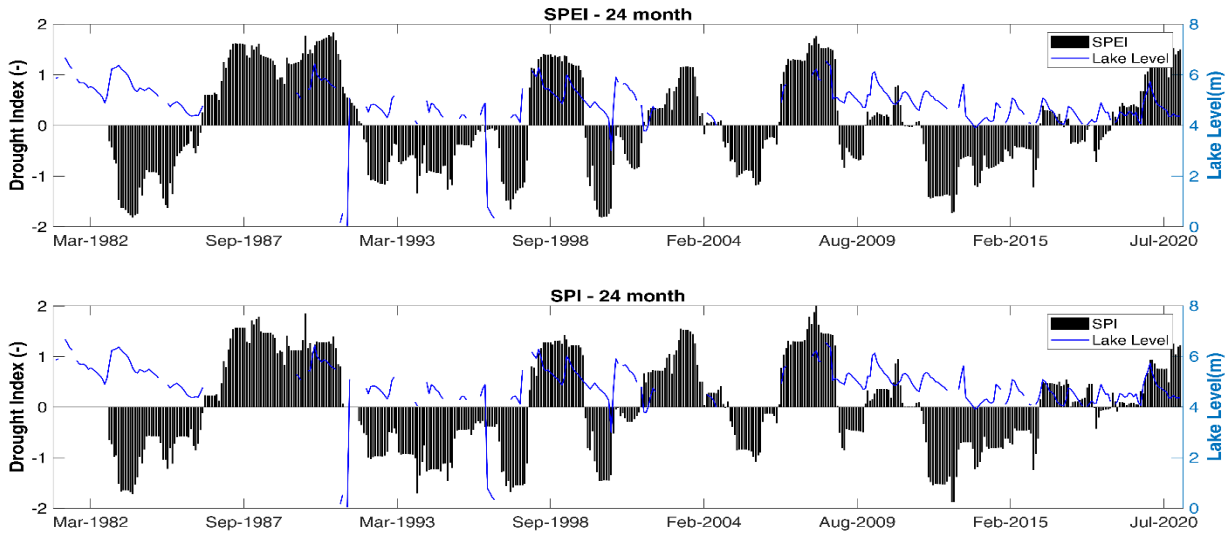

Figure 30: Variation of Lake level against drought severity at 24 months aggregation

Some extremely wet conditions did not increase the lake levels, especially when they preceded extreme or severe drought conditions, such as in August 1999. This was probably due to the influence of antecedent conditions and the large regional scale climatic phenomenon, such as the positive IOD in raising the lake levels. At the seasonal aggregation level (3 months period), SPEI and SPI reported severe or extreme wet conditions in August and September. However, that was not true because the months usually have little rainfall. The errors resulted from the SPEI and SPI computation where low rainfall average values (aggregated from the dry months of June and July) are divided by the low rainfall, giving high SPEI and SPI values interpreted as severely wet conditions.

A comparison between the monthly average lake levels and the SPEI computed at the monthly aggregation level indicated no correlation with the Spearman Rank correlation rho of only 0.01. However, the Spearman Rank correlation rho improved with increased aggregation levels. At nine months aggregation level, the correlation coefficient increased to 0.28 (Table 14). In all cases where the aggregation level was < 6 months, the SPEI and SPI explained minimal variations, all of which were insignificant (p-value > 0.05). As the aggregation level was increased, the correlation of both SPEI and SPI with the lake level improved in a similar pattern. At aggregation levels of three, six, and nine months, the correlation coefficients were slightly lower than for SPEI, but they improved to become better than SPEI with aggregation levels at 12 and 24 months. This improved correlation from increased aggregation levels suggested a response delay in the lake level during adverse climatic conditions. Byakatonda *et al.* (2018) argued that the aggregation level when correlation becomes significant is when the meteorological drought becomes a hydrological drought. This corresponds to when the residual antecedent conditions influence the lake variability significantly.

Table 14: Summary of Spearman Rank's correlation of the lake level with drought indices at different aggregation scales

Scales	SPEI_Penman & Lake Level		SPEI_Hargreaves & Lake Level		SPI & Lake Level	
	Spearman coefficient, r	p-value	Spearman coefficient, r	p-value	Spearman coefficient, r	p-value
1 - month	-0.0130	0.8390	0.0100	0.5000		
3 - month	0.0855	0.3050	0.0840	0.1600	0.0488	0.466
6 - month	0.1878	0.0180	0.1797	0.0140	0.1680	0.029
9 - month	0.2869	0.0009	0.2857	0.0005	0.2684	0.0005
12 - month	0.2766	0.0013	0.2899	0.0004	0.2954	0.0002
24 - month	0.3698	0.0022	0.3826	0.0008	0.3846	0.0001

The regression equations of the 6 months aggregated SPEI and SPI, which significantly correlated with the lake level, were compared to measure the influence of evapotranspiration in driving the lake levels. No significant difference (p-value = 0.08869) was observed when using either the SPEI

or SPI to predict the lake level. This further confirms that the influence of evapotranspiration is not significant in driving the lake level. Therefore, Lake Babati catchment experiences a 6 – 9 months lag between meteorological and hydrological drought. A similar lag was observed in the onset of hydrological drought after the meteorological drought in the Okavango River systems in Botswana. The meteorological drought lagged the hydrological drought by 6 months in the Okavango river systems, while the lag was 7 months in the River Limpopo catchment (Byakatonda, 2018).

Conclusively, drought analysis by SPEI and SPI showed that the area was neither becoming drier nor wetter. No correlation was observed between the lake level and the drought indices in the shorter time scales. The drought indices only became positively and significantly correlated with the lake levels when aggregated at time scales longer than six months. The observed phenomenon implied that the meteorological drought did not immediately affect the Lake Babati level variability but was lagged by about 6 - 9 months after the onset of the meteorological drought. Thus, it could be concluded that drought did not drive the observed seasonal decline of the lake level, although it had a long-term influence on the lake level.

4.1.6 Land-use and Land Cover Changes And Patterns

(i) Accuracy Assessment of Land Cover Classification

The supervised classification method in ArcGIS was used to classify Landsat images, and the Google Earth images and the open street map data were applied to validate the classification. The forests and the water were the most accurately produced maps (Table 15), while the built-up class had the least producer and user accuracies. In addition, the agricultural land and forests were simpler to distinguish than the bare land from the urban areas because they were distinct in the dry season. Nonetheless, the accuracy assessments were acceptable, with the least overall accuracy of 69.4% and the least Kappa coefficient of 0.6 for images of the year 2000.

Table 15: Accuracy assessments of land cover and land use classification

Class Name	Producer's accuracy (%)						User's accuracy (%)					
	1991	**2000**	**2003**	**2013**	**2015**	**2019**	**1991**	**2000**	**2003**	**2013**	**2015**	**2019**
Water	100.0	100.0	100.0	100.0	100.0	100.0	100.0	100.0	100.0	100.0	100.0	100.0
Built-up and Bare land	56.0	30.0	66.7	55.6	67.9	61.2	66.7	35.3	61.5	90.9	90.5	93.8
Agricultural land and grassland	71.1	84.2	82.6	86.9	90.9	94.2	64.3	53.3	73.1	75.7	86.2	66.2
Shrubs and scattered trees	71.8	42.9	68.0	61.8	73.5	61.9	80.0	88.2	73.9	42.0	71.4	72.2
Forests	96.2	96.6	80.0	68.9	81.0	91.5	83.3	100.0	100.0	75.6	70.8	89.6
	Overall accuracy (%)						**Kappa Coefficient (k)**					
	76.39	69.40	78.26	71.50	82.24	79.31	0.70	0.60	0.72	0.63	0.76	0.73

(ii) Classification Results

Between 1991 and 2003, forests saw the most significant conversion into shrubs and sparse vegetation and finally into agricultural land, as shown in Fig. 32 to Fig. 37. As a result, the forests were reduced from 110 km^2 in 1991 to 33 km^2 in 2019 (70.16% reduction). As shown in Table 16, the agricultural land and grassland, built-up and bare land, have consistently increased while the forests have reduced through the years.

Table 16: The variation of land cover (absolute) sizes through the years

Class no	Class Name /Year	Area (km^2)					
		1991	2000	2003	2013	2015	2019
1	Water	11.98	14.01	13.87	11.73	11.07	12.64
2	Built-up and bare land	21.74	22.54	33.84	21.15	25.84	26.56
3	Agricultural land and grassland	73.79	75.56	111.84	142.44	159.21	169.80
4	Shrubs and sparse vegetation	171.93	231.66	123.16	141.29	165.11	148.12
5	Forests	110.72	46.40	107.45	73.56	28.93	33.04

As a transitional land cover between forests and agriculture, the shrubs and sparse vegetation gained in 2000 from 171.93 $km^{2,}$ reaching 231.66 $km^{2,}$ before falling to 148.12 km^2 between 2000 and 2019. The noticeable pathway of land cover change was a gradual conversion of forests into shrubs and sparse vegetation before the arable parts became agricultural land and grassland. This was probably because of the consistent forest degradation by local communities searching for firewood or deforestation for agriculture, except in the established forest reserves under legal protections. Therefore, the conversion from "shrubs and sparse vegetation" to agriculture and vice versa was primarily noticeable. The conversion of sisal estates into agricultural land and settlements provided evidence of this trend of change in the study area.

The agricultural land cover gained consistently from 73.79 km^2 in 1991 to 169.8 km^2 (130.12% gain over the years). The highest gains were after 2000 when the government implemented the first phase of the Agricultural sector development programme that expanded the land under cultivation (URT, 2017). Similarly, built-up and bare land gained by 22% consistently in the 28 years under consideration, increasing from 21.74 km^2 in 1991 to 26.56 km^2 in 2019. However, the fluctuation in the water area has not been consistent. At first, it increased to 14.01 km^2 in 2000 but reduced to 11.07 km^2 in 2015 before increasing to 12.64 km^2 in September 2019. As a result, the average surface area of Lake Babati (free water surface) from the classified map was 12.55 km^2 compared to the 17 km^2 marked as the lake by the 1960's topographic map (Mineral Resources Division, 1966). The 1960s topographic map extended to the lake floodplains of Lake Babati,

which are presently classified as forests or shrubs and sparse vegetation depending on the type and density of the trees covering the lake shores.

(iii) Land Cover Change Pattern

Water and agricultural land were the most stable land cover between 1991 and 2015. Water maintained 89.6 % (10.7 km^2) of the 1991 water surface in 2015; in 2015, agricultural land maintained 81.1% (59.1 km^2) of its 1991 cover. The forest was the most unstable land cover type; by 2015, it had only 21.1% (23.2 km^2 out of 109.8 km^2) of the 1991 forest land available. The stable forests were in the forest reserves with legal protections. The built-up and bare land maintained only 21.7% of the 1991 cover by 2015, while the shrubs retained 42.3% (73.4 km^2) of the 1991 shrubs in 2015. Figure 37 captures succinctly where the changes happened. The diagonal columns in the confusion matrix in Table 17 show the total area of land use types, which did not change between 1991 and 2015.

Table 17: A confusion matrix showing absolute land use and land cover changes to different forms between 1991 and 2015

		2015 land cover					
		Agricultural land (km^2)	**Built up & bare land (km^2)**	**Forests (km^2)**	**Shrubs (km^2)**	**Water (km^2)**	**1991 Total (km^2)**
1991 Land cover	Agricultural land	59.1	3.8	0.5	9.4	0.0	72.8
	Built up & bare land	6.2	4.3	0.3	9.0	0.0	19.9
	Forests	10.9	2.7	23.2	72.8	0.3	109.8
	Shrubs	83.4	14.2	2.6	73.4	0.0	173.6
	Water	0.1	0.0	0.3	0.9	10.7	12.0
	2015 Total	159.6	25.0	26.9	165.5	11.1	388.1

Agricultural land gained the most, increasing from 72.8 km^2 in 1991 to 159.6 km^2 (119.2% increase) over the 24 years of consideration, while forests lost 75.5% of their coverage within the same period (falling from 109.8 km^2 to 26.9 km^2). The shrubs lost 4.7% of their land cover, shrinking from 173.6 km^2 in 1991 to 165.5 km^2 in 2015. The built-up and bare land expanded from 19.9 km^2 to 25.0 Km^2 in 2015 (25.9% gain), while the water cover shrank by 7.4% from 12.0 km^2 to 11.1 km^2 in 2015. The disappearance of a small crater lake that occupied the northeastern part of the catchment was the most noticeable change in the water coverage type. The area of the crater lake has since become shrubs and agricultural land.

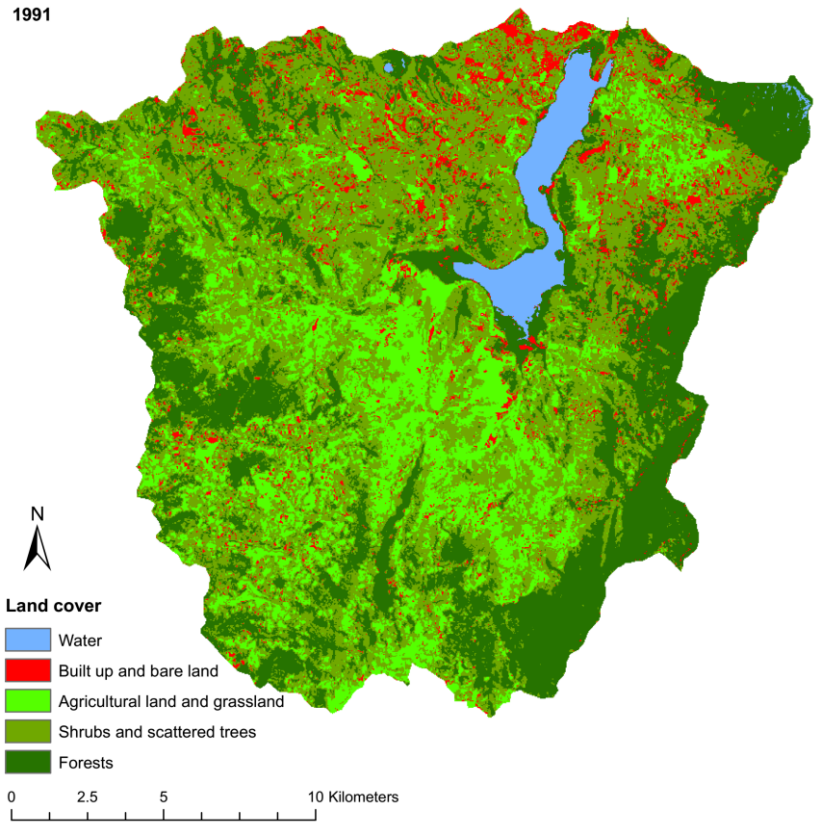

Figure 31: Babati catchment land cover in September 1991

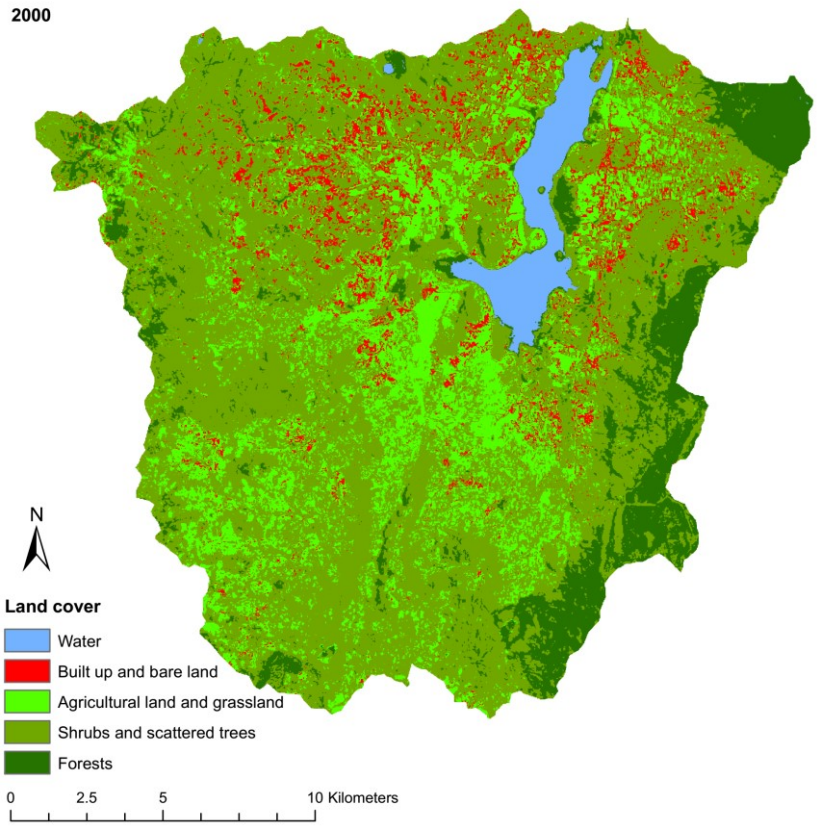

Figure 32: Babati catchment land cover in September 2000

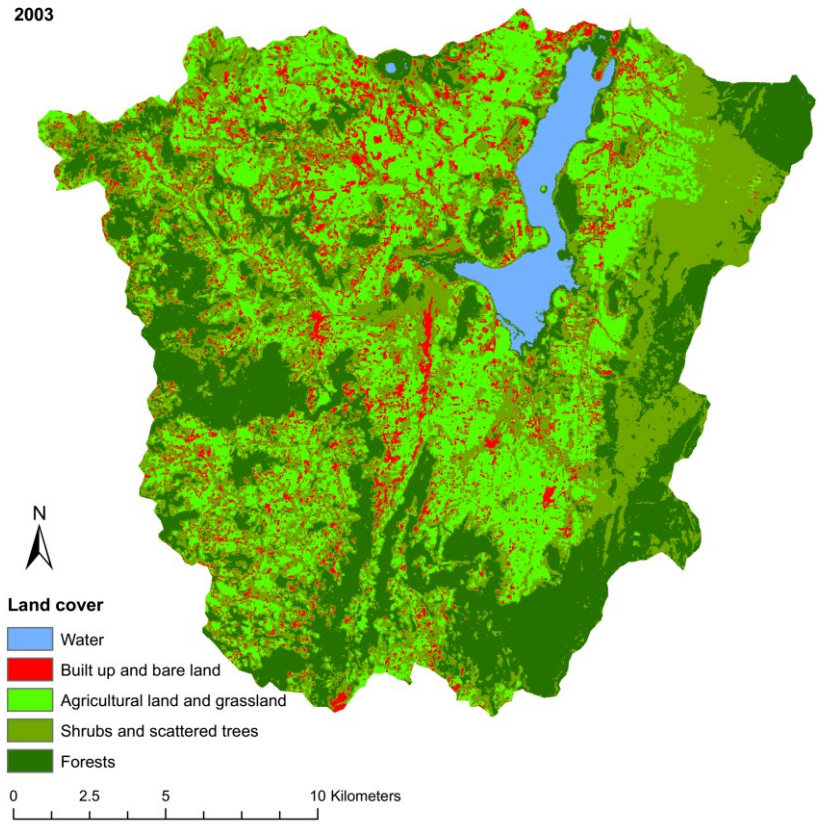

Figure 33: Babati catchment land cover in September 2003

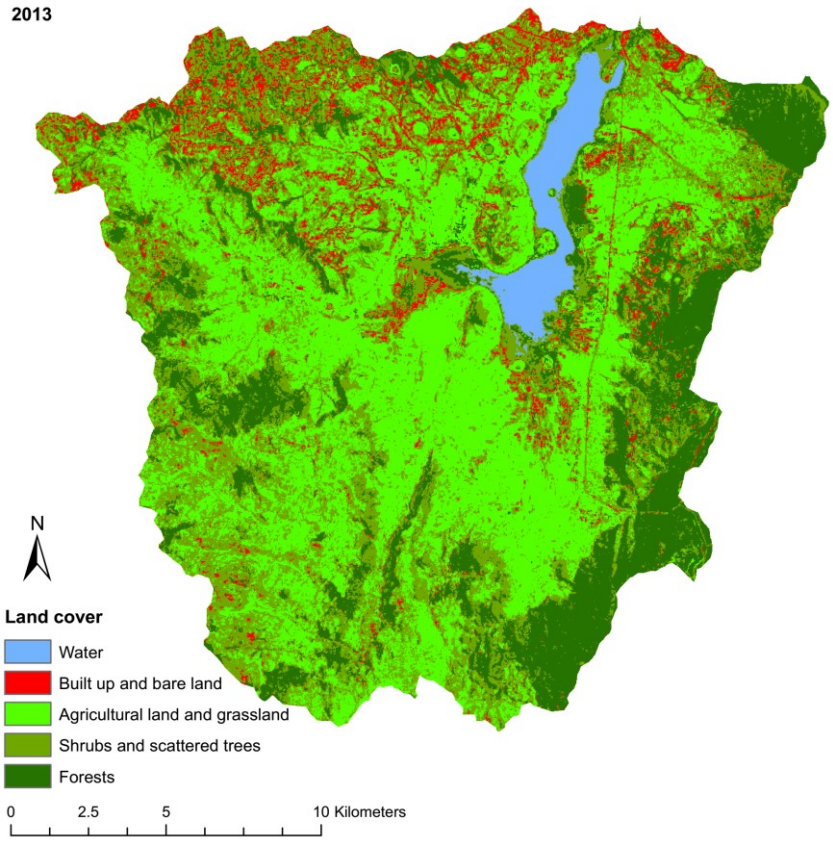

Figure 34: Babati catchment land cover in September 2013

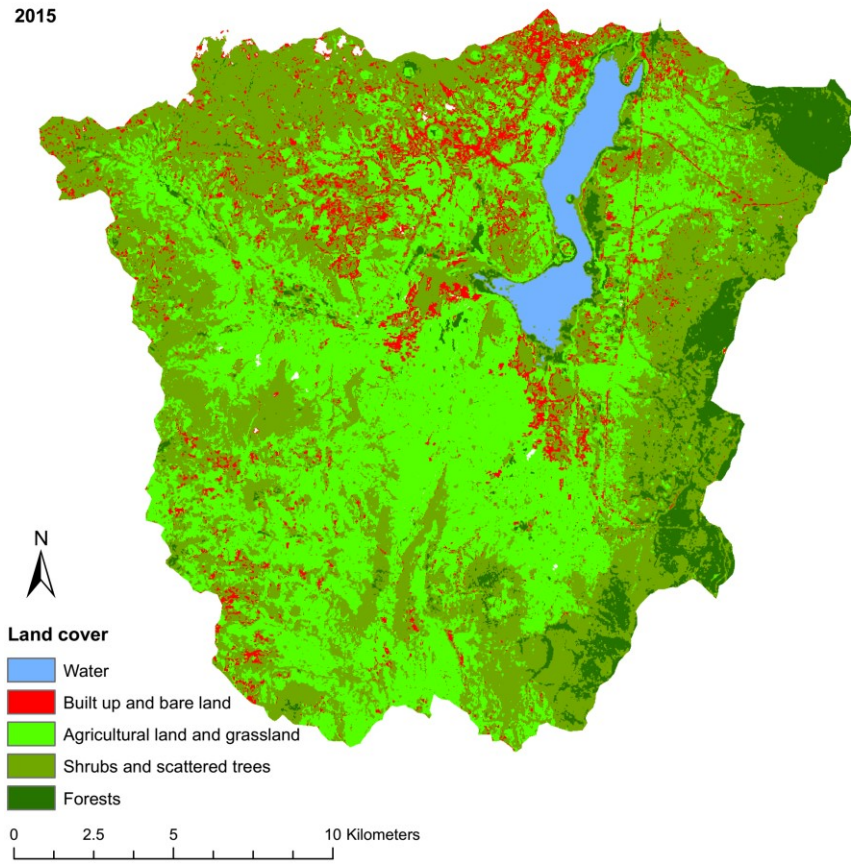

Figure 35: Babati catchment land cover in September 2015

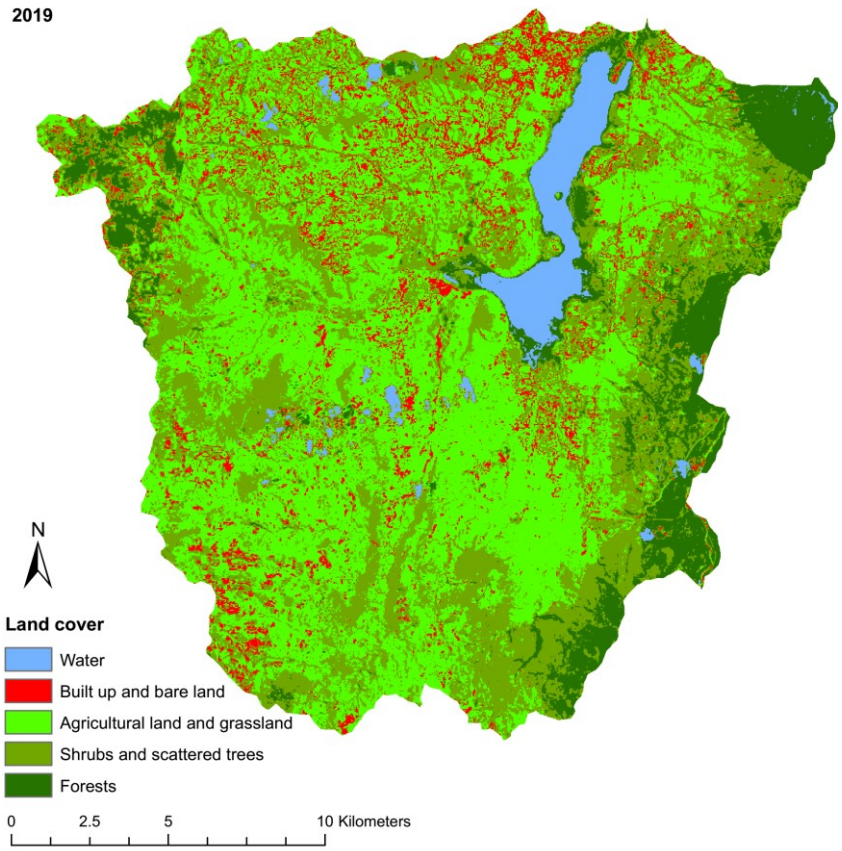

Figure 36: Babati catchment land cover in September 2019

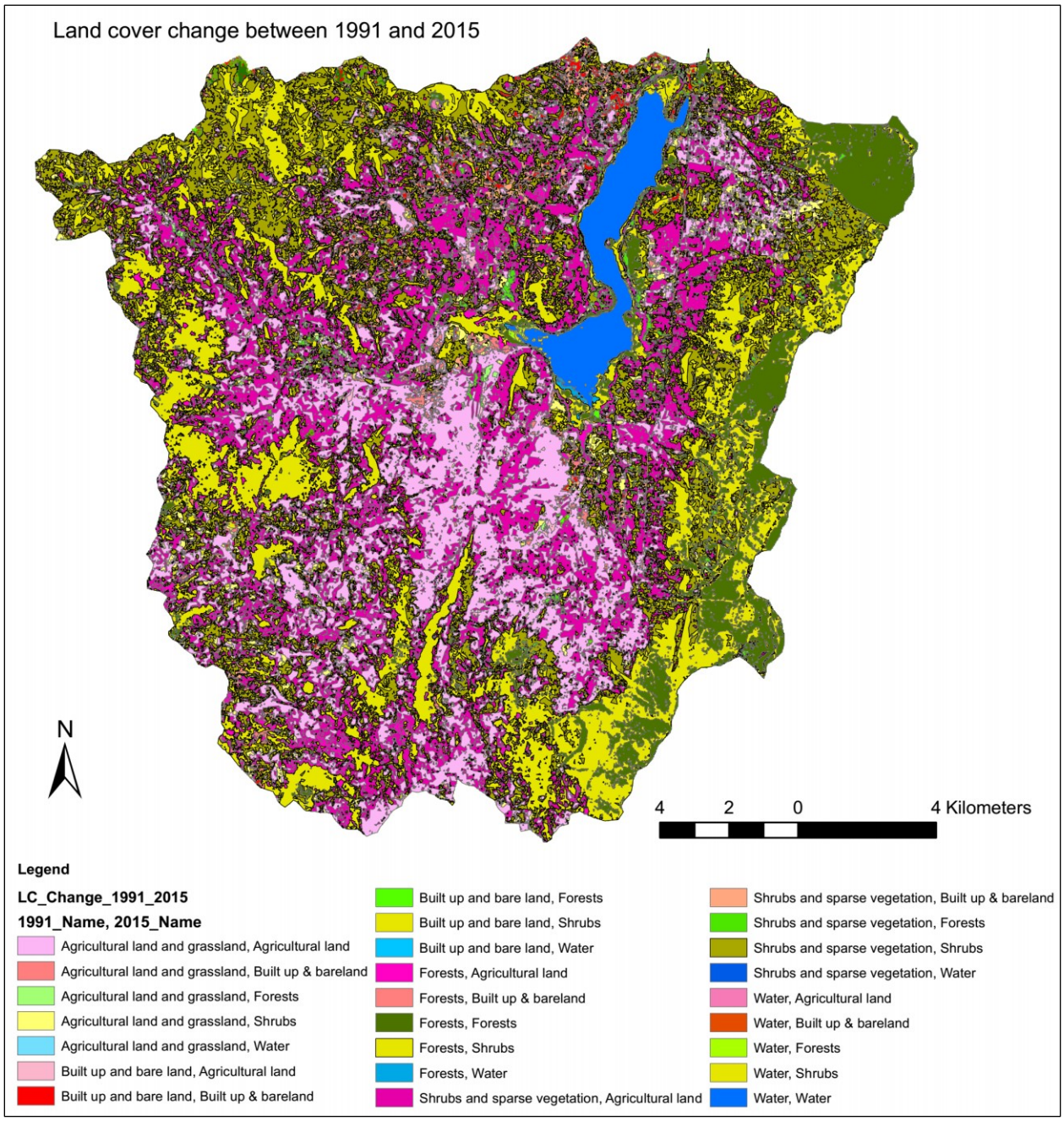

Figure 37: Patterns of land use and land cover changes from 1991 through 2015. The legend shows the 1991 land use and land cover first, and after the comma is the 2015 land use and land cover

The gradual conversion of forest land into agricultural land alters the topsoil configuration and reduces vegetation cover, resulting in increased surface runoff and reduced infiltration. Land cover changes from forests to agriculture and urban settlements were reported to have contributed to increased streamflow of the Ganga catchment of North India (Anand *et al.* 2018). In a review of Kenyan and Tanzania catchment studies, Guzha *et al.* (2018) revealed that the reduction in forest cover did not significantly increase streamflow. However, they noted a reduction in the dry season flow when forests shrank and the agricultural land expanded. As Lin *et al.* (2015) argued, the responses, however, depend on how the agricultural practices disturb the vegetation and modify the soil structure. Within the catchment, a reduced forest cover with a rapid expansion in the

agricultural land was anticipated to result in no increase in stream flow amounts over the years. However, the loss of forests which attenuates stream flows over a long period was thought to amplify the temporal variability of stream flow. The likely effect of reduced forest covers on baseflow, and the general catchment response to the observed land use and land cover changes are subjects for future investigations.

4.1.7 Population Growth and Water Abstraction

The records of water abstraction were not available. However, the catchment covered 11 wards, including Babati town council, Nangara, Singe, Bonga, Bagara, Sigino, Arii, Riroda, Duru, Ayasanda, and a small part of Gidas and Boay wards. The population in these areas increased from 54 864 in 2002 to 137 357 people by 2012 (NBS, 2013). Despite a moderate population growth rate of 3.2% reported for the Manyara region between 2002 and 2012, the population in study areas rapidly grew at an average of 15.04% (NBS, 2013). The rapid population growth was attributed to the rapid urbanization around Babati town council, the regional capital for the Manyara region.

URT (2014) estimated the water demand for the entire Lake Manyara sub-basin to be 95.6 million cubic metres (MCM) per annum in 2010. The estimate included irrigation and domestic water demand, which was approximately 47.4 and 31.88 MCM, respectively. The water requirements for industries, mining, and wildlife conservation were the least in the basin (URT, 2014), while livestock water demand was 11.82 MCM. The consumptive water demand for the Lake Manyara sub-basin was estimated to increase to 440.86 MCM by 2035. The projected 2035 demand would be driven by irrigation water demand which was 356.6 MCM, implying a considerable increase in water demand to support irrigated agriculture.

Lake Babati catchment, an elevated upstream catchment within the Lake Manyara sub-basin is small, with a catchment area of 390 km^2 against 18 740 km^2 for Manyara (Deus & Gloaguen, 2013). Despite its small areal size, Lake Babati catchment was home to 137 357 people in 2012 at the time when 1 425 131 people were living in the Manyara region (National Bureau of Statistics, 2013). In terms of the catchment area, Lake Babati is only 2.08% of Lake Manyara catchment but hosted 9.6% of the people in the Manyara region. Therefore, scaling the water demand by URT (2014) based on the population ratio in Lake Babati catchment and Manyara region, this study estimated water demand within Lake Babati catchment as presented in Table 18. The study did not consider environmental and hydropower water needs but concentrated on consumptive water uses, which have the potential to deplete water resources.

Table 18: Estimated water demand in Lake Babati and Lake Manyara catchments through the years measured in a million cubic meters (MCM) per annum

Sub Basin	Irrigation	Domestic	Livestock	Mining & Industry	Wildlife	Tourism & Recreation	Aquaculture	Total
Lake Manyara catchment								
2010	47.4	31.88	11.82	3.19	1.26	0.06	0.021	95.63
2015	144.8	40.29	12.53	6.04	1.26	0.11	0.041	205.07
2025	350.5	48.61	15.54	7.29	1.26	0.19	0.06	423.45
2035	356.5	56	18.34	8.4	1.26	0.28	0.08	440.86
Lake Babati catchment								
2010	4.55	3.06	1.13	0.31	0.12	0.01	0.00	9.18
2015	13.90	3.87	1.20	0.58	0.12	0.01	0.00	19.68
2025	33.65	4.67	1.49	0.70	0.12	0.02	0.01	40.65
2035	34.22	5.38	1.76	0.81	0.12	0.03	0.01	42.32

URT (2014)

The estimates indicated that water demand would increase, and by 2025, the total water demand of Lake Babat catchment would be 40.65 MCM, with irrigation water demand accounting for 82.7% of the total (33.65 MCM). Satisfying that demand would need a supply of 111 369 m^3 of water per day. Currently, some crops are grown under irrigation, but very scanty information was available on the scale of irrigated land or the amount of water used explicitly for irrigation. Extensive irrigation was not observed within the Lake Babati catchment, so the irrigation water requirement could have been overestimated.

The estimate of the domestic water appeared close to reality. For example, by 2025, the estimated domestic water demand was 4.67 MCM, translating to 12 794 m^3/day. At the time of the study in 2019, Babati Water Supply Authority (BAWASA) was supplying 50 000 m^3/week, which translated to 7142 m^3/day, but it was still inadequate. The BAWASA was actively expanding its water supply capacity and coverage beyond the urban areas to the rural communities, which were dependent on shallow wells for domestic water. Groundwater sources constituted 78% of the water supplied, while a spring from Girala Mountain contributed the remaining 22%. Generally, water abstractions indicated a tremendous increase to accommodate the rapidly growing urban population and economic activities.

4.1.8 Lake Water Balance Simulation

Using the available lake levels, the lake bathymetric data, the rainfall, and the lake evaporation, an HEC-HMS model was built, calibrated, and its performance validated. The graphical evaluation

of the calibrated model and the statistical measure of the performance are shown in Fig. 39 and Table 19, respectively.

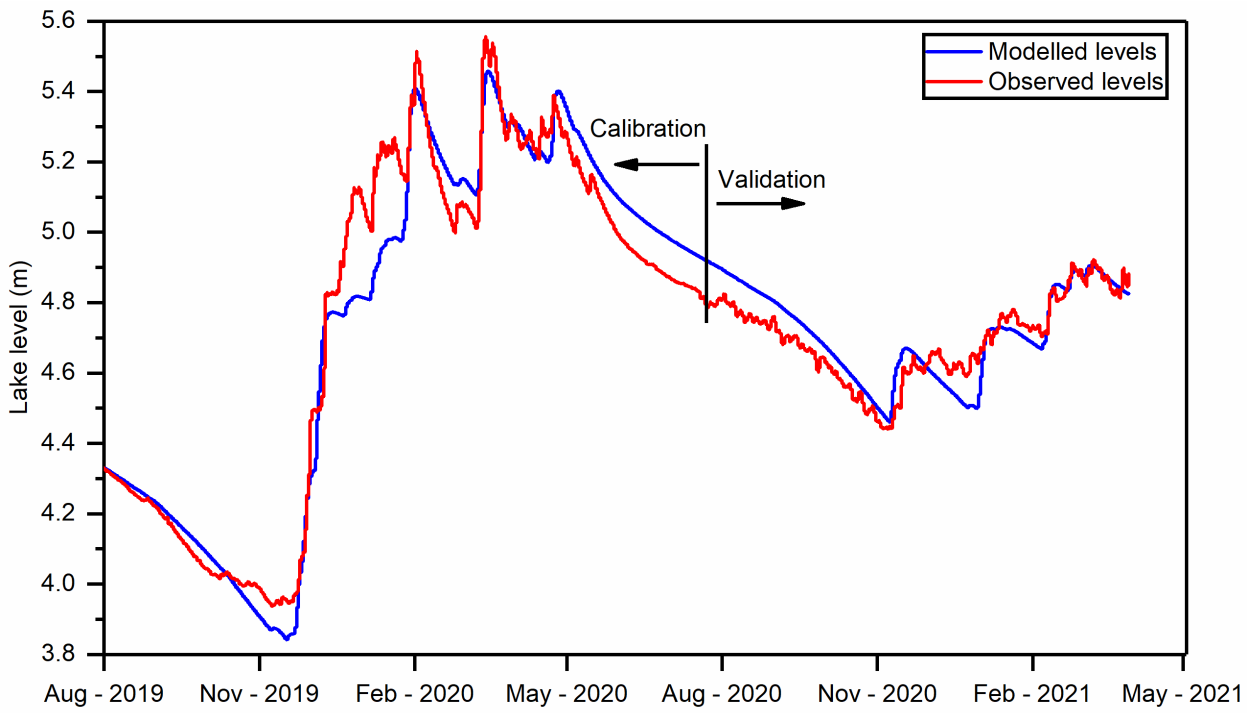

Figure 38: Graphical comparison of the observed lake level and the simulated lake level during the calibration and validation phases

Table 19: Goodness of fit measurements of the model at the calibration and validation phases

The goodness of fit statistics	Calibration phase	Validation phase
Sum of Absolute errors (m)	-29.22	-256.05
Sum of Squared Residuals (m^2)	212.04	50.40
Simulated Peak Level	5.45	4.936
Observed Peak Level	5.56	4.93
The Percent error in peak level (%)	-2.01	0.12
Mean Observed Level (m)	4.757	4.701
Nash Sutcliffe Efficiency	0.95	0.71

The statistical goodness of fit in Table 19 and Fig. 39 indicated that the model was excellent for prediction. The model had an NSE of 0.95, which indicated its excellent performance for predictive purposes (Moriasi *et al.,* 2015). Figure 38 suggests that the model is more accurate in predicting the low lake levels, but its performance during peak seasons harbours some errors. Generally, the model underestimated the lake level during the rainy season and offset the peak level in time compared to the observed lake level. Although the offset in the peak lake level could result from model inefficiency, the available cumulative daily rainfall depths do not capture the exact time for peak rainfall. Since each sub-basins have a time of concentration of less than 12 hours, the exact peak time of the rainfall is essential for predicting the lake levels. The synthetic unit hydrograph with an arbitrary frequency duration curve may cause a mismatch in the modelled and observed

lake level peaks. Improvement of the model calibration for flood studies requires rainfall captured at time steps shorter than the time of concentration of the sub-basin with the shortest time of concentration.

The model matched the low flow conditions well, making it most suitable for low flow studies and relevant for water supply and drought studies. However, it slightly underestimated the peak flows, as shown in Fig. 39 and Table 19. Therefore, the model may not accurately capture the peak flows, and thus, users may need to apply it with caution for flood studies. In addition, the model may require rainfall data collected at a 30 minutes timestep for a finer calibration. The calibrated model parameters are summarized in Table 7. Nonetheless, the model is handy for studies in a data-scarce catchment and can be improved further when more data for long-term calibration and validation is available.

4.1.9 Grey Relational Order Ranking

The factors driving the lake level or storage variability were assessed and ranked by GRA. The most important driver of the lake level variability was the inflow to the lake (runoff and baseflow), followed by direct rainfall. Lake evaporation came in third, while lake outflow was the least important. When GRA was performed with the lake storage as the reference series, the lake inflow and rainfall maintained their first and second order of importance; however, the lake evaporation and lake outflow tied in the third position. The grey relational coefficient (Table 20) of lake evaporation and lake outflow were insignificantly different (p = 0.97), thus implying both have equal magnitude/influence in the control of Lake Babati level variability when based on the lake storage.

Table 20: Comparison of Grey relational grades based on the lake level and lake storage

Reference series	Inflow (m^3/s)	Lake Evaporation (mm)	Direct Rainfall (mm)	Computed Outflow (m^3/s)
Lake Level (m)	0.8591	0.6320	0.8652	0.6120
Lake Storage (m^3)	0.8590	0.6152	0.8658	0.6155

Evaporation was expected to have a higher weight than direct rainfall because direct rainfall over the lake surface is smaller (with a lower depth) than lake evaporation. However, the high correlation of the direct rainfall to the lake inflow seems to have biased the analysis. The lake outflow had more control over the lake level variability during the rainy year (2019 -20 hydrological year) when more water was removed from the lake during peak seasons than evaporation. On the other hand, the hydrological year 2020 – 21 had low rainfall; therefore, the lake experienced more lake evaporation than lake outflow. Therefore, in the 2020 – 21 year, the study agreed with Kumambala and Ervine (2013), who suggested that lake evaporation is often

the most significant outflow component since the evaporation rates are unlimited because the water is always available. Further, it partly agreed with Mbanguka *et al.* (2016), who reported that lake evaporation and runoff control the hydrological balance of Lake Babati. Mbanguka *et al.* (2016) did not recognize the influence of large outflows during high rainfall seasons.

4.1.10 Stepwise regression analysis

We performed a stepwise regression analysis of precipitation over the lake area, lake inflow, lake outflow, and lake evaporation to determine the most influential drivers of the lake water level. The analysis indicated that the lake inflow, evaporation, and outflow were the most significant parameters for predicting daily lake levels, while direct rainfall was the least important parameter. The stepwise regression removed the direct rainfall in backward elimination. It did not substitute it in the forward elimination, implying that an optimal model prediction could be achieved without the direct rainfall.

(i) Fitting the Parameters using the Lake Level

The daily lake level in meters (L_{daily}) can be predicted using the daily precipitation (P in mm), inflow to the lake (R_{in} in m^3/s), lake outflow (R_{out} in m^3/s) and lake evaporation (E_L in mm/day) using a regression formula expressed in Equation (68). All the added parameters improved the model. The coefficients of the parameters were not zero (p-value < 0.01) and had the F – statistics of 273.8 on 4 and 608 degrees of freedom and the multiple $R^2 = 0.6443$.

$$L_{daily} = 5.6403 \ + 0.0017P + 0.0081R_{in} + 0.1761R_{out} - 0.1537E_L \tag{68}$$

The stepwise elimination improved the model by removing the less sensitive or adding the most sensitive parameters. At the daily time step, the regression showed that the lake level was not very sensitive to direct rainfall over the lake, and it was eliminated, giving Equation (69) as the final optimized equation. Thus, the final model improved with the multiple $R^2 = 0.6437$, F – statistics of 363.8 on 3 and 604 degrees of freedom, and a p-value < 0.01.

$$L_{daily} = 5.6478 \ + 0.0041R_{in} + 0.1786R_{out} - 0.1547E_L \tag{69}$$

(ii) Fitting the Parameters using the Lake Storage

The prediction of the daily lake storage using the same parameters had the following goodness of fit statistics: A multiple $R^2 = 0.7415$, the F – statistics of 432.4 on 4 and 603 degrees of freedom, and a p-value < 0.01. Equation (70) gives the regression of the lake storage with input parameters. As indicated by the R^2, the prediction of the lake storage was more accurate than the lake level.

$$LS_{daily} = 67127331 - 34253P + 66873R_{in} + 3105860R_{out} - 2583060E_L \quad (70)$$

where LS_{daily} is lake storage in m^3, P is precipitation in mm, R_{in} is inflow to the lake in m^3/s and R_{out} is the outflow from the lake in m^3/s and lake evaporation (E_L in mm/day).

Direct rainfall was removed from Equation (70) on a stepwise analysis optimization to give an optimized and parsimonious model with no significant loss in the model's predictive power, as shown in Equation (71). The goodness of fit statistics was; a multiple $R^2 = 0.7407$, F – statistics of 575 on 3 and 604 degrees of freedom, and a p-value < 0.01.

$$LS_{daily} = 67276591 - 13723R_{in} + 3155399R_{out} - 2601460E_L \quad (71)$$

The catchment inflow (including runoff and baseflow) was the most significant parameter in driving lake level variability. The effect of direct rainfall was minimal due to the small lake surface area compared to the large catchment area. With the catchment–lake surface area ratio of 26:1, 1 mm of catchment runoff would translate into a 26 mm depth of inflow over the lake surface, masking the effect of direct rainfall. The evaporation amount was equally substantial compared to the direct rainfall. At an average depth of 6 mm per day, the lake evaporation outstripped direct rainfall, reaching about 2000 mm per year compared to the annual rainfall. Although evaporation is the main depleting factor for closed lakes (Kumambala & Ervine, 2013), the insignificant change (no trend) in evaporation in Lake Babati suggested that additional factors could have influenced the consistent declines observed in the lake levels. In years of heavy rainfall, the lake outflow during peak lake level seasons withdrew more water from the lake than evaporation. The most significant effect of evaporation occurred in the dry season (December – February) when temperatures were elevated. Whereas both the lake outflow and evaporation played essential roles in controlling lake storage/level, the usually large volume of water spilt during peak levels appeared to drive the continuous depletion of the lake water.

As observed, the most important variables in predicting the lake level or storage were the inflow, evaporation, and outflow. The GRA corroborated these findings by ranking the lake's inflow as the most sensitive parameter, followed by the evaporation and outflow at the same magnitude as the second most sensitive parameter. Although GRA ranked direct rainfall as the most sensitive parameter, the stepwise analysis showed that direct rainfall over the lake area played a minimal role in driving the lake level because of the relatively smaller lake surface to the catchment area. The strong correlation of direct rainfall with the lake inflow could have influenced the GRA to rank it as the second most sensitive parameter.

Generally, the lake level control depended on the largest outflow component. For example, in the 2019 – 20 hydrological year, the lake outflow had more control over the lake level variability as

the outflow removed more water from the lake during peak seasons than evaporation. Evaporation regained control of the lake level in the hydrological year 2020 – 21, which had low rainfall; subsequently, the lake outflow was less than lake evaporation. The effect of water abstractions was perceived as small on the lake level. If the 2025 water demand of 111 369 m^3 were abstracted directly from the lake, water abstractions would exceed all the daily outflow and evaporations currently controlling the lake level. The result would be a more rapid decline in the lake levels. The current scenario is still tenable because the irrigation water demand is still less than estimated, and there are no direct abstractions from the lake. However, it is worth noting that the future shifts in the lake level could be driven by unregulated water abstractions for irrigation. Without pressure from abstractions, the observed rate of lake level decline of 25 mm per year would reduce, especially when the lake levels are below the outflow level (spillway level). This is so because evaporation would be the only remaining depletion factor whose depletion effect could still be restored by lake inflow.

Whereas outflow terms controlled the observed declining lake level scenarios, it was worth noting that factors that affect the lake's inflow (runoff and baseflow) could also significantly influence the lake level variability. One such factor is the recent land-use change dominated by the conversion of forest-dominated catchments into agriculture-dominated ones. The transition to built-up and bare land was still low, although expected to expand rapidly because of the economic boom in Babati town, the capital of the Manyara region. These transitions were anticipated to increase the catchment runoff but reduce baseflow in the future. However, the impact of these changes could be short-lived if farmers adopt agricultural practices that increase infield storage of runoffs, thus potentially reducing runoff inflows. These changes and their impact on lake inflow and sedimentation could be the subject of future investigations.

Lake Babati catchment faces deforestation due to pressure from farming and pastoralism. Unfortunately, the activities expose the soil surfaces or loosen the soil structures, thus exacerbating soil erosions. Soil erosion drives the siltation of reservoirs as the detached and suspended materials are deposited in reservoirs. Siltation does not only reduce reservoir volumes but causes high turbidity, which interferes with the diversity of aquatic life (Lévêque, 2001; Lwenya & Yongo, 2010). This is an emerging threat that future studies should assess its scale and possible influence on the lake volume and level variability.

In summary, this section has shown that Lake Babati level is declining due to increased outflow occasioned by the expansion of spillways. Lake evaporation remained an outflow term with the potential to deplete lake levels; however, its influence was stronger in dry seasons and years. Water abstraction was still smaller than lake evaporation and thus with the least influence on lake level variability. Given the probable implications of lake level declines, the subsequent section reports

on evidence of hydraulic connections and interactions between surface water and groundwater systems to assess if the variability of one system could influence the other.

4.2 Hydro Geochemical Variations

4.2.1 The Abundance of Major Cations and Anions

Sodium ions (Na^+) and Magnesium ions (Mg^{2+}) were the main cations that altogether made 80% of the cation concentration, while bicarbonate ion (HCO_3^-) alone made 66%, followed by Chloride (Cl^-) at 17% of the anions. The carbonates (CO_3^{2-}) formed a tiny portion of the anions and were mostly zero for many samples except in two lake samples (LS3 and LS4). The trend of cation abundance was Na^+>Mg^{2+}>Ca^{2+}(Calcium ions)>K^+, while for anions, the abundance was in the order of HCO_3^->Cl^->CO_3^{2-}>SO_4^{2-}(Sulphate ions). These seemed to be the order of abundance of ions for lakes within the East African rift valley, as the reviews by Lameck *et al.* (2023) showed similar orders of abundance, except that K^+ was higher than reported here.

Appendix J provides details of all the measured variables and compares each sample against the World Health Organization guideline for drinking water (WHO, 2011) wherever the guideline values are defined. Most of the measured parameters were within the drinking water standards except for fluoride in samples LS4 and RV3 and nitrate in samples DW3 and SW3. Flouride concentrations from this study were within the range of 0.18 – 2.27 mg/L reported by Pantaleo *et al.* (2018). Comparatively, fluoride concentrations are low and thus placing the area in a fluoride cool spot, as Ijumulana *et al.* (2020) observed.

Despite the semi-arid nature of the study area, where excessive evaporation was expected to influence the concentration of salts (Ahmed *et al.,* 2019), the Cl^- concentration was relatively low, possibly due to the diluting effect of rainfall and runoffs into the lake which offset the evaporation effect on Cl^- concentration. However, the lake and deep wells exhibited higher Cl^- concentrations than other water sources.

4.2.2 Distribution of the Hydrogeochemical Parameters

The lake had a high concentration of all the ions, contrasting with the rainfall-driven sources like the crater, rivers, and springs (Fig. 40 (a) – (l)). The springs, represented by their EC, had the second least concentration of ions. The Ca^{2+} was highest in the deep wells with a mean of 29.16 mg/L, followed by the lake at 22.06 mg/L and the shallow wells at 20.12 mg/L. However, the lake had the highest concentration of Mg^{2+}, followed by the deep wells. The deep wells may have acquired more Ca^{2+} and Mg^{2+} salts because their waters had longer rock dissolution time than spring and river waters. The intermediate composition of the lake chemistry suggested that the

lake contains a mixture of ions from different sources. Ahmed *et al.* (2019) reported similar results in the eastern desert of Egypt, where groundwater at the downstream points (in the low altitude) had relatively higher ion concentrations and TDS than at the upstream point in the high altitude.

The EC varied among the different groups. The EC of water samples from the bottom of Lake Babati varied from 542 to 677 µS/cm with a mean of 631 µS/cm. In contrast, water samples from the lake surface had an EC range of 475 to 670 µS/cm and an average of 575 µS/cm. The EC of deep wells varied broadly from 415 to 683 µS/cm with a mean of 550 µS/cm, lower than for the lake water. The EC for the shallow wells, rivers, springs, and crater was below 500 µS/cm (Fig. 40 (c)), implying that Lake Babati catchment water is freshwater. However, it varied distinctly from Lake Manyara with an average EC of >2000 µS/cm despite simultaneously sampling Lake Babati and Manyara. Lake Manyara was sampled from two locations (one near the middle and another near the fluvial inputs at the northern part of the lake).

In contrast, the lake water and deep wells were in the category of marginal waters, with EC ranging between 500 – 1500 µS/cm (Davis & Dewiest, 1966). As always expected, the TDS followed the same trend as EC. The deep wells had intermediate values of TDS and EC (Fig. 40 (b)), falling between the lake and the rivers and springs (which are freshwater of meteoric origin). This suggested that the deep wells were a mixture of lake water, recently recharged rainwater, and water with dissolved rocks. Although Lake Babati is shallow and semi-closed with excessive evaporation, it maintained a low level of salination. The high influx of runoff seemed to have diluted the lake and retarded the salinization effect of evaporation.

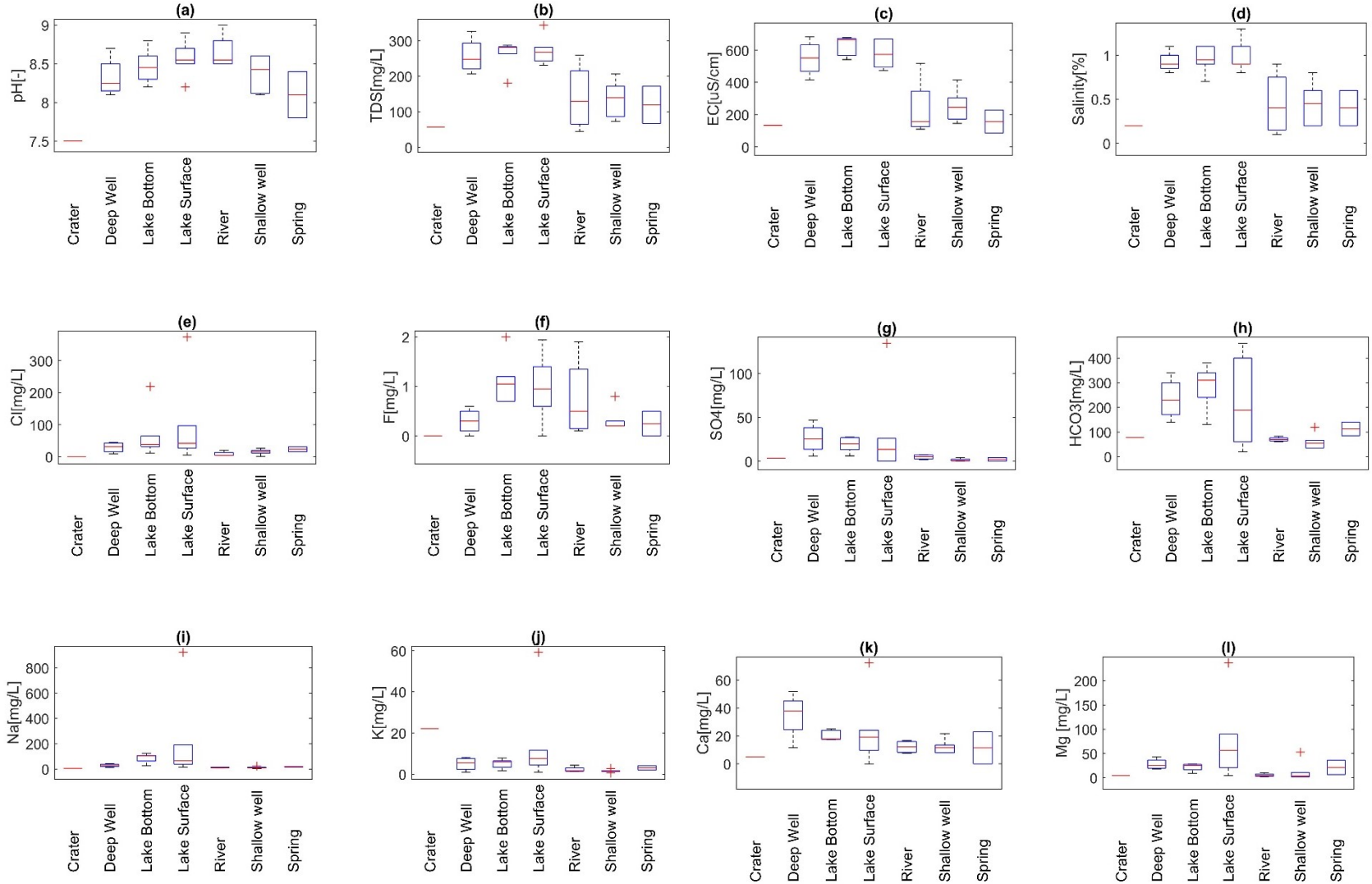

Figure 39: Variation of physical and chemical properties (a) pH, (b)TDS, (c) EC, (d) Salinity, (e) Cl^-, (f) F^-, (g) $SO4^{2-}$, (h) HCO3, (i) Na^+, (j) K^+, (k) Ca^{2+} and (l) Mg^{2+}

The results revealed that the springs, rivers, and shallow wells have lower nitrate (NO_3^-) concentrations than the bottom of the lake, suggesting they were less contaminated. Water plants on the lake surface near the bank and underwater observed during the bathymetric survey reinforce the notion that the lake has a considerable amount of nitrate pollutants. The higher NO_3^- concentrations at the bottom of the lake may have resulted from contamination by animal manure, fertilizers, or sewerage effluents from nearby communities. Elisante and Muzuka (2017) opined that animal manure might be the primary source of the high nitrate reported within the Internal Drainage Basin because the areas practice pastoralism and crop farming but with limited application of commercial fertilizers.

Although a reduction of NO_3^- concentration was expected with depth due to the presence of reducing conditions at deeper depths (Nazzal *et al.,* 2014), deep wells had the most extensive variations of NO_3^- concentration from 5.6 to 66.4 mg/L. The wide NO_3^- concentration variation in deep wells may suggest that the deep aquifer waters mixed with NO_3^- polluted surface waters since the natural occurrence of NO_3^- in water is rare. The concentration of NO_3^- in deep wells was an intermediate value between the concentration at the bottom of the lake and the shallow wells. This suggested that perhaps the waters were mixing. Mixing of the shallow well, lake, and deep well waters could only be possible if a hydraulic connection existed. The deep wells within the catchment have well screens installed to abstract water from both the confined and unconfined aquifers, attesting to the abstraction of mixed water. Therefore, the unconfined aquifers are likely in hydraulic connection with the lake through alluvial deposits, a mixture of fine to medium sand with silty clay on top that forms an aquifer surrounding the lake.

Like NO_3^-, phosphate (PO_4^{3-}) naturally has a low concentration in water or soil since phosphate is biologically active and a limiting nutrient. Therefore, the observed higher than the naturally occurring PO_4^{3-} concentration in Lake Babati suggested that perhaps the PO_4^{3-} originated from artificial sources such as sewerage deposition or leakage from farms using Nitrogen, Phosphorus, and Potassium (NPK) fertilizers which are the primary sources of PO_4^{3-} and NO_3^-. Further, the presence of both NO_3^- and PO_4^{3-} in the crater water with a comparatively higher concentration of Potassium (K^+) than Na^+ attested to the possibility of pollution of the water sources by NPK fertilizers, probably from neighbouring farms. As Timperley (1983) observed in the volcanic regions of Taupo in New Zealand, acid dissolution of some rocks may also result in elevated phosphorus concentrations. However, PO_4^{3-} concentration would be widespread in such a case, and a very high concentration would be expected in deep wells due to the prolonged contact with rocks and dissolution time. The selective PO_4^{3-} distribution in surface water sources in the Lake Babati catchment implied that PO_4^{3-} may be derived from point sources. Further, this scenario may

also suggest that the processes supplying phosphorus are higher than the biological processes depleting it, which is more likely when surface water loading of the pollutant occurs.

Although pollution from sewerage, industries, and agriculture also contribute to sulphate (SO_4^{2-}) in water (Nazzal *et al.,* 2014), the low levels of industrialization and the limited use of fertilizers in agriculture in the Lake Babati catchment area were anticipated to have minimal impact.

Generally, the deep boreholes had higher alkalinity, EC, and dissolved salts with more elevated Ca^{2+}, Mg^{2+}, and K^+ concentrations than the shallow wells. The possible dissolution of calcium–magnesium silicate or limestone rocks could have yielded Ca^{2+}, $Mg^{2+,}$ and CO_3^{2-} (Ahmed *et al.,* 2019). Kenoyer and Bowser (1992) observed that the alkalinity and concentration of some cations increase when water passes through longer subsurface flow paths. Similar results were observed in the deep wells, probably due to the long residence time resulting in rock mineral dissolution. In contrast, the shallow wells, perhaps because they are recharged from recent water, had far less dissolved solids attributed to the short interaction time with the mineral contents of the aquifer.

4.2.3 Correlation Matrix Of Parameters

Appendix K presents Pearson's correlation matrix of the physicochemical parameters of the studied waters. Variables with correlation coefficients > 0.75 were considered strong, while those with correlation coefficients between 0.5 and 0.75 were considered moderate. Total Hardness (TH) was positively correlated with many ions as follows: Fluoride ion (F^-) ($r = 0.90$, $p < 0.01$), Cl^- ($r = 0.84$, $p < 0.01$), CO_3^{2-} ($r = 0.71$, $p < 0.01$), SO_4^{2-} ($r = 0.88$, $p < 0.01$), Ca^{2+} ($r = 0.73$), Mg^{2+} ($r = 0.97$), Na^+ ($r = 0.91$) and K^+ ($r = 0.88$) as shown in Appendix K. Magnesium showed strong positive correlations with Cl^- ($r=0.80$), SO_4^{2-} ($r = 0.79$) and CO_3^{2-} ($r = 0.75$). Similarly, Ca^{2+} had a strong positive correlation with F^-, Cl^-, SO_4^{2-}, and NO_3^-. These strong correlations may suggest that the parameters co-exist or that the same processes drive their concentrations.

As always expected, samples with high TDS have high EC, as indicated by the strong Pearson's correlation ($r = 0.88$, $p < 0.01$). The pH generally showed a weak correlation with other parameters. Its strongest correlation was with TDS ($r = 0.43$, $p < 0.05$), but a correlation with CO_3^{2-} was moderate and insignificant ($r = 0.36$, $p > 0.05$). These are consistent with Ligate *et al.* (2022), who observed a similarly weak correlation between pH and other ions in groundwater from Geita and Mara districts in Tanzania. The weak correlation of the pH with other parameters might suggest that salts and rock dissolution were not related to acidic conditions (Amiri *et al.,* 2016). Similarly, a strong correlation between Mg^{2+} and CO_3^{2-} ($r= 0.75$, $p < 0.01$) might suggest that both ions coexisted and were vital parameters responsible for high pH in the water samples.

A deeper analysis of the principal components showed (Fig. 41) that EC, TDS, salinity, F^-, Cl^-, CO_3^{2-}, SO_4^{2-}, Ca^{2+}, Mg^{2+}, Na^+, and K^+ are negatively but strongly correlated with Principal Component One (PC1). The TDS showed a very significant correlation ($p < 0.01$) with CO_3^{2-}, SO_4^{2-}, Ca^{2+}, Mg^{2+}, and Na^+, which the loading plots of PC1 against Principal Component Two (PC2) (Fig. 41) indicated were due to multicollinearity, thus increasing or decreasing together. A further investigation also showed significant spatial clustering among some parameters, as shown in Fig. 24.

Table 21: Measure of global spatial autocorrelation using the Moran Index of the different water quality parameters from the study area

	Moran Index	Expected Index	Standard Deviation	p-value	Z - score
pH	-0.0701	-0.0357	0.0365	0.3466	-0.9415
EC	0.1015	-0.0357	0.0384	**0.0004**	3.5729
TDS	0.0591	-0.0357	0.0380	**0.0127**	2.4913
Salinity	0.0537	-0.0357	0.0380	**0.0186**	2.3524
F^-	-0.0412	-0.0357	0.0133	0.6801	-0.4134
Cl-	-0.0678	-0.0357	0.0281	0.2533	-1.1429
HCO_3^-	0.0617	-0.0357	0.0380	**0.0103**	2.5660
CO_3^{2-}	0.0348	-0.0357	0.0293	**0.0160**	2.4081
SO_4^{2-}	-0.0393	-0.0357	0.0257	0.8897	-0.1392
NO_3^-	-0.0628	-0.0357	0.0351	0.4412	-0.7706
Ca^{2+}	-0.0338	-0.0357	0.0345	0.9549	0.0562
Mg^{2+}	-0.0111	-0.0357	0.0267	0.3564	0.9217
Na^+	-0.0306	-0.0357	0.0175	0.7723	0.2885
K^+	-0.0146	-0.0357	0.0229	0.3562	0.9219

The EC, TDS, Salinity, HCO_3^- and CO_3^{2-} were clustered (p-value < 0.05), especially among samples from the lake and its neighbourhood, forming a hotspot near the lake, which alluded that the lake interacts with samples in its northern boundary. It was clear that areas outside the Lake Babati catchment had very distinctive patterns from the clustered samples, which suggested the sample sites were probably not interacting with the lake. These clusterings could have influenced some descriptive statistics presented here since clustering reduces the effective sample sizes.

Although all water samples were fresh with TDS < 1000 mg/L (Freeze & Cherry, 1979), the lake and deep wells exhibited higher TDS than the rivers, shallow wells, and springs, attesting to higher salt concentration. Similar patterns of TDS being higher in deep wells (boreholes) than in shallow wells, streams, and springs were reported by Ligate *et al.* (2022) around Lake Victoria gold fields in northern Tanzania. Thus, the high ion concentration in the deep wells and the lake are probably due to water that has had prolonged contact (dissolution) time with geological formation (rocks) from which most of the salts originate (Freeze & Cherry, 1979; Sakakibara *et al.,* 2016).

A significant positive correlation (r = 0.91, $p < 0.01$) of Na^+ and K^+ with Cl^- (Appendix K) suggested the dissolution of halite in the lake water. Similarly, the positive correlation of SO_4^{2-} with Ca^{2+} (r = 0.87, $p < 0.01$) and Mg^{2+} (r = 0.79, $p < 0.01$) suggested the dissolution of dolomite and gypsum rocks, especially in the waters of the deep wells and some shallow wells. This agreed with Bennett *et al.* (2021), who reported and attributed similar ion associations on Mount Merua's slopes to rock–water interactions. The F^-, Cl^-, CO_3^{2-} and SO_4^{2-} showed significant positive correlations with Mg^{2+}, Na^+ and K^+, suggesting that SO_4^{2-}, Cl^-, and CO_3^{2-} salts have a common origin. The HCO_3^- were the most dominant anions in the water samples, and their strong positive correlation (r = 0.90, $p < 0.01$) with EC, TDS, and salinity indicate their importance in driving the respective physical properties of freshwater characteristics. The increase in PC2 with a reduction in HCO_3^-, EC, TDS, and salinity hinted that the HCO_3^- concentration varied with the EC, TDS, and salinity. Therefore, the PC2 was possibly a measure of the control of the water softness since it increases with the concentration of F^-, Cl^-, CO_3^{2-}, Mg^{2+}, Na^+, and K^+, which determines water softness.

The overlap in Fig. 41 (b) in the principal components of shallow wells with deep wells and rivers implied that the shallow wells were a mixture of deep wells and river water (recently recharged water). Although the data points for the crater and springs were few for ellipsoidal representation of their spread, their locations within the cluster for rivers and shallow wells (Fig. 41 (b)) indicated their similarities. The similarity of water from the crater and springs with the rivers and shallow wells suggests that the waters originate from similar water sources (meteoric water). The deep wells had a wide range of concentrations that completely engulfed the lake bottom waters and overlapped with the water from the lake surface, shallow wells, and river waters, implying appreciable mixing levels. The striking similarity of the lake bottom water with deep wells in principal components 1 and 2, shown in Fig. 41 (b), suggests a common origin of both waters and the mixing of the two.

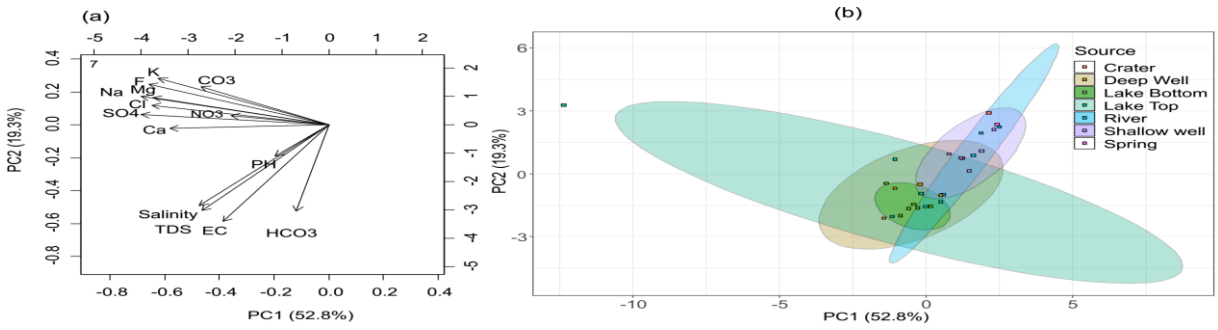

Figure 40 **(a): The loading plot of PC1 against PC2 for all the parameters considered across different water types sampled in the study, while Figure 40(b) is the cluster of eigenvalues, and principal components 1 and 2 were based on four deep wells, 6 Lake bottom, six lake top, four rivers, six shallow wells, two springs, and one craterdata**

The ellipse could not be drawn around the samples from the crater and springs because they had so few datasets

4.2.4 Piper Trilinear Diagram

From the Piper diagram classification (Fig. 42), the alkaline earth metals (Mg + Ca) exceeded the alkalis (Na + K), and the weak acids (CO_3 + HCO_3) dominated the strong acids (SO4 + Cl) in most samples. The water samples fell into three main facies types, as summarized in Table 22. However, most samples belonged to the Ca – Mg – HCO_3 facies indicating temporary hardness due to ion-exchange reaction. Carbonate hardness exceeded 50% in most samples, suggesting a substantial dissolution of possibly dolomitic rocks into the water.

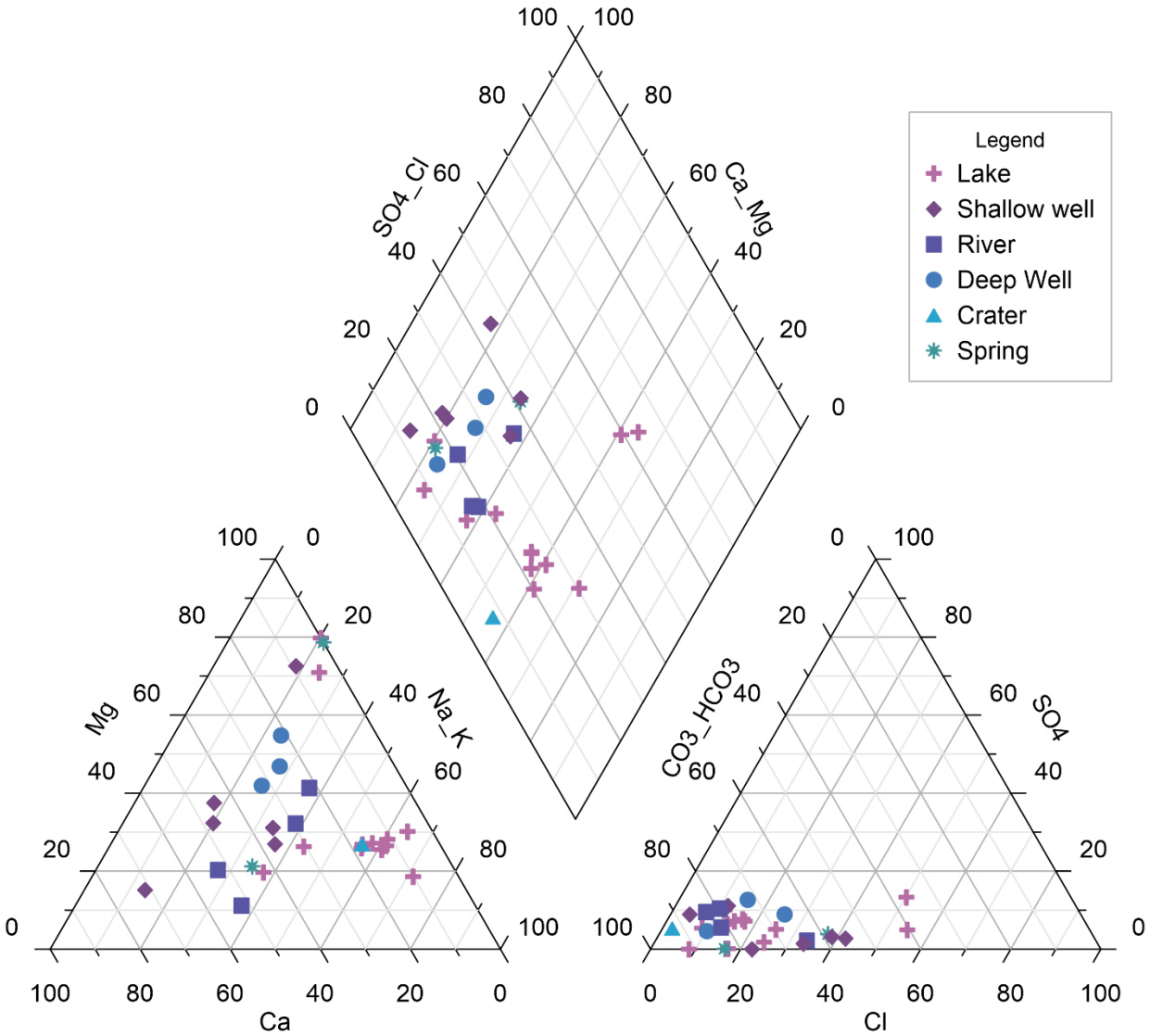

Figure 41: Distribution of the main cations and anions in the Piper diagram

Three water types occur in Lake Babati, i.e., the mixed Ca-Na – HCO_3, Na – Cl, and Ca – HCO_3, suggesting water from different sources is mixing. Moreover, four out of six locations sampled in the lake had different water types at the surface and bottom, meaning the lake is not well mixed. Location L6 in the lake was homogenous with Ca – Na – HCO_3 water type both at the surface (L6S) and bottom (L6B), while location L4 had a Na – Cl water type both at the surface (L4S) and bottom (L4B). The deep wells, springs, and some shallow wells had Mg – Ca – HCO_3 water type,

indicating the influence of rock water dissolution. In contrast, the shallow wells (SW1 and SW2) had purely Ca – HCO_3 water type.

Table 22: Classification of the dominant water types based on the Piper Diagram (Piper, 1944)

Type	Composition	Sample IDs
Non-carbonate alkali exceeds 50%	Na – Cl (Sodium – Chloride)	L4S, L4B
Carbonate hardness exceeds 50%	Ca – HCO_3 (alkaline earth exceeds alkalis – Calcium – Carbonate)	L1S, L2B, L3S, L5S, SW1, SW2, SW3, SW4, SW6, SW5, DW1, DW2, DW3, DW4, SP1, SP2, RV1, RV2, RV3, RV4
None of the cation or anion pairs exceeds 50%	Mixed – Ca – Na – HCO_3 (Calcium (Ca) – Sodium (Na) – Carbonate (HCO_3)	CR1, L1B, L2S, L3B, L5B, L6S, L6B

4.2.5 Gibbs Diagram

The Gibbs diagram of water samples from Lake Babati (Fig. 43) indicated that rock weathering and rainfall control water chemistry from most sources but the rock–water interactions dominated the cations composition of most sources (Fig. 43 (a)). The rock weathering and rainfall processes influenced the cations sources of the crater (CR), shallow well (SW4), and rivers such as RV1, RV3, and RV4. Similarly, both the rock and rainfall dominated the cations sources of spring SP2, although with a significant contribution from rainfall. Except for LB2, all the lake sources fell in the middle of the Gibbs diagram, reflecting the influence of evaporation, rock interaction, and rainfall in driving the cation composition of the lake water sources. As Dun *et al.* (2022) observed in the Pearl River Estuary in China, rock–water interactions often characterize flow delayed in porous aquifers. As such, the samples within the Babati catchment with higher ion concentrations must have had the opportunity for rock–water dissolution.

However, all the anions came from rock–water interaction dominated processes except for LS4 and LB3, where the sources were a mixture of rainfall, evaporation, and rock sources. In general, the rock–water interactions dominated the water chemistry of the different sources in Babati, except for the ephemeral rivers and some shallow wells where rainfall dominated. The rock–water interaction processes dominated the chemistry of deep wells. The strong influence of the rock weathering with a low evaporation influence and the dilution effect of the rainfall was probably responsible for maintaining the low salinity levels in the semi-closed Lake Babati. In most closed lakes, high evaporation leads to high salinity as it concentrates chloride ions (Akker *et al.,* 2011).

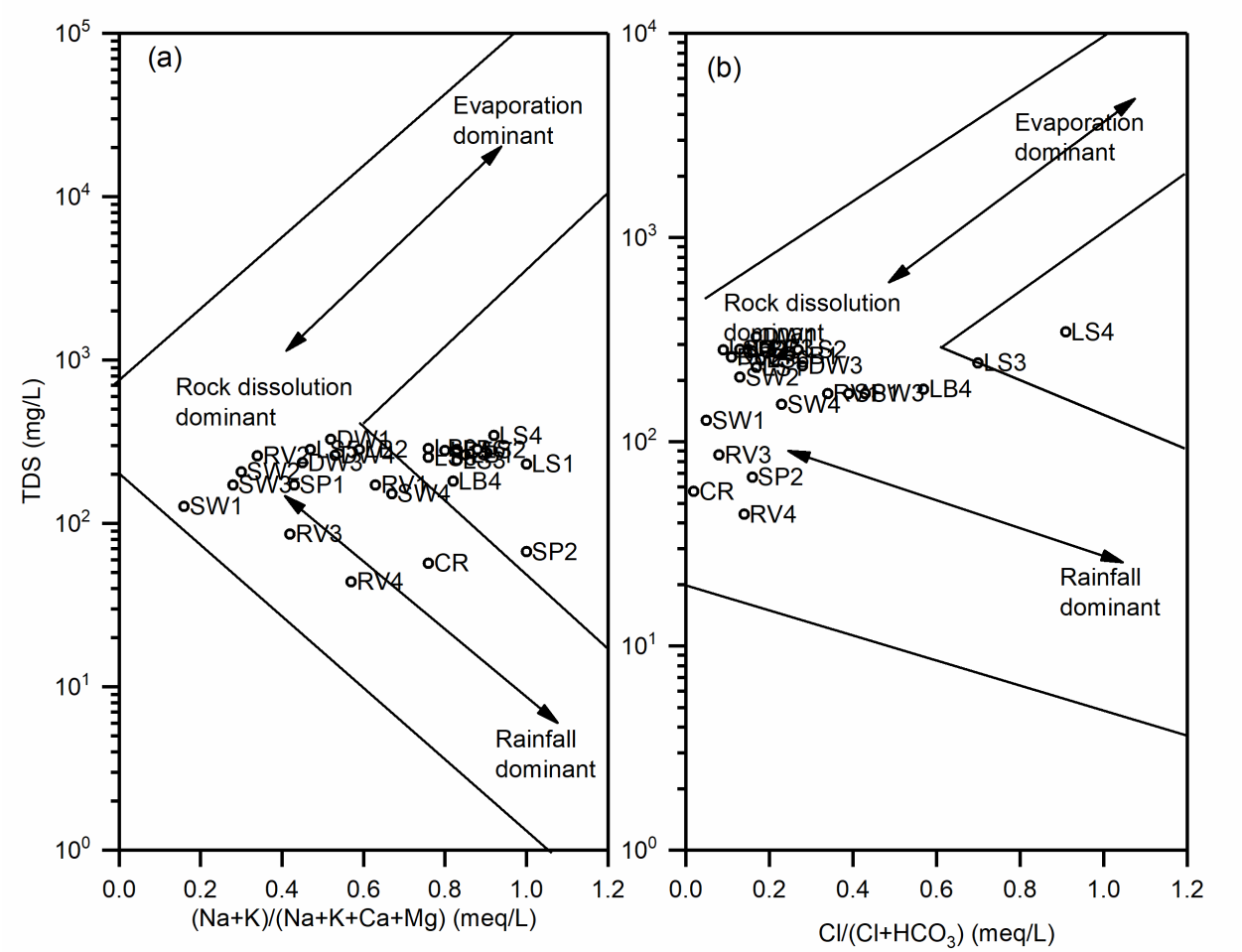

Figure 42: Distribution of sources of cations (a) and anions (b) in the water samples from Babati catchment according to Gibbs diagram

4.3 Isotopic Compositions and Variations

4.3.1 Oxygen – 18 and Deuterium Variation

The Local Meteoric Water Lines (LMWL based on the isotopic composition of precipitation from Dar es Salaam (IAEA, 2019), a coastal area that is only 10 MASL (Indian Ocean), and Dodoma, an inland town that is 1100 m higher in altitude than Dar es Salaam, were not significantly different (*p*-value = 0.22). However, the proximity of the Dodoma station to the study area and the fact that Dodoma LMWL is closer to the GMWL (Dansgard, 1964) motivated its choice to represent the isotopic composition in precipitation at Babati. Similar to the GMWL, which is a crucial reference line for understanding processes driving air masses circulation under different climatic conditions around the globe (Dansgard, 1964; Kendall & Doctor, 2003), the LMWL is useful for analysing the effect of evaporation on precipitation and the prevailing conditions during groundwater recharge.

Dodoma sampling site for the isotope in precipitation recorded the most depleted $\delta^{18}O$ value of -10.15‰ and the most enriched $\delta^{18}O$ value of 3.36‰ in April 2016 and January 2016, respectively. These $\delta^{18}O$ and δD values contrast with isotope in precipitation at the Dar es Salaam sampling

station, which ranged from -8.95 to 2.6‰ and 2.1‰ to 126.9‰, respectively. The $\delta^{18}O$ and δD values reduced in a similar pattern (not shown) with an increase in the rainfall amount, highlighting the effects of rainfall amount on the isotopic compositions (Kendall & Doctor, 2003; Scholl *et al.,* 2014). The precipitation volume-weighted isotopic composition at the Dar es Salaam station was -2.92‰ for $\delta^{18}O$ and -13.11‰ for δD. The volume-weighted composition for the Dodoma site could not be computed since the precipitation volume at the sampling time was not available. The average isotopic composition in precipitation at Dar es Salaam (a coastal site, based on 11 observations) in May, the month of water sampling in the study, was -2.22‰ for $\delta^{18}O$ and 0.69‰ for δD while the $\delta^{18}O$ at Dodoma (based on a single observation) was more depleted at -3.48‰ and δD was -17.4‰. Dodoma, the inland site, perhaps had the ocean-inland distance influencing its fractionation (Pfahl & Sodemann, 2014). This agrees with Gibson *et al.* (2016) and González-Trinidad *et al.* (2017), who reported that isotopic enrichment declines with altitude and distance from the ocean.

Generally, the isotopic compositions showed relative depletion in the peak rainy season, perhaps due to the amounts' effects, while relative enrichment was observed in the dry season. The historical data showed the relative depletion in the rainy season and enrichment as long-term seasonal patterns. Therefore, the seasonal variations of the isotopic compositions implied that rain-fed water sources such as shallow wells and springs would have similar seasonal variations in their isotopic compositions.

The variations in δD and $\delta^{18}O$ have been applied to establish aquifer replenishment sources and determine water origins, groundwater flow dynamics, and the interconnections with different sources (Jabal *et al.,* 2018; Krishan *et al.,* 2019; Maurya *et al.,* 2019). Specifically, the relative enrichment of $\delta^{18}O$ and δD in samples indicates the extent of water evaporation since lighter isotopes evaporate faster than heavy isotopes, leaving the remaining water enriched with heavy isotopes (Akker *et al.,* 2011; Kendall & Doctor, 2003). Therefore, the spread and clustering of the isotopic composition of the collected water samples shown in Fig. 44 indicated the evaporation extent of the original water source. As shown in Fig. 44 , the lake water was distinctly different from the river, springs, and shallow well waters. Specifically, DW1 and DW3 fell between the lake and springs, suggesting that those deep boreholes abstract a mixture of lake and recently-recharged meteoric water. The two other deep wells (DW2 and DW4), distant from the lake (at least 2 km away from the lakeshore), had isotopic compositions close to the precipitation, signifying that they are mainly recharged from the precipitation, which did not undergo significant evaporation. This suggested that the aquifers of these deep wells are in hydraulic connection with the local groundwater flow system where water has a short residence time or travel route.

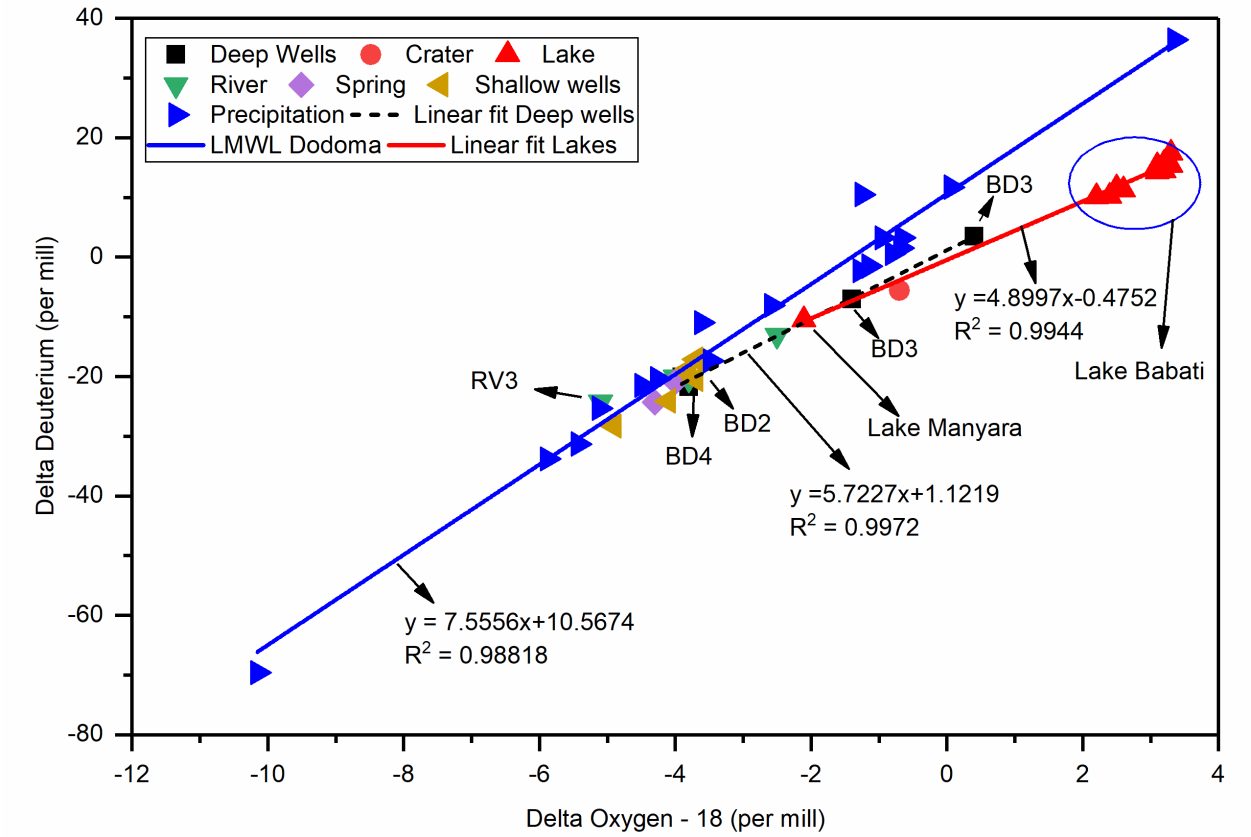

Figure 43: The comparison of variation of Deuterium with Oxygen – 18 from the study area clustered according to the water source against the Dodoma LMWL Dodoma based on 18 monthly isotopic values in precipitation

The closeness of the isotopic composition of the spring, rivers, and shallow wells to the LMWL suggests their meteoric origin. For example, the water sample from the Mrara River (RV3) was significantly depleted in heavy isotopes like precipitation and plotted near the meteoric line. It was, therefore, conclusive that the springs, shallow wells, and rivers were driven mainly by rainfall and less by the baseflow. Chacha *et al.* (2018) likewise reported similar isotopic compositions for springs in Arusha, Tanzania, and observed that the source of the flowing springs was linked to precipitation and its seasonal variations. The transient characteristics of the rivers and springs in the area further support this observation.

In contrast, River Kiongozi (RV2) had an isotopically enriched signature falling between the LMWL and Lake Babati isotopic signatures. This observation supported the notion that River Kiongozi receives isotopically rich water from Lake Babati and runoff water. Furthermore, the groundwater head contour map (Fig. 6) drawn from water levels of shallow wells substantiated that groundwater flow from Lake Babati is northeast in the flow direction of River Kiongozi.

Lake Babati water was enriched in both $\delta^{18}O$ and δD. It plotted below the LMWL with a negative intercept of -0.48 and a regression line slope of 4.89 compared to the LMWL's slope of 7.56 (Fig. 44). This deviation was most likely due to the high temperature and excess evaporation that removed the lighter isotopes and concentrated the heavier ones in the lake (Akker *et al.,* 2011).

However, Lake Manyara, (about 60 km north and downstream of Lake Babati) diverged from this with a distinctive isotopic signature and hydro-geochemistry, although it was sampled simultaneously with this study. The average EC of Lake Manyara (based on two samples, one in the Lake middle and another at the northernmost part close to a river mouth) was > 2000 µS/cm against Lake Babati's 527 µS/cm. The former had spatially varying water chemistry and isotopic signature (not shown) with more depleted water ($\delta^{18}O$ deviation of -2.1‰) near the river input, probably due to its large size and low chances of mixing. Casanova and Hillaire - Marcel (1992) similarly reported high spatial variability in Lake Manyara's hydro-geochemistry and isotopic composition depending on the distance from the fluvial inputs. The higher concentration of ions in Lake Manyara than in Lake Babati agrees with Ala-aho *et al.* (2013), who observed that closed lakes in higher altitudes at the Finnish Rokua Esker aquifer had lower solute/tracer concentrations than flowing lakes in the lower altitudes. The low salt concentration in Lake Babati was consistent with the notion that runoff and recently-recharged groundwater seep into the lake. The low solute concentration in recently-recharged water was probably due to the short contact time with rocks or the short flow path of the local groundwater flow systems, which characterize elevated catchments such as Lake Babati catchment (Toth, 1963).

4.3.2 Deuterium: Excess Variation against Delta Oxygen – 18 ($\delta^{18}O$)

A plot of d – excess against $\delta^{18}O$ indicated a spread, implying the variation in the water sources (Fig. 45). The lake water clustered in a zone with enriched $\delta^{18}O$ but very low d – excess (Fig. 45), which indicated that it experienced significant evaporation (Pfahl & Sodemann, 2014; Chacha *et al.,* 2018). In contrast, the clustering of shallow wells, springs, rivers, and two deep wells (DW2 and DW4) in a zone with high d – excess but a depleted $\delta^{18}O$, just like precipitation, implied that the shallow wells, springs, rivers, and the two deep wells away from the lake receive precipitation water before evaporation.

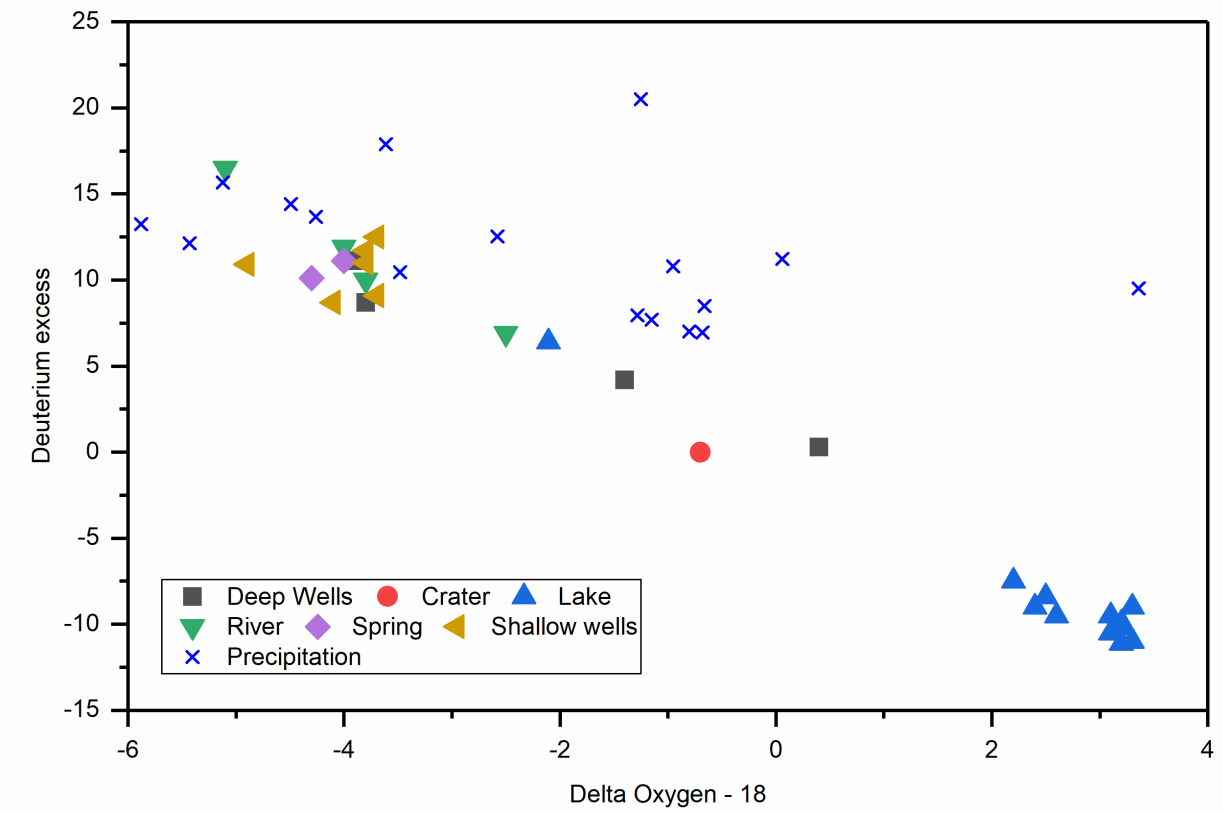

Figure 44: Distribution of the Deuterium excess against oxygen - 18 fractionization

Two deep wells (DW1 and DW3) had a d – excess intermediate to those of the lake water and precipitation, suggesting that they are in a hydraulic connection with the lake and are possibly abstracting a mixture of recently-recharged groundwater (from precipitation) and lake water enriched by evaporation. Similarly, River Kiongozi (sample RV2) recorded a d – excess of 6.9‰ and $\delta^{18}O$ of -2.5‰ (Fig. 44), closer to the d - excess of Lake Babati (-9.6‰) than any other river. This implied that a portion of the river's baseflow could be sourced from Lake Babati.

4.3.3 Lake Water Mixing

Lake Babati, although small, shallow with occasional outflow, and without the ability to turn, exhibited variations in the isotopic composition both spatially and with depth (Fig. 46). Although the isotopic variations in depth were insignificant (p-value = 0.35 for δD and p-value = 0.41 for $\delta^{18}O$), the difference indicated that the lake was not well–mixed. The spatial variation of the isotopic composition in Fig. 46 further showed a small fractionation gradient within the lake, both at the surface and bottom. The depletion at the southernmost lake boundary (upstream), closer to the inflowing streams, could be attributed to the dilution of the lake water by runoffs. On the other hand, the increase in enrichment downstream and northwards in the flow direction was probably due to the concentration of heavy isotopes by evaporation as water moved downstream with a reduction in dilution since the lake only has small seasonal streams draining into those sections. The enrichment at the lake centre might be related to a higher evaporation intensity, the concentration of enriched waters at the lake centre during seasons of low lake level, and the

reduced dilution effect from the inflowing water. The evidence of evaporation influencing the hydro-geochemistry at the lake centre near locations of samples L4S and L3S further corroborated the uniqueness of the lake at this point. Furthermore, it confirmed that the lake was not well mixed.

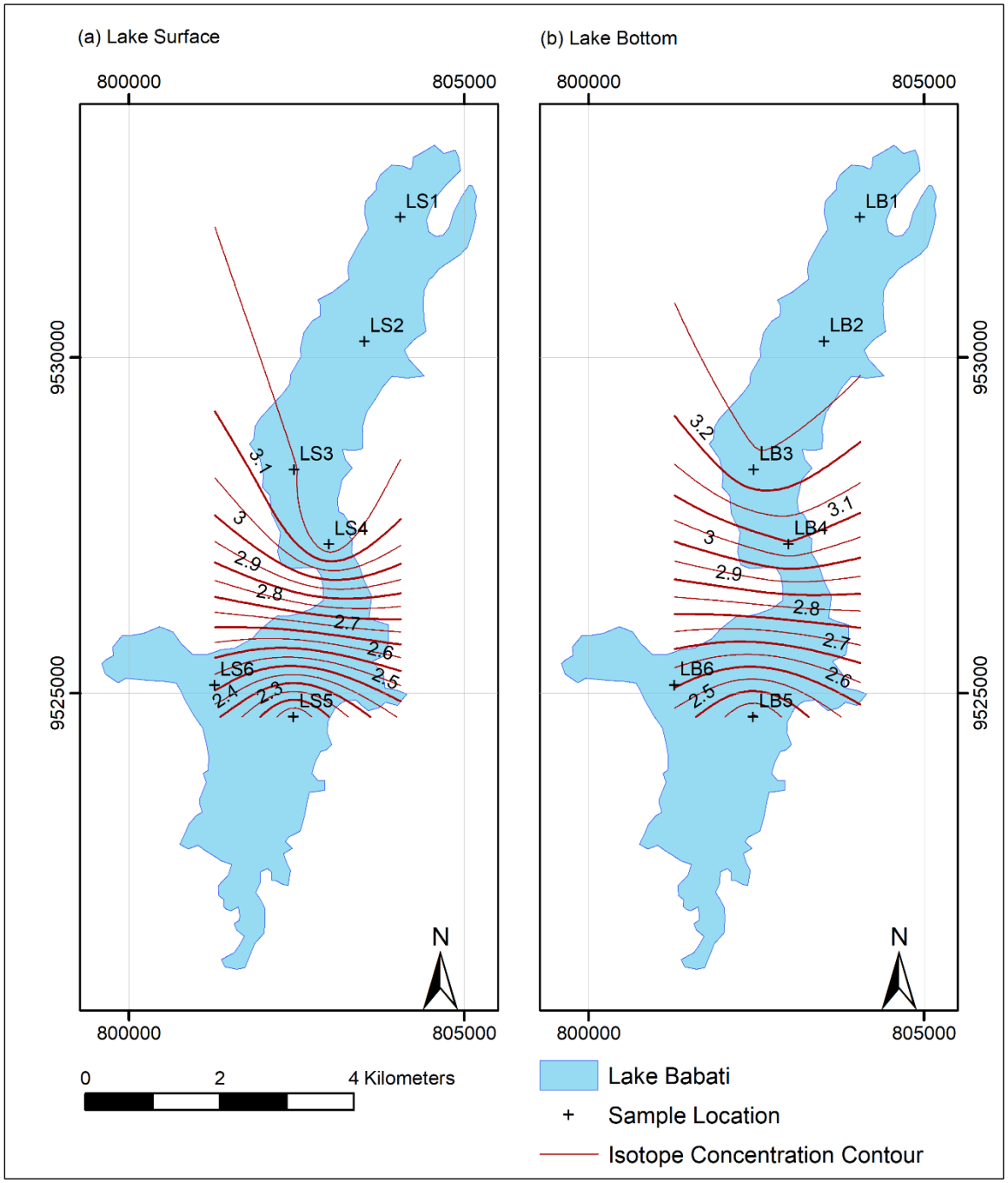

Figure 45: The spatial variation of δ^18 O within Lake Babati at the lake surface and bottom: The Lake bottom was based on water sampled at 1/3rd of the lake depth

4.3.4 Conceptual Surface Water: Groundwater Interactions

The recharge-discharge dynamics often reflect surface water–groundwater interactions as water fluxes move from one reservoir to another. Physiographic factors such as topography and geology control surface water–groundwater interactions, while climatic factors influence recharge (Khan & Khan, 2019). The recharge–discharge dynamics depend on the groundwater flow systems,

which Toth (1963) classified into local, intermediate, and regional groundwater flow systems. The recharge of regional flow systems occurs across regional surface water divides, and discharge occurs into streams of a higher order through deep, steady slow processes with highly mineralized water. In contrast, recharge and discharge of a local flow system happen at local water divides and at lower-order local streams at a relatively shallower, faster with an unsteady flux of less mineralization (Khan & Khan, 2019).

As observed in this study, the groundwater systems on the eastern bank of Lake Babati seem to discharge into the lake due to its steep groundwater level gradient. Whereas the groundwater gradient in the western banks is also inclined to the lake, groundwater influx into Lake Babati is anticipated to be lower than influx from the eastern side. The southern parts of the catchment have steep gradients with ephemeral rivers which discharge into the lake. Although the rivers are seasonal, their beds usually remain wet, attracting farmers to grow paddy rice in waterlogged areas. Whereas areas can become waterlogged for various reasons, these indicate that some groundwater from the area is discharged into the lake. The close association of River Kiongozi to Lake Babati in hydrogeochemistry and isotopic composition indicates a northward discharge of lake water into the groundwater systems. These observations suggest that Lake Babati interacts with the groundwater systems.

As Khan and Khan (2019) observed, when the water table is higher than the surface water level, the surface water will receive groundwater inflow. Whereas the general assumption is that surface water receives groundwater if the water table is higher than the elevation of the surface water bed, Khan and Khan (2019) noted that the deeper portions of the surface water body may still discharge into the groundwater system even when water table stands at a higher position. This is a likely scenario in Lake Babati, especially in its deep sections where similar hydrogeochemistry and isotopic composition were observed between samples of the lake and some deep wells.

4.3.5 Mapping Groundwater Potential using Topography: Based Methods

Conscious of the popularity of groundwater sources in the region where data paucity has limited the understanding of groundwater availability, this study undertook an innovative approach to study the GWP. It applied topography, readily available data at a reasonable quality, to predict distributions of groundwater and suitable locations for groundwater development.

4.3.6 Groundwater Potential Determinants

(i) Distribution of HAND and Topographic Wetness Index

The HAND provides hydrologically helpful information about soil water conditions and dynamics that have been applied to measure the relative potential gravitational energy (Nobre *et al.,* 2011). Therefore, the areas of high HAND captured in Fig. 47 (a) are thought to have a high drainage potential, while the low HAND areas are likely waterlogged or have low drainage potential. The areas closer to the lake and drainage lines showed low HAND, implying a high likelihood of GWP. Such areas can be groundwater discharge or recharge points depending on the groundwater level in the neighbourhood.

Topographic Wetness Index assigns high indices for the areas along the streams and low indices for hilly areas away from the water sources. Similar patterns were observed in Fig. 47 (b), affirming the influence of topography on the groundwater processes within the Lake Babati catchment. Furthermore, groundwater depth becomes shallower as TWI increases (higher wetness index), demonstrating that TWI measures topography control of groundwater depth (Rinderer *et al.,* 2014). This was also corroborated by Nejad *et al.* (2017), who showed that GWP increases with TWI because a local slope is a proxy of the hydraulic gradient, and the upslope area contributes to groundwater flow.

(ii) Land Use and Land Cover

Although the land cover strongly correlates with HAND (Renno *et al.,* 2008), its constantly evolving nature driven by anthropogenic activities influences GWP. It is observed that the reduction of forested cover results in reduced infiltration, whereas the increase of the built-up environments amplifies runoffs and the reduction of groundwater infiltration (Calder *et al.,* 1995). Furthermore, agricultural land generally encourages infiltration, although the magnitude of the influence varies depending on the actual water conservation practices employed (Singh *et al.,* 2017; Anand *et al.,* 2018). Therefore, Lake Babati catchment, predominantly shrubs and sparse vegetation (42.6% cover), followed by agriculture at 41.1% (159.6 km^2), a higher infiltration was anticipated as both large land cover types encourage infiltration. The built-up and the bare and barren land that encourage runoff make up 4 and 19.2%, respectively, while the open water covers 3.1%. The effect of bare soils is an intermediate between agriculture and built-up areas because bare soils have sparse vegetation. Figure 46 (c) presents the spatial and overall effect of the land cover types considered an indicative measure of groundwater recharge. A higher GWP was expected in the water cover, forested areas, and paddy fields (classified as agriculture). This is so because the standing water would infiltrate and percolate more through the enormous deposits of

the chromic – luvi Phaeozams soil type, where a low gradient restricts lateral flows. However, areas with high groundwater recharge may not have high GWP unless favoured by factors that restrict water movement.

(iii) Soils

The catchment has mainly three soil types distributed, as shown in Fig. 47 (d). Humi-rhodic luvisols primarily occupy the gently sloping areas of the southern portion of the catchment. Luvisols are moderately weathered soils that overlay unconsolidated alluvial deposits, forming the catchment's principal aquifer. The profiles of luvisols have less clay at the top than in the subsurface (Driessen *et al.,* 2001). Eutric leptosols were expected to have a higher GWP because they sometimes have shallow groundwater depths and low water retention capacity, which result from well-drained soils due to the high gravel content. However, the shallow depth to the bedrock of leptosols was anticipated to limit the GWP in some areas due to the high erosion rates on the steep slopes (Driessen *et al.,* 2001).

The chromic – luvi phaeozams, due to their attributes of being porous, well-aerated, organic matter-rich soils in the flat or gently undulating landform was ranked higher in GWP. These soils often cover the unconsolidated parent material of either aeolian or alluvial origin (Driessen *et al.,* 2001), which provides a higher chance of infiltration. Soils with a higher infiltration rate received the highest weights for groundwater recharge due to their perceived capacity to infiltrate and percolate more water into the groundwater aquifers.

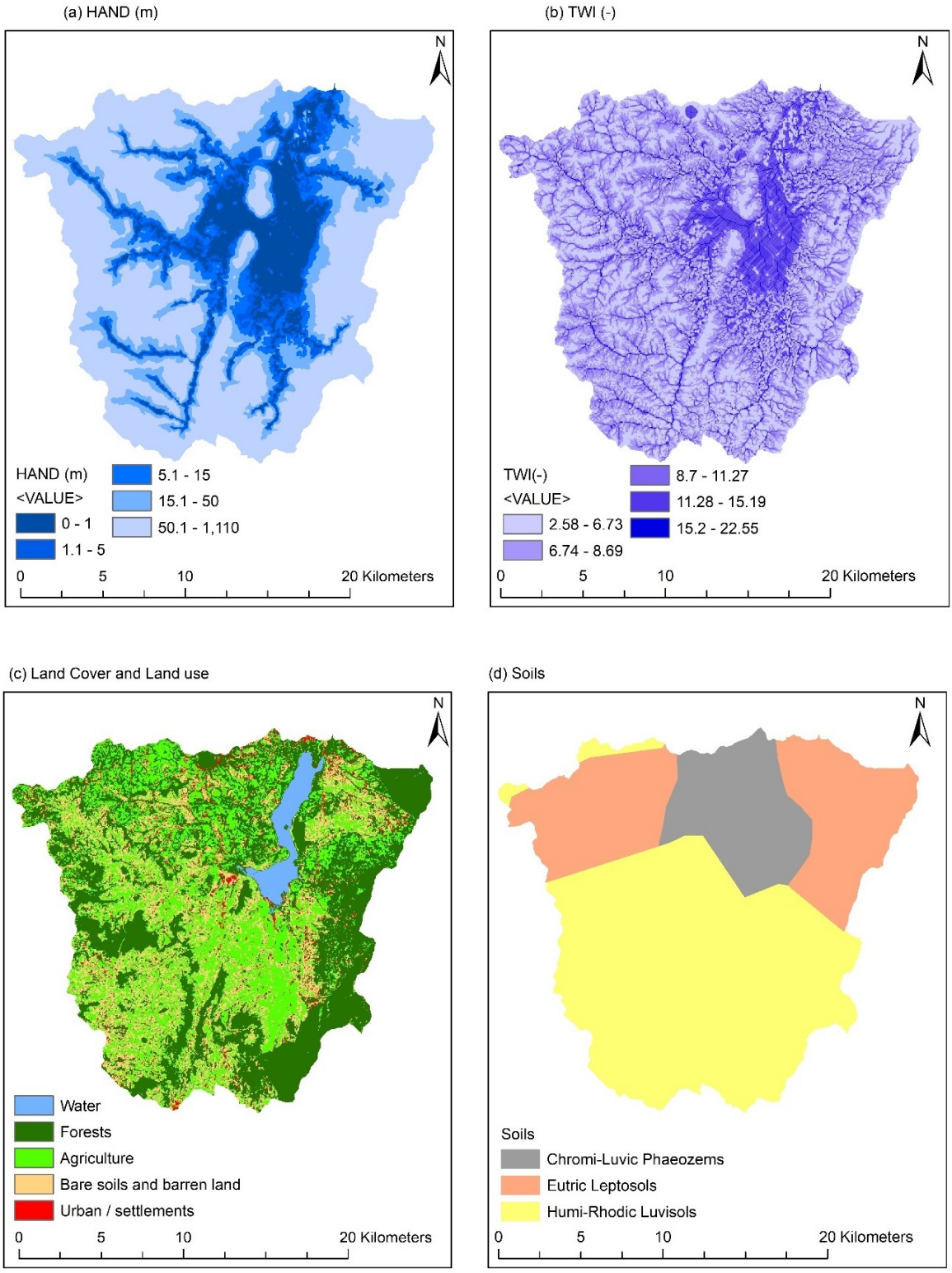

Figure 46: Input maps for mapping the groundwater potential; (a) Height Above Nearest Drainage (HAND), (b) Topographic Wetness Index (TWI), (c) Land use and land cover, (d) Soils

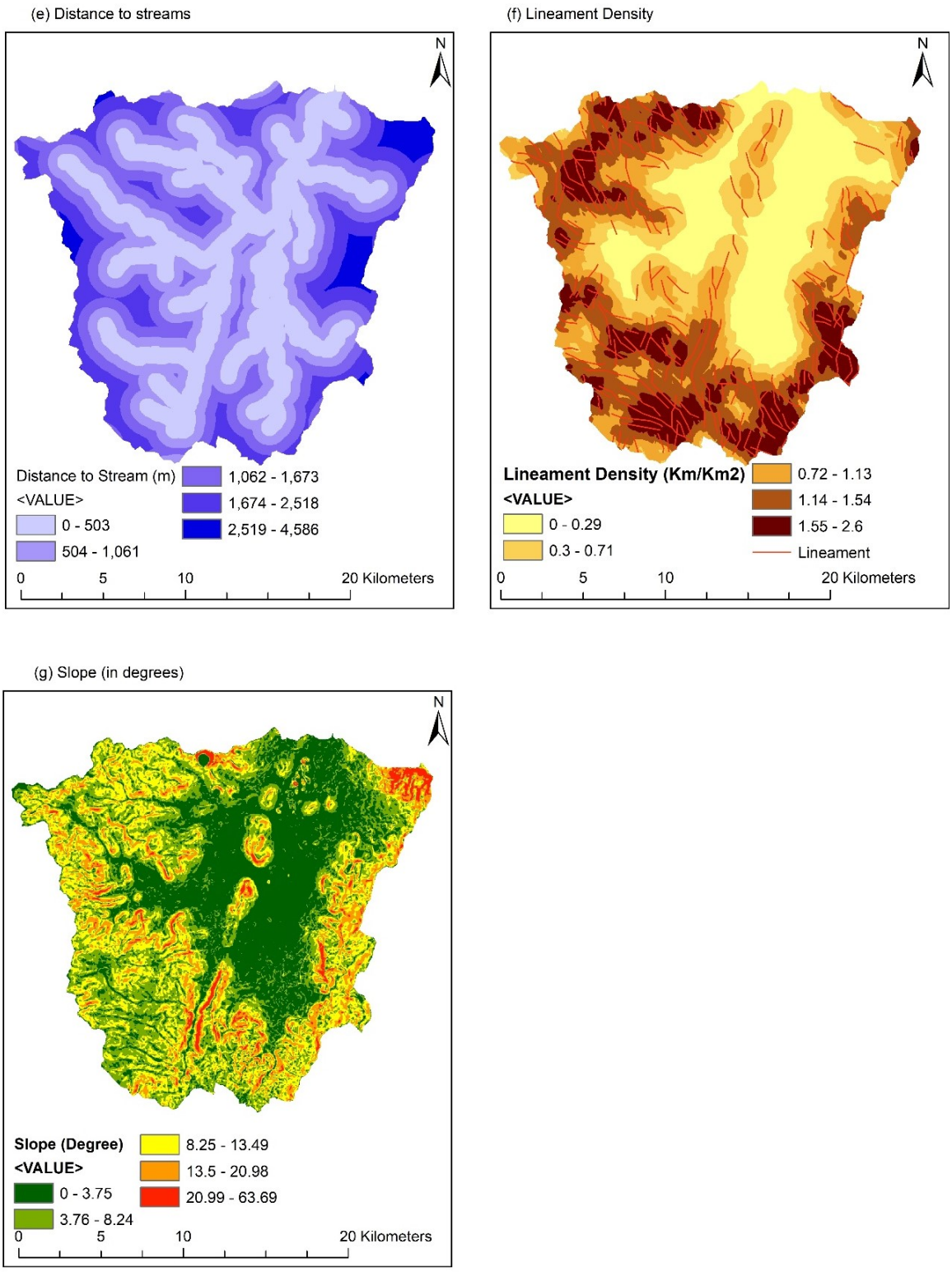

Figure 47: Additional input for mapping the groundwater potential; (e) Distance to the streams, (f) is the lineament density, and (g) is the slope in percent

(iv) Slopes

The slope is vital for understanding hydrology as it influences recharge, runoff, surface water occurrence, and movement (Shekhar & Pandey, 2014; Ghorbani Nejad *et al.,* 2017). Steep slope areas will likely have low GWP due to higher runoff potential and low infiltration (Hamdani & Baali, 2019). On the other hand, gently sloping areas favour water retention and facilitate more

infiltration and groundwater recharge (Tolche, 2020), indicating a higher potential for groundwater (Shekhar & Pandey, 2014). The gently sloping areas (slope < 3.75°) around the lake and streams (Fig. 48 (g)) were expected to have high GWP because of reduced horizontal water movement. They can be recharge or discharge points depending on the groundwater level in the neighbourhood. The steeply sloping (slope > 8.25°) areas around the mountain faces and hills are likely to have low infiltration rates and GWP unless influenced by lineaments and forests that favour infiltration.

(v) Geology

Geology controls the infiltration rate and porosity (water storage capacity). The Precambrian metasediments of quartzo – feldspathic gneiss, micaceous quartzite, and amphibolite (all metamorphic rocks) rocks which abound the southern border (Fig. 2), act as aquiclude with low water yield. The southern part of the catchment (Fig. 2) has a high likelihood of GWP because it has Bubu cataclastic, a Precambrian rock characterized by faults and micropores that permit groundwater flow.

The patches of volcanic agglomerate, volcanic tuffs, and fragments interspersing the superficial deposits that dominate the catchment's northern parts also have a potential for groundwater. The superficial deposits in the northern and central catchment form the principal aquifer of the catchment as it is covered by alluvium materials, red and brown soils, mbuga soils, and water (Fig. 2). The zone received the highest ranking for GWP, and it was thus not surprising that most wells (deep and shallow wells) were located within the formation of superficial deposits.

(vi) Distance to the Streams

Areas closer to the rivers are likely to have a higher GWP because surface water infiltration is the primary step in groundwater recharge (Arulbalaji *et al.,* 2019; Benjmel *et al.,* 2020). However, the slope and direction of groundwater flow can redirect water and affect the GWP. Nonetheless, the areas closer to the river (Fig. 48 (e)) are generally likely to receive water from or drain into the rivers. Therefore, those areas were weighted higher for GWP.

(vii) Lineaments Density

In Babati, the lineaments are located on the hilltops (Fig. 48 (f)), with very few wells sited to benefit from the high GWP. This is probably because the hills are conservation areas (forests) with very sparse or no settlements. The sparse settlements ensured the catchment recharge areas were free from anthropogenic-related pollution. Lineaments often become paths for groundwater flow and express the underlying geological structure (Kim *et al.,* 2004; Salui, 2018). Therefore,

information on lineaments is often exploited to establish mineral distribution, groundwater, and runoff potential zones because areas of high lineament zones denote good groundwater recharge and flow points through secondary porosity (Corgne *et al.,* 2010; Shekhar & Pandey, 2014; Andualem & Demeke, 2019).

Although lineament information alone is inadequate for drilling success, it was used to zone potential groundwater areas (Das *et al.,* 2019; Hamdani & Baali, 2019). For example, in the Soudano – Sahelian region, a semi-arid region of Niger, Corgne *et al.* (2010) found that 85% of lineaments were within 500 m from producing wells, and 40 – 50% of these wells were located within 200 m from lineaments.

4.3.7 Groundwater Potential Zones

Using the AHP with seven input parameters, this study delineated and classified the GWP zones into five groups based on GWP indices as follows: Very Poor (0.07 – 0.14), Poor (0.14 – 0.17), Moderate (0.17 – 0.21), Good (0.21 – 0.25), and Very Good (0.25 – 0.32) GWP zones. The "Very Good" GWP zones lay mainly in Lake Babati valleys and stream banks (Fig. 49), characterized by low HAND values, high TWI, and low slopes. This agrees with Nobre *et al.* (2011) on categorizing low HAND or high TWI areas as wetlands. In addition, it indicated the influence of both HAND and TWI in defining the GWP zones. The "Very Poor" and "Poor" zones of GWP were usually located in regions with steep slopes away from drainage lines. The findings agreed with Condon and Maxwell (2015), who also showed that the water table is deep in areas of steep topography and vice versa.

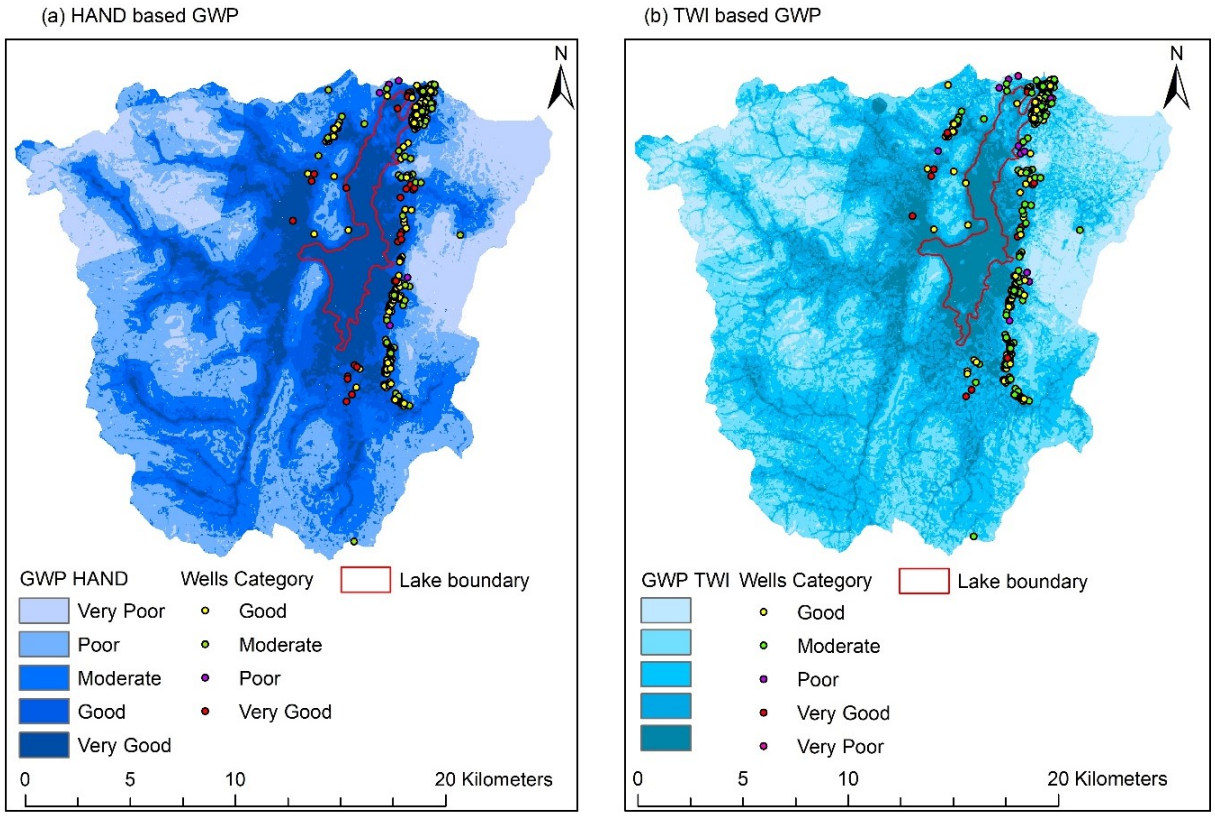

Figure 48: Comparison of Groundwater Potential (GWP) zone with shallow and deep wells classes. (a) is GWP computed based on Height Above Nearest Drainage, and (b) is GWP computed based on the Topographic Wetness Index

Both methods showed a spatial similarity of GWP zones. The variation of areas in each class was compared, as shown in Table 23. The "Very Good" potential zones generally had fewer wells than the "Good" potential zone. The "Good" GWP zone had the highest number of wells (61.31%) in the HAND–based zone compared to only 35.71% (total of 120 wells) of wells in TWI-based maps. This was despite the "Good" GWP zone occupying only 15.15% of the area in the HAND-based GWP classification and 18.27% of the total catchment in the TWI-based GWP zones. In contrast, the TWI-based GWP classification had the highest number of wells (183 wells which translated to 54.46% of the total wells) in the "Moderate" GWP zone. The HAND-based GWP zone had five wells in the "Poor" zone, which occupied 121.16 km^2 (31.16% of the catchment), and none in its 55.88 km^2 (14.37%) classified as zones of "Very Poor" GWP. However, the TWI-based GWP had as many as 16 wells (4.76% of wells) in its 110.55 km^2 (28.43%) areas classified as the "Poor" GWP zone and one well in the "Very Poor" GWP zone, which occupied 46.52 km^2.

Table 23: Distribution of wells within the groundwater potential zones based on the HAND and TWI classification methods

No	HAND based GWP zone					TWI based GWP zone			
	GWP Class	Area (km^2)	Area (%)	Wells distribution (Shallow & deep)		Area (km^2)	Area (%)	Wells distribution (Shallow & deep)	
				Number	%			Number	%
1	Very Good	51.87	13.34	28	8.33	43.72	11.24	16	4.76
2	Good	58.91	15.15	206	61.31	71.04	18.27	120	35.71
3	Moderate	100.99	25.97	97	28.87	116.95	30.08	183	54.46
4	Poor	121.16	31.16	5	1.49	110.55	28.43	16	4.76
5	Very Poor	55.88	14.37	0	0.00	46.52	11.97	1	0.30

Shallow wells (depth < 30 m) are generally located in areas with a higher success of getting water and close to users (Pantaleo *et al.,* 2018). However, successful drilling depends on groundwater exploration efforts, methods applied, and perhaps the team's expertise. Therefore, the restriction of locating a shallow well in the owners' property seems to have dictated or limited the exploitation of GWP in some cases. These restrictions could explain why few wells were located within the "Very Good" GWP. In addition, physical restrictions such as the lake and ephemeral rivers could have further limited the number of wells in some parts of the "Very Good" GWP area.

Nevertheless, the prospect of locating shallow wells in "Very Poor" GWP areas was expected to be minimal. The inconsistent distribution of wells among all the TWI-based GWP classes, including in the "Very Poor" GWP zone where none or very few wells were expected, suggests that the TWI – based methods harbour some randomness in wells' allocation. The HAND-based classification appeared free from such random classification, implying it is more robust and definite than TWI-based methods in predicting the potential groundwater zones. A linear correlation between the number of wells within a GWP zone and the zone area was positive for the TWI-based classification with a coefficient of determination (r^2) = 0.3224.

In contrast, the HAND-based classification showed no correlation with the zone area, and the coefficient of determination (r^2) was just 0.0387. If the wells' allocation were random, the number of wells in each GWP zone would positively correlate to the proportion of each zone's area in the catchment. On the other hand, the TWI-based classification had a positive correlation implying a limited degree of randomness in its classification of the GWP zones. Further, the weak correlation between TWI and groundwater reported by Rinderer *et al.* (2014) in gently sloping topography probably explains the random distribution of wells by the TWI-based GWP classification method. This meant that the upstream contributing areas had less influence on the groundwater flow in the area but rather the height above the nearest drainage, which measures the gravitational potential (Nobre *et al.,* 2011).

4.3.8 Parameter Sensitivity

The soil was the most influential and sensitive parameter with the highest effective parameter weights than the assigned theoretical weights (Table 24). It had an average effective weight of 22.11% for HAND–based GWP zonation and 21.94% for the TWI – based method. The average effective weights were greater than the theoretical weight in both cases. The second most sensitive parameter was the slope (measured in degrees) at 19.88% and 19.77% in the HAND-based and TWI-based classification methods of GWP, respectively. The distance to streams came third as the most influential and sensitive parameter, with an average effective weight of 16.58% for both methods. These sensitivities implied that any misidentification of the soils, slopes, and distance to streams could influence GWP mapping efforts. Therefore, the arbitrary definition of the stream initiation threshold area (the minimum area before a stream develops) could strongly influence the distance to the streams. However, the same distance to the stream map and weight were maintained in both methods.

The effective weight of TWI was significantly higher than the effective weight of HAND (t – statistics = 37, p-value < 0.001). The TWI had an average effective weight of 11.32 %, with a standard deviation of 6.31% in the GWP zonation compared to the 10.74 % average and a 7.29% standard deviation attained by HAND. The TWI showed more sensitivity than HAND in the zonation of GWP in the area. The sensitivity analysis further revealed that the soil and the distance to streams had a more substantial influence than assumed theoretically (Table 24). The sensitivity of lineament density, land use and land cover were closer to their assumed theoretical values. At the same time, the effective magnitude of geology was lower than its assumed theoretical magnitude.

Table 24: Sensitivity analysis of input parameters for groundwater potential indices using HAND and TWI

Theme	Normalized theme weight	Effective weight in HAND based GWP				Effective weight in TWI based GWP			
		Min	Max	Mean	Standard Deviation	Min	Max	Mean	Standard Deviation
HAND/ TWI	0.1875	3.08	33.57	10.74	7.29	2.95	37.95	11.32	6.31
Geology	0.2188	3.59	29.67	9.88	4.25	3.59	29.67	9.92	4.48
LULC	0.0938	2..43	27.87	10.35	3.5	2.49	27.87	10.2	3.24
Lineament Density	0.0938	2.32	28.76	10.29	5.88	2.32	28.76	10.03	5.54
Distance to streams	0.1250	2.79	35.41	16.58	5.33	2.16	35.42	16.65	5.7
Slope (Degree)	0.1563	4.88	42.2	19.88	4.85	4.88	42.2	19.77	4.77
Soil	0.1250	6.78	45.38	22.11	7.37	6.87	45.38	21.94	7.09

GWP means Groundwater Potential, HAND is the Height Above Nearest Drainage, TWI is Topographihc Wetness Index , LULC is Land Use and Land Cover, Min is Minimum and Max is Maximum

Weighting values assigned to parameters were subjective and varied with different studies and environments. For example, Andualem and Demeke (2019) ranked thematic maps with high GWP in the order of geology > slope gradient > geomorphology > lineament density > drainage density > land cover > soil type. However, Pande *et al.* (2017) accorded geology a smaller weight and ranked the thematic maps in the order of hydro-geomorphic = depth to groundwater > land cover > geomorphology = elevation. Magesh *et al.* (2012) ranked the thematic maps in the order of importance to GWP as follows: lithology > land use > slope gradient > lineament density > rainfall =drainage density > soil.

4.3.9 Validation of GWP with Wells Data

The effectiveness of GWP zonation was validated using water levels and depths of 323 shallow wells (depth < 30 m) collected in June 2017 by Pantaleo *et al.* (2018). The wells' depths varied from 3 m to 30 m, while the depths to the water level varied from the ground surface (0 metres below ground surface (mbgs)) to a maximum of 24.62 mbgs. The shallow wells were clustered near the lake, implying that their depths were guided by other reasons besides water availability. The detailed statistics of the wells per GWP classes captured in the box and whisker plots were presented in Fig. 50.

Some wells had water levels on the ground surface in the HAND classification. The shallow wells within the "Very Good" GWP zones had an average depth of 9.40 mbgs, while the average depth of shallow wells in the "Good" GWP zone was 8.44 mbgs. The average well depth increased to 14.61 mbgs in the "Moderate" GWP zone and 20.16 mbgs in the "Poor" zone (Fig. 50 (b)). These variations in the well depths and depths to water levels were realistic as areas with high GWP tend to have a shallow water level and would, therefore, have shallow wells. Wells tend to be deeper in low GWP areas. However, well depths alone are not a good indicator of GWP because wells are often excavated/drilled further after water strikes to abstract more water or as a precaution against seasonal fluctuations in groundwater levels. Thus, without well yields for defining GWP, the complementary use of well depths and water levels becomes very informative. However, the validations with well depths and water levels would be misleading, especially in the perched water table or low-yielding wells, as the water levels would inaccurately reflect the GWP.

The TWI-based classification of the GWP showed similar patterns as the HAND-based classification. The depth to water levels of shallow wells in the "Very Good" GWP zones was an average of 4.51 mbgs and 7.37 mbgs for the "Good" zone but increased to 12.68 mbgs in the "Poor" GWP zone (Fig. 50 (c)). Similarly, the mean well depth increased from 8.64 mbgs in the "Very Good" GWP zone to 16.64 mbgs in the "Poor" potential zone, as shown in Fig. 50 (d). Despite the observed differences between the average water level in the HAND–based and TWI-

based GWP classification, no significant differences were observed in the depths to water levels and well depths of a similar class between the two methods.

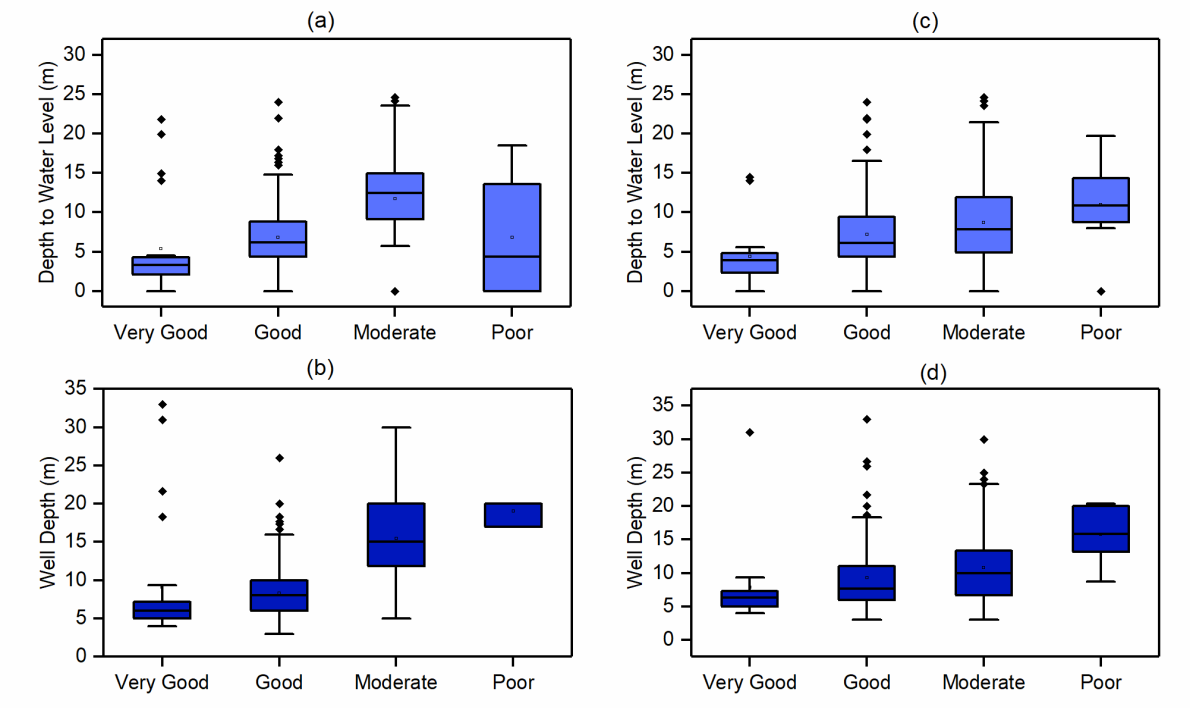

Figure 49: Comparison of depths to water level and wells depths in different groundwater potential classes by the HAND-based and TWI-based method

(a) is depths to water level classified by the HAND-based method, while (c) is depths to water levels for shallow wells classified by TWI-based groundwater potential zonation. (b) is the depths of the wells classified by HAND, and (d) is the depths of wells classified based on TWI groundwater potential classes

For the HAND-based classification, the average depth to water levels was significantly different from one class to another, except for the close classes such as "Very Good" and "Good" (p-value = 0.31), and "Moderate" and "Poor" classes where p-value = 0.37, higher than the 0.05 alpha value of significance. The water levels showed a similar pattern with the well depths in the groundwater class of "Very Good" and "Good" being insignificantly different (p-value = 0.6), just as "Moderate" and "Poor" with insignificant depth differences with p-value = 0.13. Wells in the "Very Good" and "Moderate" areas were significantly different at a p-value < 0.05 for the two methods. Similarly, wells in the "Poor" and "Good" zones showed significant differences in depths to water level (for the TWI-based method, p-value < 0.001) and p-value = 0.09 for the HAND-based method).

The depths of wells in all the other zones were significantly different (p-value < 0.05) except for wells between the "Very Good" and "Good" zones, with a p-value = 0.61 for the HAND and p-value = 0.78 for the TWI-based method. Similarly, the depth of wells in the "Very Good" was insignificantly different from wells in the "Moderate" zones (p-value = 0.43 for the HAND-based method and p-value = 0.51 for the TWI-based method). The insignificant differences in the water levels and well depth among the wells could indicate the inadequacy of the groundwater zone

classification methods. However, some groundwater potential classes had very few wells which influenced the statistical analysis and resulted in an unreasonably high standard deviation. For example, in the HAND-based method, out of 13 wells in the "Very Good" category, only 11 had wells depth compared to 158 wells with well depths in the "Moderate" zones. Nonetheless, it was logical that wells should be deeper (Fig. 50) in areas of low groundwater potential.

As shown in Fig. 50 (a), (b), (c), and (d), both methods indicated that the average depths to water level and well depths were shallow in "Very Good" GWP zones but deepened in areas of lower/poor GWP. The concentration of wells in the "Good" zone indicated that the HAND method classified wells better than the TWI method. None of the allocated a shallow well in the "Very Poor" zone. The TWI-based method had one well in the "Very Poor" zone but as many as 16 wells in the "Poor" zone, yet HAND had only five wells in the "Poor" zone. Since shallow wells primarily derive water from shallow aquifers, it was inconsistent for "Poor" and "Very Poor" GWP areas to have many shallow wells. Moreover, the distribution of shallow wells in the different classes of the TWI classification correlated positively, though insignificantly, with the area of GWP classes. This suggested that the TWI-based method was slightly random in predicting the GWP zones. The distribution of the 13 deep wells (> 30 m) in the various classes presented inTable 25 corroborated the randomness of the TWI-based method.

Due to professional drillers' rigorous and extensive groundwater prospecting efforts before developing deep wells, GWP validation using the deep wells was given more weight than the shallow wells. The deep wells also indicated that the wells' depths increased as the GWP reduced except for wells in the "Good" GWP, which were few. Test pumping results could have validated the groundwater zones better, but the data was unavailable.

Both methods accurately delineated the "Very Poor" GWP zones, and none of the deep wells was located within the zone. Technically, the location of four deep wells in the 'Very Good" zone by HAND compared to three deep wells by the TWI-based method might have indicated the superiority of the HAND–based method in defining the GWP classes over the TWI. However, we were also cautious because non-technical criteria such as land ownership and availability can dictate the siting of wells.

Table 25: The distribution of the deep wells (depth > 30 m) among the different groundwater potential classes

Classes	HAND based classification		TWI based classification	
	No of deep wells	Average of well depth (m)	No of deep wells	Average of well depth (m)
Very Good	4	57.89	3	41.84
Good	3	56	2	90.73
Moderate	5	87.15	7	73.19
Poor	1	150	1	150

Generally, the location of very few shallow wells in the "Poor" and "Very Poor" zones indicated that the local shallow well excavators had implemented an adequate groundwater prospecting method that has proven successful and effective in identifying the "Poor" GWP areas. Conclusively, using either of these methods to predict the GWP map can help drillers/excavators improve well-drilling success while minimizing prospecting costs. The maps can narrow the extent of geophysical surveys and other groundwater prospecting efforts. In addition, the GWP map provided valuable information for further research and detailed modelling of groundwater-lake interactions, as areas of high GWP can be identified.

4.3.10 Comparison between HAND and TWI Groundwater Potential Areas

In the comparison, the GWP map based on HAND was referenced against the GWP map based on TWI. The TWI's percentage correct or agreement was measured against the GWP produced by HAND. Table 26 provides the basis for calculating the percentage of the agreement as it compares, cell by cell, the classification of the GWP by the two methods.

The class agreement percentage between the two GWP zoning methods are shown in the diagonal values. The best agreement was obtained in the "Very Good" zone, with 90.70% of the zones defined by TWI as the "Very Good" GWP zones defined similarly as so by HAND. Again, the two methods reached 83.66% agreement in defining the "Very Poor" GWP area. However, the TWI method had only 51.03% agreement with the HAND classification to define the "Poor" GWP. The misclassified zones were placed in either the next higher or lower class. For example, 25.47% of the areas TWI classified as "Moderate" belonged to the "Good" zone, while HAND classified another 13.41% of the moderate zone as "Poor". Although these could have resulted from differences in the two methods, the arbitrary class definition of the input parameters by Jenk's natural breaks (Benjmel *et al.,* 2020) was another source of errors in GWP zonation. The TWI further had a 77.64% agreement in classifying the "Good" GWP. However, 11.96% of what TWI classified as "Good" fell in the "Very Good" zone by the HAND-based method.

Table 26: Confusion matrix comparing the cell-by-cell classification of groundwater potential by TWI against the groundwater potential map based on HAND

Percent correct (%)		TWI – based Groundwater Potential Classes				
Class No	Class Name	Very Good	Good	Moderate	Poor	Very Poor
	HAND – based Groundwater potential classes	1	2	3	4	5
1	Very Good	90.70	11.96	0.39	0.00	0.00
2	Good	9.28	77.64	25.47	1.71	0.00
3	Moderate	0.02	10.05	60.52	26.10	1.26
4	Poor	0.00	0.34	13.41	51.03	15.08
5	Very Poor	0.00	0.00	0.22	21.17	83.66

The producer's accuracy (Table 27) showed that it was more accurate to reproduce the extreme zones, i.e., the "Very Good" and the "Very Poor" of the HAND-based groundwater zones using the TWI-based method with better user accuracy of the same classes at 75.53% and 70.52% respectively. Similarly, the "Good" and the "Moderate" GWP zone had a fair user accuracy at 70.85% and 70.09%, respectively (Table 27). The results showed that the two methods have a better agreement in defining extreme classes of GWP zones. Generally, the local communities use topographical and vegetation indicators (e.g., the presence of fig trees) as aids for groundwater prospecting. Future studies could explore opportunities provided by these topographic based methods and their relationships with the groundwater prospecting approaches adopted by the local community.

The overall accuracy of prediction of HAND-based GWP using the TWI-based GWP was 69.87%, with a Kappa coefficient of 0.61. This implied that significant relationships existed between the two methods regarding GWP identification. While the two methods do not ideally give the same results, they help define the potential of groundwater. Therefore, either method is suitable for preliminary groundwater exploration with considerable potential to minimize groundwater prospecting efforts and costs. Overall, the study finds that groundwater potential varies with the spatial variability of the catchment parameters.

Table 27: The accuracy of using the TWI-based groundwater potential to predict the HAND-based groundwater potential classification

S/NO	Groundwater class	Producer's Accuracy			User's Accuracy (%)		
		Correct Pixels	Total no. of reference pixels	Producer's accuracy (%)	Correct Pixels	Total no. of pixels in the class	User's accuracy (%)
1	Very Good	42450	46802	90.70	42450	56205	75.53
2	Good	86344	111208	77.64	86344	121871	70.85
3	Moderate	71198	117651	60.52	71198	101587	70.09
4	Poor	36467	71461	51.03	36467	59261	61.54
5	Very Poor	36793	43978	83.66	36793	52176	70.52

Producer's accuracy is a percent of the correctly classified number of pixels for a given class divided by the total number of reference pixels for that class, while the users' accuracy is the accuracy of using the TWI based groundwater potential zones to predict the HAND based groundwater potential zones calculated as a percentage of correct pixels divided by the total number of pixels in the class

CHAPTER FIVE

CONCLUSION AND RECOMMENDATIONS

5.1 Conclusion

This study investigated surface water – groundwater interaction within a semi-closed lake catchment. To achieve the study's objectives while relating it locally, Lake Babati, a semi-closed rift valley lake, was chosen as a case study. It was observed that Lake Babati responds to different hydrological parameters. Lake Babati's level is significantly declining (p-value < 0.01) at about 25 mm per annum. Contrary to the expectations, the lake levels declined significantly (p-value < 0.05) in all months and seasons. Although the lake level has varied, often reflecting the cycles of the rainy and dry seasons, and with the lake level peaks corresponding to the rainfall peaks, no significant correlation was observed between the lake level and rainfall at daily and monthly timesteps.

Interestingly, the lake level declines occurred when the lake evaporation remained constant, and the rainfall did not show any significant change either seasonally or annually. Drought analysis by SPEI and SPI also showed that the area was neither becoming drier nor wetter. Therefore, the direct attribution of the decline in the lake levels to the rainfall variability was not supported. Given that the rainfall (the driver of runoff) did not change significantly, and the evaporation remained constant, the logical explanation for the declining lake levels would be the increased outflow that resulted after expanding and lowering the spillway level. Therefore, the interventions to control Lake Babati's flooding have reduced lake volume.

On the other hand, the hydro-geochemistry and isotope data showed that the lake water and groundwater interact. The similarity of the isotopic and hydro-geochemical compositions of the deep wells and the lake suggested that the lake water recharges the deep wells in its neighbourhood while the shallow wells drain into the lake. Further, the nitrate in deep wells attested that deeper aquifers receive both the lake water and the recently-recharged water polluted with nitrate, implying a hydraulic connection between the wells and the lake. Other water sources also showed such clustering. For example, shallow wells' hydro-geochemical and isotopic composition were strikingly similar to those of the springs and crater water. Their isotopic signatures were more depleted in Oxygen – 18 and Deuterium, suggesting that the shallow wells, springs, and crater water came from similar sources of meteoric (rainfall and runoff) origin. On the other hand, the deep wells were characterized by carbonate and sulphate salts of calcium and magnesium, probably from rocks that dissolved as water travelled. The high salt concentration in the deep wells indicated they were extracting a portion of water with a long residence time mixed with the recently recharged water from the local groundwater flow systems.

Further, the similarity of the isotopic signature of water from the Kiongozi River with the deep boreholes in the lake neighbourhood and the groundwater suggested its hydraulic connection to the groundwater flow systems of Lake Babati. This connection will likely impact surface water especailly when groundwater abstraction is at unsustainable rates or either water source is contaminated. If unchecked, this is a likely future scenario given that Babati town, a regional capital for the Manyara region, is bursting with economic activities and rapid population growth. This is a genuine concern given that most abstractions are currently groundwater-based but are not well monitored.

The study further sought to appreciate the influence of catchment heterogeneity on groundwater distribution. It used HAND-based and TWI-based methods to map GWP as a proxy for groundwater distributions and compared the suitability of the two methods in identifying areas of GWP. Subsequent validation of GWP maps from both methods with shallow and deep wells emphasized the importance of HAND and TWI in understanding groundwater spatial variability. Both methods showed similarities in the GWP classifications, with an overall Kappa coefficient of 0.61 and an overall efficiency of 69.87%. Therefore, using either method for preliminary prospecting can yield promising results and minimize groundwater prospecting efforts and associated costs.

Nevertheless, the HAND-based method demonstrated superiority to the TWI-based method in the present study based on the distribution of the shallow wells. The HAND-based GWP had a more realistic classification of shallow wells in the identified GWP classes. In contrast, the TWI-based method appeared to incorporate randomness in allocating shallow wells among the different GWP classes. The groundwater potential maps developed are proxy indicators of surface water – groundwater interactions as the good groundwater potential areas indicated are likely locations of groundwater discharge. The hilly areas with very poor groundwater potential are groundwater recharge points. Thus, these locations need protection to avoid contamination.

5.2 Recommendations

Lake Babati Level is declining, yet it is hydraulically connected to the groundwater system. The linkage between lake catchment and groundwater system makes them vulnerable as overexploitation of one would influence the other. Therefore, a holistic assessment of surface and groundwater systems is required for sustainable water resources development and integrated management in the catchment.

As the population in the catchment rapidly grows, it might be accompanied by urban sprawl. These often lead to increased water abstractions, and land use and land cover may change in commensurate rates. Therefore, the subsequent changes in the lake levels could be driven by water

abstractions or changes in stream inflow occasioned by land use and land cover changes. Thus, future studies should investigate the evolution of these changes and their possible impact on lake level variability. The abstractions from the groundwater systems must be limited to the safe yields of the aquifer determined through test pumping.

A variable control gate is recommended at the outlet of Lake Babati for dynamic and optimized control of the lake level. This will give Lake Babati a dual purpose of being a water reservoir with controlled outflow and a reservoir for controlling floods. Further, mandatory and continuous monitoring of the water resources (groundwater levels, river flows, and lake levels) is recommended for timely remediation efforts. Additionally, a detailed 3 Dimensional modelling of integrated surface water–groundwater system may quantify the fluxes exchanged and offer more insight into the interdependence of the surface water and groundwater systems.

Siltation is an emerging threat to lakes and reservoirs, which irresponsible land use practices can exacerbate. It would be interesting for future investigations to analyse the evolution of siltation under the current trends of land cover and land use change and its possible effect on lake volume and levels variability.

The topography-based methods applied for mapping groundwater suitability predicted the GWP areas. However, a similar study is recommended in other catchments to validate HAND's superiority over TWI in defining the GWP. Furthermore, the water balance model developed should be calibrated and validated with longer records for instrumental observations taken at timesteps shorter than daily.

REFERENCES

Abdullah, A., Akhir, J. M., & Abdullah, I. (2010). Automatic Mapping of Lineaments Using Shaded Relief Images Derived from Digital Elevation Model in the Maran: Sungi Lembing Area. *Electronic Journal of Geotechnical Engineering*, *15*, 949–957.

Abramowitz, M., & Stegun, I. A. (Eds.). (1970). *Handbook of Mathematical Functions with Formulas, Graphs and Mathematical Tables* (9th ed.). Washington, D.C: National Bureau of Standards.

Ahmed, A. A., Shabana, A. R., & Saleh, A. A. (2019). Using hydrochemical and isotopic data to determine sources of recharge and groundwater evolution in arid region from Eastern Desert, Egypt. *Journal of African Earth Sciences*, *151*(May 2018), 36–46.

Akaike, H. (1973). *Information Theory as an Extension of the Maximum Likelihood Principle. In B. . Petrov & F. C. saki (Eds.), Second International Symposium on Information Theory (pp. 267–281)*. Akademiai Kiado, Budapest.

Ala-aho, P., Rossi, P. M., & Kløve, B. (2013). Interaction of esker groundwater with headwater lakes and streams. *Journal of Hydrology*, *500*, 144–156.

Allen, R. G., Pereira, L S, Raes, D., & Smith, M. (1998). Crop Evapotranspiration: Guidelines for Computing Crop Water Requirements. http://www.fao.org

Gonzales Amaya, A., Villazon, M. F., & Willems, P. (2018). Assessment of rainfall variability and its relationship to ENSO in a sub-Andean watershed in central Bolivia. *Water,* 10(6), 701.

Rice, E. W., Bridgewater, L., & American Public Health Association (Eds.). (2012). *Standard Methods for the Examination of Water and Wastewater (Vol. 10)*. Washington, DC: American public health association.

Amiri, V., Nakhaei, M., Lak, R., & Kholghi, M. (2016). Investigating the salinization and freshening processes of coastal groundwater resources in Urmia aquifer, NW Iran. *Environmental Monitoring and Assessment,* 188, 1-23.

Anand, J., Gosain, A. K., & Khosa, R. (2018). Prediction of land use changes based on Land Change Modeler and attribution of changes in the water balance of Ganga basin to land use change using the SWAT model. *Science of the Total Environment*, *644*, 503–519. https://doi.org/10.1016/j.scitotenv.2018.07.017

Anand, J., Gosain, A. K., Khosa, R., & Srinivasan, R. (2018). Regional scale hydrologic modelling for prediction of water balance, analysis of trends in streamflow and variations in streamflow: The case study of the Ganga River basin. *Journal of Hydrology: Regional Studies*, *16*(3), 32–53. https://doi.org/10.1016/j.ejrh.2018.02.007

napalli, S. S., Green, T. R., Reddy, K. N., Gowda, P. H., Sui, R., Fisher, D. K., Moorhead, J. E., & Marek, G. W. (2018). Application of an energy balance method for estimating evapotranspiration in cropping systems. *Agricultural Water Management,* 204, 107-117.

Anderson, M. P. (2005). The Wisconsin roots of ground water hydrology. *Ground Water*, *43*(1), 142–145.

Andualem, T. G., & Demeke, G. G. (2019). Groundwater potential assessment using GIS and remote sensing: A case study of Guna tana landscape, upper Blue Nile Basin, Ethiopia. *Journal of Hydrology: Regional Studies*, *24*(6), 100610.

Arulbalaji, P., Padmalal, D., & Sreelash, K. (2019). GIS and AHP Techniques Based Delineation of Groundwater Potential Zones: A case study from Southern Western Ghats, India. *Scientific Reports*, 1, 1–17.

As-syakur, A. R., Adnyana, I. W. S., Arthana, I. W., & Nuarsa, I. W. (2012). Enhanced built-UP and bareness index (EBBI) for mapping built-UP and bare land in an urban area. *Remote Sensing*, *4*(10), 2957–2970. https://doi.org/10.3390/rs4102957

Awange, J. L., Schumacher, M., Forootan, E., & Heck, B. (2016). Exploring hydro-meteorological drought patterns over the Greater Horn of Africa (1979–2014) using remote sensing and reanalysis products. *Advances in Water Resources*, 94, 45-59.

Baguis, P., Roulin, E., Willems, P., & Ntegeka, V. (2009). Climate change scenarios for precipitation and potential evapotranspiration over central Belgium. *Theoretical and Applied Climatology*, *99*(3–4), 273–286. https://doi.org/10.1007/s00704-009-0146-5

Bailey, R., Rathjens, H., Bieger, K., Chaubey, I., & Arnold, J. (2017). SWATMOD‐Prep: Graphical user interface for preparing coupled SWAT‐MODFLOW simulations. *Journal of the American Water Resources Association,* 53(2), 400-410.

Bailey, R. T., Wible, T. C., Arabi, M., Records, R. M., & Ditty, J. (2016). Assessing regional-scale spatio-temporal patterns of groundwate: Surface water interactions using a coupled SWAT-MODFLOW model. *Hydrological Processes*, *4433*(8), 4420–4433.

Batelaan, O., & Smedt, F. D. E. (2001). WetSpass: A flexible, GIS based, distributed recharge methodology for regional groundwater modelling. *Impact of Human Activity on Groundwater Dynamics,* 269, 11–17.

Bedient, P. B., Huber, W. C., & Vieux, B. E. (2013). *Hydrology and Floodplain Analysis.* https://doi.org/10.5860/choice.27-2736

Benjmel, K., Amraoui, F., Boutaleb, S., Ouchchen, M., Tahiri, A., & Touab, A. (2020). Mapping of groundwater potential zones in crystalline terrain using remote sensing, GIS techniques, and multicriteria data analysis (Case of the Ighrem Region, Western Anti-Atlas, Morocco). *Water*, 12(2), 471.

Bennett, G., Van Reybrouck, J., Shemsanga, C., Kisaka, M., Tomašek, I., Fontijn, K., Kervyn, M., & Walraevens, K. (2021). Hydrochemical characterisation of high-fluoride groundwater and development of a conceptual groundwater flow model using a combined hydrogeological and hydrochemical approach on an active volcano: Mount meru, Northern Tanzania. *Water,* 13(16), 2159.

Berhanu, K. G., & Hatiye, S. D. (2020). Identification of Groundwater Potential Zones Using Proxy Data: Case study of Megech Watershed, Ethiopia. *Journal of Hydrology: Regional Studies*, *28*(1), 100676. https://doi.org/10.1016/j.ejrh.2020.100676

Biggs, E. M., Bruce, E., Boruff, B., Duncan, J. M., Horsley, J., Pauli, N., McNeill, K., Neef, A., Van Ogtrop, F., Curnow, J., & Haworth, B. (2015). Sustainable development and the water-energy-food nexus: A perspective on livelihoods. *Environmental Science and Policy*, *54*, 389–397.

Brassington, R. (2007). *Field Hydrogeology* (3rd ed.). John Wiley & Sons.

Bretzke, K., Drechsler, P., & Conard, N. J. (2012). Water availability and landuse during the Upper and Epipaleolithic in southwestern Syria. *Journal of Archaeological Science*, *39*(7), 2272–2279. https://doi.org/10.1016/j.jas.2012.02.033

Byakatonda, J, Parida, B. P., Kenabatho, P. K., & Moalafhi, D. B. (2016). Modelling dryness severity using artificial neural network at Okavango Delta, Botswana. *Global Nest Journal*, *18*(3), 463–481.

Byakatonda, Jimmy, Parida, B. P., & Kenabatho, P. K. (2018). Relating the dynamics of climatological and hydrological droughts in semiarid Botswana. *Physics and Chemistry of the Earth*, *105*, 2017, 12–24. https://doi.org/10.1016/j.pce.2018.02.004

Byakatonda, Jimmy, Parida, B. P., Moalafhi, D. B., & Kenabatho, P. K. (2018). Analysis of long term drought severity characteristics and trends across semiarid Botswana using two drought indices. *Atmospheric Research*, *213*(3), 492–508.

Calder, I. R., Hall, R. L., Bastable, H. G., Gunston, H. M., Shela, O., Chirwa, A., & Kafundu, R. (1995). The impact of land use change on water resources in sub-Saharan Africa: A modelling study of Lake Malawi. *Journal of Hydrology*, *170*(1–4), 123–135.

Casanova, J., & Hillaire - Marcel, C. (1992). Chronology and Paleohydrology of Late Quaternary High Lake Levels in the Manyara Basin (Tanzania) from Isotopic Data (“0, 13C, 14C, Th/U) on Fossil Stromatolites. *Quaternary Research*, *38*, 205–226.

Chacha, N., Njau, K. N., Lugomela, G. V., & Muzuka, A. N. (2018). Groundwater age dating and recharge mechanism of Arusha aquifer, northern Tanzania: application of radioisotope and stable isotope techniques. *Hydrogeology Journal,* 26(8), 2693-2706.

Chow, V. T., Maidment, D. R., & Mays, L. W. (1988). *Applied Hydrology*. New Delhi: McGraw-Hill Book Co.

Christensen, N. S., Wood, A. W., Voisin, N., Lettenmaier, D. P., & Palmer, R. N. (2004). *The Effects of Climate Change on the Hydrology and Water Resources of the Colorado River Basin*. https://scholar.google.com/

Clifton, C., Evans, R., Hayes, S., Hirji, R., Puz, G., & Pizarro, C. (2010). *Water and Climate change: Impacts on Groundwater Resources and Adaptation Options* (No. 55027). https://scholar.google.com

Condon, L. E., & Maxwell, R. M. (2015). Evaluating the relationship between topography and groundwater using outputs from a continental‐scale integrated hydrology model. *Water Resources Research,* 51(8), 6602-6621.

Corgne, S., Magagi, R., Yergeau, M., & Sylla, D. (2010). Remote Sensing of Environment An integrated approach to hydrogeological lineament mapping of a semi-arid region of West Africa using Radarsat-1 and GIS. *Remote Sensing of Environment*, *114*(9), 1863–1875. https://doi.org/10.1016/j.rse.2010.03.004

Dansgard, W. (1964). *Stable Isotopes in Precipitation.* https://doi.org/10.1111/j.2153-3490.1964.tb00181.x

Das, B., Pal, S. C., Malik, S., & Chakrabortty, R. (2019). Modeling groundwater potential zones of Puruliya district, West Bengal, India using remote sensing and GIS techniques.

Geology, Ecology, and Landscapes, 3(3), 223-237.

Davis, S. N., & Dewiest, R. J. M. (1966). *Hydrogeology*. Wiley and sons.

Debnath, J., Das (Pan), N., Ahmed, I., & Bhowmik, M. (2017). Channel migration and its impact on land use/land cover using RS and GIS: A study on Khowai River of Tripura, North-East India. *Egyptian Journal of Remote Sensing and Space Science*, *20*(2), 197–210.

Detty, J. M., & McGuire, K. J. (2010). Topographic controls on shallow groundwater dynamics: Implications of hydrologic connectivity between hillslopes and riparian zones in a till mantled catchment. *Hydrological Processes*, *24*(16), 2222–2236.

Deus, D., & Gloaguen, R. (2013). Remote sensing analysis of lake dynamics in semi-arid regions: Implication for water resource management. Lake Manyara, East African Rift, Northern Tanzania. *Water (Switzerland)*, *5*(2), 698–727. https://doi.org/10.3390/w5020698

Deus, D., Gloaguen, R., & Krause, P. (2013). Water Balance Modeling in a Semi-arid Environment with limited in situ data using remote sensing in Lake Manyara, East African rift, Tanzania. *Remote Sensing*, *5*(4), 1651–1680. https://doi.org/10.3390/rs5041651

Dijkshoorn, J. A. (2003). *SOTER Database for Southern Africa (SOTERAF): Technical Report*. https://doi.org/https://www.persistent-identifier.nl/urn:nbn:nl:ui:32-452227

Draper, N., & Smith, H. (1998). *Applied-Regression-Analysis-Third-Edition Norman Draper and Hary Smith.pdf* (3rd ed.). New York: Wiley and sons.

Driessen, P., Deckers, J., Spaargaren, O., & Nachtergaele, F. (2000). *Lecture notes on the Major Soils of the World (No. 94).* Food and Agriculture Organization (FAO).

Duan, Z., Tuo, Y., Liu, J., Gao, H., Song, X., & Zhang, Z. (2018). Hydrological evaluation of open-access precipitation and air temperature datasets using SWAT in a poorly gauged basin in Ethiopia. *Journal of hydrology, 569, 612-626.*

Dun, Y., Ling, J., Wang, R., Wei, J., Zhou, Q., Cao, Y., Zhang, Y., & Xuan, Y. (2022). Hydrochemical Evolution and Nitrogen Behaviors in Coastal Groundwater Suffered From Seawater Intrusion and Anthropogenic Inputs. *Frontiers in Marine Science*, *9*(9), 1–14.

Elisante, E., & Muzuka, A. N. N. (2017). Occurrence of nitrate in Tanzanian groundwater aquifers: A review. *Applied Water Science*, *7*(1), 71–87. https://doi.org/10.1007/s13201-015-0269-z

Ershadi, A., Mccabe, M. F., Evans, J. P., & Walker, J. P. (2011). Evaluation of energy balance , combination , and complementary schemes for estimation of evaporation. *Hydro-Climatology: Variability and Change*, 2011(7), 52–56.

Ewen, J., Parkin, G., & O'Connell, P. E. (2000). Shetran: Distributed River B Asin F Low Modeling System. *Journal of Hydrologic Engineering*, *5*(7), 250–258.

Fajri, S. N., Surtiyono, E., & Nalendra, S. (2019). *Lineament Analysis of Digital Elevation Model to Identification of Geological Structure in Northern Manna Sub-Basin, Bengkulu.* https://scholar.google.com

Fitts, C. R. (2002). *Groundwater Science*. Elsevier. https://scholar.google.com

Fleckenstein, J. H., Krause, S., Hannah, D. M., & Boano, F. (2010). Groundwater-surface water interactions: New methods and models to improve understanding of processes and dynamics. *Advances in Water Resources*, *33*(11), 1291–1295.

Foody, G. M. (2002). Status of land cover classification accuracy assessment. *Remote Sensing of Environment*, *80*(1), 185–201.

Freeze, R. A., & Cherry, J. A. (1979). *Groundwater*. London: Prentice - Hall. https:// scholar. google. com

Funk, C. C., & Brown, M. E. (2009). Declining global per capita agricultural production and warming oceans threaten food security. *Food Security*, *1*(3), 271–289.

Gao, H., Birkel, C., Hrachowitz, M., Tetzlaff, D., Soulsby, C., & Savenije, H. H. G. (2019). A simple topography-driven and calibration-free runoff generation module. *Hydrology and Earth System Sciences*, *23*(2), 787–809. https://doi.org/10.5194/hess-23-787-2019

Gao, H., Hrachowitz, M., Fenicia, F., Gharari, S., & Savenije, H. H. G. (2014). Testing the realism of a topography-driven model (FLEX-Topo) in the nested catchments of the Upper Heihe, China. *Hydrology and Earth System Sciences*, *18*, 1895–1915. https://doi.org/10.5194/hess-18-1895-2014

Gharari, S., Hrachowitz, M., Fenicia, F., & Savenije, H. H. G. (2011). Hydrological landscape classification: investigating the performance of HAND based landscape classifications in a central European meso-scale catchment. *Hydrology and Earth System Sciences*, 2011, 3275–3291. https://doi.org/10.5194/hess-15-3275-2011

Ghorbani-Nejad, S., Falah, F., Daneshfar, M., Haghizadeh, A., & Rahmati, O. (2017). Delineation

of groundwater potential zones using remote sensing and GIS-based data-driven models. *Geocarto International*, *32*(2), 167–187.

Gibson, J. J., Birks, S. J., & Yi, Y. (2016). Stable isotope mass balance of lakes: A contemporary perspective. *Quaternary Science Reviews*, *131*, 316–328.

Gilbert, R. O. (1987). *Statistical Methods for Environmental Pollution monitoring*. New York. https://scholar.google.com

Gilfedder, M., Rassam, D. W., Stenson, M. P., Jolly, I. D., Walker, G. R., & Littleboy, M. (2012). Incorporating land-use changes and surface-groundwater interactions in a simple catchment water yield model. *Environmental Modelling and Software*, *38*, 62–73.

Global Modeling and Assimilation Office. (2022). *Modern-Era Retrospective Analysis for Research and Applications, Version 2 (MEERA-2).* https://scholar.google.com

Gonfiantini, R., Roche, M., Olivry, J., Fontes, J., & Maria, G. (2001). The altitude effect on the isotopic composition of tropical rains. *Chemical Geology*, *181*, 147–167.

González-Trinidad, J., Pacheco-Guerrero, A., Júnez-Ferreira, H., Bautista-Capetillo, C., & Hernández-Antonio, A. (2017). Identifying groundwater recharge sites through environmental stable isotopes in an alluvial aquifer. *Water*, *9*(8), 1–12.

Grabs, T., Seibert, J., Bishop, K., & Laudon, H. (2009). Modeling spatial patterns of saturated areas : A comparison of the topographic wetness index and a dynamic distributed model. *Journal of Hydrology*, *373*(1–2), 15–23. https://doi.org/10.1016/j.jhydrol.2009.03.031

Hamdani, N., & Baali, A. (2019). Height Above Nearest Drainage model coupled with lineament mapping for delineating groundwater potential areas. *Groundwater for Sustainable Development*, *9*(6), 100256. https://doi.org/10.1016/j.gsd.2019.100256

Hassan, A. A., & Jin, S. (2014). Lake level change and total water discharge in East Africa Rift Valley from satellite-based observations. *Global and Planetary Change*, *117*, 79–90. https://doi.org/10.1016/j.gloplacha.2014.03.005

Hayashi, M., & Van der Kamp, G. (2007). Water Level Changes in Ponds and Lakes. The Hydrological Processes. *Plant Disturbance Ecology*, 2007, 311–339.

Hayes, M. J., Svoboda, M. D., & Wilhite, D. A. (2000). *Chapter 12 Monitoring Drought Using the Standardized Precipitation Index.* https://scholar.google.com

HEC. (2000). *Hydrologic Modeling System HEC-HMS Technical Reference Manual*.

https://scholar.google.com

HEC. (2021). *HEC-HMS User's Manual*. https://scholar.google.com/

Hongoa, P. S. (2014). The Impact of Population Increase Around Lake Babati [The Open University of Tanzania]. https://scholar.google.com

Hussain, M. M., Mahmud, I., & Bari, S. H. (2023). pyHomogeneity: A Python Package for Homogeneity Test of Time Series Data. *Journal of Open Research Software*, *11*, 1–10. https://doi.org/10.5334/jors.427

IAEA. (2019). *Global Network of Isotopes in Precipitation.* https://scholar.google.com

Idowu, O. A. (2007). Hydrological Processes of Interaction Between Surface Water and Groundwater. *An International Journal*, *6*(2), 172–190.

Ijumulana, J., Ligate, F., Bhattacharya, P., Mtalo, F., & Zhang, C. (2020). Spatial analysis and GIS mapping of regional hotspots and potential health risk of fluoride concentrations in groundwater of northern Tanzania. *Science of the Total Environment*, *735*, 139584.

Infascelli, R., Faugno, S., Pindozzi, S., Boccia, L., & Merot, P. (2013). Testing Different Topographic Indexes to Predict Wetlands Distribution. *Procedia Environmental Sciences*, *19*, 733–746. https://doi.org/10.1016/j.proenv.2013.06.082

Ishizaka, A. (2014). Comparison of Fuzzy logic, AHP, FAHP and Hybrid Fuzzy AHP for new supplier selection and its performance analysis. *International Journal of Integrated Supply Management*, (9), 1–22. https://doi.org/10.1504/IJISM.2014.064353

Jabal, M. S. A., Abustan, I., Rozaimy, M. R., & El Najar, H. (2018). The deuterium and oxygen-18 isotopic composition of the groundwater in Khan Younis City, southern Gaza Strip (Palestine). *Environmental Earth Sciences*, *77*(4), 1–11.

Jenk, G. F. (1967). The Data Model Concept in Statistical Mapping. *International Yearbook of Cartography*, *7*, 186–190.

Kalacska, M., Arroyo-Mora, J. P., Lucanus, O., & Kishe-Machumu, M. A. (2017). Land cover, land use, and climate change impacts on endemic cichlid habitats in Northern Tanzania. *Remote Sensing*, *9*(6), 1–25. https://doi.org/10.3390/rs9060623

Kebede, S., Travi, Y., Alemayehu, T., & Marc, V. (2006). Water balance of Lake Tana and its sensitivity to fluctuations in rainfall, Blue Nile basin, Ethiopia. *Journal of Hydrology*, *316*(1–4), 233–247. https://doi.org/10.1016/j.jhydrol.2005.05.011

Keijzer, T. (2020). *Drought Analysis of the Lake Manyara Catchment: Meteorological Drought Occurence, Influence of Atmospheric Teleconnections and Impact on Lake Manyara* (Universiteit Utrecht).

Kendall, C., & Doctor, D. H. (2003). *Stable Isotope Applications in Hydrological Studies*. https://doi.org/http://dx.doi.org/10.1016/B0-08-043751-6/05081-7

Kendall, M. G. (1975). *Rank Correlation Methods (4th Ed.).* London: Griffin.

Kenoyer, G. J., & Bowser, C. J. (1992). Groundwater chemical evolution in a sandy silicate aquifer in northern Wisconsin: Patterns and rates of change. *Water Resources Research*, *28*(2), 579–589. https://doi.org/10.1029/91WR02302

Khan, H. H., & Khan, A. (2019). *Groundwater and Surface Water Interaction. https:// scholar. google. com*

Kim, G. B., Lee, J. Y., & Lee, K. K. (2004). Application of representative elementary area (REA) to lineament density analysis for groundwater implications. *Geosciences Journal*, *8*(1), 27–42. https://doi.org/10.1007/BF02910276

Kløve, B., Ala-Aho, P., Bertrand, G., Gurdak, J. J., Kupfersberger, H., Kværner, J., Muotka, T., Mykrä, H., Preda, E., Rossi, P., & Uvo, C. B. (2014). Climate change impacts on groundwater and dependent ecosystems. *Journal of Hydrology*, 518, 250-266.

Kopecký, M., & Čížková, Š. (2010). Using topographic wetness index in vegetation ecology: Does the algorithm matter?. *Applied Vegetation Science,* 13(4), 450-459.

Krishan, G., Singh, S., Thayyen, R. J., Ghosh, N. C., Rai, S. P., & Arora, M. (2020). Understanding river–subsurface water interactions in upper Ganga basin, India. *International Journal of River Basin Management,* 18(2), 243-253.

Kumambala, P. G., & Ervine, A. (2013). Water Balance Model of Lake Malawi and its Sensitivity to Climate Change. *The Open Hydrology Journal*, *4*(1), 152–162.

Kung, C., & Wen, K. (2007). Applying Grey Relational Analysis and Grey Decision-Making to evaluate the relationship between company attributes and its financial performance: A case study of venture capital enterprises in Taiwan. *Decision Support Systems*, *43*, 842–852. https://doi.org/10.1016/j.dss.2006.12.012

Kwak, S. G., & Kim, J. H. (2017). Central limit theorem: the cornerstone of modern statistics. *Korean Journal of Anesthesiology*, *70*(2), 144–156. https://doi.org/pISSN 2005-6419

Lalika, M. C. S., Meire, P., Ngaga, Y. M., & Chang'a, L. (2015). Understanding watershed dynamics and impacts of climate change and variability in the Pangani River Basin, Tanzania. *Ecohydrology and Hydrobiology*, *15*(1), 26–38.

Lameck, A. S., Skutai, J., & Boros, E. (2023). Review of chemical properties of inland soda and saline waters in East Africa (rift valley region). *Journal of Hydrology: Regional Studies*, *46*(2022), 101323. https://doi.org/10.1016/j.ejrh.2023.101323

Lévêque, C. (2001). *Lake and Pond Ecosystems.* https://scholar.google.com

Li, X., Li, G., & Zhang, Y. (2014). Identifying Major Factors Affecting Groundwater Change in the North China Plain with Grey Relational Analysis. *Water*, 2014, 1581–1600.

Ligate, F., Ijumulana, J., Ahmad, A., Kimambo, V., Irunde, R., Mtamba, J. O., Mtalo, F., & Bhattacharya, P. (2021). Groundwater resources in the East African Rift Valley: Understanding the geogenic contamination and water quality challenges in Tanzania. *Scientific African*, 13, e00831.

Song, F., Gu, L., Zhu, N., & Yuan, H. (2013). Leaching behavior of heavy metals from sewage sludge solidified by cement-based binders. *Chemosphere*, 92(4), 344-350.

Liliane, M., & Jouzel, J. (1979). Global Climatic Interpretationof theDeuterium-Oxygen 18 Relationship for Precipitation. *Jounral of Geophysical Research*, *84*(9), 5029–5033.

Llamas, M., & Martínez-Santos, P. (2005). Intensive groundwater use: Silent revolution and potential source of social conflicts. *Journal of Water Resources*, *131*(10), 337–341. https://doi.org/10.1061/(ASCE)0733-9496(2005)131:5(337)

Lopez, M. G. (2011). *Modelling Climatic and Hydrological Variability in Lake Babati, Northern Tanzania [MSc thesis Stockholm University]*.

Lwenya, C., & Yongo, E. (2010). Human aspects of siltation of Lake Baringo: Causes, impacts and interventions. *Aquatic Ecosystem Health and Management*, *13*(4), 437–441.

MacDonald, A. M., Bonsor, H. C., Dochartaigh, B. É. Ó., & Taylor, R. G. (2012). Quantitative maps of groundwater resources in Africa. *Environmental Research Letters*, *7*(2), 1-9. https://doi.org/10.1088/1748-9326/7/2/024009

Magesh, N. S., Chandrasekar, N., & Soundranayagam, J. P. (2012). Delineation of groundwater potential zones in Theni district, Tamil Nadu, using remote sensing, GIS and MIF techniques. *Geoscience Frontiers*, *3*(2), 189–196.

Malczewski, J. (2006). GIS - based multicriteria decision analysis: A survey of the literature. *International Journal of Geographical Information Science*, *20*(17), 703–726.

Maliva, R., & Missimer, T. (2012). Arid Lands Water Evaluation and Management. *Environmental Science and Engineering*, (1948), 21–40. https://doi.org/10.1007/978-3-642-29104-3

Mallick, J., Khan, R. A., Ahmed, M., Alqadhi, S. D., Alsubih, M., Falqi, I., & Hasan, M. A. (2019). Modeling groundwater potential zone in a semi-arid region of Aseer using fuzzy-AHP and geoinformation techniques. *Water*, 11(12), 2656.

Mann, H. B. (1945). Nonparametric test against trend. *Econometrica*, *13*(3), 245–259. https://doi.org/10.2307/1907187

MARI. (2006). *Soils of Tanzania Potential for Agriculture Development*. Tanga, Tanzania. https://scholar.google.com

Markstrom, S. L., Niswonger, R. G., Regan, R. S., Prudic, D. E., & Barlow, P. M. (2005). *GSFLOW: Coupled Ground-Water and Surface-Water Flow Model Based on the Integration of the Precipitation-Runoff Modeling System (PRMS) and the Modular Ground-Water Flow Model*. Reston, Virginia: U.S. Geological Survey Techniques and Methods 6-D1. https://scholar.google.com

Mashnik, D., Jacobus, H., Barghouth, A., Jiayu Wang, E., Blanchard, J., & Shelby, R. (2017). Increasing productivity through irrigation: Problems and solutions implemented in Africa and Asia. *Sustainable Energy Technologies and Assessments*, *22*, 220–227.

Maurya, P., Kumari, R., & Mukherjee, S. (2019). Hydrochemistry in integration with stable isotopes ($\delta^{18}O$ and δD) to assess seawater intrusion in coastal aquifers of Kachchh district, Gujarat, India. *Journal of Geochemical Exploration*, *196*(2018), 42–56.

Mavromatis, T. (2007). Drought index evaluation for assessing future wheat production in Greece. *International Journal of Climatology*, *924*(2006), 911–924. https://doi.org/10.1002/joc

Mbanguka, R. P., Lyon, S. W., Holmgren, K., Girons Lopez, M., & Jarsjö, J. (2016). Water balance and level change of Lake Babati, Tanzania: sensitivity to hydroclimatic forcings. *Water,* 8(12), 572.

McDonald, M. G., & Harbaugh, A. W. (1988). *A Modular Three Dimensional Finite DIfference Groundwater Flow Model*. *Book 6*. U.S Geological Survey. https://scholar.google.com

Mckee, T. B., Doesken, N. J., & Kleist, J. (1993). The relationship of drought frequency and

duration to time scales. *Eighth Conference on Applied Climatology*, 1, 17–22.

Meijerink, A. M. J., Bannert, D., Batelaan, O., Lubczynski, M. W., & Pointet, T. (2007). *Remote Sensing to Groundwater Applications to Groundwater*. https:// doi. org/ IHP/ 2007/ GW/ 16

Mineral Resources Division. (1966). *Quarter Degree Sheet 85 Babati*. Dodoma, Tanzania. https://scholar.google.com

Moriasi, D. N., Gitau, M. W., Pai, N., & Daggupati, P. (2015). Hydrologic and water quality models: Performance measures and evaluation criteria. *Transactions of the ASABE*, *58*(6), 1763–1785. https://doi.org/10.13031/trans.58.10715

Mul, M. L., Mutiibwa, R. K., Foppen, J. W. A., Uhlenbrook, S., & Savenije, H. H. G. (2007). Identification of groundwater flow systems using geological mapping and chemical spring analysis in South Pare Mountains, Tanzania. *Physics and Chemistry of the Earth, Parts A/B/C*, 32(15-18), 1015-1022.

National Bureau of Statistics. (2013). 2012 *Population and Housing Census Population Distribution by Administrative areas*. https://scholar.google.com

Nazzal, Y., Ahmed, I., Al-Arifi, N. S., Ghrefat, H., Zaidi, F. K., El-Waheidi, M. M., Batayneh, A., & Zumlot, T. (2014). A pragmatic approach to study the groundwater quality suitability for domestic and agricultural usage, Saq aquifer, northwest of Saudi Arabia. *Environmental Monitoring and Assessment*, 186, 4655-4667.

NBS. (2013). *United Republic of Tanzania: 2012 Population and Housing Census*. https://www.nbs.go.tz/index.php/en

Nejad, S. G., Falah, F., Daneshfar, M., & Haghizadeh, A. (2017). Delineation of groundwater potential zones using remote sensing and GIS-based data-driven models. *Geocarto International*, *6049*(5), 1–22. https://doi.org/10.1080/10106049.2015.1132481

Nobre, A. D., Cuartas, L. A., Hodnett, M., Rennó, C. D., Rodrigues, G., Silveira, A., & Saleska, S. (2011). Height Above the Nearest Drainage: A hydrologically relevant new terrain model. *Journal of Hydrology,* 404(1-2), 13-29.

Nystrom, E. A., & Burns, D. A. (2011). *TOPMODEL Simulations of Streamflow and Depth to Water Table in Fishing Brook Watershed, New York, 2007–09: U.S. Geological Survey Scientific Investigations Report 2011–5190.* http://pubs.usgs.gov/sir/2011/5190/

Ogiramoi, P. N. (2011). *Climate Change Impacts on Hydrological Extremes and Water resources in Lake Victoria catchments, Upper Nile Basin*. Katholieke Universiteit Leuven - Faculteite Ingenieurswetenschappen, Arenberg Doctoraatsschool, Kasteelpark, Leuven, Belgium.

Okwir, G., Kumar, S., Pramod, K. S., Gao, H., & Njau, K. N. (2023). Conceptualization of groundwater-surface water interaction with evidence from environmental isotopes and hydrogeochemistry in lake Babati Basin in Northern Tanzania. *Groundwater for Sustainable Development*, *21*(2021), 100940.

Olaka, L. A., Odada, E. O., Trauth, M. H., & Olago, D. O. (2010). The sensitivity of East African rift lakes to climate fluctuations. *Journal of Paleolimnology*, *44*(2), 629–644.

Olofsson, P., Foody, G. M., Herold, M., Stehman, S. V., Woodcock, C. E., & Wulder, M. A. (2014). Good practices for estimating area and assessing accuracy of land change. *Remote Sensing of Environment*, *148*, 42–57. https://doi.org/10.1016/j.rse.2014.02.015

Palmer, W. C. (1965). *Meteorological Drought*. https://www.ncdc.noaa.gov

Pande, C. B., Khadri, S. F. R., Moharir, K. N., & Patode, R. S. (2018). Assessment of groundwater potential zonation of Mahesh River basin Akola and Buldhana districts, Maharashtra, India using remote sensing and GIS techniques. *Sustainable Water Resources Management,* 4, 965-979.

Pantaleo, P. A., Komakech, H. C., Mtei, K. M., & Njau, K. N. (2018). Contamination of groundwater sources in emerging African towns: The case of Babati town, Tanzania. *Water Practice & Technology*, *13*(4), 980–990. https://doi.org/10.2166/wpt.2018.104

Pavelic, P., Giordano, M., Keraita, B., Ramesh, V., & Rao, T. (Eds.). (2012). *Groundwater Availability and use in Sub - Saharan Africa: A review of 15 countries*. https:// scholar. google. com

PCI. (2019). *Geomatica Banff*. pcigeomatics.com

Pfahl, S., & Sodemann, H. (2014). What controls deuterium excess in global precipitation? *Climate of the Past*, *10*(2), 771–781

Piper, A. M. (1944). A graphic procedure in the geochemical interpretation of water-analyses. *Transactions, American Geophysical Union*,1944, 914–928.

Prasad, A. D., Jain, K., & Gairola, A. (2013). Mapping of lineaments and knowledge base

preparation using geomatics techniques for part of the Godavari and Tapi basins, India: A case study. *International Journal of Computer Applications,* 70(9), 39-47.

Lima, I. Q., Ramos, O. R., Munoz, M. O., Aguirre, J. Q., Duwig, C., Maity, J. P., Sracek, O., & Bhattacharya, P. (2020). Spatial dependency of arsenic, antimony, boron and other trace elements in the shallow groundwater systems of the Lower Katari Basin, Bolivian Altiplano. *Science of the Total Environment*, 719, 137505.

Rahman, M. R., Islam, A. H. M. H., & Rahman, M. A. (2004). NDVI derived sugarcane area identification and crop condition assessment. *Plan Plus,* 1(2), 1-12.

Rahmati, O., Kornejady, A., Samadi, M., Nobre, A. D., & Melesse, A. M. (2018). Development of an automated GIS tool for reproducing the HAND terrain model. *Environmental Modelling and Software*, *102*, 1–12. https://doi.org/10.1016/j.envsoft.2018.01.004

Rawlings, J. O., & Dickey, D. A. (1998). *Applied Regression Analysis: A Research Tool* (2nd Ed.). New York: Springer. https://scholar.google.com

Razmkhah, H. (2016). Comparing performance of different loss methods in rainfall-runoff modeling. *Water Resources*, *43*(1), 207–224.

Reig-Mullor, J., Pla-Santamaria, D., & Garcia-Bernabeu, A. (2020). Extended fuzzy analytic hierarchy process (E-fahp): A general approach. *Mathematics*, *8*(11), 1–14.

Renno, C. D., Nobre, A. D., Cuartas, L. A., Soares, J. V., Hodnett, M. G., Tomasella, J., & Waterloo, M. J. (2008). Remote Sensing of Environment HAND, a new terrain descriptor using SRTM-DEM: Mapping terra-firme rainforest environments in Amazonia. *Remote Sensing of Environment*, *112*, 3469–3481.

Rinderer, M., Meerveld, H. J. van, & Seibert, J. (2014). Topographic controls on shallow groundwater levels in a steep, prealpine catchment: When are the TWI assumptions valid? *Water Resources Research*, *50*, 6067–6080.

Saaty, R. W. (1987). The Analytic Hierarchy Process: What it is and how it is used. *Mathematical Modelling*, *9*(3), 161–176. https://doi.org/10.1016/0270-0255(87)90473-8

Sakakibara, K., Tsujimura, M., Song, X., & Zhang, J. (2016). Interaction between surface water and groundwater revealed by multi-tracer and statistical approaches in the Baiyangdian Lake watershed, North China plain. *Hydrological Research Letters*, *10*(2), 74–80.

Salui, C. L. (2018). Methodological Validation for Automated Lineament Extraction by LINE

Method in PCI Geomatica and MATLAB based Hough Transformation. *Journal of the Geological Society of India*, *92*(9), 321–328. https://doi.org/10.1007/s12594-018-1015-6

Sandstrom, K. (1995). The recent Lake Babati floods in semi-arid Tanzania: A response to changes in land cover? *Geografiska Annaler, Series A*, *77 A*(1–2), 35–44.

Saranya, T., & Saravanan, S. (2020). Groundwater potential zone mapping using analytical hierarchy process and GIS for Kancheepuram District, Tamilnadu, India. *Modeling Earth Systems and Environment,* 6(2), 1105-1122.

Savenije, H. H. (2010). HESS Opinions" Topography driven conceptual modelling (FLEX-Topo)". *Hydrology and Earth System Sciences,* 14(12), 2681-2692.

Scholl, M. A., Shanley, J. B., Zegarra, J. P., & Coplen, T. B. (2009). The stable isotope amount effect: New insights from NEXRAD echo tops, Luquillo Mountains, Puerto Rico. *Water Resources Research,* 45(12), 1-14.

Seeteram, N. A., Hyera, P. T., Kaaya, L. T., Lalika, M. C., & Anderson, E. P. (2019). Conserving rivers and their biodiversity in Tanzania. *Water,* 11(12), 2612.

Sen, P. K. (1968). Estimates of the Regression Coefficient Based on Kendall's Tau. *Journal of the American Statistical Association*, *63*(324), 1379–1389.

Sene, K., Piper, B., Wykeham, D., McSweeney, R. T., Tych, W., & Beven, K. (2017). Long-term variations in the net inflow record for Lake Malawi. *Hydrology Research*, *48*(3), 851–866. https://doi.org/10.2166/nh.2016.143

Serdeczny, O., Adams, S., Coumou, D., Hare, W., & Perrette, M. (2016). Climate change impacts in Sub-Saharan Africa: from physical changes to their social repercussions. *Regional Environmental Change,* 17, 1585-1600. https://doi.org/10.1007/s10113-015-0910-2

Shekhar, S., & Pandey, A. C. (2014). Delineation of groundwater potential zone in hard rock terrain of India using remote sensing, geographical information system and analytic hierarchy process techniques. *Geocarto International*, *30*(4), 402–421.

Simcore Software. (2011). *Processing Modflow: An Integrated Modeling Environment for the Simulation of Groundwater Flow, Transport and Reactive Processes*. Simcore Software. https://scholar.google.com

Singh, P., Javed, S., Shashtri, S., Singh, R. P., Vishwakarma, C. A., & Mukherjee, S. (2017).

Influence of changes in watershed landuse pattern on the wetland of Sultanpur National Park, Haryana using remote sensing techniques and hydrochemical analysis. *Remote Sensing Applications: Society and Environment*, *7*(1), 84–92.

Sjoin, E. (2010). *Leaking or Waterproof Organization ? Babati Town and the Current Capacity to*. https://scholar.google.com

Stagl, J., Mayr, E., Koch, H., & Hattermann, F. F. (2014). Effects of Climate Change on the Hydrological Cycle in Central and Eastern Europe. *Advances in Global Change Research*, *58*, 31–43. https://doi.org/10.1007/978-94-007-7960-0

Stromquist, L. (1992). Environmental Impact Assessment of Natural Disasters, a Case Study of the Recent Lake Babati Floods in Northern Tanzania. *Swedish Society for Anthropology and Geography*, *74*(2), 81–91. https://doi.org/10.2307/521286

Swenson, S., & Wahr, J. (2009). Monitoring the water balance of Lake Victoria, East Africa, from space. *Journal of Hydrology*, *370*(1–4), 163–176.

Tanzania Survey Division. (1967). *East Africa (Tanzania) 1:50,000*. Dar es salaam. https://scholar.google.com

Tapley, B. D., Bettadpur, S., Watkins, M., & Reigber, C. (2004). The gravity recovery and climate experiment: Mission overview and early results. *Geophysical Research Letters,* 31(9), 1-4.

Tarboron, G. (1997). A new method for the determination of flow directions and upslope areas in grid digital elevation models. *Water Resources Research*, *33*(2), 309–319. https://doi.org/10.1029/96WR03137

Tate, E., Sutclifffe, J., Conway, D., & Farquharson, F. (2004). Water balance of Lake Victoria: upadate to 2000 and climate change modelling to 2100. *Hydrological Sciences-Journal-Des Sciences Hydrologiques*, *49*(4), 563–574.

Taye, M. T., Ntegeka, V., Ogiramoi, N. P., & Willems, P. (2011). Assessment of climate change impact on hydrological extremes in two source regions of the Nile River Basin. *Hydrology and Earth System Sciences*, *15*(1), 209–222. https://doi.org/10.5194/hess-15-209-2011

Timperley, M. H. (1983). Phosporus in spring waters of the Taupo Volcanic Zone, North Island, New Zealand. *Chemical Geology*, *38*, 287–306. https://doi.org/0009-2541/83/0000--0000/$03.00

Tolche, A. D. (2020). Groundwater potential mapping using geospatial techniques: A case study of Dhungeta-Ramis sub-basin, Ethiopia. *Geology, Ecology, and Landscapes*, *00*(00), 1–16. https://doi.org/10.1080/24749508.2020.1728882

Toth, J. (1963). A theoretical analysis of groundwater flow in small drainage basins. *Journal of Geophysical Research,* 68(16), 4795-4812.

Trajkovic, Slavisa. "Hargreaves versus Penman-Monteith under humid conditions." *Journal of Irrigation and Drainage Engineering,* 133, 1, 38-42.

Tzeng, C. J., Lin, Y. H., Yang, Y. K., & Jeng, M. C. (2009). Optimization of turning operations with multiple performance characteristics using the Taguchi method and Grey relational analysis. *Journal of Materials Processing Technology*, *209*(6), 2753–2759.

UNICEF. (2015). *Progress on Sanitation and Drinking Water: The 2015 Update and MDG. https://scholar.google.com*

URT. (2014). *Integrated Water Resources Management and Development Plans (IWRMDP) for the Internal Drainage Basin Final Report*. Dar es salaam. https://scholar.google.com/

URT. (2017). *The United Republic of Tanzania Agricultural Sector Development Programme Phase II*. https://www.kilimo.go.tz

USACE. (1994). *Engineering and Design: Flood-Runoff Analysis*. https://doi.org/EM 1110-2-1417

USACE. (1998). *HEC-1 Flood Hydrograph Package User's Manual*. Davis, California: Hydrologic Engineering Center, US Army Corps of Engineers.

USGS. (2018). *Shuttle Radar Topographic Mission*. http://www.landcover.org/data/srtm

Van Den Akker, J., Simmons, C. T., & Hutson, J. L. (2011). Salinity effects from evaporation and transpiration under flood irrigation. Journal of Irrigation and Drainage Engineering, 137(12), 754-764.

Vicente-Serrano, S. M., Beguería, S., & López-Moreno, J. I. (2010). A multiscalar drought index sensitive to global warming: The standardized precipitation evapotranspiration index. *Journal of Climate,* 23(7), 1696-1718.

Weitz, J., & Demlie, M. (2014). Conceptual modelling of groundwater–surface water interactions in the Lake Sibayi Catchment, Eastern South Africa. *Journal of African Earth Sciences*, 99, 613-624.

WHO. (2011). *WHO Guidelines for drinking water quality* (4th Ed.). Geneva, Switzerland: World Health Organization. https://scholar.google.com

Winter, T. C. (1995). Recent advances in understanding the interaction of groundwater and surface water. *Reviews of Geophysics*, *33*(2 S), 985–994. https://doi.org/10.1029/95RG00115

Woldeamlak, S. T., Batelaan, O., & De Smedt, F. (2007). Effects of climate change on the groundwater system in the Grote-Nete catchment, Belgium. *Hydrogeology Journal*, *15*(5), 891–901. https://doi.org/10.1007/s10040-006-0145-x

Wolock, D. M., & Price, C. V. (1994). Effects of digital elevation model map scale and data resolution on a topography-based watershed model. *Water Resources Research*, *30*(11), 3041–3052. https://doi.org/10.1029/94WR01971

Wong, H., Hu, B. Q., Ip, W. C., & Xia, J. (2006). Change-point analysis of hydrological time series using grey relational method. *Journal of Hydrology*, *324*, 323–338.

WREM International. (2015). *Rufiji IWRMDP Final Report, Volume I: Rufiji IWRMD Plan*. Atlanta, Georgia. https://scholar.google.com

WWAP. (2012). *The United Nations World Water Development Report 4 Volume 1: Managing Water under Uncertainty and Risk*. http://www.unesco.org

WWAP. (2019). *The United Nations World Water Development Report 2019: Leaving No One Behind*. Paris: UNESCO. https://scholar.google.com

Yu, M., Hayes, M. J., & Svoboda, M. (2013). Are droughts becoming more frequent or severe in China based on the Standardized Precipitation Evapotranspiration Index: 1951 – 2010 ? Are droughts becoming more frequent or severe in China based on the Standardized Precipitation. *International Journal of Climatology*, *34*, 345–558. https:// doi. org/ 10. 1002/ joc.3701

Zohary, T., & Ostrovsky, I. (2011). Ecological impacts of excessive water level fluctuations in stratified freshwater lakes. *Inland Waters*, *1*(1), 47–59. https://doi.org/10.5268/IW-1.1.406

APPENDICES

Appendix 1: AHP pairwise weighting of the HAND classes with respect to their groundwater potential

Class No	HAND (m)	HAND Class Weight	<1	1.1-5	5.1-15	15.1-50	50.1-803.7	Geometric mean	Normalized weight
1	<1	9	1.00	1.29	1.80	3.00	9.00	2.29	0.36
2	1.1-5	7	0.78	1.00	1.40	2.33	7.00	1.78	0.28
3	5.1-15	5	0.56	0.71	1.00	1.67	5.00	1.27	0.20
4	15.1-50	3	0.33	0.43	0.60	1.00	3.00	0.76	0.12
5	50.1-1118	1	0.11	0.14	0.20	0.33	1.00	0.25	0.04

Appendix 2: AHP pairwise weighting of the TWI classes with respect to their groundwater potential

Class No	TWI (-)	TWI Class Weight	>11.94	11.94 - 9.25	9.25 - 7.61	7.61-6.37	2.58 - 6.37	Geo metric mean	Norma lized weight
1	>15.19	9	1.00	1.29	1.80	3.00	9.00	2.29	0.36
2	15.19-11.27	7	0.78	1.00	1.40	2.33	7.00	1.78	0.28
3	11.27-8.69	5	0.56	0.71	1.00	1.67	5.00	1.27	0.20
4	8.69-6.73	3	0.33	0.43	0.60	1.00	3.00	0.76	0.12
5	2.58 - 6.73	1	0.11	0.14	0.20	0.33	1.00	0.25	0.04

Appendix 3: AHP pairwise weighting of the land use and land cover types with respect to their groundwater potential

Class	Class weight	Water	Urban / Settlements	Agricultural land	Bare soil & barren land	Forests	Geo metric mean	Normalized weight
Water	9	1.00	4.50	1.80	2.25	1.50	1.94	0.35
Urban / Settlements	2	0.22	1.00	0.40	0.50	0.33	0.43	0.08
Agricultural land	5	0.56	2.50	1.00	1.25	0.83	1.08	0.19
Bare soil and barren land	4	0.44	2.00	0.80	1.00	0.67	0.86	0.15
Forests	6	0.67	3.00	1.20	1.50	1.00	1.29	0.23

Appendix 4: AHP pairwise weighting of the lineament density classes with respect to their groundwater potential

Class No	Lineament density (km/km2)	Class weight	<0.29	0.3 - 0.71	0.72 - 1.13	1.14 - 1.54	1.55 - 2.6	Geo metric mean	Norma lized weight
1	<0.29	2	1.00	0.67	0.40	0.29	0.22	0.44	0.08
2	0.3 - 0.71	3	1.50	1.00	0.60	0.43	0.33	0.66	0.12
3	0.72 - 1.13	5	2.50	1.67	1.00	0.71	0.56	1.11	0.19
4	1.14 - 1.54	7	3.50	2.33	1.40	1.00	0.78	1.55	0.27
5	1.55 - 2.6	9	4.50	3.00	1.80	1.29	1.00	1.99	0.35

Appendix 5: AHP pairwise weighting of the drainage distance classes with respect to their groundwater potential

Class No	Drainage distance (m)	Class weight	<278	278 - 582	582 - 913	913 - 1304	1304 - 2217	Geo metric mean	Normalized weight
1	<503	9	1.00	1.29	2.25	3.00	9.00	2.39	0.38
2	503 - 1061	7	0.78	1.00	1.75	2.33	7.00	1.86	0.29
3	1061 - 1673	4	0.44	0.57	1.00	1.33	4.00	1.06	0.17
4	1673 - 2518	3	0.33	0.43	0.75	1.00	3.00	0.80	0.13
5	2518 - 4586	1	0.11	0.14	0.25	0.33	1.00	0.27	0.04

Appendix 6: AHP pairwise weighting of the slope classes in respect to their groundwater potential

Class No	Slope (Degree)	Class weight	<3.75	3.73 - 8.24	8.25 - 13.49	13.5 - 20.98	20.99 - 63.69	Geometric mean	Normalized weight
1	<3.75	9	1.00	1.29	2.25	3.00	9.00	2.39	0.38
2	3.73 - 8.24	7	0.78	1.00	1.75	2.33	7.00	1.86	0.29
3	8.25 - 13.49	4	0.44	0.57	1.00	1.33	4.00	1.06	0.17
4	13.5 - 20.98	3	0.33	0.43	0.75	1.00	3.00	0.80	0.13
5	20.99 - 63.69	1	0.11	0.14	0.25	0.33	1.00	0.27	0.04

Appendix 7: AHP pairwise weighting of the soil types with respect to their groundwater potential

Class No	Soil type	Soil weight	Eutric Leptosols	Humi-Rhodic Luvisols	Chromi-Luvic Phaeozems	Geometric mean	Normalized weight
1	Eutric Leptosols	3	1.00	0.38	0.33	0.50	0.15
2	Humi-Rhodic Luvisols	8	2.67	1.00	0.89	1.33	0.40
3	Chromi-Luvic Phaeozems	9	3.00	1.13	1.00	1.50	0.45

Appendix 8: AHP pairwise weighting of the lithology types in respect to their groundwater potential

Potentials	AHP Rank	Water	Mbuga soils	Alluvium	Red and brown soils	Volcanic crystal tuff & fragments	Volcanic agglomerate	Meta sediments	Bubu cataclastics	Geometric mean	Normalized weight
Superficial deposits, Water	9	1.00	1.29	1.13	1.80	1.50	3.00	4.50	3.00	1.88	0.21
Superficial deposits, Mbuga soils	7	0.78	1.00	0.88	1.40	1.17	2.33	3.50	2.33	1.46	0.16
Superficial deposits, Alluvium	8	0.89	1.14	1.00	1.60	1.33	2.67	4.00	2.67	1.67	0.19
Superficial deposits, Red and brown soils	5	0.56	0.71	0.63	1.00	0.83	1.67	2.50	1.67	1.05	0.12
Volcanic crystal tuff & fragments	6	0.67	0.86	0.75	1.20	1.00	2.00	3.00	2.00	1.26	0.14
Volcanic agglomerate	3	0.33	0.43	0.38	0.60	0.50	1.00	1.50	1.00	0.63	0.07
Meta sediments	2	0.22	0.29	0.25	0.40	0.33	0.67	1.00	0.67	0.42	0.05
Bubu cataclastics	3	0.33	0.43	0.38	0.60	0.50	1.00	1.50	1.00	0.63	0.07

Appendix 9: Prospective locations for well drilling / /excavation

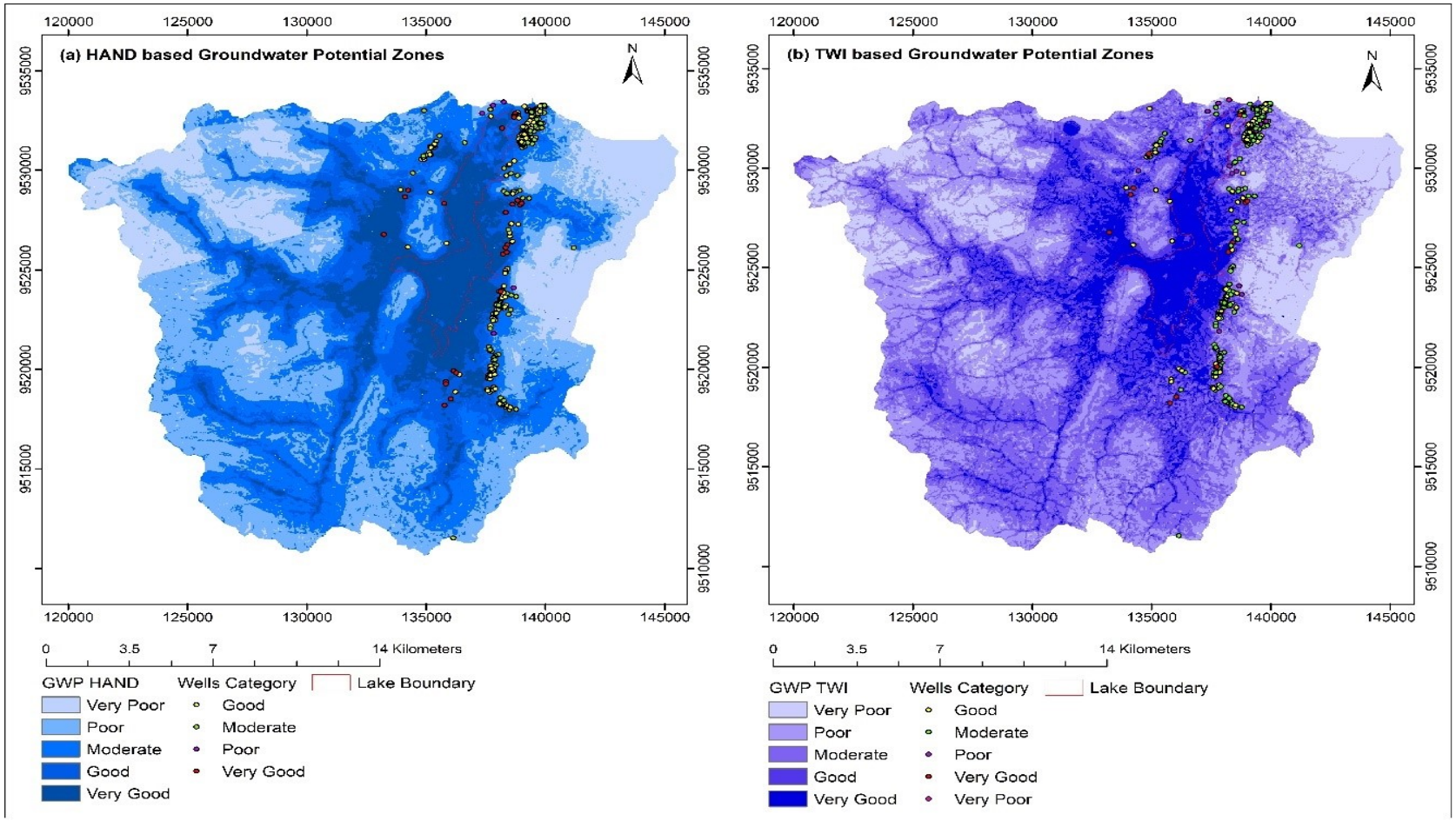

Appendix 10: Hydrogeochemical and isotopic parameters of the water samples

No	Sample ID	Source	pH (-)	EC (µS/cm)	TDS (mg/L)	Salinity (%)	F^- (mg/L)	Cl^- (mg/L)	$HCO3^-$ (mg/L)	$CO3^{2-}$ (mg/L)	$SO4^{2-}$ (mg/L)	$NO3^-$ (mg/L)	Ca^{2+} (mg/L)	Mg^{2+} (mg/L)	Na^+ (mg/L)	K^+ (mg/L)	$\delta^{18}O$ $^o/_{oo}$	δ^2H $^o/_{oo}$
1	CR	Crater	7.5	133	57	0.2	0	1.1	77.5	0	3.5	8.2	5.1	4.8	6	22.1	-0.7	-5.6
2	DW1	Deep Well	8.2	683	326	1.1	0.4	41.7	340	0	47.1	5.6	38.3	42.8	42.8	8.1	0.4	3.5
3	DW2	Deep Well	8.1	415	207	0.8	0	22.9	260	0	29.4	17	51.8	21.4	24.5	0.9	-3.9	-20.1
4	DW3	Deep Well	8.3	582	235	0.9	0.6	44.9	200	0	21.3	66.4	37.6	29.9	30.9	7.2	-1.4	-7.0
5	DW4	Deep Well	8.7	521	261	0.9	0.2	9.7	140	0	6	10	11.5	18	12.6	3.7	-3.8	-21.7
6	LS1	Lake Surface	8.6	670	231	0.8	0	48.2	400	0	0.2	0.4	0	90	38.3	8.5	3.2	15.7
7	LB1	Lake Bottom	8.2	672	263	0.9	2	65.2	340	0	6.2	5.1	17.6	27.5	107.8	7.8	3.3	15.4
8	LS2	Lake Surface	8.5	669	282	0.9	1.2	97.6	460	0	26.1	0	24.2	27	191.7	6.6	3.2	15.7
9	LB2	Lake Bottom	8.8	567	283	1.1	0.7	11	130	0	13.1	0.1	17.6	9.2	27.6	1.7	3.3	17.4
10	LS3	Lake Surface	8.9	474	243	0.9	0.6	27.6	20	239.9	0.2	0.1	9.7	85.9	48.8	11.6	3.1	14.3
11	LB3	Lake Bottom	8.6	542	287	1.1	0.7	32.1	240	0	17.9	13.5	17.5	16.5	63.5	3.3	3.2	14.5
12	LS4	Lake Surface	8.7	582	344	1.3	19.4	374	60	199.9	134.7	47.4	72.5	237	922.8	59.2	3.2	15.4
13	LB4	Lake Bottom	8.4	677	181	0.7	1.2	219.3	280	0	26.9	31.7	25.1	28.6	125.3	6.4	3.1	15.3
14	LS5	Lake Surface	8.5	565	282	1.1	0.7	5.8	97	0	4.8	2.9	14.9	4.2	14.5	0.9	2.2	10.1
15	LB5	Lake Bottom	8.5	663	279	1	1	42.8	380	0	27.6	13.9	24	26.7	104.7	5.6	2.4	10.2
16	LS6	Lake Surface	8.2	494	253	0.9	1.4	35.7	280	0	22.4	6.6	23.4	20.6	81.9	4.5	2.5	11.6
17	LB6	Lake Bottom	8.3	667	283	0.9	1.1	34.5	340	0	21.6	21.1	18.3	24.3	102.4	6.4	2.6	11.3
18	RV1	River	8.5	173.8	172	0.6	0.2	21.3	70	0	1.8	2.9	8.8	10.1	16.2	1.6	-4.0	-20.1
19	RV2	River	9.0	518	259	0.9	0.8	5	67	0	6.9	0.8	15.5	3.7	8.2	1.8	-2.5	-13.1
20	RV3	River	8.5	140.5	86	0.2	1.9	4.4	82.5	0	7.5	0.6	16.6	2.2	11	4.3	-5.1	-24.3
21	RV4	River	8.6	109.9	44	0.1	0.1	5.5	60	0	3.3	2.7	7.7	5.1	10.7	1.3	-3.8	-20.4
22	SP1	Spring	8.4	228	172	0.6	0	31.6	85	0	4.4	7.3	22.9	6.6	19.1	2	-4.3	-24.3
23	SP2	Spring	7.8	86.4	67	0.2	0.5	16	140	0	0.1	0.3	0	36.2	16.2	4.1	-4.0	-20.9
24	SW1	Shallow well	8.6	254.7	127	0.4	0.3	1.4	50	0	4	0.2	13.5	1.7	2.6	0.6	-4.9	-28.3

No	Sample ID	Source	pH (-)	EC (µS/cm)	TDS (mg/L)	Salinity (%)	F^- (mg/L)	Cl^- (mg/L)	$HCO3^-$ (mg/L)	$CO3^{2-}$ (mg/L)	$SO4^{2-}$ (mg/L)	$NO3^-$ (mg/L)	Ca^{2+} (mg/L)	Mg^{2+} (mg/L)	Na^+ (mg/L)	K^+ (mg/L)	$\delta^{18}O$ $^o/_{oo}$	δ^2H $^o/_{oo}$
25	SW2	Shallow well	8.5	172.3	86.1	0.2	0.2	11.5	35	0	0.5	0	7.9	2.0	9.0	1.4	-3.7	-17.1
26	SW3	Shallow well	8.4	235	172	0.6	0.2	26.5	60	0	2.3	57.3	21.7	11	8.9	1.6	-3.8	-18.7
27	SW4	Shallow well	8.1	145.6	73	0.2	0.2	19.9	67	0	1.1	4	12.2	5.5	13.2	1.3	-4.1	-24.1
28	SW5	Shallow well	8.12	415	207	0.8	0.2	11.5	35	0	0.5	0	7.9	2	9	1.4	-3.8	-19.4
29	SW6	Shallow well	8.6	304	152	0.5	0.8	20.3	120	0	0.1	0.3	10.8	52.6	23.5	2.8	-3.7	-20.5
30	MLK	Lake Manyara	7.16	21.67													-2.1	-10.4
	WHO Guideline Value		-		-		1.5	-			-	50			-	-		

Appendix 11: **Matrix of Pearson rank correlation coefficient (r) amongst physicochemical parameters across samples from all water types reported. NB: ** p<0.01 and * p <0.05: Abbreviations pH = Potential of Hydrogen [-], EC = Electrical Conductivity [µS/cm], TDS = Total Dissolved Solids [mg/L], F^- = Fluoride ion [mg/L], Cl^- = Chloride ion [mg/L], HCO_3^- = Bicarbonate ion [mg/L], CO_3^- = Carbonate ion [mg/L], SO_4^{2-} = Sulphate ion [mg/L], NO_3^- = Nitrate ion [mg/L], Ca^{2+} = Calcium ion [mg/L], Mg^{2+} = Magnesium ion [mg/L], Na^+ = Sodium ion [mg/L], K^+ = Potassium ion [mg/L], TH = Total Hardness [mg/L]**

	PH	EC	TDS	Salinity	F^-	Cl^-	HCO_3^-	CO_3^{2-}	SO_4^{2-}	NO_3^-	Ca^{2+}	Mg^{2+}	Na^+	K^+	TH	Total Alkalinity
PH	1.00															
EC	0.26	1.00														
TDS	0.43*	0.88**	1.00													
Salinity	0.42*	0.86**	0.99**	1.00												
F^-	0.19	0.20	0.35	0.36	1.00											
Cl-	0.12	0.38*	0.37	0.39*	0.86**	1.00										
HCO_3^-	-0.19	0.72**	0.48**	0.41*	-0.11	0.14	1.00									
CO_3^{2-}	0.36	0.13	0.27	0.30	0.62**	0.51**	-0.30	1.00								
SO_4^{2-}	0.10	0.41*	0.52**	0.53**	0.90**	0.85**	0.16	0.49**	1.00							
NO_3^-	-0.08	0.21	0.20	0.25	0.38*	0.48**	0.01	0.16	0.46*	1.00						
Ca^{2+}	0.06	0.39*	0.51**	0.53**	0.68**	0.68**	0.16	0.34	0.87**	0.59**	1.00					
Mg^{2+}	0.22	0.32	0.40*	0.41*	0.86**	0.80**	0.03	0.75**	0.79**	0.32	0.55*	1.00				
Na^+	0.17	0.31	0.42*	0.43*	0.98**	0.91**	0.04	0.61**	0.92**	0.39*	0.70**	0.87**	1.00			
K^+	-0.01	0.20	0.28	0.30	0.91**	0.80**	-0.07	0.67**	0.83**	0.38*	0.58**	0.87**	0.91**	1.00		
TH	0.19	0.37	0.46*	0.48*	0.90**	0.84**	0.07	0.71**	0.88**	0.42*	0.73*	0.97**	0.91**	0.88**	1.00	
Total Alkalinity	-0.03	0.80**	0.62**	0.57**	0.17	0.38	0.90**	0.15	0.38	0.08	0.32	0.38*	0.32	0.24	0.43*	1.00

Appendix 12: Summary of Mann - Kendall trend test of the Lake Babati levels and rainfall received in Babati

	Lake Babati Level			Rainfall in Babati			Minimum temperature			Maximum Temperature			Lake Babati Evaporation		
Series\Test	Kendall's tau	p-value	Sen's slope	Kendall's tau	p-value	Sen's slope	Kendall's tau	p-value	Sen's slope	Kendall's tau	p-value	Sen's slope	Kendall's tau	p-value	Sen's slope
Jan	-0.06	0.61	-0.01	0.10	0.44	1.57	0.25	0.019	0.02	-0.118	0.289	-0.03	-0.13	0.23	-0.25
Feb	-0.10	0.46	-0.01	0.11	0.39	0.98	0.32	0.003	0.02	-0.054	0.633	-0.015	0.0025	0.99	0.01
Mar	-0.26	0.07	-0.04	0.07	0.61	0.58	0.26	0.018	0.017	-0.21	0.057	-0.06	-0.283	0.01	-0.47
Apr	-0.30	0.02	-0.03	-0.12	0.40	-1.46	0.27	0.013	0.015	0.018	0.87	0.003	-0.03	0.73	-0.07
May	-0.38	0.00	-0.03	-0.15	0.27	-0.55	0.15	0.16	0.009	0.095	0.395	0.015	0.003	0.98	0.005
Jun	-0.15	0.27	-0.01	-0.04	0.80	0.00	0.338	0.002	0.035	0.137	0.217	0.021	0.070	0.53	0.071
Jul	-0.20	0.14	-0.02	-0.19	0.23	0.00	0.331	0.002	0.031	0.264	0.017	0.031	0.065	0.56	0.041
Aug	-0.12	0.34	-0.01	-0.11	0.41	0.00	0.42	0.0001	0.036	0.264	0.026	0.024	0.079	0.47	0.049
Sep	0.00	1.00	0.00	0.08	0.64	0.00	0.49	0.0000	0.032	0.279	0.011	0.021	0.074	0.50	0.038
Oct	-0.29	0.05	-0.02	0.00	1.00	0.00	0.443	0.0000	0.029	0.218	0.048	0.024	-0.028	0.80	-0.01
Nov	-0.265	0.07	-0.01	-0.01	0.94	-0.08	0.502	0.0000	0.032	-0.074	0.506	-0.009	-0.20	0.06	-0.22
Dec	-0.35	0.02	-0.03	0.08	0.59	1.66	0.456	0.0000	0.021	-0.087	0.435	-0.013	-0.209	0.059	-033
Annual	-0.35	0.02	-0.03	-0.05	0.76	-2.23	0.58	0.0000	0.025	0.064	0.574	0.005	-0.148	0.18	-0.97
Minor rainy season (ONDJ)	-0.38	0.01	-0.03	0.07	0.64	2.07	0.591	0.0000	0.025	-0.058	0.607	-0.005	-0.261	0.018	-0.90
Major rainy season (FMAM)	-0.26	0.03	-0.03	-0.09	0.51	-1.86	0.388	0.0006	0.017	-0.0544	0.632	-0.007	-0.12	0.278	-0.43
Rainy season (ONDJFMAM)	-0.36	0.00	-0.03	-0.09	0.53	-4.34	0.595	0.0000	0.022	-0.062	0.583	-0.005	-0.249	0.024	-1.41

	Lake Babati Level			**Rainfall in Babati**			**Minimum temperature**			**Maximum Temperature**			**Lake Babati Evaporation**		
Series\Test	Kendall's tau	p-value	Sen's slope	Kendall's tau	p-value	Sen's slope	Kendall's tau	p-value	Sen's slope	Kendall's tau	p-value	Sen's slope	Kendall's tau	p-value	Sen's slope
Dry season (JJAS)	-0.12	0.31	-0.01	-0.10	0.51	0.00	0.505	0.0000	0.036	0.253	0.023	0.025	0.084	0.45	0.18

RESEARCH OUTPUTS

(i) Publication

Okwir, G., Kumar, S. P., Gao, H., Selemani, J. R., & Njau, K. N. (2022). Multi-variate regression analysis of lake level variability: A case of semi-closed, shallow rift valley lake in Northern Tanzania. *Environmental Challenges*, 7, 100533.

Okwir, G., Kumar, S., Pramod, K. S., Gao, H., & Njau, K. N. (2023). Conceptualization of groundwater-surface water interaction with evidence from environmental isotopes and hydrogeochemistry in lake Babati Basin in Northern Tanzania. *Groundwater for Sustainable Development,* 21, 100940.

Okwir, G., Komakech, H. C., Kumar, S. P., Gao, H., & Njau, K. N. (2022). Mapping groundwater in ungauged lake basin in Tanzania: A comparison between two topography based methods. *Groundwater for Sustainable Development*, 16, 100697.

(ii) Poster Presentation